INFORMATION TO USERS

This manuscript has been reproduced from the microfilm master. UMI films the text directly from the original or copy submitted. Thus, some thesis and dissertation copies are in typewriter face, while others may be from any type of computer printer.

The quality of this reproduction is dependent upon the quality of the copy submitted. Broken or indistinct print, colored or poor quality illustrations and photographs, print bleedthrough, substandard margins, and improper alignment can adversely affect reproduction.

In the unlikely event that the author did not send UMI a complete manuscript and there are missing pages, these will be noted. Also, if unauthorized copyright material had to be removed, a note will indicate the deletion.

Oversize materials (e.g., maps, drawings, charts) are reproduced by sectioning the original, beginning at the upper left-hand corner and continuing from left to right in equal sections with small overlaps.

Photographs included in the original manuscript have been reproduced xerographically in this copy. Higher quality 6" x 9" black and white photographic prints are available for any photographs or illustrations appearing in this copy for an additional charge. Contact UMI directly to order.

Bell & Howell Information and Learning
300 North Zeeb Road, Ann Arbor, MI 48106-1346 USA
800-521-0600

Seismic Analysis of Lattice Towers

by

Mohamed Abdel Halim Khedr

October 1998

Department of Civil Engineering and Applied Mechanics
McGill University
Montreal, Canada

A thesis submitted to
the Faculty of Graduate Studies and Research
in partial fulfillment of the requirements for the degree of
Doctor of Philosophy

In the Name of Allah the most merciful the most compassionate

To my beautiful Rania
To my son Omar
To my father's soul
To my mother
To my sister

ABSTRACT

In the absence of specific guidelines for the seismic analysis of self-supporting telecommunication towers, designers may be tempted to apply simplified building code approaches to these structures. However, these towers respond to earthquakes in a different fashion than that of shear buildings. The objective of this research is to propose simplified methods for the seismic analysis of self-supporting telecommunication towers.

The author studied the specific problem of self-supporting lattice telecommunication towers using numerical simulations and applying the modal superposition method and the response spectrum technique on ten existing towers, typical of microwave towers usually erected in Canada. The analyses are carried out using a set of 45 strong motion horizontal accelerograms to study the horizontal effects. Vertical dynamic effects are studied using two approaches: the first considering the same horizontal accelerograms in the vertical direction after reducing their amplitudes to 75%, the second using a distinct set of 55 vertical accelerograms.

As a first stage, simple regression analyses are performed on the results to yield earthquake amplification factors for the base shear and the total vertical reaction. These factors are presented as functions of the tower's largest flexural period or largest axial period of vibration as appropriate and peak ground acceleration at tower site. They can be used by designers to estimate the expected level of dynamic forces in self-supporting telecommunication towers due to an earthquake.

As a second stage, a simplified static method is proposed to estimate the member forces in self-supporting telecommunication lattice towers due to both horizontal and

vertical earthquake excitations. It is assumed that the lowest three flexural modes of vibration are sufficient to estimate the structure's response to horizontal excitation accurately, while only the first axial mode will reflect the actual behavior of towers in response to vertical excitation. An acceleration profile along the height of the tower is defined using the spectral acceleration values corresponding to the lowest three flexural mode shapes or the lowest axial mode as appropriate. The mass of the tower is calculated and then lumped at the leg joints. A set of equivalent static lateral or vertical loads can be determined by simply multiplying the mass by the acceleration. The tower is then analyzed statically under the effect of these forces to evaluate the member forces. The maximum error associated with the proposed simplified static method is found to be 25% in the extreme cases with an average error of ±7%.

The effect of including antennae clusters is also addressed in the analysis and findings are summarized in the thesis.

The study is extended to include transmission line towers in order to simplify the response of coupled tower-cable system by replacing the cables with an equivalent mass. Several frequency analyses were performed on the system in order to achieve a better understanding of the behavior of the coupled system, however, it was not possible to simplify this interaction in the way desired. Several observations are presented which may help in further studies.

SOMMAIRE

Faute de directives spécifiques à l'analyse sismique des pylônes de télécommunications, les concepteurs peuvent être tentés d'appliquer les approches simplifiées proposées dans codes pour les structures de bâtiments aux pylônes de type autoporteur. Une mise en garde s'impose toutefois car ces pylônes ne présentent pas le même type de réponse sismique que le modèle simplifié de bâtiment élevé avec déformation latérale en cisaillement. L'objectif de cette recherche est de fournir aux concepteurs de pylônes de télécommunications des outils appropriés à l'analyse sismique simplifiée.

L'auteur a étudié le problème spécifique aux pylônes de télécommunications autoporteurs à treillis en acier à l'aide de simulations numériques par superposition modale et par analyse spectrale sur dix modèles détaillés de pylônes existants, typiques de l'expérience canadienne. Ces structures présentent un comportement essentiellement linéaire et élastique dans la gamme des efforts considérés. Les analyses ont utilisé les accélérogrammes de 45 tremblements de terre réels pour les effets horizontaux. Pour les effets verticaux, deux séries de sollicitations ont été considérées : la première consiste à utiliser les mêmes accélérogrammes que pour les effets horizontaux mais avec une amplitude réduite à 75%, et la seconde est composée de 55 accélérogrammes verticaux réels.

Dans une première étape, l'analyse des résultats des réactions à la base des pylônes a permis d'établir des facteurs d'amplification du cisaillement à la base et de la composante dynamique de la réaction verticale. Ces deux facteurs sont exprimés en fonction de la période naturelle de vibration du pylône en modes transversal et axial, et en fonction de l'accélération maximale à la base de la structure. L'auteur propose l'utilisation

de ces facteurs comme des indicateurs de réponse seulement, i.e. pour estimer le niveau probable des effets dynamiques d'ensemble sur la structure.

En seconde étape, l'analyse des résultats s'est faite au niveau détaillé des efforts dans les membrures principales, soit les montants, les diagonales principales ainsi que les contreventements horizontaux. L'auteur propose maintenant une méthode simplifiée, par analyse statique avec forces équivalentes aux effets d'inertie, pour estimer les efforts dans les membrures individuelles. Une courbe enveloppe des accélérations maximales le long du pylône est définie à partir des accélérations spectrales correspondant aux fréquences des trois premiers modes de vibration transversaux, pour les effets latéraux, et du premier mode de vibration axial, pour les effets verticaux. La méthode proposée présuppose donc la connaissance de ces fréquences naturelles. La masse de la structure est discrétisée sur les noeuds des montants principaux et un profil de charges équivalentes aux effets d'inertie est obtenu en multipliant directement le profil de masse avec le profil d'accélération. L'analyse statique usuelle sous charges équivalentes permet ensuite d'obtenir les forces dans les membrures. La comparaison des résultats de l'analyse simplifiée avec ceux de l'analyse des détaillée des dix pylônes étudiés indique des variations dans l'évaluation des forces internes de l'ordre de ± 7% en moyenne avec des écarts allant jusqu'à 25%.

L'étude a également considéré l'effet de la masse de groupes d'antennes sur la réponse sismique des pylônes et les principales conclusions sont résumées dans la thèse.

L'auteur a tenté d'étendre l'application de sa méthode simplifiée au problème des pylônes de lignes aériennes de transport d'énergie, mais en vain. L'idée de base consistait à évaluer s'il était possible de remplacer l'effet des câbles de la ligne par une masse équivalente au pylône. Après avoir fait plusieurs analyses de fréquences sur des modèles couplés câbles-pylônes, l'auteur n'a pu généraliser ses résultats. Quelques observations présentées dans la thèse pourront servir de point de départ pour des recherches futures.

ACKNOWLEDGMENTS

The author is indebted to Professor Ghyslaine McClure for her valuable suggestions, long discussions, support, encouragement, and understanding to the student personal life and feelings. This work would have never been completed in such a way without such supervision. It is near impossible to describe how lucky I am for having her as my supervisor, many thanks.

The financial assistance provided by the Natural Science and Engineering Research Council of Canada (NSERC) in the form of post graduate scholarship to the author and research grant is greatly appreciated.

The financial assistance provided by Le Fonds pour la Formation de Chercheurs et l'Aide à la Recherche (Fonds FCAR) in the form of post graduate scholarship to the author is greatly appreciated.

The author appreciates the contribution of both Hydro-Quebec and Martoni, Cyr and Associates in this work by providing the drawings and detailed data for the telecommunication and transmission towers used in this study.

TABLE OF CONTENTS

ABSTRACT i

SOMMAIRE iii

ACKNOWLEDGMENTS v

TABLE OF CONTENTS vi

LIST OF FIGURES x

LIST OF TABLES xix

LIST OF SYMBOLS xx

CHAPTER 1

INTRODUCTION 1

1.1 Introduction 1

1.2 Objectives 3

1.3 Organization of Text 4

CHAPTER 2

LITERATURE REVIEW 6

2.1 Introduction 6

2.2 Dynamic Response of Self-supporting Lattice Towers 6

2.2.1 Response to wind 6

2.2.2 Seismic response 9

2.3 Dynamic Response of Transmission Line Structures 14

2.4 Seismic Response of Tower-shaped Structures 21

2.4.1 Seismic response of offshore towers 21

2.4.2 Seismic response of intake-outlet towers 23

2.5 Design Code Approaches for Seismic Analysis 25

2.5.1 Code approaches for different types of structures 25

2.5.2 Standards and codes of practice for towers 28

2.6 Conclusions 32

CHAPTER 3

METHODOLOGY 34

3.1 Telecommunication Towers Used in the Study 34

3.2 Numerical Modeling of Telecommunication Towers 45

3.3 Classification of Telecommunication Towers 45

3.4 Transmission Line Towers 48

3.5 Modeling and Analysis of Transmission Towers 55

3.6 Earthquake Records Used in The Study 56

CHAPTER 4

EARTHQUAKE AMPLIFICATION FACTORS FOR TELECOMMUNICATION TOWERS 58

4.1 Introduction 58

4.2 Method of Analysis 59

4.3 The Use of NBCC 1995 59

4.4 Horizontal Earthquake Excitation 63

4.5 Vertical Earthquake Excitation 77

4.6 Discussion 90

4.7 Conclusions 93

CHAPTER 5

PROPOSED STATIC METHOD OF ANALYSIS 94

5.1 Theoretical Background 94

5.1.1 Equation of motion and response spectrum 94

5.1.2 Modal analysis 96

5.1.3 Seismic response of MDOF systems 97

5.2 Proposed Method for Horizontal Earthquake Excitation 99

5.3 Verification of the Proposed Method 111

5.4 Vertical Earthquake Excitation 116

5.5 Verification of The Proposed Vertical Acceleration Profile 119

5.6 Effect of Concentrated Mass of Antennae 120

CHAPTER 6

SEISMIC CONSIDERATION FOR TRANSMISSION TOWERS 131

6.1 Introduction 131

6.2 Mathematical Modeling 131

6.2.1 Modeling of towers 132

6.2.2 Modeling of cables 132

6.3 Methods of Analysis 135

6.3.1 Nonlinear static analysis 135

6.3.2 Frequency analysis 136

6.4 Parametric Study 136

6.5 Equivalent Mass 145

6.6 Conclusions 146

CHAPTER 7

SUMMARY AND CONCLUSIONS 148

7.1 Summary 148

7.2 Earthquake Amplification Factors 149

7.3 Simplified Methods of Analysis 150

7.4 Analysis of Transmission Line Towers 151

7.5 Recommendations for Future Work 152

Statement of Originality 153

REFERENCES 154

APPENDIX A

EARTHQUAKE RECORDS 159

APPENDIX B

VERIFICATION OF THE PROPOSED EXPRESSIONS FOR THE EARTHQUAKE AMPLIFICATION FACTORS 205

APPENDIX C

VERTICAL EARTHQUAKE AMPLIFICATION FACTORS FOR TELECOMMUNICATION TOWERS 212

C. 1 Introduction 213

C.2 Vertical Earthquake Records 213

C.3 Vertical Earthquake Excitation 214

C.4 Discussion 221

APPENDIX D

VERIFICATION OF THE PROPOSED STATIC METHOD 223

LIST OF FIGURES

Fig. 3.1 Layout of tower TC1 (dimensions are in m) 35

Fig. 3.2 Layout of tower TC2 (dimensions are in m) 36

Fig. 3.3 Layout of tower TC3 (dimensions are in m) 37

Fig. 3.4 Layout of tower TC4 (dimensions are in m) 38

Fig. 3.5 Layout of tower TC5 (dimensions are in m) 39

Fig. 3.6 Layout of tower TC6 (dimensions are in m) 40

Fig. 3.7 Layout of tower TC7 (dimensions are in m) 41

Fig. 3.8 Layout of tower TC8 (dimensions are in m) 42

Fig. 3.9 Layout of tower TC9 (dimensions are in m) 43

Fig. 3.10 Layout of tower TC10 (dimensions are in m) 44

Fig. 3.11 Definition of the main symbols used in categorizing the lattice towers 45

Fig. 3.12 Layout of tower TR1 (dimensions are in m) 49

Fig. 3.13 Layout of tower TR2 (dimensions are in m) 50

Fig. 3.14 Layout of tower TR3 (dimensions are in m) 51

Fig. 3.15 Layout of tower TR4 (dimensions are in m) 52

Fig. 3.16 Layout of tower TR5 (dimensions are in m) 53

Fig. 3.17 Layout of tower TR6 (dimensions are in m) 54

Fig. 4.1 NBCC 1995 acceleration design spectrum evaluated for 5% damping 60

Fig. 4.2 Maximum base shear values for tower TC1 65

Fig. 4.3 Maximum base shear values for tower TC2 66

Fig. 4.4 Maximum base shear values for tower TC3 67

Fig. 4.5 Maximum base shear values for tower TC4 68

Fig. 4.6 Maximum base shear values for tower TC5 69

Fig. 4.7 Maximum base shear values for tower TC6 70

Fig. 4.8 Maximum base shear values for tower TC7 71

Fig. 4.9 Maximum base shear values for tower TC8 72

Fig. 4.10 Maximum base shear values for tower TC9 73

Fig. 4.11 Maximum base shear values for tower TC10 74

Fig. 4.12 Base shear amplification factors 76

Fig. 4.13 Total vertical dynamic reaction for tower TC1 78

Fig. 4.14 Total vertical dynamic reaction for tower TC2 79

Fig. 4.15 Total vertical dynamic reaction for tower TC3 80

Fig. 4.16 Total vertical dynamic reaction for tower TC4 81

Fig. 4.17 Total vertical dynamic reaction for tower TC5 82

Fig. 4.18 Total vertical dynamic reaction for tower TC6 83

Fig. 4.19 Total vertical dynamic reaction for tower TC7 84

Fig. 4.20 Total vertical dynamic reaction for tower TC8 85

Fig. 4.21 Total vertical dynamic reaction for tower TC9 86

Fig. 4.22 Total vertical dynamic reaction for tower TC10 87

Fig. 4.23 Vertical reaction amplification factors 89

Fig. 4.24 Acceleration response spectra evaluated for 3% damping 91

Fig. 4.25 Maximum base shear vs. peak ground acceleration in TC3 92

Fig. 4.26 Maximum dynamic vertical reaction vs. peak ground acceleration in TC3 92

Fig. 5.1 Concept of the proposed method 100

Fig. 5.2 Acceleration profiles for tower TC9 103

Fig. 5.3 Comparison between member forces obtained from dynamic analysis and the proposed method 103

Fig. 5.4 Lateral mode shapes and mass distribution for Group A1 106

Fig. 5.5 Lateral mode shapes and mass distribution for Group A2 106

Fig. 5.6 Lateral mode shapes and mass distribution for Group B 107

Fig. 5.7 The a_i coefficients for Group A1 108

Fig. 5.8 The a_i coefficients for Group A2 109

Fig. 5.9 The a_i coefficients for Group B 110

Fig. 5.10 Member forces for tower TC1 113

Fig. 5.11 Member forces in tower TC1 using NBCC spectrum 115

Fig. 5.12 Proposed vertical acceleration profile 118

Fig. 5.13 Member forces in tower TC1 under vertical excitation 120

Fig. 5.14 Tower TC3 with antennae 122

Fig. 5.15 Member forces including the effect of antenna mass for tower TC3 using NBCC 1995 for $Z_a<Z_v$ ratio in the horizontal direction 122

Fig. 5.16 Member forces including the effect of antenna mass for tower TC3 using NBCC 1995 for $Z_a<Z_v$ ratio in the vertical direction 123

Fig. 5.17 Effect of including heavy antennae on tower TC1 124

Fig. 5.18 Effect of including heavy antennae on tower TC2 125

Fig. 5.19 Effect of including heavy antennae on tower TC3 125

Fig. 5.20 Effect of including heavy antennae on tower TC5 126

Fig. 5.21 Effect of including heavy antennae on tower TC6 126

Fig. 5.22 Effect of including heavy antennae on tower TC7 127

Fig. 5.23 Effect of including heavy antennae on tower TC8 127

Fig. 5.24 Effect of including heavy antennae on tower TC9 128

Fig. 5.25 Effect of including heavy antennae on tower TC10 128

Fig. 6.1 Components of transmission line section on double-circuit lattice towers 133

Fig. 6.2 Mesh convergence for the lowest transversal mode 134

Fig. 6.3 Ratio between calculated natural periods of the coupled line system and the bare tower for tower TR2 with Condor 139

Fig. 6.4 Ratio between calculated natural periods of the coupled line system and the bare tower for tower TR2 with Curlew 140

Fig. 6.5 Ratio between calculated natural periods of the coupled line system and the bare tower for tower TR2 with Bersfort 141

Fig. 6.6 Ratio between calculated natural periods of the coupled line system and the bare tower for tower TR6 with Condor 142

Fig. 6.7 Ratio between calculated natural periods of the coupled line system and the bare tower for tower TR6 with Curlew 143

Fig. 6.8 The lowest two calculated longitudinal modes of tower TR6 144

Fig. A1.1 Earthquake record Long Beach, N51W (L1) 160

Fig. A1.2 Earthquake record Long Beach N39E (L2) 161

Fig. A1.3 Earthquake record Lower California S00W (L3) 162

Fig. A1.4 Earthquake record San Fernando N61W (L4) 163

Fig. A1.5 Earthquake record San Fernando West (L5) 164

Fig. A1.6 Earthquake record San Fernando S37W (L6) 165

Fig. A1.7 Earthquake record San Fernando S90W (L7) 166

Fig. A1.8 Earthquake record San Fernando N15E (L8) 167

Fig. A1.9 Earthquake record San Fernando S38W (L9) 168

Fig. A1.10 Earthquake record San Fernando S00W (L10) 169

Fig. A1.11 Earthquake record Near E. Cost of Honshu NS (L11) 170

Fig. A1.12 Earthquake record Near E. Coast of Honshu (L12) 171

Fig. A1.13 Earthquake record Michoacan S00E (L13) 172

Fig. A1.14 Earthquake record Michoacan N00E (L14) 173

Fig. A1.15 Earthquake record Michoacan N90W (L15) 174

Fig. A2.1 Earthquake record Imperial Valley S00E (N1) 175

Fig. A2.2 Earthquake record Kern County S69E (N2) 176

Fig. A2.3 Earthquake record Kern County N21E (N3) 177

Fig. A2.4 Earthquake record Borrego Mountain N57W (N4) 178

Fig. A2.5 Earthquake record Borrego Mountain N33E (N5) 179

Fig. A2.6 Earthquake record San Fernando S90W (N6) 180

Fig. A2.7 Earthquake record San Fernando N90E (N7) 181

Fig. A2.8 Earthquake record San Fernando N90E (N8) 182

Fig. A2.9 Earthquake record San Fernando S00W (N9) 183

Fig. A2.10 Earthquake record San Fernando N37E (N10) 184

Fig. A2.11 Earthquake record Near E. Coast of Honshu NS (N11) 185

Fig. A2.12 Earthquake record Near S. Coast of Honshu EW (N12) 186

Fig. A2.13 Earthquake record Monte Negro N00W (N13) 187

Fig. A2.14 Earthquake record Michoacan S00E (N14) 188

Fig. A2.15 Earthquake record Michoacan N90E (N15) 189

Fig. A3.1 Earthquake record Parkfield N65W (H1) 190

Fig. A3.2 Earthquake record Parkfield N85E (H2) 191

Fig. A3.3 Earthquake record San Francisco S80E (H3) 192

Fig. A3.4 Earthquake record San Francisco S09E (H4) 193

Fig. A3.5 Earthquake record Helena Montana S00W (H5) 194

Fig. A3.6 Earthquake record Lytle Creek S25W (H6) 195

Fig. A3.7 Earthquake record Oroville N53W (H7) 196

Fig. A3.8 Earthquake record San Fernando S74W (H8) 197

Fig. A3.9 Earthquake record San Fernando S21W (H9) 198

Fig. A3.10 Earthquake record Nahanni Longitudinal (H10) 199

Fig. A3.11 Earthquake record Centeral Honshu TR (H11) 200

Fig. A3.12 Earthquake record Near E. Coast of Honshu NS (H12) 201

Fig. A3.13 Earthquake record Honshu NS (H13) 202

Fig. A3.14 Earthquake record Monte Negro N00W (H14) 203

Fig. A3.15 Earthquake record Banja Luka N90W (H15) 204

Fig. B.1 Maximum base shear vs. peak ground acceleration in TC1 206

Fig. B.2 Maximum base shear vs. peak ground acceleration in TC2 206

Fig. B.3 Maximum base shear vs. peak ground acceleration in TC4 206

Fig. B.4 Maximum base shear vs. peak ground acceleration in TC5 207

Fig. B.5 Maximum base shear vs. peak ground acceleration in TC6 207

Fig. B.6 Maximum base shear vs. peak ground acceleration in TC7 207

Fig. B.7 Maximum base shear vs. peak ground acceleration in TC8 208

Fig. B.8 Maximum base shear vs. peak ground acceleration in TC9 208

Fig. B.9 Maximum base shear vs. peak ground acceleration in TC10 208

Fig. B.10 Maximum dynamic vertical reaction vs. peak ground acceleration in TC1 209

Fig. B.11 Maximum dynamic vertical reaction vs. peak ground acceleration in TC2 209

Fig. B.12 Maximum dynamic vertical reaction vs. peak ground acceleration in TC4 209

Fig. B.13 Maximum dynamic vertical reaction vs. peak ground acceleration in TC5 210

Fig. B.14 Maximum dynamic vertical reaction vs. peak ground acceleration in TC6 210

Fig. B.15 Maximum dynamic vertical reaction vs. peak ground acceleration in TC7 210

Fig. B.16 Maximum dynamic vertical reaction vs. peak ground acceleration in TC8 211

Fig. B.17 Maximum dynamic vertical reaction vs. peak ground acceleration in TC9 211

Fig. B.18 Maximum dynamic vertical reaction vs. peak ground acceleration in TC10 211

Fig. C.1 Total vertical dynamic reaction for tower TC1 215

Fig. C.2 Total vertical dynamic reaction for tower TC2 215

Fig. C.3 Total vertical dynamic reaction for tower TC3 215

Fig. C.4 Total vertical dynamic reaction for tower TC4 216

Fig. C.5 Total vertical dynamic reaction for tower TC5 216

Fig. C.6 Total vertical dynamic reaction for tower TC6 216

Fig. C.7 Total vertical dynamic reaction for tower TC7 217

Fig. C.8 Total vertical dynamic reaction for tower TC8 217

Fig. C.9 Total vertical dynamic reaction for tower TC9 217

Fig. C.10 Total vertical dynamic reaction for tower TC10 218

Fig. C.11 Vertical reaction amplification factors 220

Fig. C.12 Maximum dynamic vertical reaction vs. peak ground acceleration in TC3 220

Fig. C.13 Maximum dynamic vertical reaction vs. peak ground acceleration in TC10 220

Fig. C.14 Comparison between the expressions for vertical amplification factor 221

Fig. D.1 Member forces in tower TC2 224

Fig. D.2 Member forces in tower TC3 225

Fig. D.3 Member forces in tower TC5 226

Fig. D.4 Member forces in tower TC6 227

Fig. D.5 Member forces in tower TC7 228

Fig. D.6 Member forces in tower TC8 229

Fig. D.7 Member forces in tower TC9 230

Fig. D.8 Member forces in tower TC10 231

Fig. D.9 Member forces in tower TC2 using NBCC spectrum 232

Fig. D.10 Member forces in tower TC3 using NBCC spectrum 233

Fig. D.11 Member forces in tower TC5 using NBCC spectrum 234

Fig. D.12 Member forces in tower TC6 using NBCC spectrum 235

Fig. D.13 Member forces in tower TC7 using NBCC spectrum 236

Fig. D.14 Member forces in tower TC8 using NBCC spectrum 237

Fig. D.15 Member forces in tower TC9 using NBCC spectrum 238

Fig. D.16 Member forces in tower TC10 using NBCC spectrum 239

Fig. D.17 Member forces in tower TC2 under vertical excitation 240

Fig. D.18 Member forces in tower TC3 under vertical excitation 240

Fig. D.19 Member forces in tower TC5 under vertical excitation 240

Fig. D.20 Member forces in tower TC6 under vertical excitation 241

Fig. D.21 Member forces in tower TC7 under vertical excitation 241

Fig. D.22 Member forces in tower TC8 under vertical excitation 241

Fig. D.23 Member forces in tower TC9 under vertical excitation 242

Fig. D.24 Member forces in tower TC10 under vertical excitation 242

LIST OF TABLES

Table 3.1 Characteristics of the telecommunication towers studied 34

Table 3.2 Classification of towers according to Sackmann (1996) 47

Table 3.3 Prediction of the lowest three flexural modes 47

Table 3.4 Characteristics of the transmission towers studied 48

Table 3.5 Earthquake records used in the study 57

Table 4.1 Base shear values using the NBCC 1995 design spectrum 61

Table 4.2 Base shear values (in kN) using the NBCC 1995 static approach 62

Table 4.3 Linear regression analysis for the maximum base shear 64

Table 4.4 Linear regression analysis for the maximum vertical reaction 77

Table 6.1 Cable data 135

Table 6.2 Cases used in the parametric study 137

Table C.1 Earthquake records used as vertical input 214

Table C.2 Linear regression analysis for the total vertical reaction 218

LIST OF SYMBOLS

a	length of truss panel
A	peak horizontal ground acceleration
A_D	cross sectional area of diagonals
a_i	coefficients used in evaluating the horizontal acceleration profile (i= 1,6)
A_L	cross sectional area of main legs
A_v	peak vertical ground acceleration
c	viscous damping constant
D	equivalent taper ratio
F	foundation factor
H_{cond}	conductor horizontal tension
I_l	second moment of area of the main leg sections at the top
I_o	second moment of area of the main leg sections at the base
k	stiffness
k^*	generalized stiffness
K_{so}	shear coefficient at the tower base
L	tower height
L_i	excitation factor for mode i
m	mass
M	total mass of the tower
m^*	generalized mass
$m(x)$	tower mass at position x
$M_f(x)$	internal bending moment at position x

M_i	generalized mass for mode *i*
M_{JMA}	Japan meteorological agency scale
M_L	local magnitude
M_S	surface wave magnitude
R	coefficient of correlation
S	dimensionless seismic response factor
S_a	spectral acceleration value corresponding to the fundamental axial period
S_{pai}	pseudo-acceleration corresponding to flexural natural period *i*
T_a	fundamental axial period of vibration
T_f	fundamental flexural period of vibration
u	relative displacement
$\dot{u}$	relative velocity
$\ddot{u}$	relative acceleration
v	zonal velocity ratio
V	peak ground velocity
$V(x)$	internal shear force at position *x*
V_e	elastic base shear
V_h	base shear
V_v	total maximum vertical reaction
W	dead load
$w_{cond.}$	conductor's weight per unit length
$w_{O.H.G.W.}$	overhead ground wire weight per unit length
x	relative position

$\ddot{y}_s$	the base acceleration
Z_a	acceleration-related seismic zone
Z_v	velocity-related seismic zone
Φ	shear parameter
ϕ_i	mode shape i
ω	undamped circular frequency of vibration
ω_D	damped circular frequency of vibration
ξ	viscous damping ratio

CHAPTER 1

INTRODUCTION

1.1 Introduction

Lattice towers are widely used today as supporting structures, namely in telecommunication network systems and in overhead power lines. They are classified into two main categories: guyed towers, also called guyed masts or simply masts, and self-supporting towers. The present study focuses on the latter.

Self-supporting telecommunication towers are three-legged or four-legged space-trussed structures with usual maximum height of 120 m to 160 m. These towers consist of main legs and horizontal and transverse bracings. Main legs are typically composed of 90° angles (in four-legged towers), 60° schifflerized or cold-formed angles (in three-legged towers), or tubular round sections. Various bracing patterns are used but the most common ones are the chevron and the cross bracing. Classical steel transmission towers are four-legged self-supporting lattice structures. Their main legs are also usually composed of 90° angles and tubular sections while built-up composite sections are less frequent. The bracing patterns used in these towers are similar to those used in self-supporting telecommunication lattice towers.

Self-supporting telecommunication towers are designed to resist environmental loads such as wind and ice accretion on their components (in cold climates), usually without considering earthquakes. However, some of these towers may be crucial structures in a telecommunication network and their owner may require that they remain operational or at least survive a severe earthquake, especially for towers located in high

risk seismic areas. The 1994 edition of the Canadian standard CSA S37 *Antennas, Towers and Antenna-Supporting Structures* (CSA 1994) introduced a new appendix (Appendix M) titled "Seismic Analysis of Towers", in order to raise the awareness of the telecommunication industry on this important issue. Specific recommendations for lattice self-supporting telecommunication towers are that, whenever necessary, a somewhat detailed dynamic analysis is to be performed using modal superposition. The base acceleration should correspond to the values prescribed by the National Building Code of Canada (NBCC 1995) for the tower site. These recommendations are very general, however, and the tower designer is left without any specific guidance to assess whether or not a detailed dynamic analysis is truly necessary. It would therefore be desirable to rely on a simplified, static method of analysis to get an estimate of the relative importance of the seismic response of the tower. If the accuracy of such a method can be proven, detailed dynamic analysis may even become unnecessary in the majority of cases. The design procedure would then include a relatively simple additional step to estimate seismic effects, which could then be compared to extreme wind or combined wind and ice effects.

The main design loads of overhead transmission line towers are conductors weight and environmental loads such as wind and ice or a combination of both, acting on the cables and directly on the towers. Several exceptional loads such as cable breakages and ice-shedding effects are also considered in some cases, using equivalent static loads methods. However, earthquake effects are not considered in tower design, even in high risk seismic areas. Nonetheless, there are a few reports (Pierre, 1995 and Kempner, 1996) of some transmission tower damages during recent earthquakes. Although in most cases damages were due to large movements of the tower foundation, it remains relevant to

determine the level of dynamic forces these structures are subjected to during earthquakes. It is noted that the main difference between the seismic behavior of classical transmission line towers and self-supporting telecommunication towers arises from the dynamic interaction between the tower and the cables supported. If it is possible to simplify this interaction, aseismic design of transmission towers could be based on analysis methods similar to those for self-supporting telecommunication towers.

1.2 Objectives

The aim of this study is to achieve the following objectives:

1. To propose a simplified static method that can be used in evaluating the member forces in self-supporting telecommunication towers due to both vertical and horizontal earthquake excitations. This is done by proposing a representative acceleration profile, which is combined to the mass profile along the height of the towers. The product of these two profiles yields a profile of lateral inertia forces. The structure is then analyzed statically under the effect of these forces.

2. To assess the sensitivity of the towers to the vertical component of the earthquake accelerations.

3. To evaluate the relative importance of the dynamic interaction between the cables and their supporting towers in transmission line systems.

4. To adapt the proposed simplified static method for transmission line towers, if feasible.

1.3 Organization of Text

Chapter Two: A literature review is presented, which includes the work concerned with general dynamic analysis of both telecommunication and transmission towers as well as seismic analysis of such structures. The review also covers seismic analysis of other tower-shaped structures (such as offshore towers and intake outlet towers), and relevant code approaches and design recommendations.

Chapter Three: A brief description of the essential structural characteristics of the telecommunication and transmission towers used in the study is presented. The main recommendations and conclusions reached in a preliminary investigation (Sackmann 1996) on telecommunication towers are presented as these results are integrated with the current work. The data base of the earthquake records used in the current study is also briefly discussed.

Chapter Four: Earthquake amplification factors for telecommunication towers are presented for both horizontal and vertical excitations. These factors are meant to be a first step in assessing the global level of forces expected to develop in telecommunication towers as a result of earthquake ground motions.

Chapter Five: In this chapter the scientific background of the proposed simplified method is briefly reviewed, after which the basic concept of the proposed method is explained. The simplified method's coefficients for the horizontal earthquake excitation are then given based on the classification explained in Chapter 3. The applicability of the proposed static method is then verified through numerical comparison between tower member forces obtained using dynamic analysis and those using the proposed method. Selected earthquake inputs are used in this

comparison in addition to the NBCC response spectrum (NBCC 1995). Coefficients for the vertical earthquake excitations are also presented, which are used to calculate the member forces due to vertical excitation. A comparison between the forces obtained from dynamic analysis and those obtained using these coefficients is also presented for selected earthquake records. The presence of antennae is also studied to show the change in tower behavior when heavy antenna clusters are added. The addition of these antennae is accounted for through two generic cases.

Chapter Six: This chapter deals with transmission line towers. The study provides more insight in the relative effect of the cables and the towers on the dynamic behavior of the line system.

Chapter Seven: In this chapter the findings and conclusions of this research are highlighted in addition to the limitations of the work. Suggestions for relevant future work are also included.

CHAPTER 2

LITERATURE REVIEW

2.1 Introduction

Earthquake loads are not routinely considered in the design of telecommunication and transmission line structures even in high seismicity regions. This neglect is tolerated without proper justification or complete understanding of the issue. In areas with low seismicity this may be justified as wind effects will likely govern member design. However, in areas with high seismicity, stresses in tower members or connections and tower movements due to earthquake loading may indeed exceed the effects of other environmental loads.

Most of the published work on lattice towers is devoted to the analysis of these structures under wind. For transmission lines, some exceptional loading cases were also studied including cable breakage, ice shedding and galloping conductors. A review of the relevant publications on dynamic wind and earthquake effects on lattice towers and tower-shaped structures is presented in the following sections. Design code approaches are also reviewed which pertain to buildings and safety-related nuclear structures.

2.2 Dynamic Response of Self-supporting Lattice Towers

2.2.1 Response to wind

Chiu and Taoka (1973) were among the first to present a rational experimental and theoretical study on the dynamic response of self-supporting lattice towers under real and simulated wind forces. A three-legged, 46 m tall self-supported lattice tower was instrumented to study its dynamic response to wind forces. The tower was also idealized as a

space truss with masses lumped at the horizontal panel points. Comparison of the measured dynamic properties of the tower indicated agreement with the calculated values. The validity of the common assumption of uncoupled motion between the two principal horizontal directions was also confirmed. The study showed that the tower response to wind is essentially governed by the fundamental mode of vibration. The average damping for the fundamental period was found to be 0.5% of the critical viscous damping value, which is considered very low.

More recently, Venkateswarlu et al. (1994) conducted a numerical study of the response of microwave lattice towers to random wind loads. The dynamic response was predicted using a stochastic approach, and a spectral analysis method (frequency-domain) was proposed for calculating the along-wind response and the resulting gust response factor. The gust response factor is defined as the ratio of the maximum expected wind load effect in a specified time period to the corresponding mean value in the same time period. A free-standing four-legged tower of 101 m height was used as a case study. The variation of the gust response factor along tower height was calculated with and without the contribution of the second and higher lateral modes of vibration of the tower, and it was found that the maximum contribution of these higher modes to the gust response factor was only about 2%. The gust response factor obtained using the proposed stochastic method varied between 1.55 and 1.58 along the height. Values calculated using the formulae recommended by the Indian (IS:875-1987), Australian (AS 1170-2-1989), British (BS 8100-1986) and American (ASCE 7-88-1990) standards, were found to be 2.03, 2.21, 1.93 and 1.89, respectively. Comparing these results, it was concluded that the

standards values are conservative with difference in the order of 20% to 40%, at least for the case study considered.

In two very important papers on the along-wind response of lattice towers, Holmes (1994,1996) proposed closed-form expressions for the gust response factor for both the shearing force and the bending moment along tower height. The generic tower used in this study was idealized with linear taper and uniform solidity ratio so that the drag coefficient was kept constant. The mass per unit height of the tower, $m(z)$, was assumed to vary with the tower elevation, z, according to the following exponential relation:

$$m(z) = m_o(1 - k(\frac{z}{h})^{\gamma}) \tag{2.1}$$

where

m_o= mass per unit length of the tower at the base

h = total height of the tower

k and γ are empirical constants determined so that $m(z)$ best fits the actual mass distribution of the tower.

In this study, only the effect of the lowest flexural natural mode of the tower was considered, which was assumed to take the following exponential shape, $\mu_1(z)$:

$$\mu_1(z) = (\frac{z}{h})^{\beta} \tag{2.2}$$

where β is also a constant determined so that $\mu_1(z)$ best fits the calculated mode shape. Using the previous assumptions, expressions for the gust response factors for the shearing force and the bending moment were obtained in a closed form.

It should be noted that three response components were included in the derivation of the previous expressions namely, mean, background and resonant response. The reader may refer to Holmes (1994,1995) for a complete explanation of the terms used.

These expressions were then compared to those recommended in the Australian standard AS 1170.2-1989 and were found to be in agreement. The advantage of the proposed expressions over the currently used is the inclusion of more factors to account for the effects of various parameters associated with characteristics of the wind and the structure. An expression for the aerodynamic damping of the tower, due to the relative motion between the tower and the surrounding air, was also derived as a ratio of critical viscous damping. In addition, a closed-form expression for the deflection of the top of the tower was proposed combining three components of deflections (namely the mean, background and resonant components). The effects of the tower height, taper ratio, and mean velocity on the gust response factors were also studied. Finally, the work was extended and simplified to predict an effective static load distribution, including the mean, background fluctuating and resonant components of the wind.

2.2.2 Seismic response

One of the first publications discussing earthquake effects on antenna-supporting lattice towers was authored by Konno and Kimura (1973). The study aimed mainly at collecting information on tower vibration mode shapes, natural frequencies and damping properties. A real case study of a tower that was instrumented when the 1968 Off-Tokachi earthquake occurred was presented. The collected data was analyzed and compared with numerically simulated results obtained from a simplified stick model of the tower with

lumped masses and a viscous damping ratio of 1% in all modes. In some members, it is interesting to note that the earthquake forces were found to exceed those due to wind. This was confirmed by observation of local damage and permanent deformations at the tower base after the earthquake.

More recently, Mikus (1994) studied the seismic response of self-supporting telecommunication towers using modal superposition analysis. The aim of this preliminary study was to improve understanding of the response of these towers to earthquakes. Six towers with height ranging from 20 m to 90 m were modeled: bare towers only, i.e. without antennae, attachments, ancillary components etc. Three earthquake records were selected as the base excitation. A detailed linear dynamic analysis was performed using modal superposition, and it was concluded that the use of the lowest four lateral modes of vibration provided sufficient accuracy. The frequency of the first axial mode of the towers was found to be in the range of 11 to 43 Hz, which was either not present in the frequency content of the earthquake records used or corresponded to small amplitudes of input accelerations. As a result, the effects of the vertical component of the earthquakes proved negligible.

A first attempt to propose an equivalent static method for the analysis of lattice self-supporting telecommunication towers was made by Gálvez (1995). The method was based on modal superposition, considering the effect of the lowest three flexural modes of vibration of the tower. As self-supporting towers behave essentially as cantilever beams, Gálvez suggested the use of natural frequencies and mode shapes expressions developed for prismatic cantilevers. The effects of taper ratio and shear deformations were included

by means of correction factors to the classical solution for prismatic Euler cantilevers. The proposed expression for the natural frequency of mode i, f_i, is:

$$f_i = \frac{\lambda_i^2}{2\pi L^2}\sqrt{\frac{EI_o}{m_o}} \tag{2.3}$$

where

L = tower height

EI_o= flexural rigidity at the tower base

m_o= mass per unit length at the tower base

The parameter λ_i (essentially a dimensionless frequency) is defined as:

$$\lambda_i = \lambda_b F_{ct} F_{cs} \tag{2.4}$$

where

λ_b= frequency parameter for prismatic cantilever

F_{ct}= taper correction factor

F_{cs}= shear correction factor.

The expression for the corresponding flexural mode shapes, $\phi_i(x)$, is

$$\phi_i(x) = \cosh(\lambda_i x/L) - \cos(\lambda_i x/L) - \sigma_i[\sinh(\lambda_i x/L) - \sin(\lambda_i x/L)] \tag{2.5}$$

where

$$\sigma_i = \frac{\sinh\lambda_i - \sin\lambda_i}{\cosh\lambda_i + \cos\lambda_i} \tag{2.6}$$

The base excitation simulated by Gálvez was a sinusoidal wave with maximum amplitude, $\ddot{u}_g$, equal to the peak ground acceleration defined by the National Building Code of Canada (NBCC 1995) for the tower site. The acceleration profile of the tower response, $\ddot{u}(x,t)$, for a sinusoidal ground motion is given by:

$$\ddot{u}(x,t) = \ddot{u}_g \Sigma_{i=1}^{3} \phi_i(x)\psi(\lambda_i)\ddot{\alpha}(\Omega, \omega_i, t) \tag{2.7}$$

where

$$\psi(\lambda_i) = 2\sigma_i/\lambda_i \tag{2.8}$$

Ω = forcing frequency of the sinusoidal input wave

$$\omega_i = 2\pi f_i \tag{2.9}$$

$\ddot{a}(\Omega, \omega_i, t)$= dynamic amplification function for mode i.

For $\Omega \neq \omega_i$ and using the frequency ratio $\beta_i = \Omega/\omega_i$,

$$\ddot{a}(\Omega, \omega_i, t) = \frac{\beta_i}{1-\beta_i^2}(\sin\omega_i t - \beta_i \sin\Omega t) \tag{2.10}$$

At resonance in mode i, $\Omega = \omega_i$,

$$\ddot{a}(\Omega, \omega_i, t) = \tfrac{1}{2}(\sin\omega_i t + \omega_i t\cos\omega_i t) \tag{2.11}$$

The base excitation is assumed to be in resonance with each of the lowest three flexural modes considered, and the modal accelerations for i=1, 2, 3 are calculated. Using the Square Root of Sum of Squares (SRSS) method, these relative modal accelerations are combined and the acceleration profile along the tower is estimated with eq. (2.7). Detailed dynamic analysis using a total of 45 base accelerograms was used to validate the method for three existing towers with heights of 90, 103 and 121m. Based on these results, simplified acceleration profiles were proposed depending on the A/V ratio (peak ground acceleration to velocity ratio) of the accelerograms. The inertia force distribution was simply found by multiplying the acceleration profile by the mass profile. The structure was then analyzed under the effect of these equivalent "static" inertia forces. Although simple, the method did not always give good estimates for the internal forces. For the main legs in general, the method yielded conservative values accurate enough for preliminary design. However, the results were not systematically reliable and conservative for other diagonal

and horizontal members. The range of differences between the force predictions and the dynamic analysis results for horizontal members was between -70% and +45%, and for cross bracings it was in the range of -35% to +25%. The method was further limited to the tower geometry used in the study, i.e. a taper ratio (change in width divided by taper height) less than 1:14.5, and a total length to tapered length ratio less than 1.15.

A draft of the American TS 13 National Earthquake Hazard Reduction Program (NEHRP) for non-building structures was released for comments in 1996, where a simple design equation (eq. 2.12) for self-supporting telecommunication towers was suggested. It was recommended that self-supporting telecommunication towers be designed to resist an earthquake lateral force, V, applied at the centroid of the tower and calculated using the following equation:

$$V = \frac{S_{a1} I W}{R T} \tag{2.12}$$

where

V= lateral force

S_{a1} = site specific design spectral acceleration at nominal period of 1 second

I = importance factor (I=1.0 for standard towers, 1.25 for essential or post-critical towers)

W= total weight of tower including all attachments

R = response modification factor

T= fundamental period of the tower in seconds.

This equation was meant to resemble the maximum base shear equation used in most building codes. However, the basis on which the equation was developed is not clear. Also

only the fundamental mode of vibration is considered in this approach, which is not accurate for this type of structure: it was first demonstrated in Mikus (1994) and later verified in Gálvez (1995) and Gálvez and McClure (1995) that the contributions of both the second and third flexural modes are usually significant.

2.3 Dynamic Response of Transmission Line Structures

The study of the complex dynamic problem arising from the coupled behavior of the tower-cable system attracted several researchers. Some of them investigated the dynamic loads on transmission towers due to galloping of the conductors (Baenziger et al. 1994), conductor breakage (McClure and Tinawi 1987 and McClure 1989), ice shedding from the cables (Jamaleddine et al. 1993) and the free vibration of the coupled system (Ozono et al. 1988 and Ozono and Maeda 1992). However, most of the published work on seismic analysis of transmission lines involves either the tower or the cable alone without considering the coupled tower-cable problem.

Long (1974) was among the first to publish on the seismic response of transmission towers, more or less at the same period as the pioneering studies on the dynamic response of telecommunication towers to wind and earthquakes (Section 2.2). Long neglected completely the effects of the overhead conductors. The study was later extended to evaluate the forces exerted by the conductors on the tower. The lattice transmission tower model was divided into two parts: The top part consisted of the prismatic part and the cross arms supporting the conductors, and was idealized as a flexible uniform cantilever, while the bottom part was simply assumed to be a rigid body. The absolute

displacement of the flexible cantilever portion, $u(x,t)$, was then approximated by the following equation:

$$u(x,t) = z(t) + \Sigma_{k=1}^{\infty} h_k(x) f_k(t) - \frac{ml^4}{EI}\ddot{z}(t)[c_1(x) - \Sigma_{k=1}^{\infty} \frac{h_k(x)}{\lambda_k^4}] \qquad (2.13)$$

where

$z(t)$ = ground displacement

$h_k(x)$ = deflection curve for normal mode of vibration k

$f_k(t)$ = displacement response to the ground motion of a simple oscillatory system in mode k

m = mass per unit length

l = length of flexible cantilever portion

EI = flexural rigidity

$\ddot{z}(t)$ = ground acceleration

$c_1(x)$ = deflection due to static uniform loading $= \frac{1}{24}(\frac{x}{l})^4 - \frac{1}{6}(\frac{x}{l})^3 + \frac{1}{4}(\frac{x}{l})^2$

λ_k = dimensionless frequency, positive root of the equation $1 + \cosh\lambda\cos\lambda = 0$ for mode k

k = mode number.

Eq. (2.13) is therefore the summation of the horizontal ground displacement, the displacement response of the structure to the ground motion using modal superposition, and a correction to the deflection resulting from the difference of acceleration loadings of ground motion and free vibration. The deflection at the top of the tower was evaluated using eq. (2.13), assuming that the maximum values of each of the three terms in the equation occurred simultaneously. A response spectrum was used to evaluate the

maximum value of the response function $f(t)$, and the maximum values of the ground displacements, $z(t)$, and accelerations, $\ddot{z}(t)$, were obtained from the earthquake records. After all these calculations for a case study of a 43 m transmission tower, it was concluded that the entire tower moved rigidly with the ground and that no amplification of stresses was produced by the ground motion. The second part of the study aimed at calculating the force exerted by the conductors on the tower due to the earthquake excitation, assuming compatibility of tower motions with conductors motions. Three orthogonal earthquake directions were considered namely, transverse, longitudinal and vertical. The forces calculated in the three cases were found to be very small and could be resisted safely. It should be noted that the tower used in the study was a relatively rigid one having a lowest frequency of vibration of about 5 Hz.

Kotsubo et al. (1985) performed dynamic measurements on three transmission towers before and after installation of the conductors. The purpose of their study was to determine the effects of the conductors on the dynamic characteristics of the towers. The three towers used were two strain towers (with conductors directly anchored to the tower) with heights of 92.5m and 68.5m, and a suspension tower with height of 92.2m. The results were published for the case of the suspension tower only. The natural frequencies and modes of vibration of the tower were calculated using both a plane truss model and a space truss model. Ambient vibration measurements for the tower were taken before the installation of the cables. The natural frequencies, modes of vibration and damping properties were extracted from these measurements using FFT analysis. After the installation of the cables, forced vibration tests using an exciter were carried out. The exciter was set up on the third arm from the top of the tower. It was observed that there were no

significant changes in the natural frequencies and the modes of vibration of the tower before and after the cable stringing, which suggested that the dynamic interaction between the cables and towers is insignificant for suspension towers. The damping ratio of the tower was found to be in the range of 0.2 to 2.0% of the critical viscous damping. The earthquake responses were then calculated using the plane truss model and the space truss model ignoring the presence of the cables. For the plane truss model, the responses were calculated for both the longitudinal and the transverse direction to the transmission line. It was concluded that it is sufficient to model the tower as a plane truss.

In a more recent study conducted by Li et al. (1991) models for long-span transmission line systems under earthquake effects were presented. The study included the derivation of mass and stiffness matrices for the tower-cable coupled system for the longitudinal and transverse directions. For the vertical direction the mass of the conductors was calculated and lumped at the appropriate joints. For each of the three principal directions a dynamic analysis was carried out using three earthquake records namely Qian'an (China), El Centro (USA) and Ninghe (China). The analyses were done for the following three cases for comparison:

I- The discretized model of the tower without the conductors;

II- The discretized model of the tower with the mass of the conductors lumped at relevant tower joints;

III- The coupled tower-conductor model.

It was found that for the vertical ground motion the seismic response of model II is greater than that of model I. For both the lateral and longitudinal ground motions, the response of model III was greater than that of model II, which in turn was greater than that of model I.

It was concluded that the effects of the conductors on the seismic response of their supporting tower are not negligible and should be taken into consideration.

Li et al. (1994) studied the seismic response of high voltage overhead transmission lines. In the study the tower was discretized as a lumped mass multi-degree-of-freedom system in the horizontal direction and assumed rigid in the vertical direction. It was further assumed that the supporting towers vibrate in phase with each other. Each cable span was divided into five equal straight segments, the mass of each being lumped at its ends. The ground motion was assumed acting in the longitudinal direction of the line. The equation of motion of the coupled tower-conductor system was presented using the previous assumptions. A numerical example was presented in which a 55 m height tower with conductors spanning 400 m was analyzed under the effect of horizontal earthquake excitation. Three earthquake records were used in the study, namely El Centro (1940) representing a soft site, San Fernando/Pacoima Dam (1971) representing a medium-stiff site and Olympia (1965) representing a stiff site. Two models were used in the analyses: one considering the presence of the conductor (model I) and one neglecting the presence of the conductors (model II). However, for model II it was not mentioned whether or not the mass of the conductors was included in the analysis. Displacements and shear forces were compared for the two models and it was found that neglecting the presence of the cables could result in an underestimation of up to 66% (in case of the Pacoima Dam earthquake) in the shear force evaluated at the tower base. It was therefore concluded that the tower cable interaction greatly affects the seismic response of the towers and neglecting their presence may lead to unsafe prediction of internal forces in the tower members.

In a preliminary study, El Attar et al. (1995) investigated the response of

transmission lines under the effect of vertical seismic forces. The tower used in the study was modeled by plane truss elements while the cables were modeled using two-node straight elements taking geometric non-linearities into consideration. Damping of the supporting towers was assumed to be 2% of the critical viscous damping (in all modes) while that of the cables was taken as only 1%. The tower alone was subjected to a horizontal sinusoidal ground acceleration of 0.28 g representing Victoria (Canada) in accordance to the NBCC 1990 recommendations. From this analysis the maximum displacement of the tower at the top level was determined, which resulted mainly from the contribution of the first mode of vibration. However, this conclusion should not be generalized as it contradicts most of the published work in this area of interest (Mikus 1994, Gálvez 1995 and Gálvez and McClure 1995), which suggests that at least the lowest three modes of vibration should be included in the analysis. This conclusion might be suitable for short and stiff towers in which the higher modes are not likely to be triggered by an earthquake. The cable was subjected to the vertical component of two earthquakes, San Fernando for low A/V ratio and Parkfield for high A/V ratio, after being scaled to a peak ground acceleration of 0.21 g representing ¾ of the horizontal component prescribed for Victoria. The vertical displacement of the cable at mid span was calculated and it was found that the displacement resulting from the low A/V earthquake was more than four times the response due to the high A/V earthquake. The effect of the change in the damping ratio of the cable on its response was also investigated and it was found more pronounced in records with low A/V ratio as a change in the damping value form 1% to 4% resulted in a decrease of 32% in the displacement at mid span in comparison to a 22%

decrease for the high A/V ratio. The study did not report any analysis of on the coupled tower-conductor system.

Ghobara et al. (1996) proposed a simplified technique to investigate the effect of multiple-support excitation on the response of transmission lines. In this study, the towers were modeled as space trusses while the conductors were modeled using linkages of two-node straight elements, duly accounting for geometric non-linearities. In modeling the ground motion along the transmission line three factors were identified namely, wave travel effect resulting from finite speed of seismic wave, incoherency effect resulting from reflection and refraction of seismic waves and finally site effect. However, only the first two factors were accounted for stochastically in the study. A numerical example illustrated the suggested technique in which the maximum lateral displacements of the cable along the span, maximum force in tower members and maximum tension in cables were evaluated for different wave velocities and considering incoherency and wave travel effects. Three conclusions were drawn from the study: Firstly, considering the same ground motion for all supporting towers does not produce the worst case for design. Secondly, although the velocity of wave propagation has a significant effect on the lateral displacement of transmission lines, the incoherency of seismic wave is more significant. Thirdly, the increase in cable tension due to lateral ground motion is small.

As a very crude approximation, Kempner (1996) suggested analyzing transmission towers statically under the effect of a single lateral force acting at the tower's center of mass, using the same equation as presented in the case of self-supporting telecommunication tower (eq. 2.12).

The definitions of the terms are the same as for the case of self-supporting towers (see section 2.2.2), except that W is the tower dead load without including the weight of the supported wires. The same lateral force is applied in both the longitudinal and transverse directions. If it is found that earthquake loading is likely to govern the design, a more detailed lateral force distribution or modal analysis is suggested.

2.4 Seismic Response of Tower-shaped Structures

Due to the scarce information available in the literature available on seismic analysis of lattice self-supporting towers, the search is directed towards other structures that behave essentially as cantilevers, namely offshore towers and intake-outlet towers. The aim of this search is to gain insight of the approaches used in analyzing such structures under seismic excitation and to find if a simplified method for analysis is available.

2.4.1 Seismic response of offshore towers

Penzien and Kaul (1972) studied the response of offshore towers to strong motion earthquakes. In their work, the response spectrum method of analysis was used and compared with their proposed stochastic method. In this proposed method, a mean ergodic Gaussian process of finite duration was used as the stochastic model for the horizontal ground acceleration. The aim of the study was to determine the transverse shear distribution and the overturning moment along the height of the tower without investigating the individual member forces. The towers were idealized as stick models with seven joints along the height on which the mass of the tower was lumped. A condensed stiffness matrix corresponding to the lateral displacements of the model was evaluated, and from

the mass and stiffness matrices of the model, the eigenproperties of the towers (frequencies and mode shapes) were predicted. The distributions of the transverse shear and overturning moment were then calculated using the response spectrum of the earthquake excitation considering the contribution of the lowest three flexural modes. The results were found to be comparable to those obtained with the more rigorous stochastic random vibration analysis.

Anagonstopoulos (1982), in his work on modal solutions for the earthquake response of offshore towers, concluded that modal superposition gives good estimates of the overall response of the towers. For some members, however, the estimated value of the bending moment was in an error by about -60%, yet the difference in total stress was less than 13% which can be reduced by increasing the number of modes in the summation. Due to the uncertainties in the earthquake loading, it was suggested to use more earthquake excitations instead of increasing the number of modes in the analysis. It was also concluded that the inclusion of the lowest three modes in each of the three principal structural directions would be adequate for design purposes.

In the work reported by Chan (1987), response spectrum techniques for multi-component seismic analysis of offshore platforms were evaluated. Two platforms were modeled taking into account the added mass of water. Three components of earthquake input were considered, two horizontal components with the ratio 0.67 : 1.0 and a vertical component with 0.5. The study aimed at evaluating the techniques used for modal combination as well as seismic component combination rules. The member forces and stresses calculated using different combination rules for both the modal summation and seismic components were compared with those obtained using detailed direct integration analysis.

The different modal combination rules studied were the Square Root of Sum of Squares (SRSS), the Complete Quadratic Combination (CQC), and the American Petroleum Institute (API) method. For different directional seismic inputs, the SRSS and the Multi Component Quadratic Combination (MCQC) rules were used. It was concluded that all of these combination rules gave comparable results, and the CQC-SRSS rule was recommended because of its conservatism. As part of this study, Chan also checked the error resulting from neglecting the effect of higher modes (above the eleventh mode) in the analysis. He concluded that because all lower modes are horizontal, the vertical forces could be underestimated by a truncated analysis which in turn would affect the support design.

2.4.2 Seismic response of intake-outlet towers

Valliappan et al. (1980) investigated the effect of earthquakes on the intake tower of Magrove Creek dam in Australia, using both dynamic and pseudo-static analyses. The design spectrum approach was used as a basis of the pseudo-static analysis considering only the lowest flexural mode of vibration. The mode shape used was that reported in Clough and Penzien (1993) in the form of a cosine function. The structure was analyzed statically under the effect of inertia forces resulting from multiplying the acceleration profile due to the first mode shape by the mass. Detailed dynamic analysis was also performed and the results obtained from both analyses were compared. From this comparison, it was concluded that the pseudo-static analysis considering the lowest flexural mode is only an approximate solution. However, this conclusion might change if higher modes were included.

A simplified method for seismic analysis of intake-outlet towers was later developed by Chopra and Goyal (1991). The method was used to estimate the maximum forces in these towers using the design earthquake spectrum. A simplified step-by-step procedure based on the Stodola and Rayleigh methods for the calculation of the lowest two natural periods was suggested. It was demonstrated that considering the lowest two flexural modes of vibration is accurate enough for the preliminary design phase. The procedure can be summarized in the following six steps:

1. Definition of a smooth design spectrum suitable for the site of the tower.
2. Calculation of the added mass associated with both the inside and outside water.
3. Definition of the structural properties of the tower:
    a. Mass per unit height, $m_s(z)$
    b. Flexural rigidity, $E_sI(z)$ and shear rigidity, $G_sK(z)A(z)$
    c. Modal damping ratio, ξ_n
4. Calculation of the lowest two natural periods of the tower using the proposed simplified procedure.
5. Calculation of the lateral force distribution for each mode of vibration using a generalized single-degree-of-freedom approach as follows:
    a. Determine the pseudo-acceleration ordinate S_a from the design spectrum corresponding to period T_n and damping ratio ξ_n .
    b. Calculate the generalized mass M_n and the generalized excitation term L_n using the following expressions:

$$M_n = \int_0^{H_s} m_s(z)[\phi_n(z)]^2 dz \qquad (2.14)$$

$$L_n = \int_0^{H_s} m_s(z)\phi_n(z)dz \qquad (2.15)$$

where

H_s = tower height

$\phi_n(z)$ = lateral displacements of the tower in the n^{th} vibration mode.

c. Calculate the equivalent lateral forces $f_n(z)$ using the following expression:

$$f_n(z) = \frac{L_n}{M_n} S_a(T_n, \xi_n) m_s(z) \phi_n(z) \tag{2.16}$$

6. Calculation of the maximum shear and bending moment at any section along the tower height using the SRSS modal combination method.

It is noted that the method for estimating the lowest two natural periods is accurate if the variation in the tower cross-sectional properties can be expressed in a closed form. Since self-supporting lattice towers usually have irregular changes in their cross-sectional properties, the use of this method will only give crude estimates for the natural periods. Also, a computer program was suggested for the implementation of the proposed procedure, which means that it is not such a "simplified" procedure.

2.5 Design Code Approaches for Seismic Analysis

Different design code approaches for the analysis of structures under earthquake loads need to be reviewed. In addition to the few available approaches for the analysis of towers under seismic effects, the recommendations for two other types of structures namely safety-related nuclear structures and buildings are presented.

2.5.1 Code approaches for different types of structures

The ASCE 1986 standard on seismic analysis of safety-related nuclear structures suggests acceptable analysis methods and provides the methodology and the input ground

motion to be used in calculating the response of such structures. The standard defines two methods for specifying the seismic input, namely design spectrum and input ground motion time history. The horizontal component of the earthquake spectral ordinates (absolute acceleration S_a, spectral velocity S_v, and spectral displacement S_d) are obtained by applying dynamic amplification factors to the corresponding maximum values of ground motion (acceleration a, velocity v, and displacement d) obtained from the response spectrum. These amplification factors depend on the amount of damping and are given as ratios of S_a/a, S_v/v, and S_d/d. The standard requires the use of two equal horizontal earthquake components in orthogonal directions. Two thirds of the horizontal component value is used as the vertical component of the input. If time histories are used, three different earthquake records should be used in three orthogonal directions. These records must be selected so as to represent the site conditions.

The standard recognizes four methods for the analysis of such structures: the direct time integration method, the response spectrum method, the complex frequency method and the equivalent static method. The first three methods are well documented in textbooks (Bathe 1982, Gupta 1992, and Clough and Penzien 1993) and need not be reviewed here. As for the equivalent static method, the standard restricts its use to cantilever models with uniform mass distribution. Multi-degree-of-freedom models (MDOF) of cantilevers with non uniform mass distribution can be analyzed using the static method only if they have a dominant lowest mode of vibration. In this case, the equivalent static load is determined by multiplying the structure's mass profile by a uniform acceleration profile of magnitude equal to 1.5 times the peak acceleration of the response spectrum. For cantilever structures with uniform mass, values of 1.0 and 1.1 applied to the peak spectral acceleration are

used to determine the tower base shear and base moment respectively. The justification of these values is not presented in the standard. The total response for the three components of seismic input is then calculated using the SRSS combination rule.

The usual approach suggested in building codes for seismic analysis of regular buildings is to evaluate a global base shear value (Paz 1994). The base shear is then distributed along the height of the structure assuming that the lowest mode of vibration is dominant and that the lateral displacement varies linearly with height. The National Building Code of Canada (NBCC 1995) specifies the minimum design base shear by the following equation:

$$V = \frac{V_e}{R} U \tag{2.17}$$

where

R = force modification factor

U = calibration factor = 0.6

V_e= equivalent lateral seismic force.

The value of V_e is given by the following equation:

$$V_e = vSIFW \tag{2.18}$$

where

v = zonal velocity ratio derived from the probabilistic study of the ground motion

S = seismic response factor which is a function of the fundamental period of the structure and the relative values of the velocity zone, Z_v, and the acceleration zone, Z_a

I = importance factor

F = foundation factor, which depends on the soil conditions at the site.

This base shear force is assumed to counteract distributed seismic forces along the height of the structure, given by:

$$F_x = (V - F_t)\left(\frac{W_x h_x}{\sum_{i=1}^{n} W_i h_i}\right) \tag{2.19}$$

where F_t is a concentrated force applied to the top of the building to account for the effect of higher modes and can be calculated using the following equation:

$$F_t = 0.07TV \leq 0.25V$$
$$F_t = 0 \text{ if } T \leq 0.7 \text{ s} \tag{2.20}$$

while W and h are the floor weight and elevation, respectively and n is the number of stories.

It should be noted that the code recommends dynamic analysis using the response spectrum method and modal techniques for buildings with irregular stiffness and/or mass distributions.

2.5.2 Standards and codes of practice for towers

It is important to review the approaches followed and the recommendations set forth in the different standards for earthquake design of towers to stand at the level of knowledge available to the designers.

In its 1994 edition, the Canadian Standard *Antennas, Towers and Antenna Supporting Structures* CSA S37-94 has introduced a new appendix (Appendix M, not a mandatory part) which addressed the issue of seismic analysis of lattice telecommunication towers, both self-supporting and guyed. In this appendix it is stated that since most

self-supporting telecommunication towers are typically of high frequency compared to dominant frequencies of earthquakes, seismic effects are not likely to be significant. The appendix therefore recommends that a frequency analysis of the tower be performed to allow for the identification of the tower's sensitive frequency range. If this range coincides with the frequency content of the dynamic loading, detailed dynamic analysis should be performed. If seismic analysis is required, modal superposition should be used for self-supporting towers only with modal viscous damping ratios between 1% to 3%. It also suggests to use accelerograms or earthquake spectra based on the seismicity levels prescribed by the NBCC for the tower site.

The Australian Standard AS 3995-1995 *Design of steel lattice towers and masts* also contains an informative appendix (Appendix C) which includes general guidelines for earthquake design of such structures. In this appendix it is stated that self-supporting lattice towers with height up to 100 m with no significant mass concentrations need not be designed for earthquake effects. For towers with significant mass and height of more than 100 m or lesser height but with significant mass concentrations, it is suggested that they may be exposed to base shears and overturning moments approaching ultimate wind actions. However, this standard does not offer any guidance as to how to estimate the tower response.

The Eurocode 8 *Design Provisions for Earthquake Resistance of Structures* ENV 1998-3 (1995 draft) devotes a complete part to towers, masts and chimneys (Part 3). This part contains a description of basic design requirements, seismic action, modeling considerations and methods of analysis. It is emphasized that the design philosophy of this code is to maintain the function of the structure and to prevent any danger to nearby buildings

or facilities. However, the code does not provide protection against damage of nonstructural components. The code suggests several methods to describe seismic input: elastic response spectrum, smoothed design spectrum and time history representations using either artificial accelerograms or recorded strong motions. A complete section is devoted to mathematical modeling which includes the rocking and translation stiffness of the foundation. For electrical transmission towers, the code specifically requires that the model include a line section of at least three towers (four spans) in order to obtain an acceptable evaluation of the coupled tower-cable system.

The code also provides a simplified method of analysis using design spectra in which the base shear is calculated using the following expression:

$$F_t = S_d(T)\,\Sigma_{i=1}^{n} W_i \tag{2.21}$$

this value is then distributed along the tower height using the following expression:

$$F_i = \frac{h_i W_i}{\Sigma_{i=1}^{n} h_i W_i} F_t \tag{2.22}$$

where

W_i= weight of the i^{th} mass

h_i= elevation of the i^{th} mass from the base

S_d= design spectrum ordinate corresponding to the fundamental period

T= fundamental period of the tower.

However, the code clearly stipulates that this approach is limited to unimportant structures with height less than 60 m. The code also allows the use of both modal superposition analysis and non-linear analysis.

The Uniform Building Code UBC 1997 devotes a specific section (No. 1632) to earthquake resistant design of non-building structures. However, for telecommunication

towers, this section does not specify any procedure different from the one used for building structures. It is suggested that when an approved national standard provides a seismic design procedure for a certain type of non-building structure, such procedure may be used under the following conditions: the seismic zones and occupancy categories must conform with the UBC, and the total base shear and overturning moment calculated must be greater than 80% of the values obtained using the UBC approach. At this point it should be noted that the philosophy of the UBC is *to safeguard against major structural failures and loss of life, not to limit damage or maintain function*, which is completely different than the philosophy behind the provisions for seismic design of towers in which the main concern is to maintain the towers' functionality.

In a recent report (EIA, 1998) released by the seismic committee of the Electronic Industry Alliance / Telecommunication Industry Association EIA/TIA several recommendations about the seismic analysis of steel antenna towers are made. The objectives of the committee were as follows: To define a methodology for use in seismic analysis of towers, to identify simple but conservative assumptions to make the analysis easier, to provide acceptable methods for more rigorous analysis techniques and to identify tower characteristics which indicate if seismic analysis should be performed. At present, however, these objectives are not all met in a satisfactory way. The committee recommends to follow the same approach as used in the Uniform Building Code UBC 1997, which is intended for building structures and is not suitable for towers. The total design base shear value is calculated using the following expression:

$$V = \frac{3ZIC}{8} W \tag{2.23}$$

and

$$C = \frac{1.25S}{T^{\frac{2}{3}}} \leq 2.75 \qquad (2.24)$$

where

V= total design base shear

Z= seismic zone factor

I= importance factor equal to 1.25 for important or hazardous facilities and 1.0 for special or standard facilities

W= total dead load

S= site coefficient

T= fundamental period of the tower in seconds.

After obtaining the base shear it is distributed along the tower height in the same manner as prescribed in the UBC 1997. The EIA/TIA report also contains a study performed in order to obtain a threshold criterion that can be used to determine whether a seismic analysis is truly needed or not. To this end, a comparison between base shear values obtained from wind effects and seismic effects was done. From this study it was concluded that it is unlikely for seismic effects to control over wind. It should be noted, however, that seismic calculations were carried out using the UBC base shear equation which makes this approach questionable.

2.6 Conclusions

From this literature review it can be seen that seismic analysis of self-supporting telecommunication towers has received little attention. Also, the work done in other fields cannot be applied directly to self-supporting lattice towers. Since the designers are left without much guidance to assess if a detailed dynamic analysis is required, earthquake

effects are usually ignored. For short towers and low risk seismic area this may be acceptable. However, in high risk areas and for tall towers the designer should be able to perform at least a simple static analysis as a quick design check. Therefore, a simplified static method is proposed in this thesis. The method is based on modal superposition and the response spectrum approach. It is anticipated that the proposed method will give reliable estimates of the member forces and in most cases performing a detailed dynamic analysis will become unnecessary.

Analyses of transmission towers under seismic excitation were conducted for particular systems such as very rigid towers, suspension towers with relatively light conductors and very long spans with heavy conductors. The researchers were divided among themselves into two groups. The first one neglected the tower-conductor interaction effects, and even went further by not including the mass of the conductors. The second group recommended the performance of a detailed analysis of the tower-conductor system. As lattice transmission towers are similar to self-supporting lattice telecommunication towers, part of this work is devoted to trying to find an equivalent added mass to replace the effect of the conductors. If this proved feasible, the work could be extended to investigate the applicability of the proposed simplified method for telecommunication towers to transmission towers. If not, this work could suggest some novel approach tailored to overhead line systems.

CHAPTER 3

METHODOLOGY

3.1 Telecommunication Towers Used in the Study

Ten existing three-legged self-supporting lattice steel telecommunication towers are used in this study with heights ranging from 30 m to 120 m: they are representative of the range of towers usually erected in Canada. Table 1 lists some important characteristics of these towers including their total mass and calculated natural periods corresponding to their fundamental flexural and axial modes of vibration in still air. It should also be noted that these values are based on calculations made for the bare conditions, without including the mass of the antennae and other non-structural attachments.

The geometric layouts of the ten towers are illustrated in Figs. 3.1 to 3.10; it should be noted that secondary or redundant members are not shown on the figures, however their mass are included in the analysis.

Table 3.1 - Characteristics of the telecommunication towers studied

Tower	Height (m)	Base Width (m)	Top Width (m)	Total Mass (kg)	Fundamental Flexural Period (s)	Fundamental Axial Period (s)
TC1	30	5.0	1.2	3,400	0.23	0.029
TC2	42	7.8	1.8	9,900	0.33	0.047
TC3	66	10.8	1.8	27,000	0.54	0.071
TC4	103	21.8	1.5	48,000	0.55	0.085
TC5	76	12.1	1.6	32,200	0.59	0.070
TC6	90	14.8	1.8	42,300	0.67	0.088
TC7	83	10.4	2.4	27,000	0.69	0.073
TC8	90	11.9	1.8	36,000	0.76	0.081
TC9	55	6.1	1.2	10,800	0.79	0.064
TC10	121	14.4	2.0	66,200	1.20	0.122

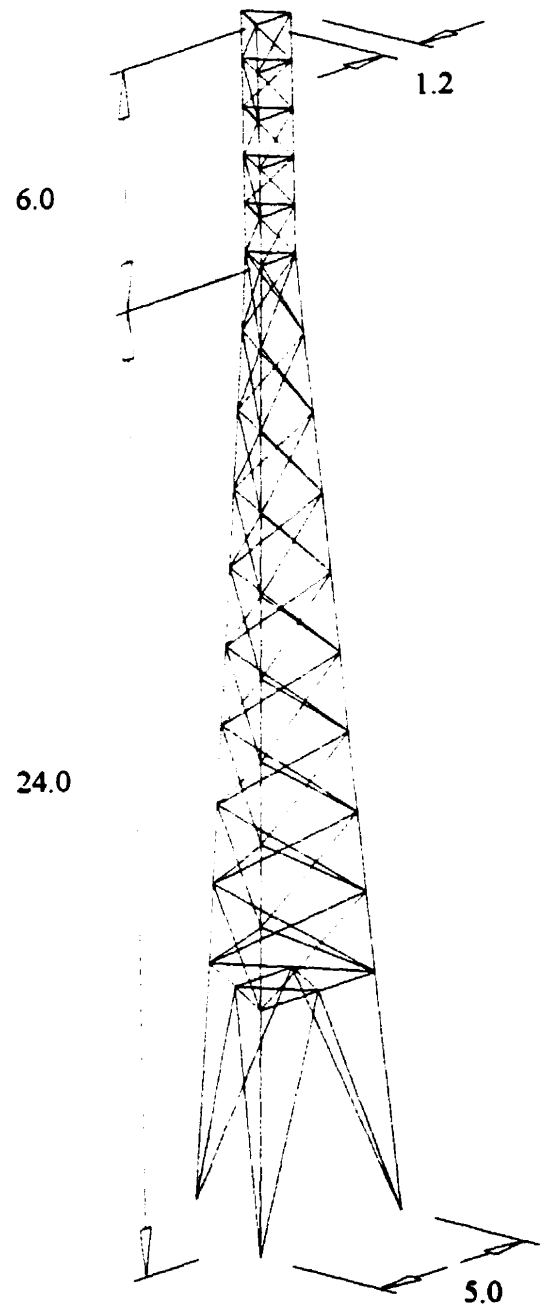

Fig. 3.1 Layout of tower TC1 (dimensions are in m)

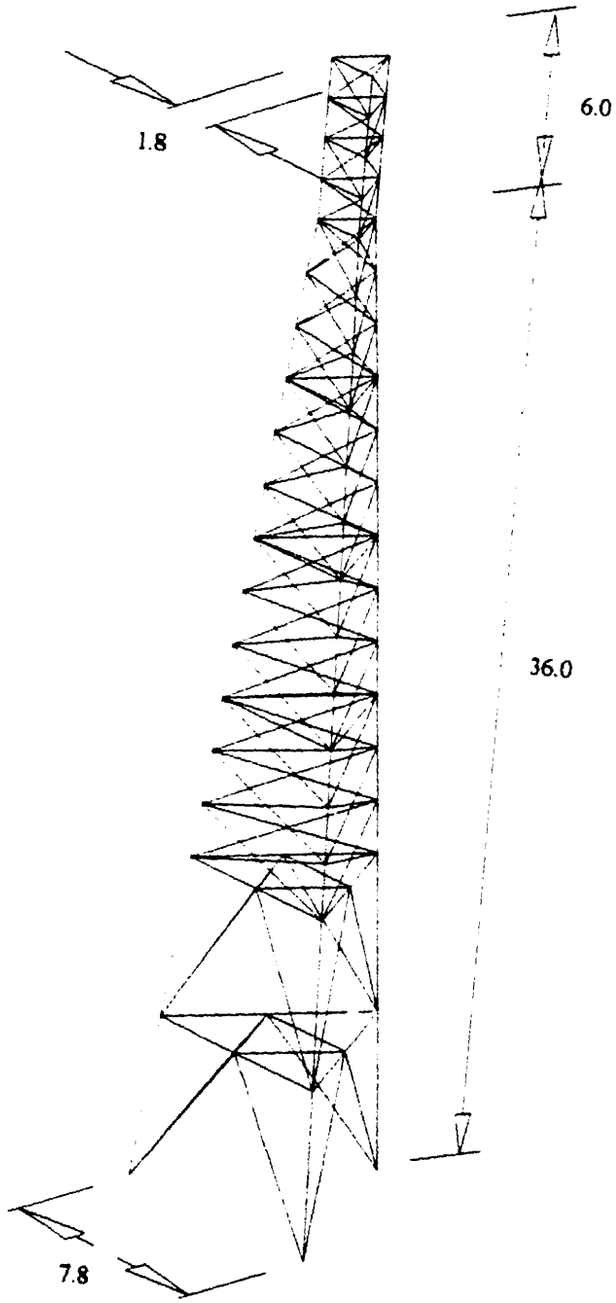

Fig. 3.2 Layout of tower TC2 (dimensions are in m)

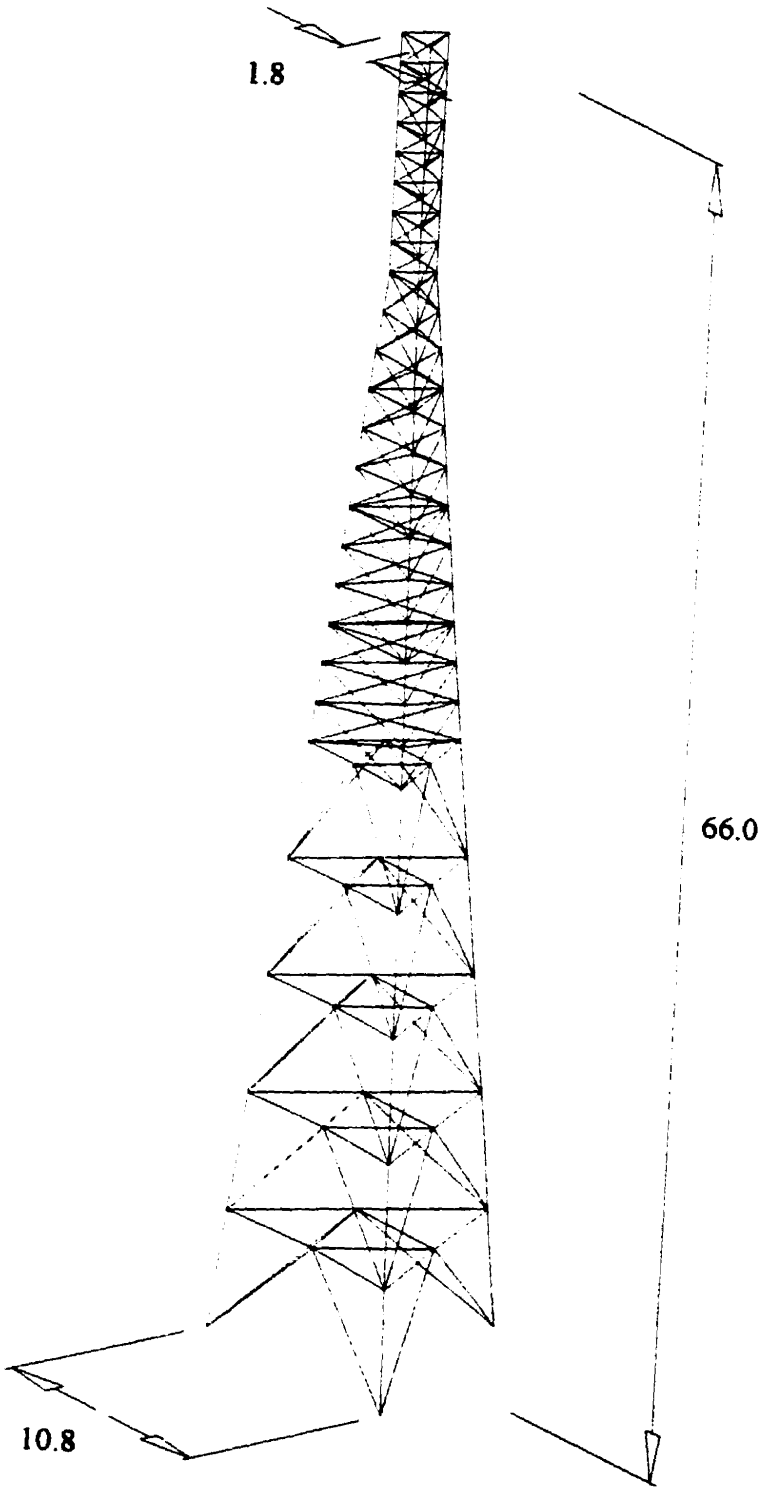

Fig. 3.3 Layout of tower TC3 (dimensions are in m)

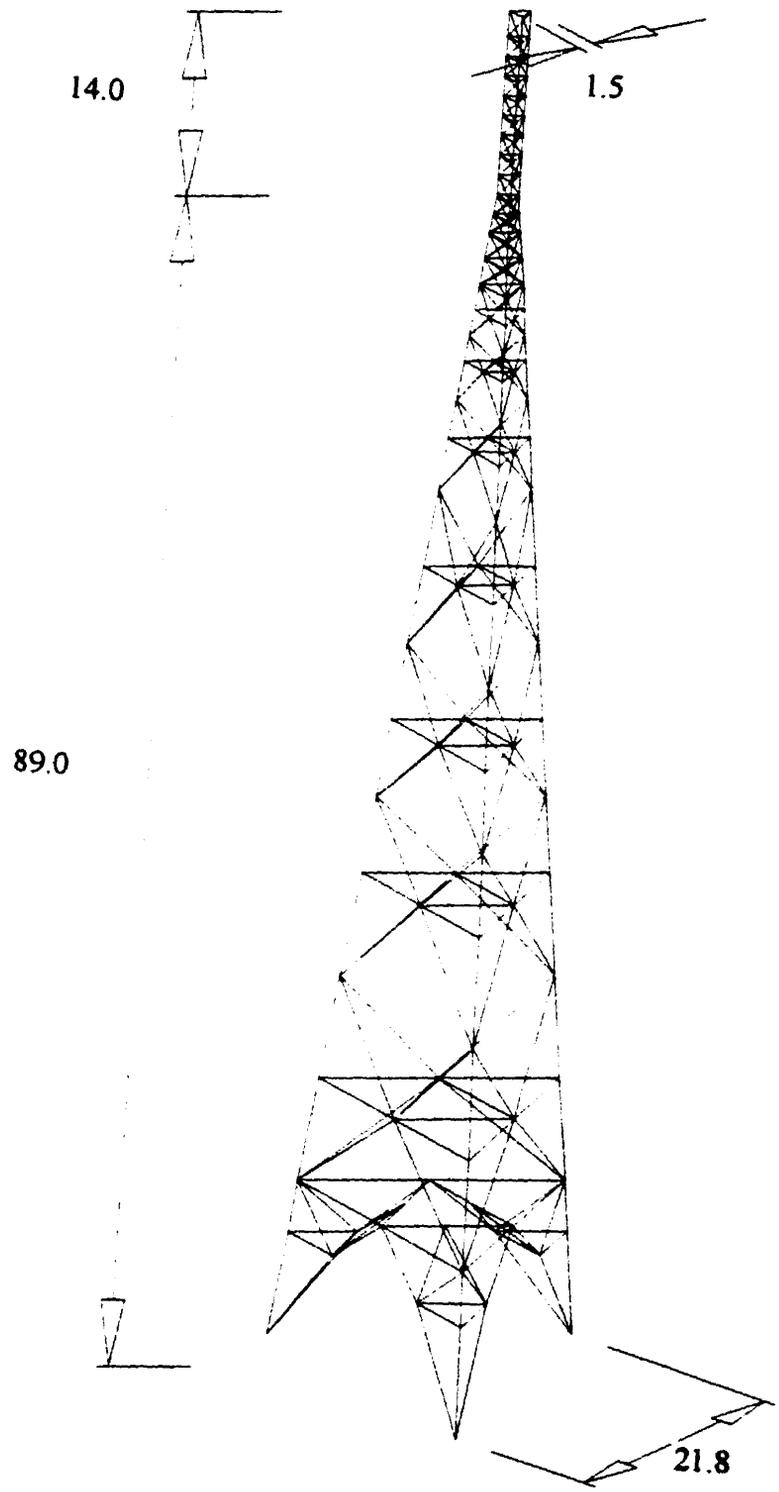

Fig. 3.4 Layout of tower TC4 (dimensions are in m)

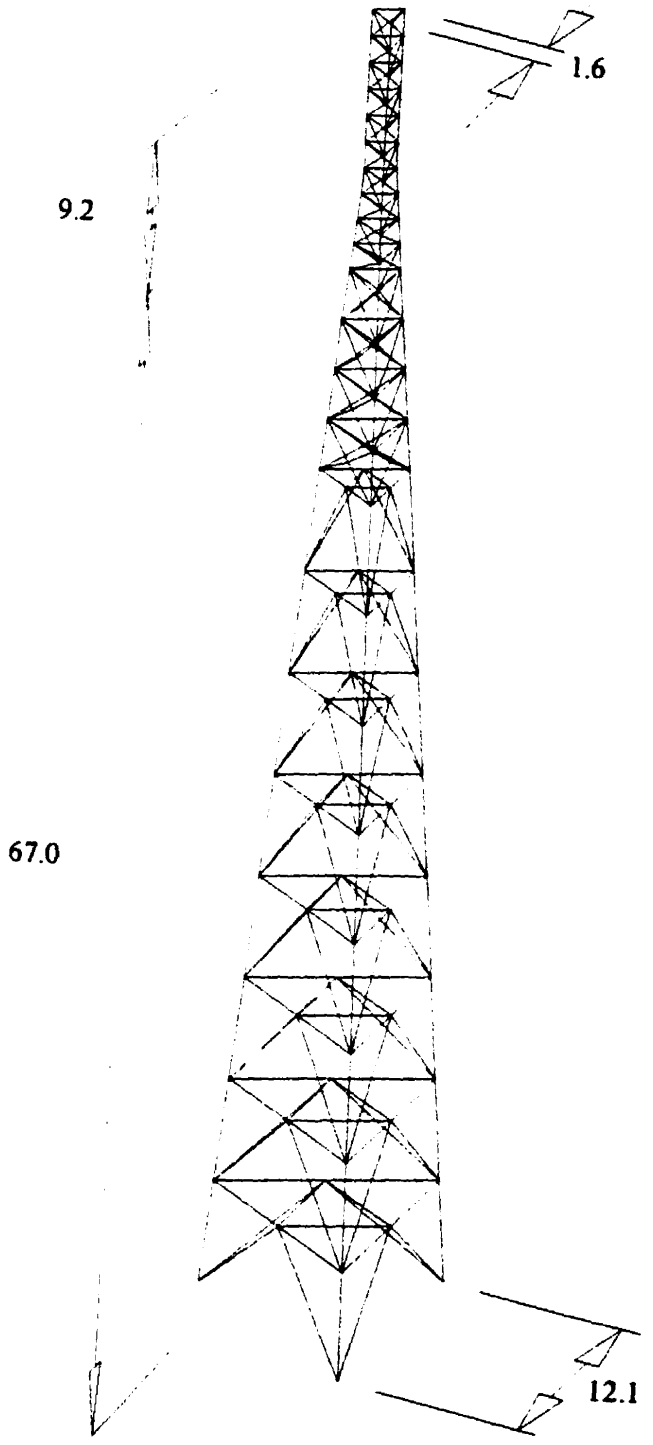

Fig. 3.5 Layout of tower TC5 (dimensions are in m)

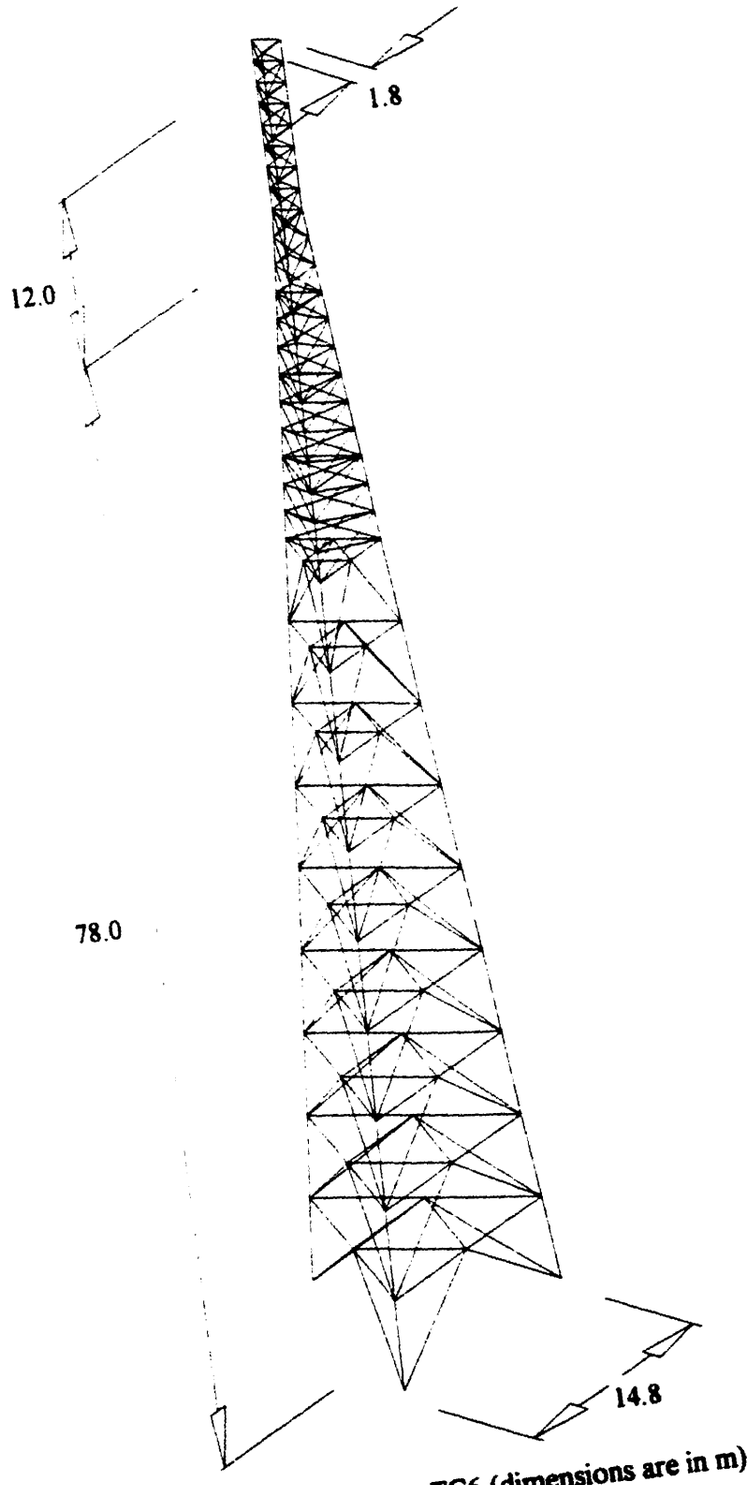

Fig. 3.6 Layout of tower TC6 (dimensions are in m)

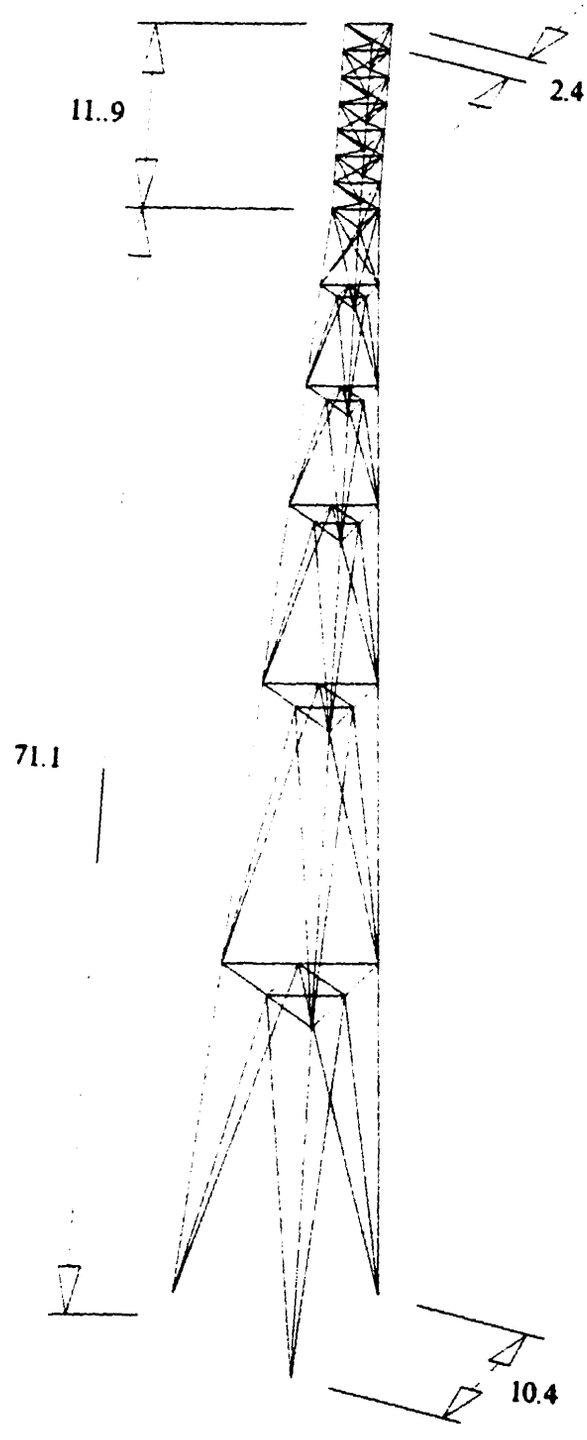

Fig. 3.7 Layout of tower TC7 (dimensions are in m)

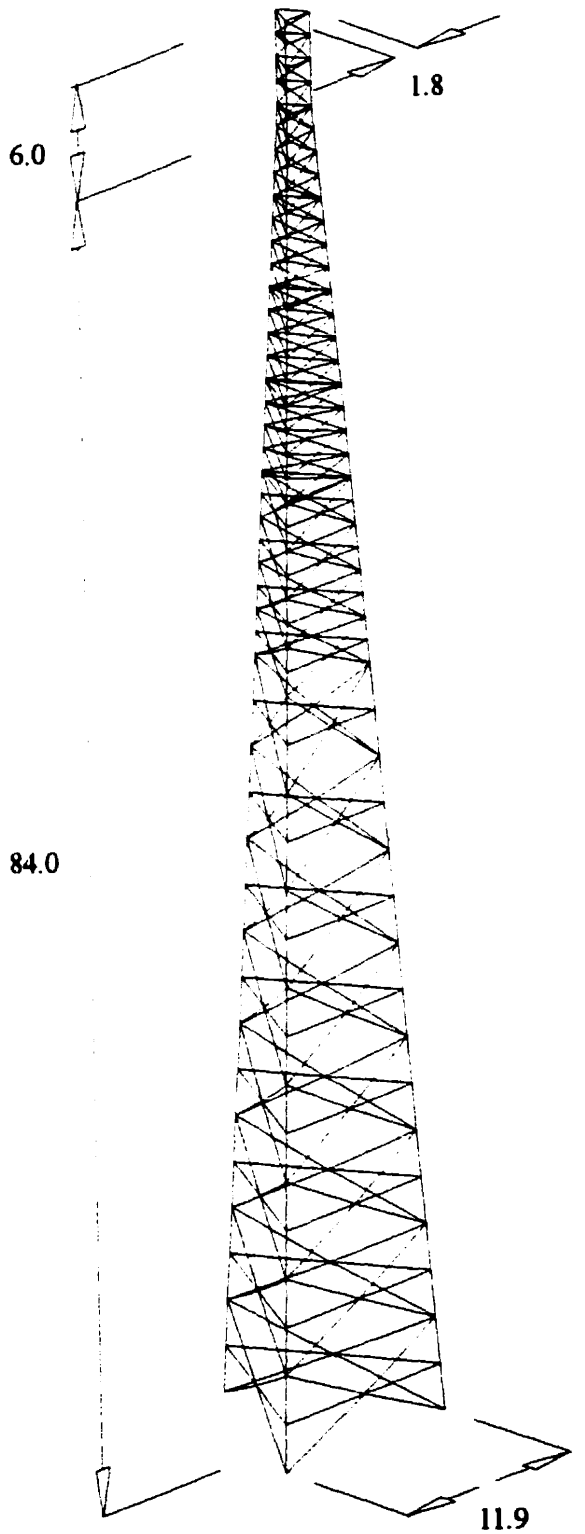

Fig. 3.8 Layout of tower TC8 (dimensions are in m)

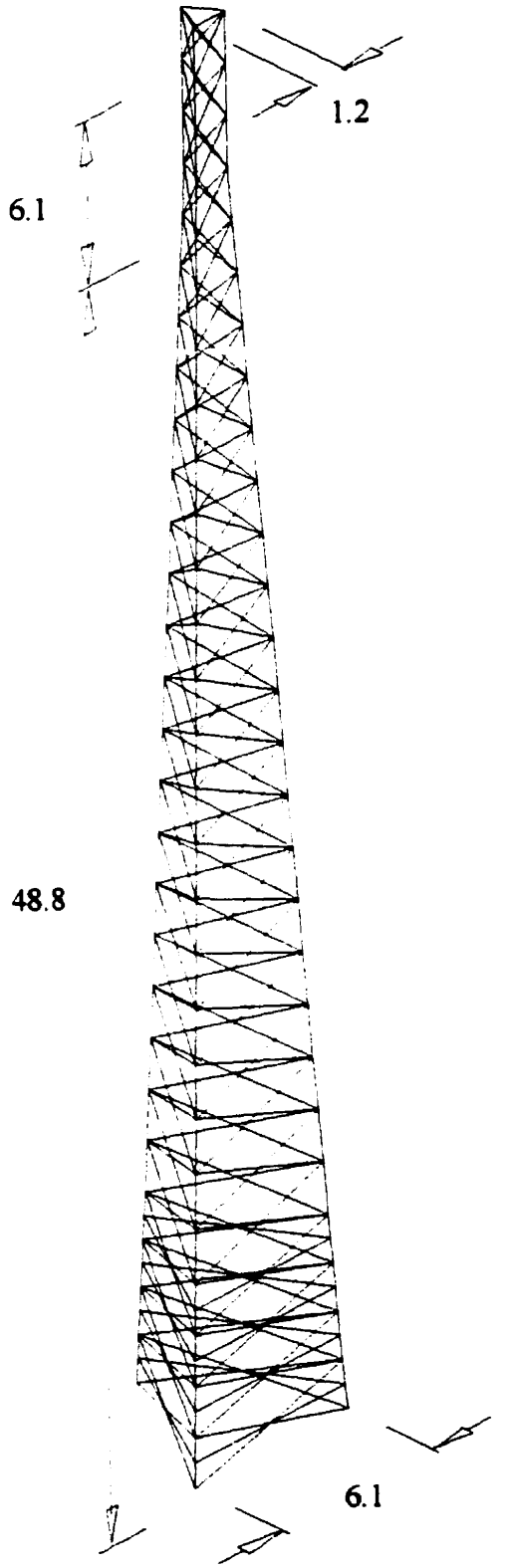

Fig. 3.9 Layout of tower TC9 (dimensions are in m)

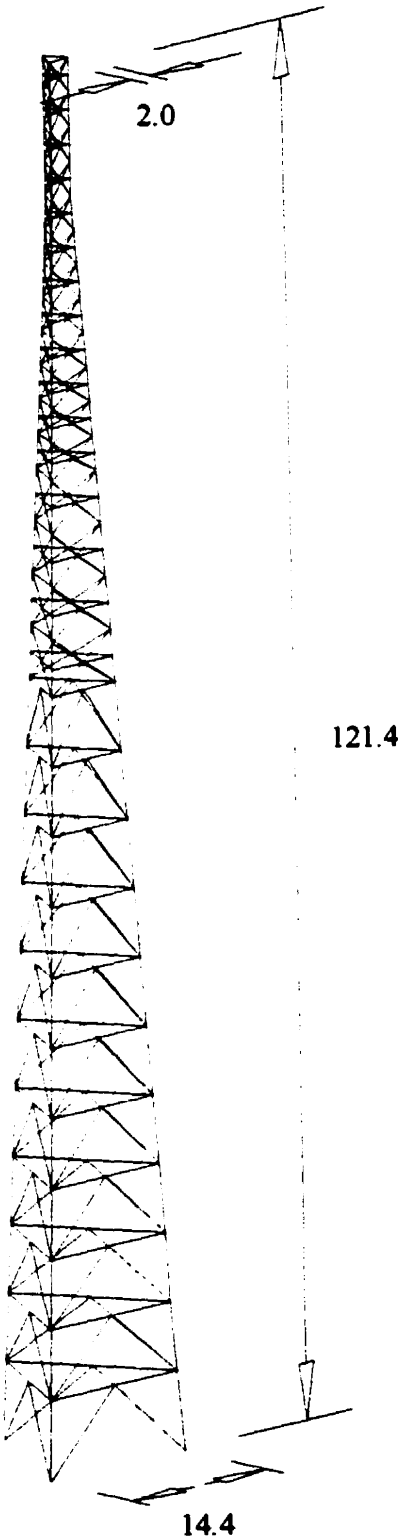

Fig. 3.10 Layout of tower TC10 (dimensions are in m)

3.2 Numerical Modeling of Telecommunication Towers

The towers are modeled as linear elastic three-dimensional structures with beam elements for the main legs and truss elements for the diagonal and horizontal members. The supports are idealized as pinned on rigid foundation. The mass of the main legs and their tributary members (bracing members spanning between the legs without any intermediate joint) are lumped at the corresponding leg joints. For truss members spanning between the legs with intermediate joints, the mass is lumped at the appropriate leg joints so that the member itself is assumed massless. All secondary or redundant members are removed from the stiffness model since they do not take any load in a linear analysis. However, their mass is calculated and lumped at the corresponding leg joints.

3.3 Classification of Telecommunication Towers

In this study the classification of the towers adopted by Sackmann (1996) is followed, where the towers are classified with respect to three main characteristics namely, the equivalent taper ratio D, the shear coefficient at the base K_{so}, and the a/L (length of truss panel/tower height) ratio of the largest panel.

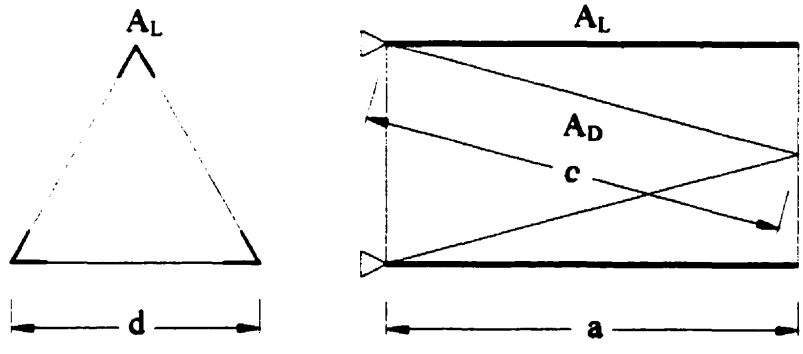

Fig. 3.11 Definition of the main symbols used in categorizing the lattice towers

The equivalent taper ratio is given by:

$$D = (\frac{I_1}{I_o})^{\frac{1}{3}} \tag{3.1}$$

where

I_1= second moment of area of the main leg sections at the top

I_o= second moment of area of the main leg sections at the base.

In calculating the second moment of area of the main leg section either at the base or at the top, the following expression can be used:

$$I = \frac{1}{2} A_L \times d^2 \tag{3.2}$$

the symbols used are defined Fig. 3.11.

The shear coefficient of the tower at the base is calculated using the shear coefficient for prismatic beams calculated for the elements of the tower at the base and using the following expression:

$$K_{so} = 0.29 \frac{a}{L} \sqrt{\Phi} \tag{3.3}$$

In the previous expression the shear parameter Φ depends on the ratio of the cross-sectional areas of the leg and diagonal members and the length and depth of the truss element, as follows:

$$\Phi = 2\frac{A_L}{A_D}(\frac{c}{a})^3 - 1 \qquad \text{for cross-braced trusses, and}$$

$$\Phi = 8\frac{A_L}{A_D}(\frac{c}{a})^3 \qquad \text{for chevron-braced trusses} \tag{3.4}$$

Two groups of towers were identified (labeled as A and B) for which a predictor of the lowest three flexural modes of vibration was proposed. The most important parameter used in classifying the groups was the a/L ratio of the largest element. From the tower data used in the study a limit of $a/L = 0.1$ is the boundary between the two groups.

Group A was further subdivided into two subgroups A1 and A2. Subgroup A1 has an equivalent taper ratio $D = 0.1$ to 0.2, while subgroup A2 has an equivalent taper ratio $D =$ 0.2 to 0.3. The prediction of the mode shapes is presented in a polynomial form. Tables 3.2 and 3.3 show the different classification parameters and the mode shapes suggested for the two groups. It should be noted that tower TC4 was not included in this prediction as it has a profound taper ratio (width at the top to width at the base ratio) of 14.5 which is higher than that of the remaining nine towers considered in this study having taper ratios in the range of 4.2 to 8.2.

Table 3.2 - Classification of towers according to Sackmann (1996)

	A1	A2	B
a/L	≤ 0.1	≤ 0.1	> 0.1
D	0.1 to 0.2	0.2 to 0.3	0.25 to 0.35
K_{xx}	0.1 to 0.25	0.1 to 0.25	0.25 to 0.4

Table 3.3 - Prediction of the lowest three flexural modes

Group A1	ϕ_1	$x^{2.2}$
	ϕ_2	$-2.9x^2 + 3.2x^3 + .7x^4$
	ϕ_3	$.8x + 5.4x^2 - 21.9x^3 + 16.7x^4$
Group A2	ϕ_1	$x^{2.2}$
	ϕ_2	$-4.4x^2 + 5.1x^3 + .3x^4$
	ϕ_3	$1.5x + 7.3x^2 - 31.2x^3 + 23.4x^4$
Group B	ϕ_1	$x^{2.2}$
	ϕ_2	$-2.1x + 1.4x^2 + 1.7x^3$
	ϕ_3	$3.8x + 1.2x^2 - 51x^3 + 81x^4 - 34x^5$

In the current study, the classification adopted by Sackmann (1996) is followed but some modifications were made for the lowest flexural mode shape. This is done because Sackmann's prediction of the lowest mode is an average for the two groups and it was found beneficial to use a specific prediction for each group as will be discussed later.

3.4 Transmission Line Towers

An investigation is carried out to assess the applicability of the proposed simplified static method to transmission towers, focusing on the effect of the conductors on tower behavior. This study aims at finding an equivalent mass that can replace the mass of the conductors in order to reflect the real behavior of the tower-conductor coupled system. To this end, a frequency analysis of the tower-conductor system is performed using the computer program ADINA. A frequency analysis of the tower alone is performed and the equivalent mass of conductor is determined. Potential dynamic interactions between the cables and the tower are evaluated. Six existing transmission towers are studied for power lines of voltage level ranging from 120 kV to 450 kV. Table 3.4 shows the basic dimensions and the lowest flexural periods of vibration in both the longitudinal and transverse directions for the six towers.

Table 3.4 - Characteristics of the transmission towers studied

Tower	Height (m)	Base Width (m)	Top Width (m)	Total Mass (kg)	Fundamental Flexural Period Transverse (s)	Fundamental Flexural Period Longitudinal (s)
TR1	48.15	16.50	2.00	13,500	0.298	0.287
TR2	41.60	7.50	1.35	5,500	0.300	0.298
TR3	48.50	10.50	1.50	6,500	0.421	0.416
TR4	34.90	2.00	1.30	5,000	0.462	0.461
TR5	58.00	11.60	2.00	13,000	0.472	0.464
TR6	36.50	1.95	1.30	4,500	0.482	0.481

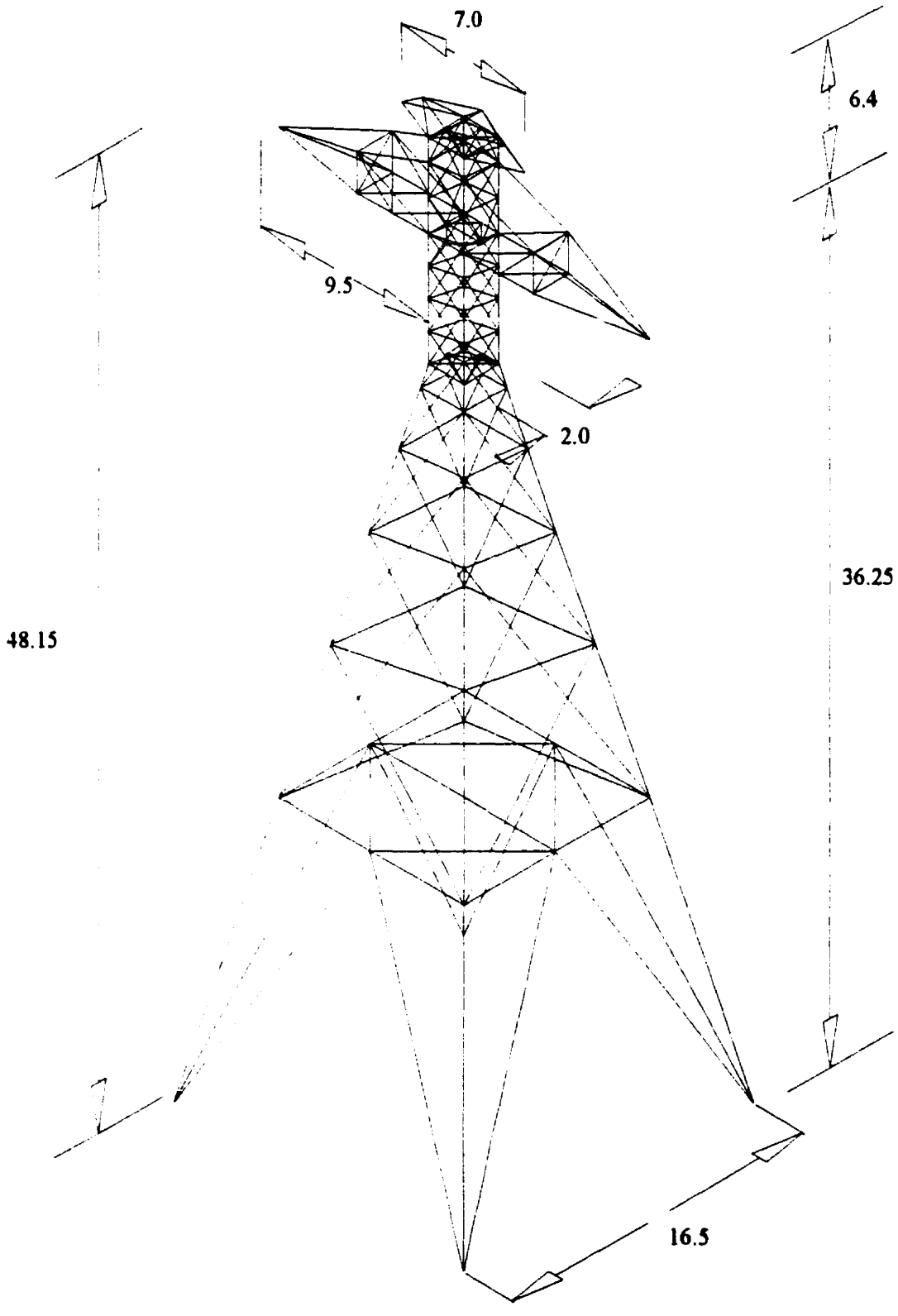

Fig. 3.12 Layout of tower TR1 (dimensions are in m)

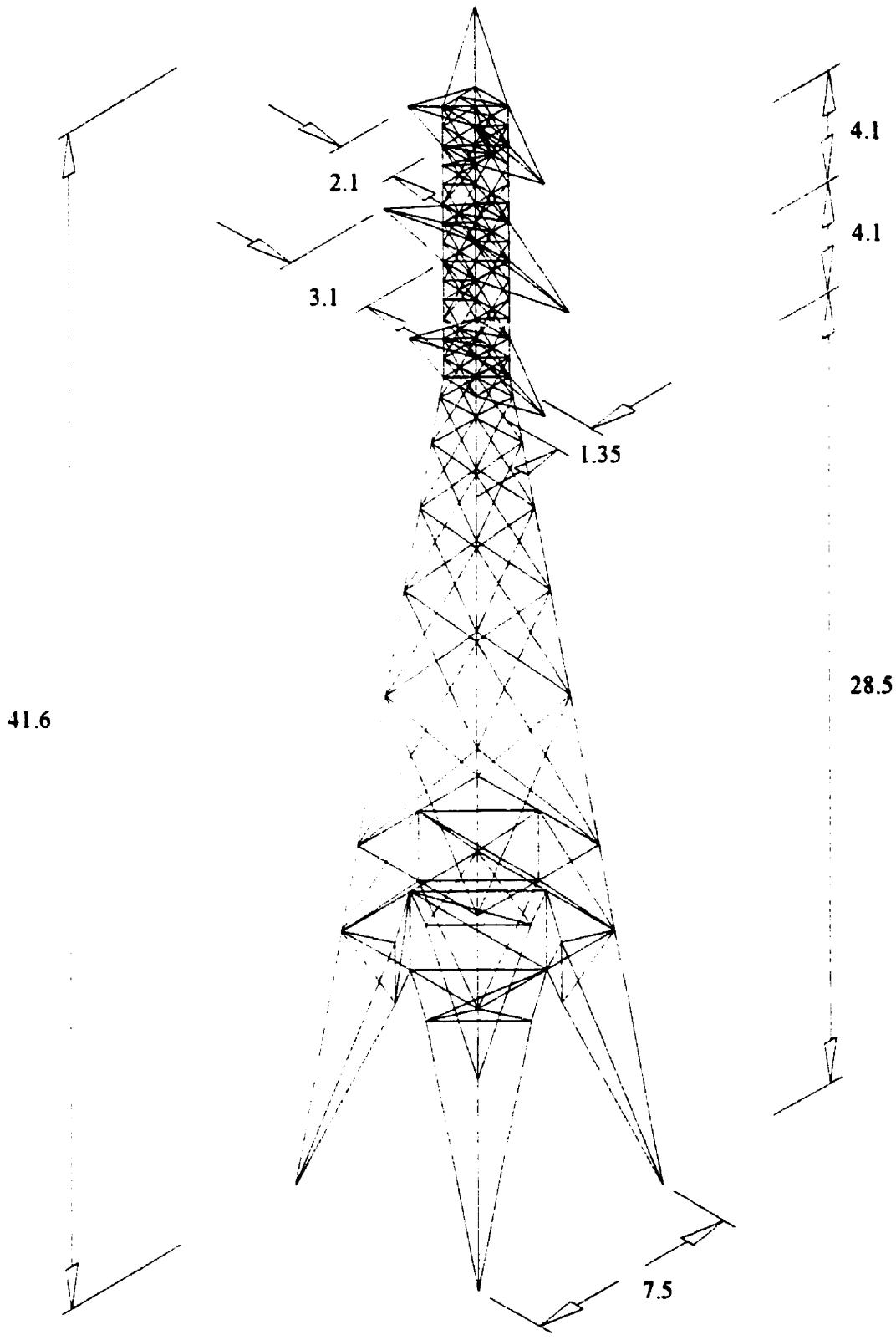

Fig. 3.13 Layout of tower TR2 (dimensions are in m)

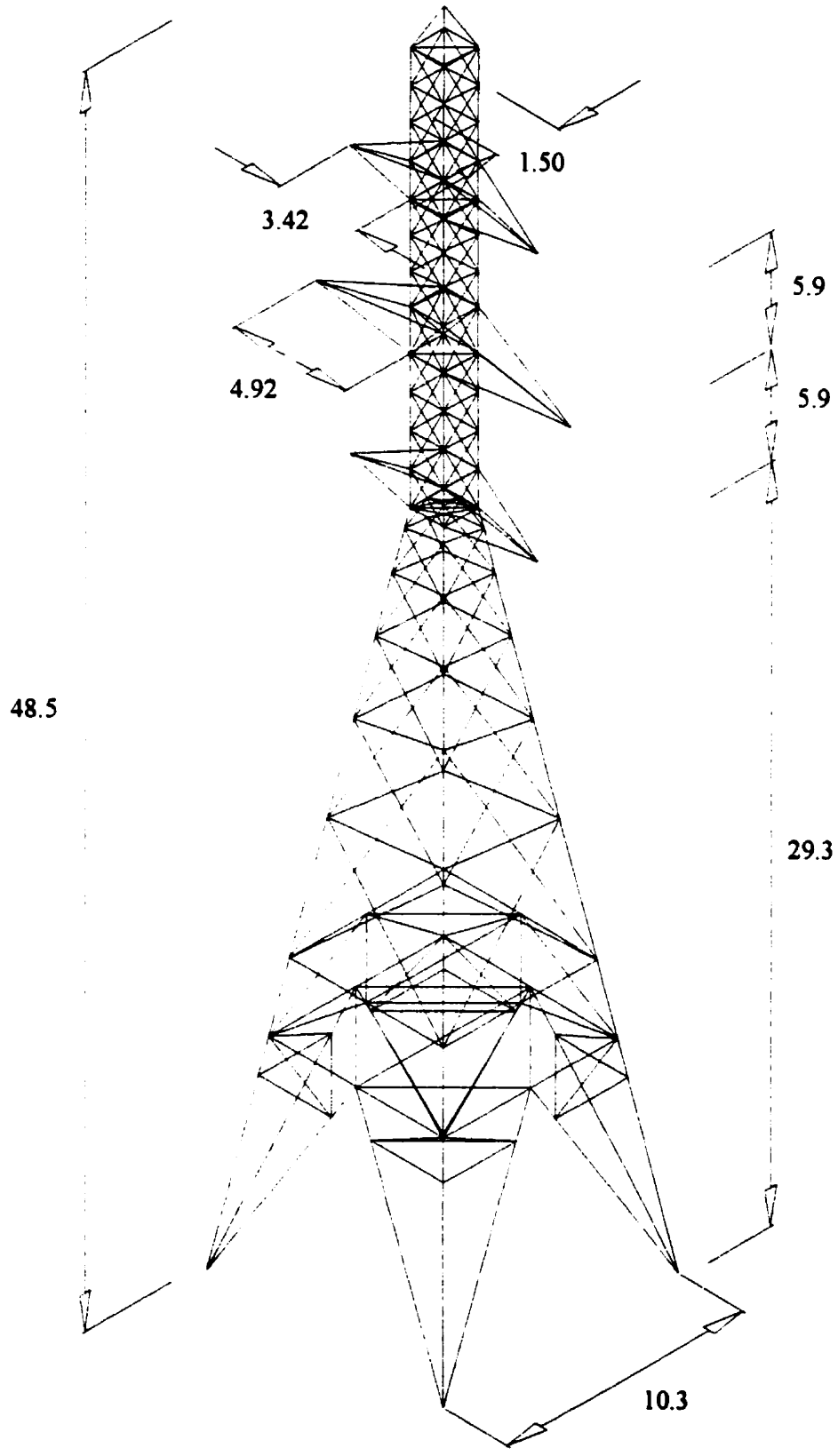

Fig. 3.14 Layout of tower TR3 (dimensions are in m)

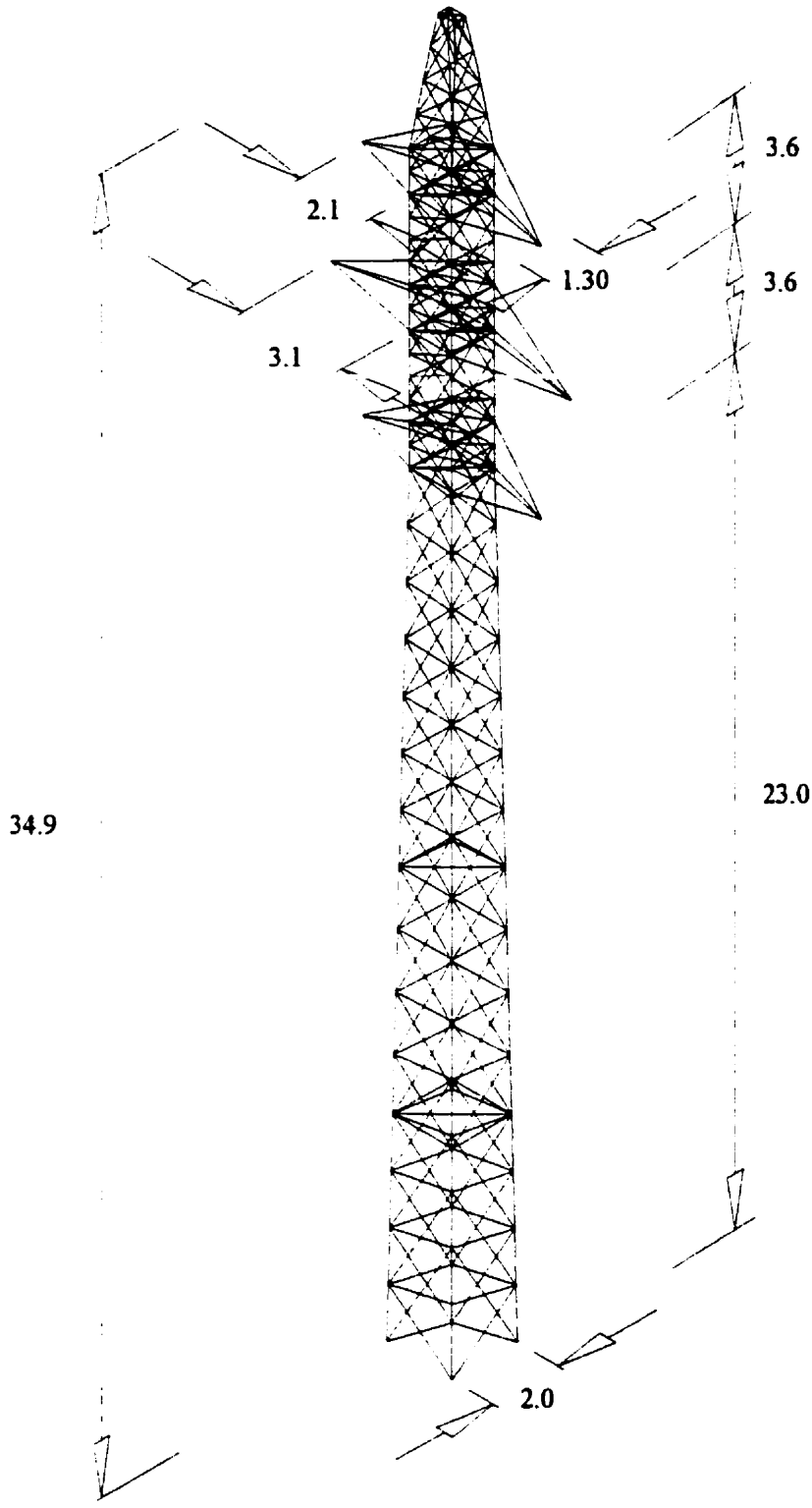

Fig. 3.15 Layout of tower TR4 (dimensions are in m)

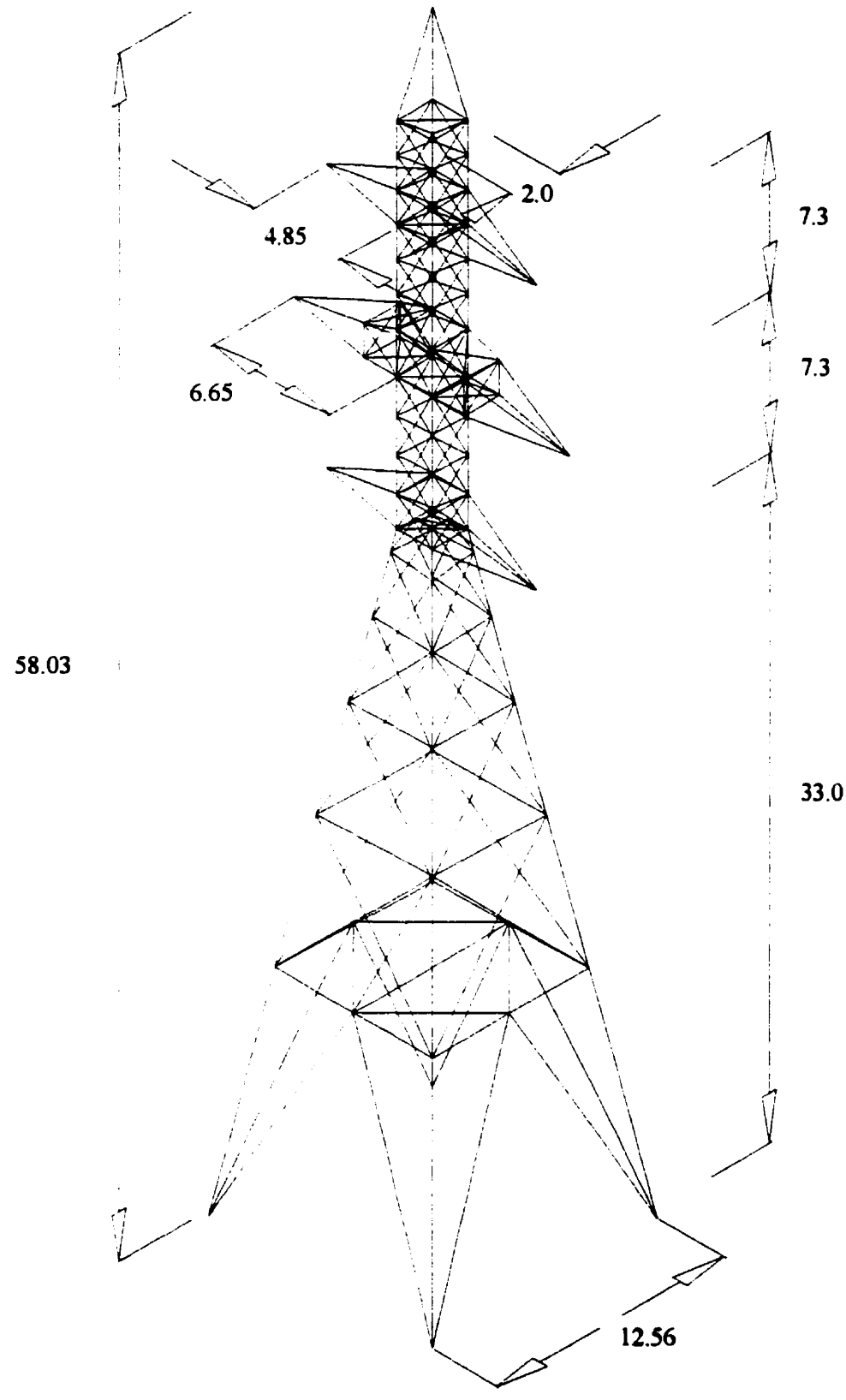

Fig. 3.16 Layout of tower TR5 (dimensions are in m)

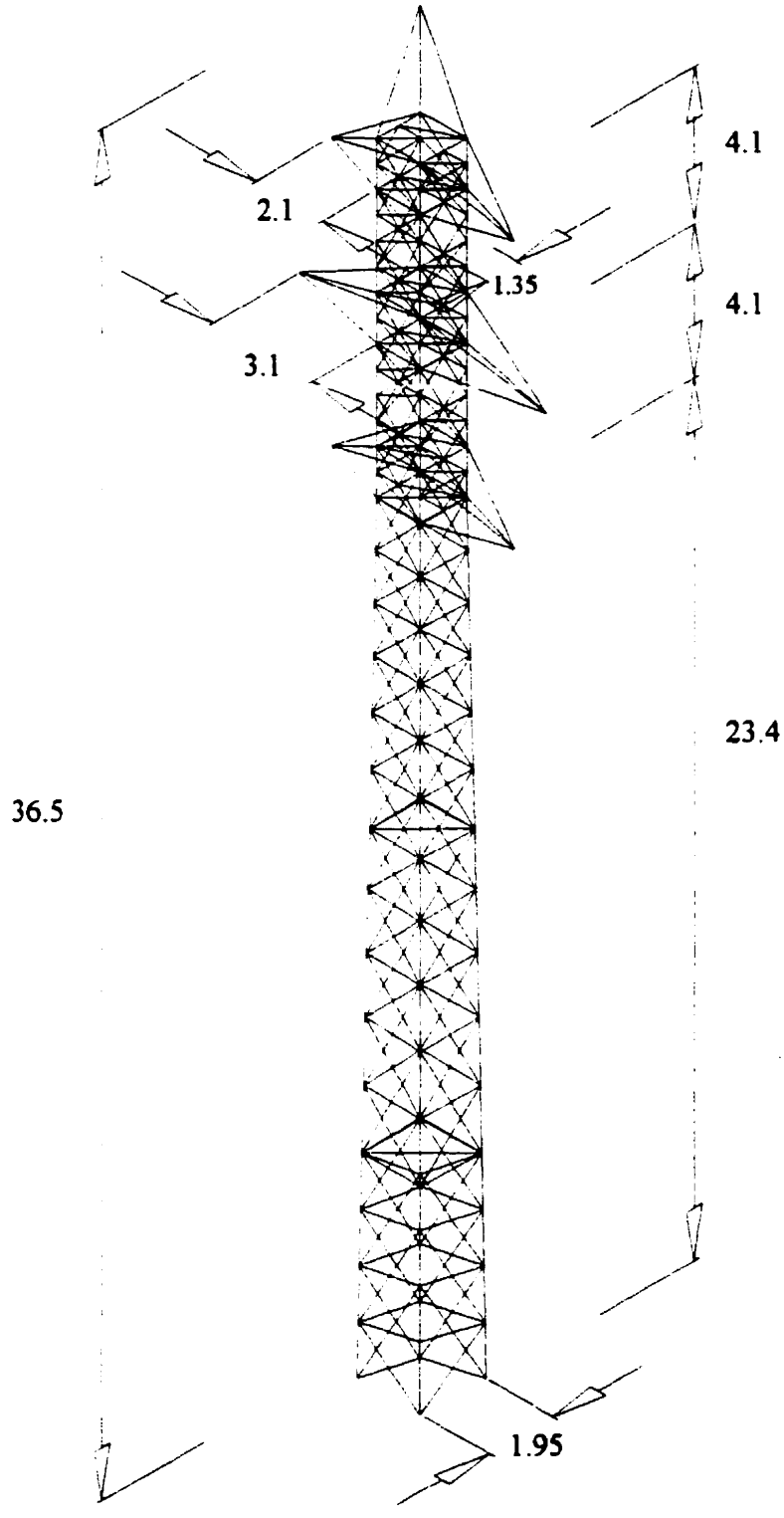

Fig. 3.17 Layout of tower TR6 (dimensions are in m)

The layouts of the six towers including the basic dimensions, section categories are illustrated in Figs. 3.12 through 3.17. It should be noted that member subdivisions and other attachments are not shown in these figures.

3.5 Modeling and Analysis of Transmission Towers

Transmission towers are modeled as three-dimensional lattice structures, in the same way as the telecommunication towers (discussed in section 3.2). The main legs are modeled as frame elements while all other elements are modeled using truss elements. In modeling the cable, however, two-node tension-only truss elements with prestressing force are used. The tower main legs are assumed to be pinned on rigid foundation. Their mass and that of their tributary members are lumped at the corresponding leg joints including the mass of truss members having intermediate joints. When modeling the coupled tower-conductor system, the mass of each cable element is calculated and divided equally on its two end nodes. However, when replacing the conductor with an equivalent mass, this mass is lumped at the appropriate cross-arm joint or at the top of the tower for the case of the overhead ground wire.

The coupled tower-conductor system problem involves geometric non-linearity due to large displacements of cable joints and therefore requires more computation effort than the tower alone. The modal method of analysis is no longer valid and a step-by-step procedure is used. However, after removing the cables, the tower alone is treated in the same manner as telecommunication towers.

3.6 Earthquake Records Used in The Study

A set of 45 strong motion earthquake records obtained from 23 different events, as listed in Table 3.5, is used in the present study. This set of accelerograms was previously used by Tso et al. (1992) in an investigation of the importance of the peak ground acceleration to the peak ground velocity ratio (A/V) as an indicator of the dynamic characteristics of an earthquake.

The data set was compiled from earthquakes that occurred in many places in the world to include a vast range of seismological conditions. The effect of localized soil conditions is not included in the present study as all selected accelerograms were recorded on rock or stiff soil sites. It should also be noted that both near-field and far-field records were included in this set, and all records have a peak ground acceleration equal to or greater than 0.04 g.

Three groups of records were identified in accordance with their maximum A/V ratio, namely low, for records with A/V < 0.8 g/m/s, intermediate, for records with 0.8 g ≤ A/V ≤1.2 g/m/s and high, for records with A/V > 1.2 g/m/s. A complete description of the earthquake component, magnitude, maximum ground acceleration, maximum ground velocity, source distance and soil conditions can be found in Tso et al. (1992). A graphical representation of the 45 accelerograms together with their response spectra (evaluated for 3% damping) is presented in Appendix A.

These records are used as both horizontal and vertical base accelerations. The records are not scaled or adjusted in any way in the analyses. However, in the case of vertical accelerations, the acceleration values are reduced to 75% of their original values to be consistent with the recommendations set forth by many design codes for

safety-related nuclear structures and building codes (ASCE 4-86 and NBCC 1995). A distinct set of 55 vertical earthquake components collected from 17 different events is also used in this study, a list of earthquake names, magnitudes and dates can be found in Appendix C.

Table 3.5 - Earthquake records used in the study

Earthquake	Magnitude	No. of records	Date
Long Beach, California	M_L=6.3	2	10/03/1933
Lower California	M_L=5.6	1	30/12/1934
Helena, Montana	M_L=6.0	1	31/10/1935
Imperial Valley, California	M_L=6.6	1	18/05/1940
Kern County, California	M_L=7.6	2	21/07/1952
San Francisco, California	M_L=5.4	2	22/03/1957
Honshu, Japan	M_{JMA}=5.4	1	5/04/1966
Parkfield, California	M_L=5.6	2	27/06/1966
Borrego Mtn., California	M_L=6.5	2	8/04/1968
Near E. Coast of Honshu, Japan	M_{JMA}=7.9	1	16/05/1968
Lytle Creek, California	M_L=5.4	1	12/09/1970
San Fernando, California	M_L=6.6	14	9/02/1971
Central Honshu, Japan	M_{JMA}=5.5	1	26/02/1971
Near S. Coast of Honshu, Japan	M_{JMA}=7.0	1	02/08/1971
Near E. Coast of Honshu, Japan	M_{JMA}=5.8	1	11/05/1972
Near E. Coast of Honshu, Japan	M_{JMA}=7.4	1	17/06/1973
Near E. Coast of Honshu, Japan	M_{JMA}=6.1	1	16/11/1974
Oroville, California	M_L=5.7	1	1/08/1975
Monte Negro, Yugoslavia	M_L=5.4	1	9/04/1979
Monte Negro, Yugoslavia	M_L=7.0	1	15/04/1979
Banja Luka, Yugoslavia	M_L=6.1	1	13/08/1981
Michoacan, Mexico	M_S=8.1	5	19/09/1985
Nahanni, N.W.T., Canada	M_S=6.9	1	23/12/1985

M_{JMA} = Japan meteorological agency scale
M_L = local magnitude
M_S = surface wave magnitude

CHAPTER 4

EARTHQUAKE AMPLIFICATION FACTORS FOR TELECOMMUNICATION TOWERS

4.1 Introduction

Earthquake amplification factors for self-supporting lattice telecommunication towers are suggested based on a numerical modeling study performed on the ten towers used, each being subjected to the set of 45 accelerograms. The dynamic analysis is carried out using modal superposition method with a uniform damping ratio of 3% of the critical viscous damping for all modes considered in the analyses as mentioned before. Each tower is analyzed twice under the effect of the same earthquake, once applying the accelerogram in one of the two principal horizontal directions, and then considering 75% of the same accelerogram acting in the vertical direction to be consistent with the NBCC 1995. From these simulations the value of the base shear and total vertical reaction are obtained. Simple regression analyses are performed on the results from which horizontal and vertical amplification factors are found.

These factors are presented as functions of the tower's largest flexural period or largest axial period of vibration as appropriate. When multiplied by the tower mass, these factors can be used by designers to estimate the expected level of base shear and vertical reaction developed in self-supporting telecommunication towers due to an earthquake event. Vertical earthquake amplification factors are presented in Appendix C using a distinct set of 55 vertical earthquake records.

4.2 Method of Analysis

The modal superposition method is used for the analysis, as implemented in the commercial software SAP90. The number of modes considered varied with each tower, the main concern being to ensure that at least 90% of the total mass is participating in the horizontal direction and 85% of the total mass is participating in the vertical direction. The damping ratio is taken as 3% of the critical viscous damping and kept constant in all modes included in the analysis. It is important to note that the results reported in this chapter are those of the dynamic analysis without including the static response due to self-weight.

4.3 The Use of NBCC 1995

It is paramount to realize that there are important differences between the behavior of buildings and that of self-supporting telecommunication towers. While most buildings respond to horizontal earthquakes essentially in their lowest lateral mode of vibration, it is not the case for self-supporting towers whose lowest three flexural modes are usually significantly excited.

To illustrate this point, the ten towers used in the study were dynamically analyzed for their base shear values using the NBCC 1995 design spectrum shown in Fig. 4.1, which has three zones $Z_a<Z_v$, $Z_a=Z_v$ and $Z_a>Z_v$, where Z_a is the acceleration-related seismic zone and Z_v is the velocity-related seismic zone. The modal superposition method was used in these analyses and two sets of base shear values were calculated, the first considering only the lowest flexural mode while the second included the effects of the lowest three flexural modes. It should be noted that although the NBCC design spectrum is given for 5%

damping, it was used in this study for illustration purposes only. The base shear values obtained from these analyses are given in Table 4.1 for a peak horizontal ground velocity v = 1 m/s. As expected, including only the lowest flexural mode greatly underestimates the maximum base shear, the percentage of error ranging from 14% to 70% . This confirms that it is essential to include at least the lowest three flexural modes in the analyses in order to capture the response of these structures under horizontal excitation.

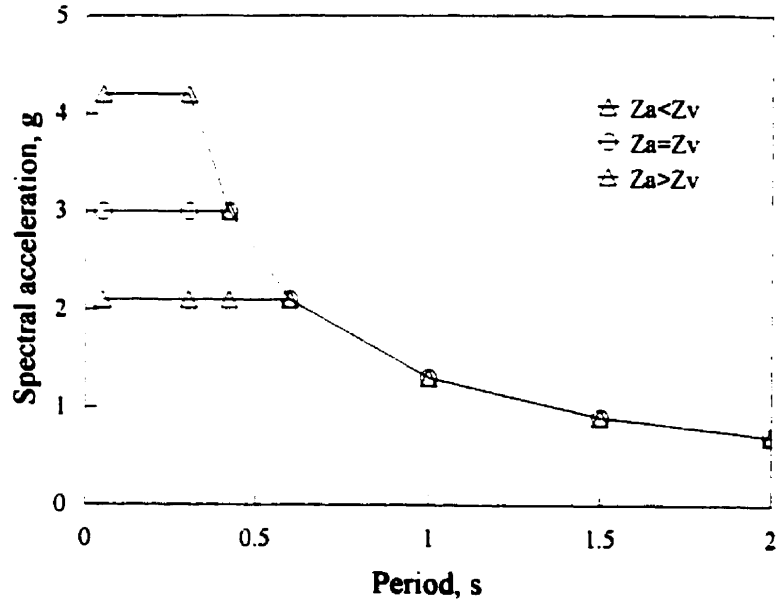

Fig. 4.1 NBCC 1995 acceleration design spectrum evaluated for 5% damping

Table 4.1 - Base shear values using the NBCC 1995 design spectrum

	Base shear [kN] considering three flexural modes			Base shear [kN] considering the lowest flexural mode		
Tower	$Z_A<Z_V$	$Z_A=Z_V$	$Z_A>Z_V$	$Z_A<Z_V$	$Z_A=Z_V$	$Z_A>Z_V$
TC1	44	64	81	34	48	67
TC2	118	160	220	99	130	170
TC3	285	350	440	210	210	210
TC4	520	690	940	270	270	270
TC5	340	410	520	260	260	260
TC6	420	510	640	300	300	300
TC7	350	370	410	300	300	300
TC8	350	410	500	280	280	280
TC9	87	110	140	61	61	61
TC10	570	620	710	390	390	390

To further prove the inability of static methods used in building codes to predict the seismic response of towers, the base shear values were also calculated for the ten towers using the static approach of the NBCC 1995. The lateral elastic seismic force, V_e, is given by the following expression:

$$V_e = vSIFW \tag{4.1}$$

where

V_e= elastic base shear in N

v = zonal velocity ratio

S = dimensionless seismic response factor

F = foundation factor

W = dead load in N.

In these calculations the importance factor, foundation factor and zonal velocity ratio were taken as unity. The results are given in Table 4.2. Comparing these base shear values with the results obtained from the response spectrum analysis presented in Table 4.1, it is clear that the static code expression consistently overestimates the tower base shear values.

Table 4.2 - Base shear values (in kN) using the NBCC 1995 static approach

		$Z_A<Z_V$		$Z_A=Z_V$		$Z_A>Z_V$	
Tower	W	S	V_e	S	V_e	S	V_e
TC1	3.3E+04	2.100	70	3.000	100	4.200	140
TC2	9.7E+04	2.100	200	2.712	260	3.528	340
TC3	2.6E+04	2.041	540	2.040	540	2.040	540
TC4	4.7E+05	2.033	960	2.030	960	2.030	960
TC5	3.2E+05	1.953	620	1.950	620	1.950	620
TC6	4.1E+05	1.833	760	1.830	760	1.830	760
TC7	2.6E+05	1.806	480	1.810	480	1.810	480
TC8	3.5E+05	1.721	610	1.720	610	1.720	610
TC9	1.1E+05	1.688	180	1.690	180	1.690	180
TC10	6.5E+05	1.369	890	1.370	890	1.370	890

From the previous discussion it is concluded that it is necessary to perform dynamic analysis in order to include the lowest three flexural modes as the base shear expressions recommended by building codes consider the fundamental lateral mode only. It is also evident that the building code static approach is not suitable for telecommunication towers. Moreover, most building codes do not account for the effects of the vertical ground motion, which may be important for telecommunication towers. Therefore, it is necessary and useful to derive earthquake amplification factors specifically for self-supporting telecommunication towers.

4.4 Horizontal Earthquake Excitation

In order to study horizontal force amplification factors, each tower is subjected to each of the 45 earthquake records selected. From this analysis, the resulting shear force at the base of each tower is recorded. The base shear values are then plotted versus the peak ground acceleration, peak ground velocity and finally A/V ratio. The purpose is to find the correlation, if any, between the base shear and each of these characteristics of the ground motion.

The results obtained for the ten towers are shown in Figs. 4.2 to 4.11. It is seen that the ten towers follow the same trend and that strong correlation exists between the base shear values and the peak ground acceleration of the earthquake. Furthermore, the relation follows a linear trend. Therefore, linear regression analyses were performed on the results obtained for each tower in order to find a relation between the base shear values and the peak ground acceleration. It is observed, however, that the correlation of the base shear does not seem to be as good with the peak ground velocity (Figs. 4.2.b to 4.11.b) and that practically no correlation is found with the A/V ratio (Figs. 4.2.c to 4.11.c).

For each tower, the value of the maximum base shear is divided by the tower mass to obtain a dimensionless factor relating the peak ground acceleration and the dynamic magnification values. Regression analyses are then performed on each of the three predefined groups of accelerograms namely, low, intermediate and high A/V ratios, as well as on the entire set. The results of these analyses are summarized in Table 4.3.

Table 4.3 - Linear regression analysis for the maximum base shear

	Low A/V		Inter. A/V		High A/V		Entire Set	
Tower	Slope	R^2	Slope	R^2	Slope	R^2	Slope	R^2
TC1	1.71	0.67	1.63	0.69	1.40	0.70	1.55	0.69
TC2	1.84	0.91	1.67	0.84	1.37	0.96	1.58	0.84
TC3	1.58	0.67	1.48	0.89	1.00	0.70	1.30	0.63
TC4	1.59	0.55	1.61	0.80	1.45	0.93	1.54	0.81
TC5	1.44	0.70	1.58	0.83	1.00	0.78	1.30	0.67
TC6	1.31	0.70	1.36	0.93	0.86	0.56	1.14	0.59
TC7	1.69	0.80	1.47	0.85	0.96	0.87	1.29	0.67
TC8	1.21	0.63	1.21	0.87	0.80	0.81	1.03	0.67
TC9	1.08	0.86	1.07	0.87	0.76	0.67	0.94	0.69
TC10	1.20	0.89	1.04	0.83	0.67	0.92	0.92	0.68

R value: coefficient of correlation

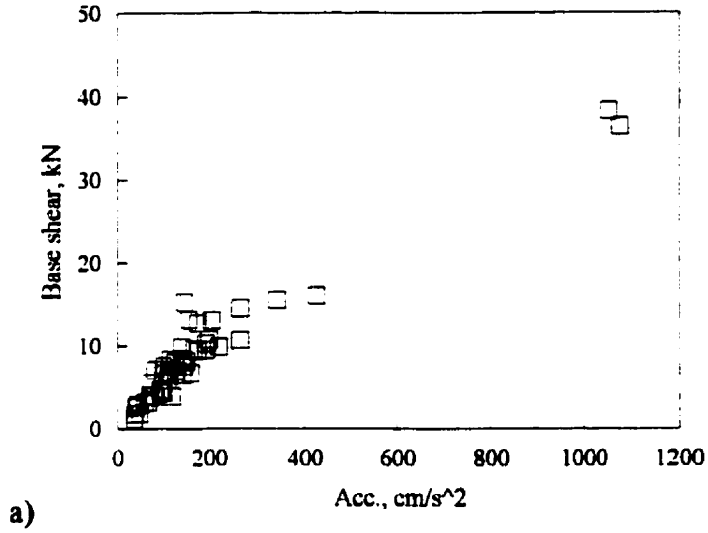

a)

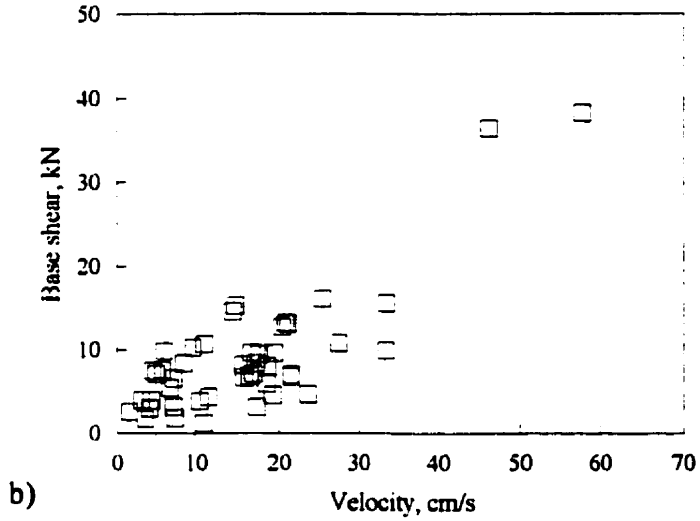

b)

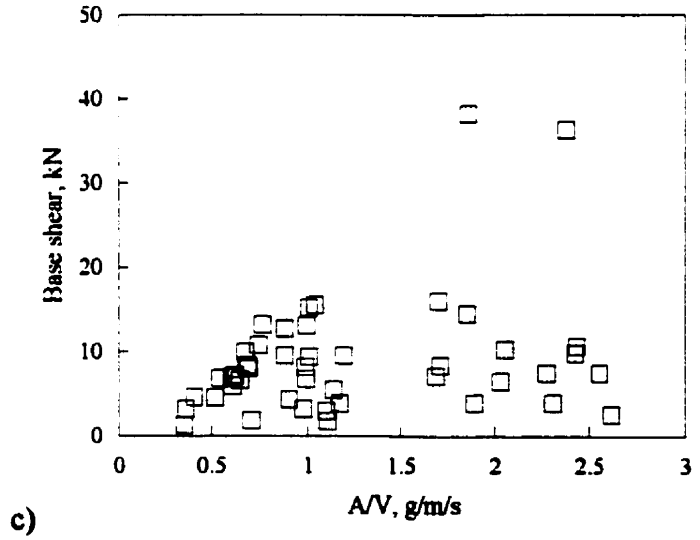

c)

Fig. 4.2 Maximum base shear values for tower TC1

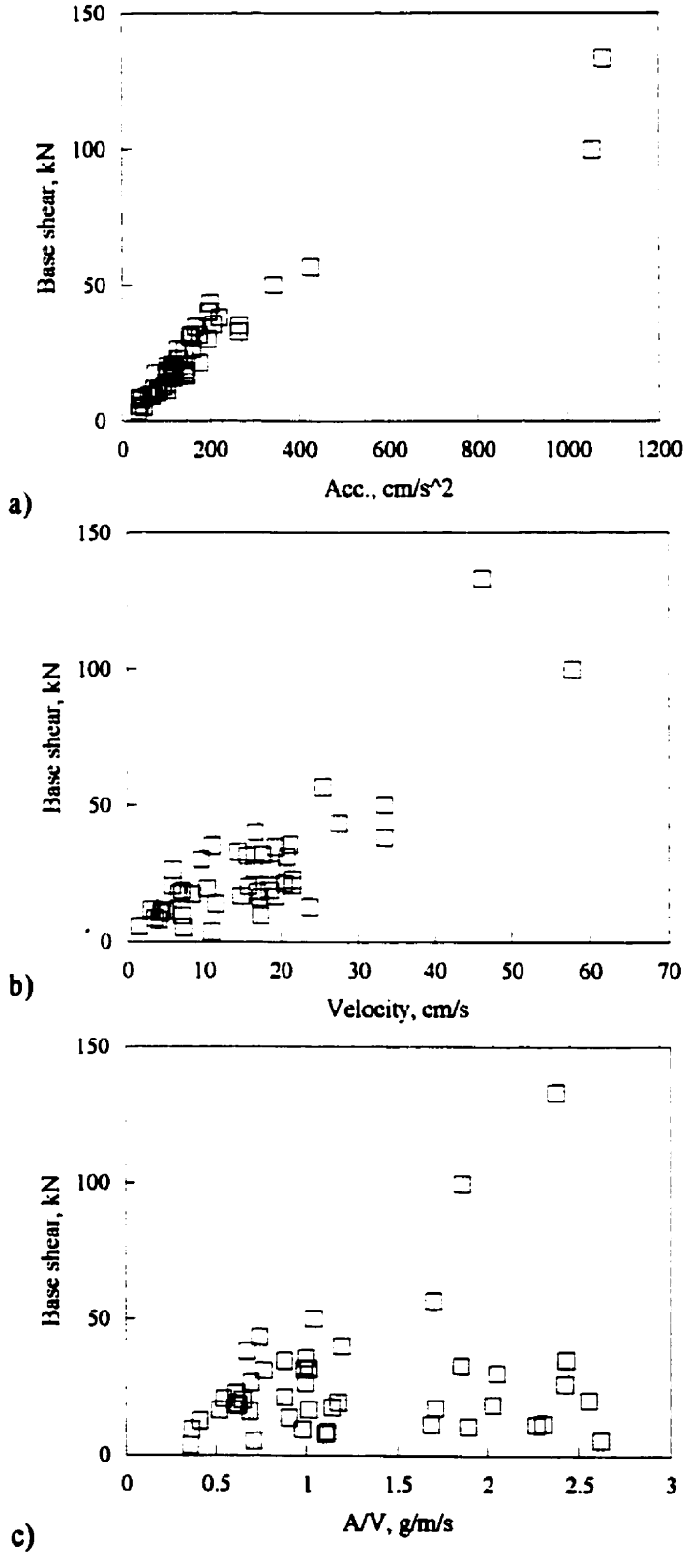

Fig. 4.3 Maximum base shear values for tower TC2

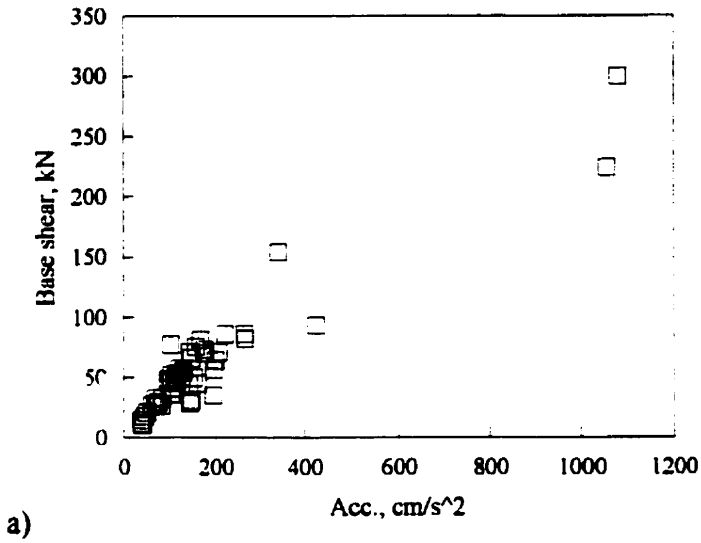

a)

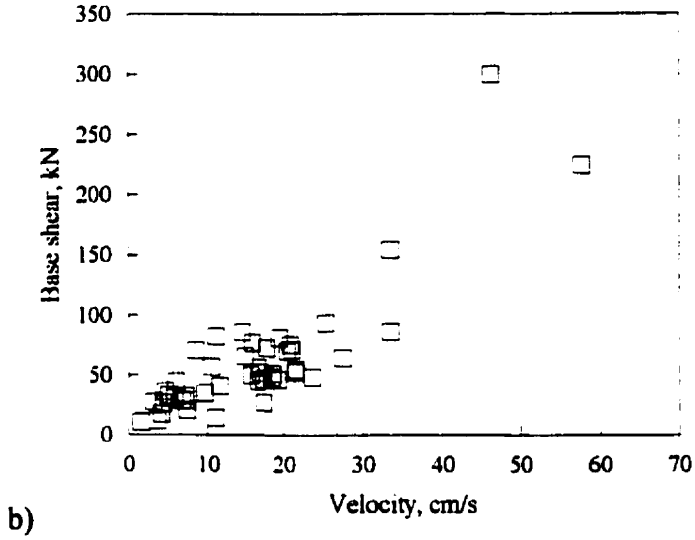

b)

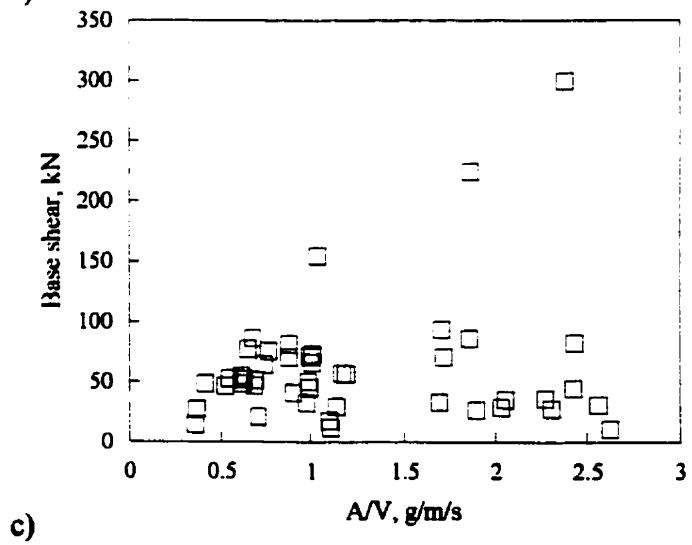

c)

Fig. 4.4 Maximum base shear values for tower TC3

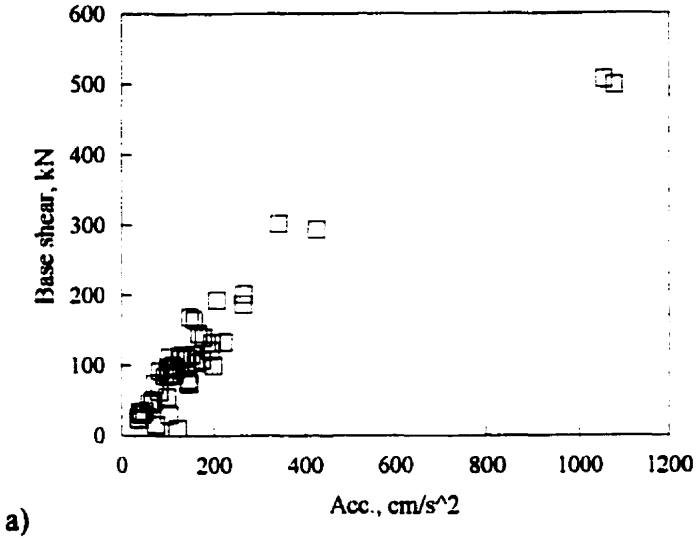

a)

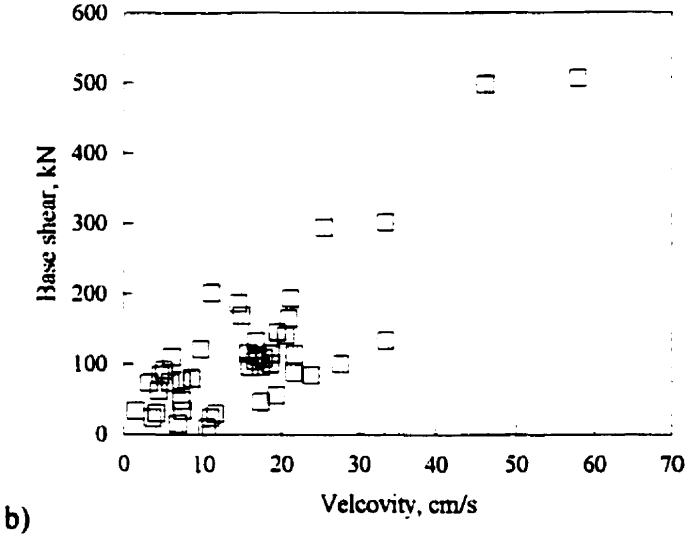

b)

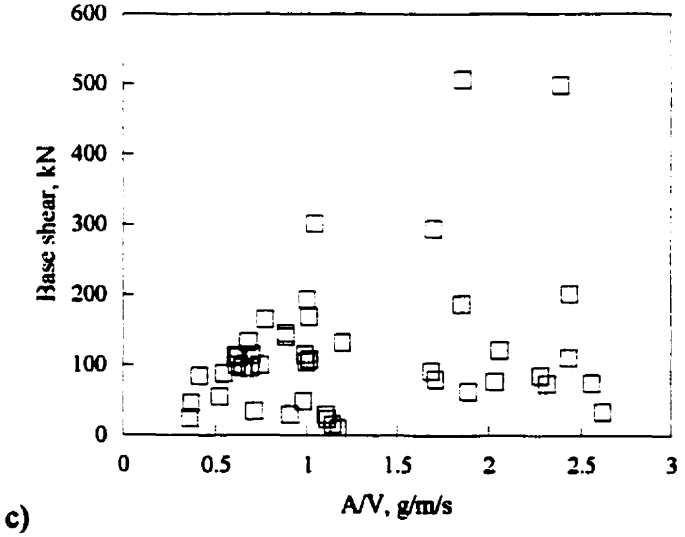

c)

Fig. 4.5 Maximum base shear values for tower TC4

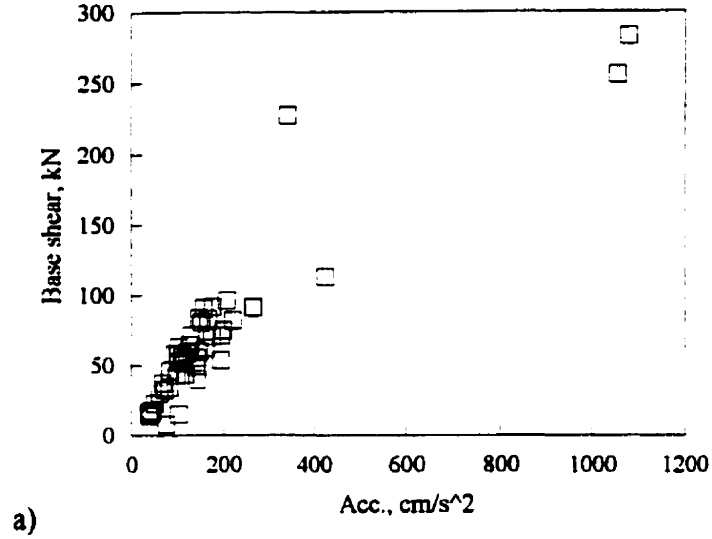

a)

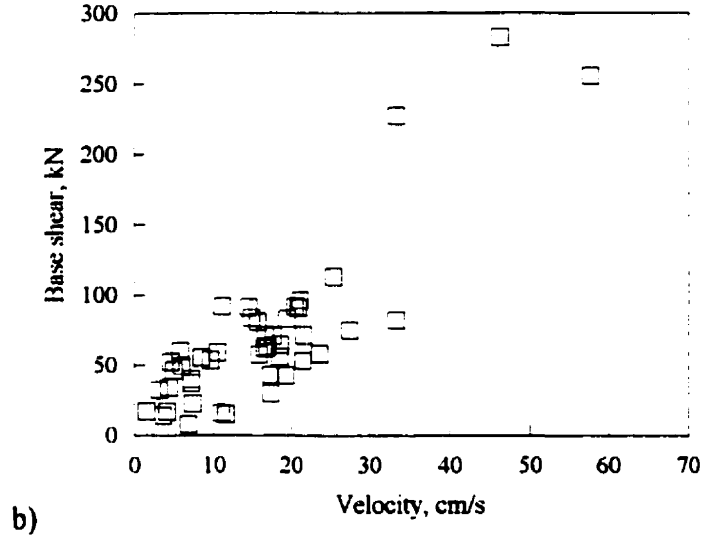

b)

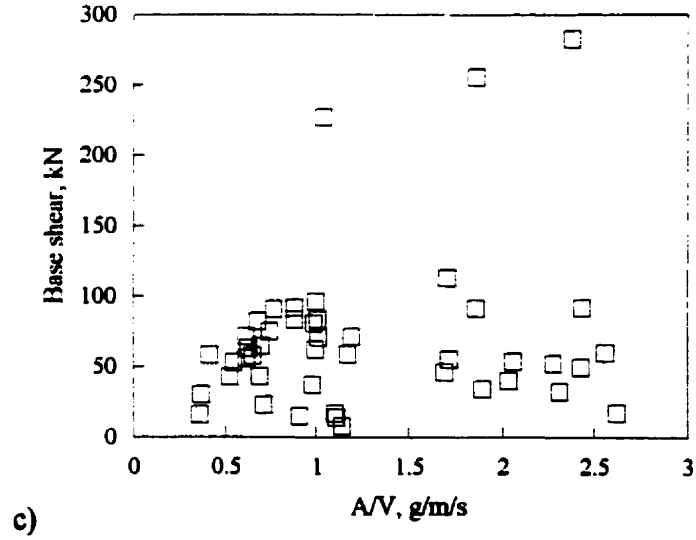

c)

Fig. 4.6 Maximum base shear values for tower TC5

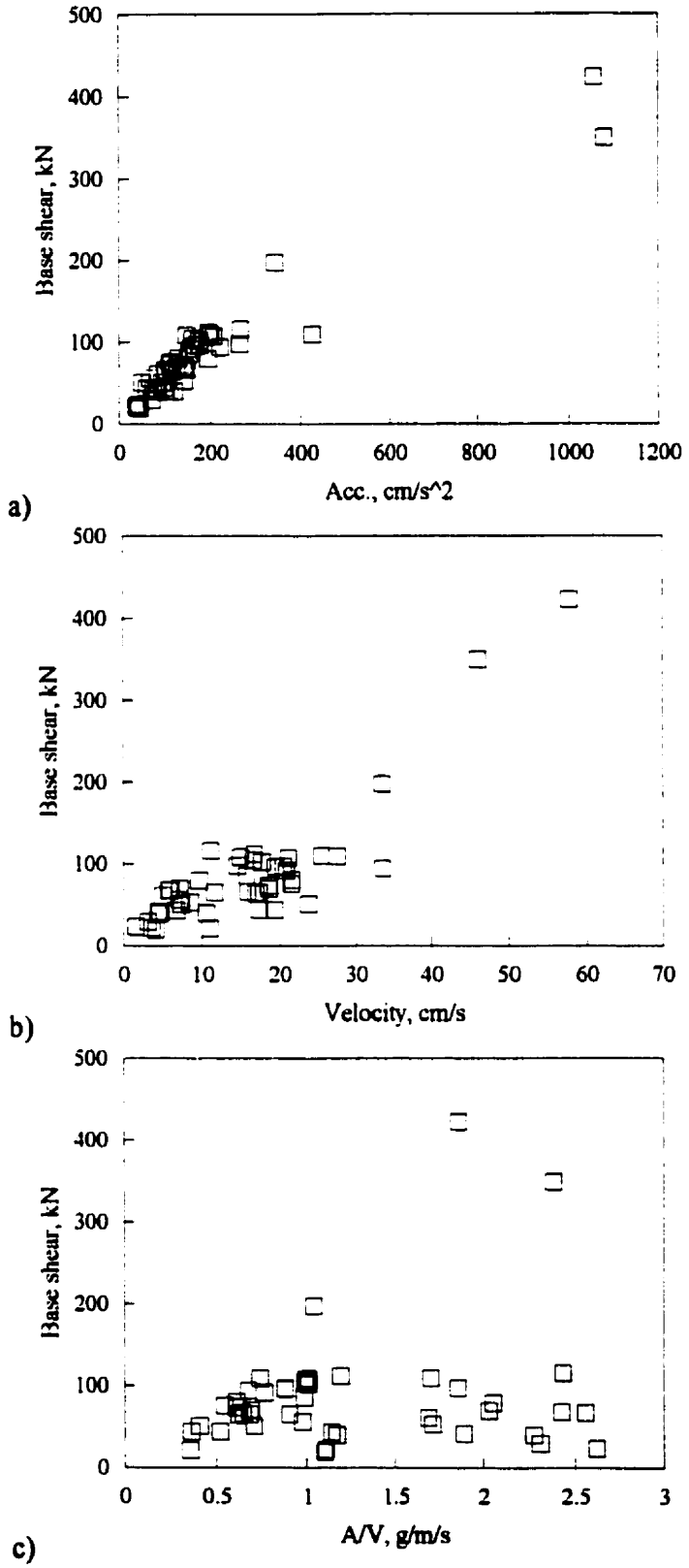

Fig. 4.7 Maximum base shear values for tower TC6

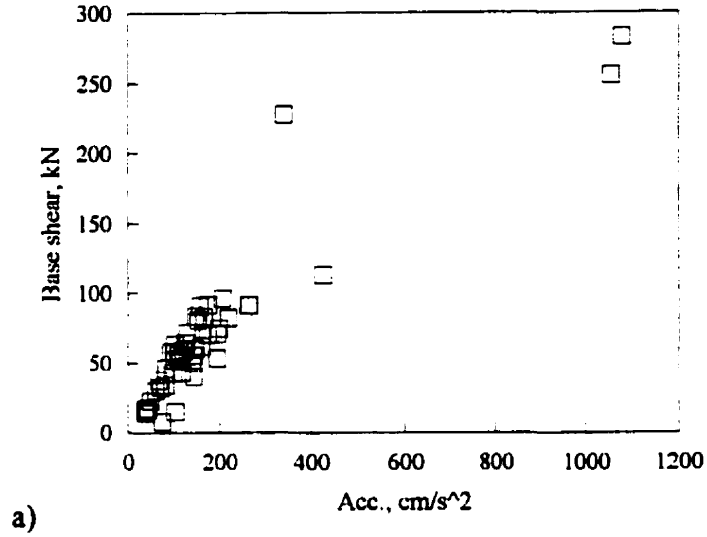

a)

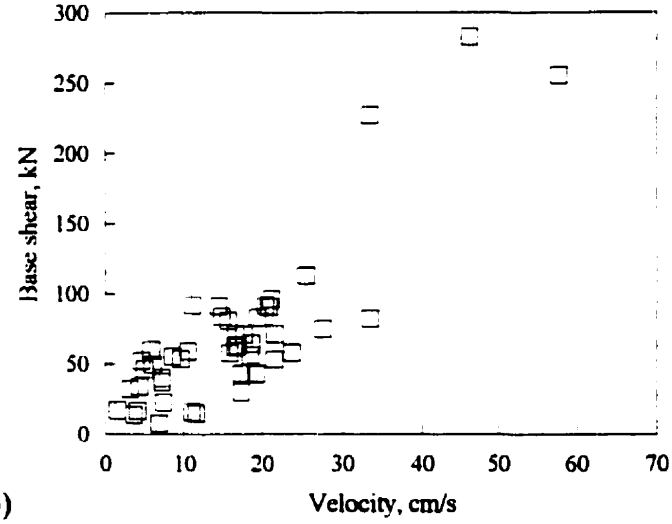

b)

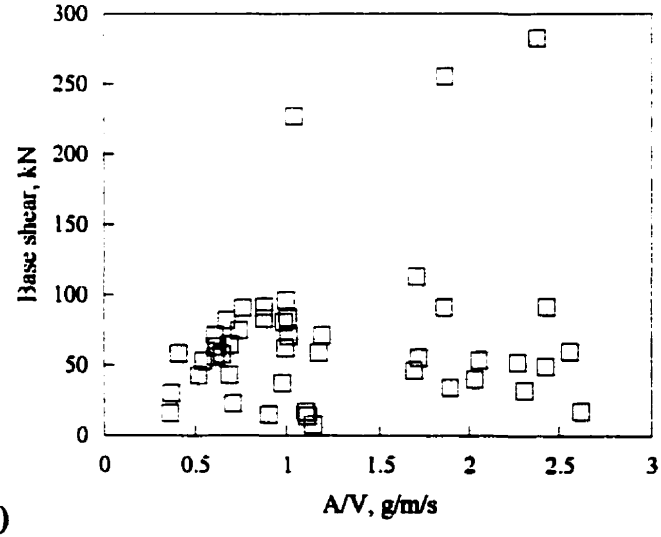

c)

Fig. 4.8 Maximum base shear values for tower TC7

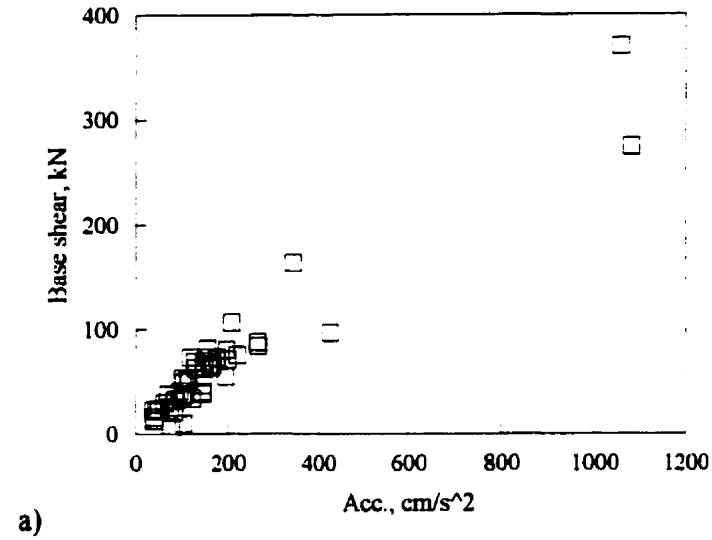

a)

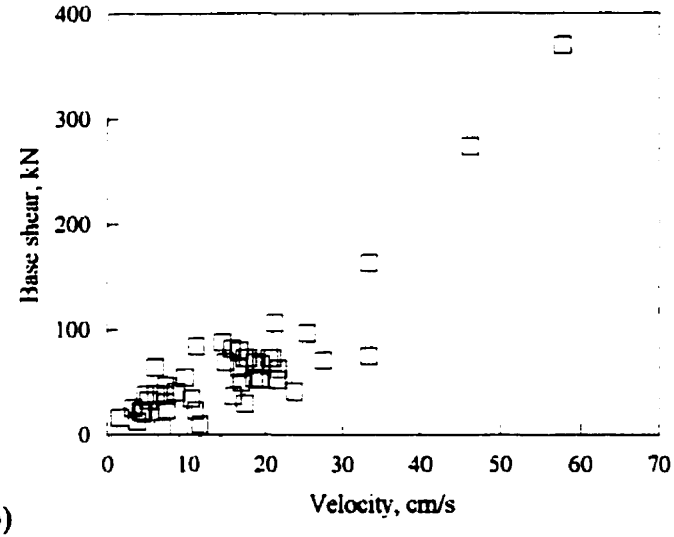

b)

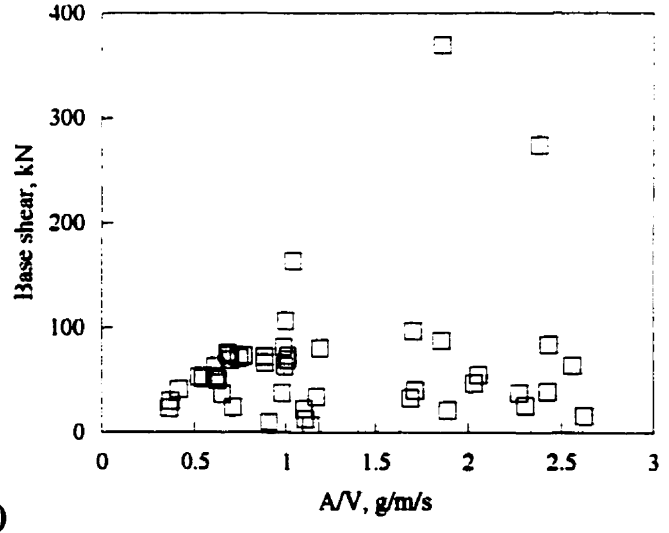

c)

Fig. 4.9 Maximum base shear values for tower TC8

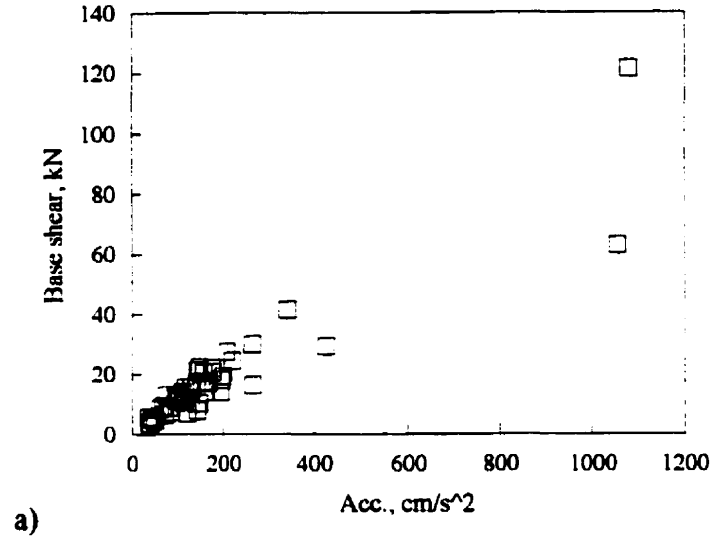

a)

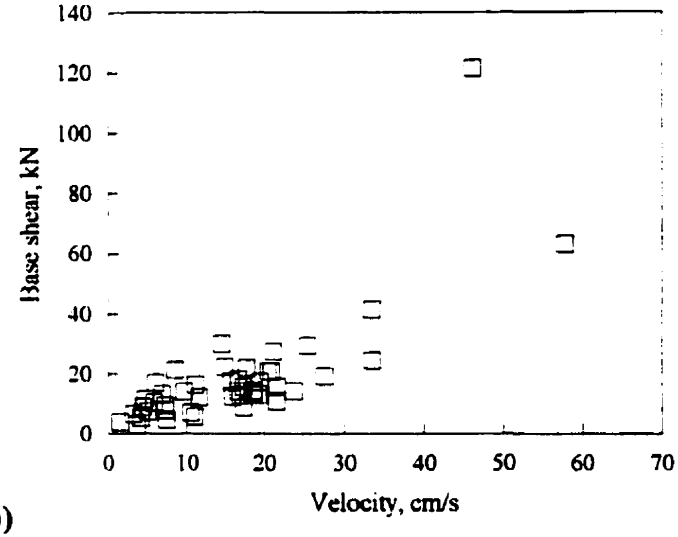

b)

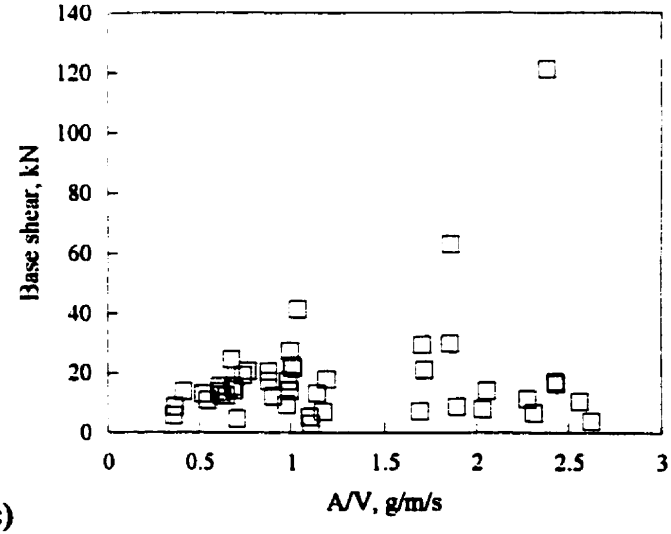

c)

Fig. 4.10 Maximum base shear values for tower TC9

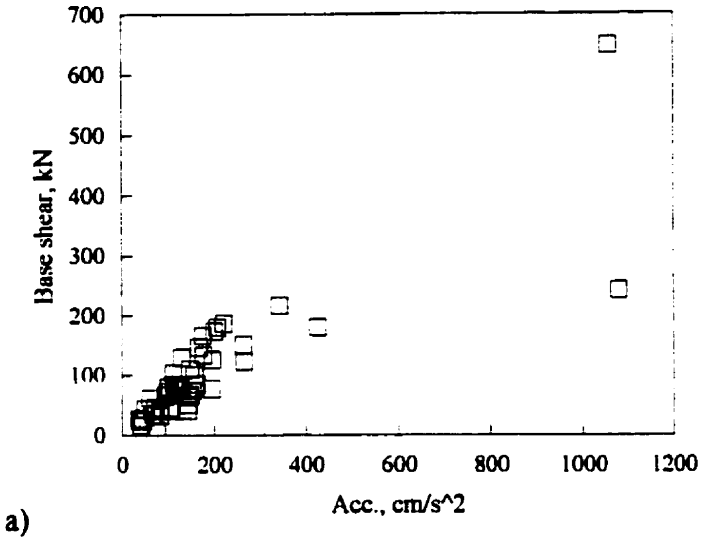

a)

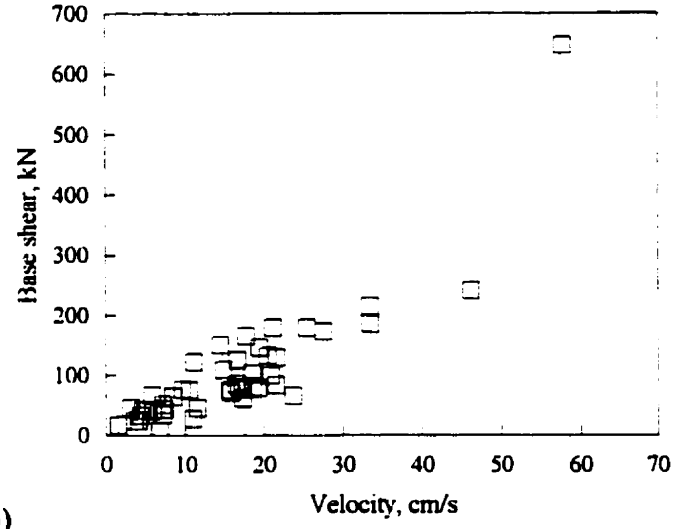

b)

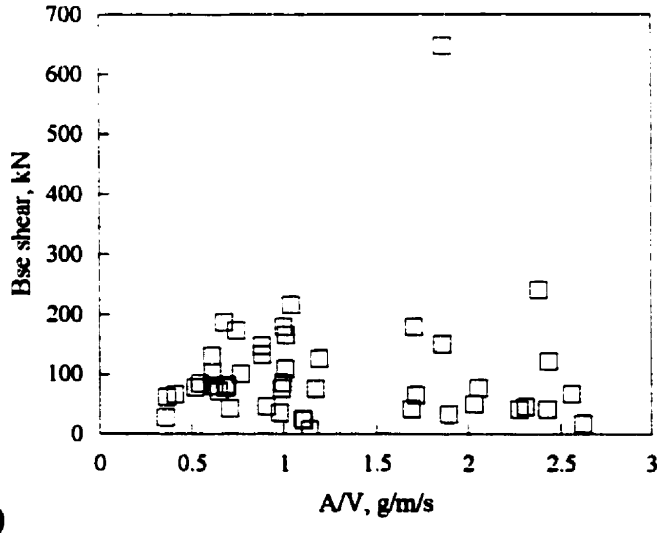

c)

Fig. 4.11 Maximum base shear values for tower TC10

For each group of results the horizontal force amplification factor (maximum base shear / tower mass x peak ground acceleration) is plotted versus the fundamental flexural period of vibration of the corresponding tower, as shown in Fig. 4.12. It is noticed that the plotted data follows a descending trend in which the tower with smallest fundamental flexural period has the largest amplification factor. Performing linear regression analysis once again, relations between the horizontal force amplification factors and the fundamental flexural period of vibration are obtained. Multiplying these factors by the mass, M, and the peak ground acceleration, A, the following expressions are obtained for estimating the maximum base shear:

$$V_h = M \times A \times (1.94 - 0.74 \times T_f) \quad \text{for low A/V ratio,} \tag{4.2}$$

$$V_h = M \times A \times (1.90 - 0.77 \times T_f) \quad \text{for intermediate A/V ratio,} \tag{4.3}$$

$$V_h = M \times A \times (1.60 - 0.90 \times T_f) \quad \text{for high A/V ratio and,} \tag{4.4}$$

$$V_h = M \times A \times (1.78 - 0.82 \times T_f) \quad \text{for the entire set} \tag{4.5}$$

where

V_h = base shear, N

M = total mass of the tower, kg

A = peak horizontal ground acceleration, m/s^2

T_f = fundamental flexural period of vibration, s.

More discussion of these results follows in section 4.6.

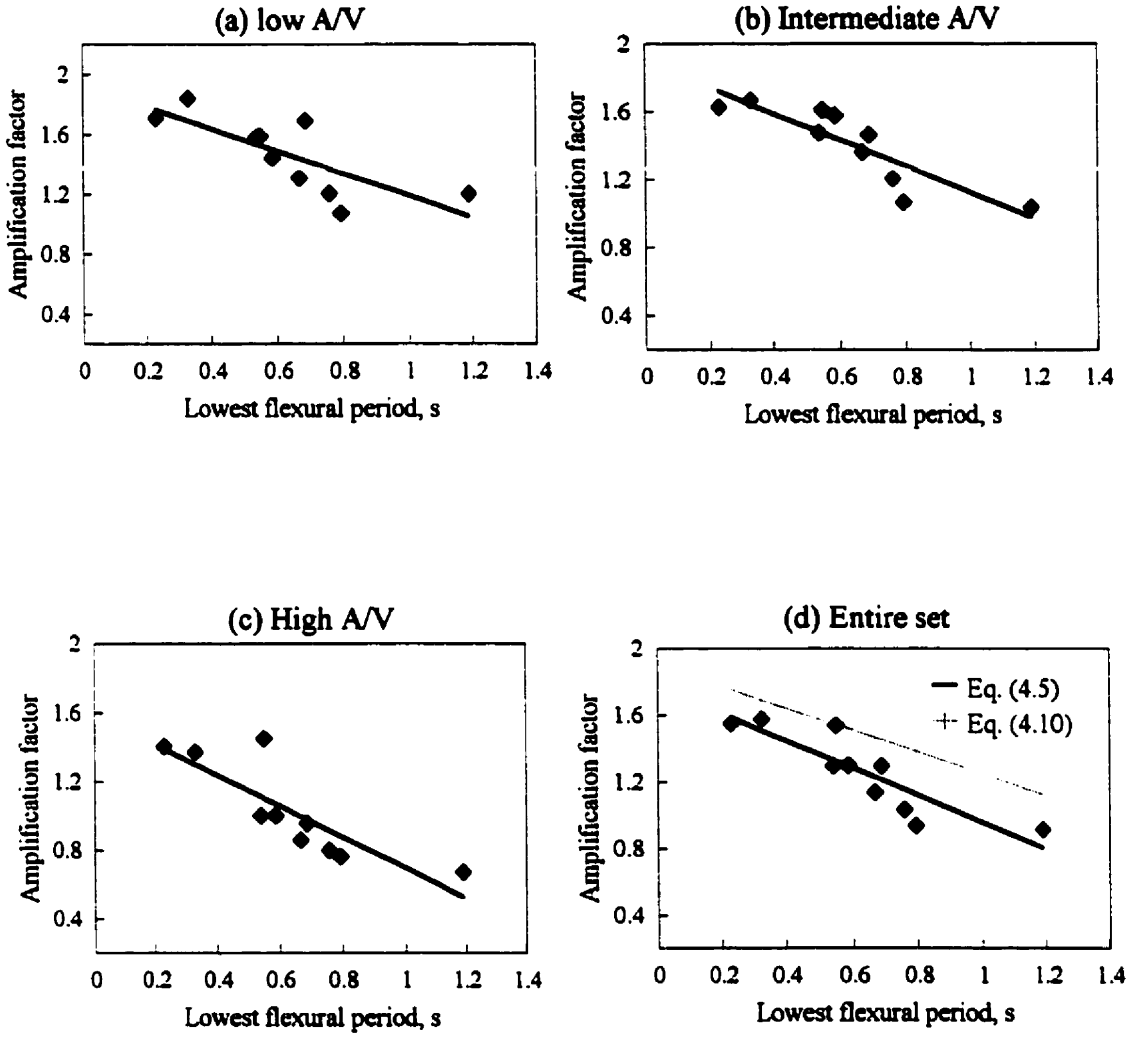

Fig. 4.12 Base shear amplification factors

4.5 Vertical Earthquake Excitation

The towers are also analyzed considering the 45 earthquakes acting in the vertical direction. The values of maximum vertical reaction at the tower base are plotted versus the peak ground acceleration, peak ground velocity and A/V ratio as before. Figs. 4.13 to 4.22 show the results obtained for the ten towers, and it is seen that a similar trend is followed by all towers. As in the case of maximum base shear the correlation between the maximum vertical reaction and both the peak ground velocity and A/V ratio does not appear very strong. However, excluding the results obtained for the record with peak ground acceleration 1.05 g (Nahanni earthquake), the relation between the vertical reaction and the peak ground acceleration follows a straight line.

Linear regression analyses are then performed and Table 4.4 summarizes the results for the ten towers. Similar to the maximum base shear, the maximum vertical reaction is divided by the product of the tower mass by peak ground acceleration in order to yield a dimensionless factor representing the importance of the dynamic amplification of the response.

Table 4.4 - Linear regression analysis for the maximum vertical reaction

	Low A/V		Inter. A/V		High A/V		Entire Set	
Tower	Slope	R^2	Slope	R^2	Slope	R^2	Slope	R^2
TC1	0.60	0.99	0.61	0.99	0.55	0.97	0.58	0.97
TC2	0.70	0.96	0.65	0.99	0.66	0.98	0.67	0.98
TC3	0.79	0.94	0.82	0.93	0.84	0.92	0.82	0.93
TC4	0.88	0.90	0.91	0.88	0.90	0.93	0.90	0.91
TC5	0.83	0.92	0.80	0.86	0.89	0.88	0.84	0.88
TC6	0.95	0.82	1.00	0.75	1.04	0.89	1.01	0.84
TC7	0.93	0.79	0.90	0.81	0.92	0.84	0.91	0.83
TC8	0.88	0.89	0.92	0.85	0.86	0.86	0.88	0.86
TC9	0.73	0.96	0.76	0.96	0.77	0.94	0.76	0.95
TC10	1.25	0.58	1.29	0.72	1.27	0.66	1.27	0.70

R value: coefficient of correlation

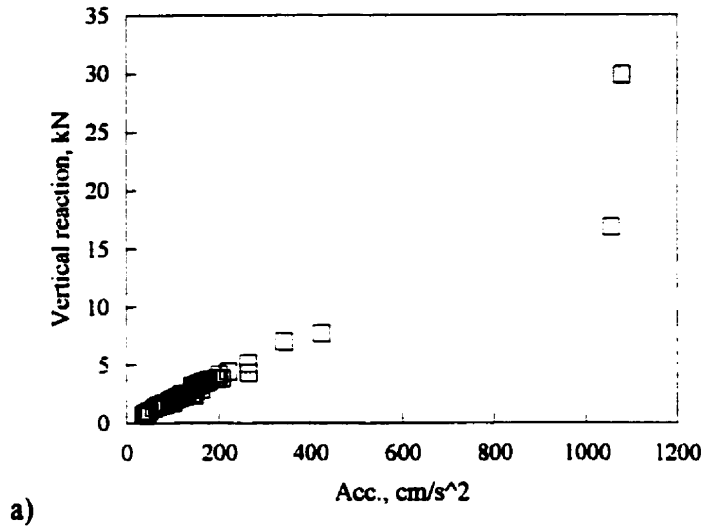

a)

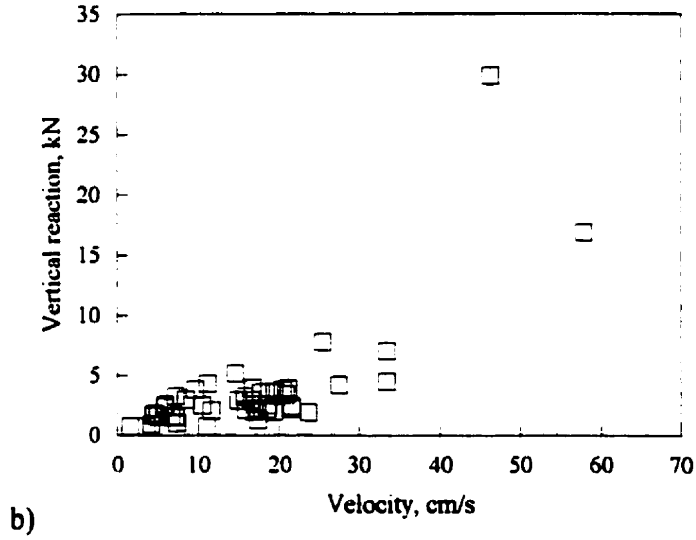

b)

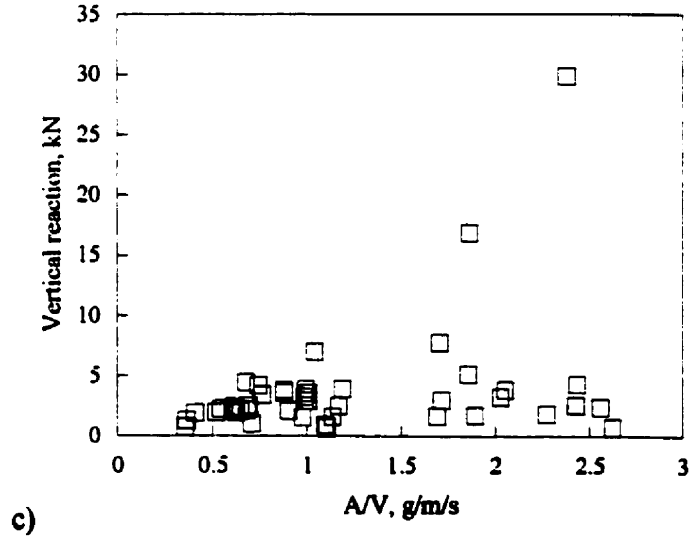

c)

Fig. 4.13 Total vertical dynamic reaction for tower TC1

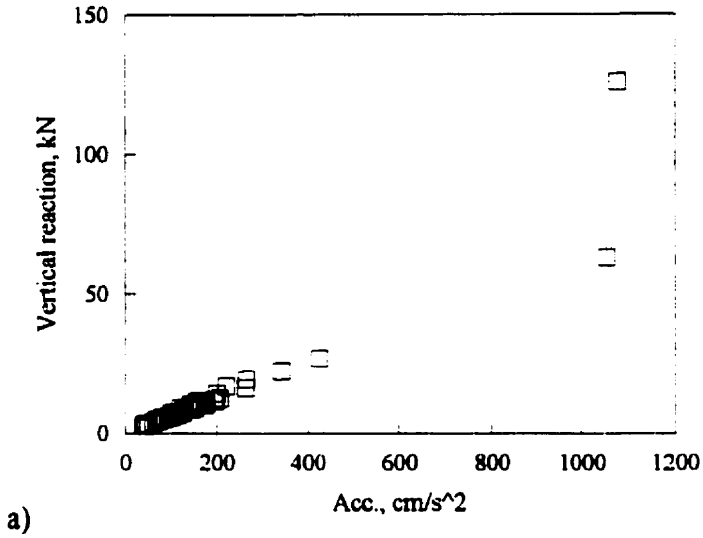

a)

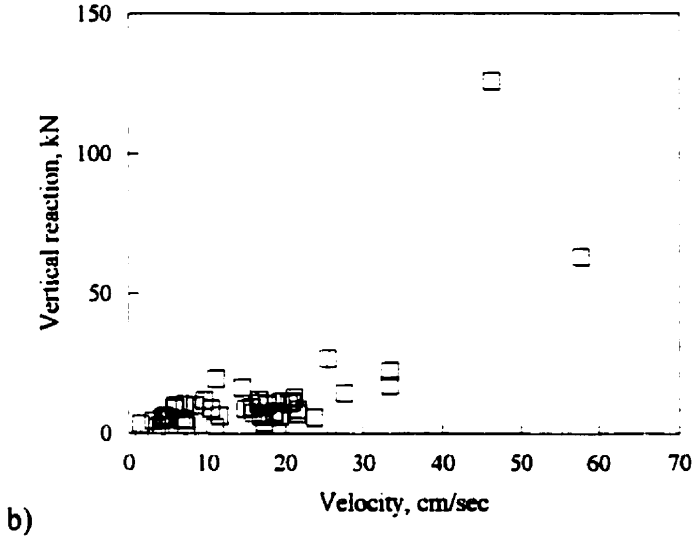

b)

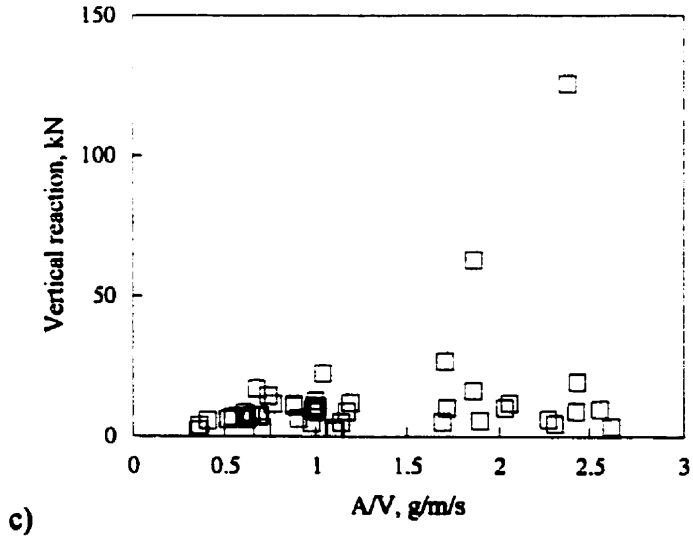

c)

Fig. 4.14 Total vertical dynamic reaction for tower TC2

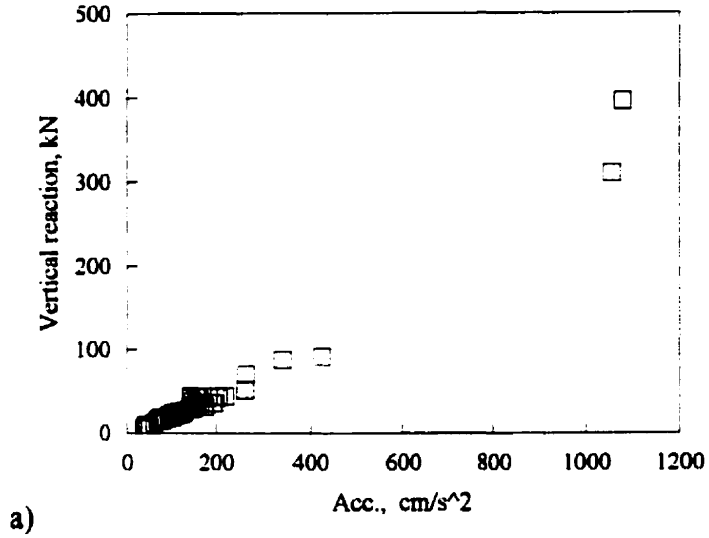

a)

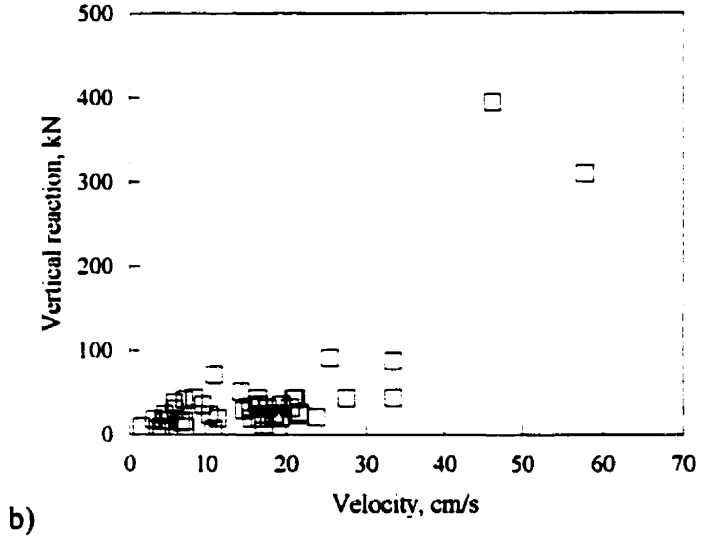

b)

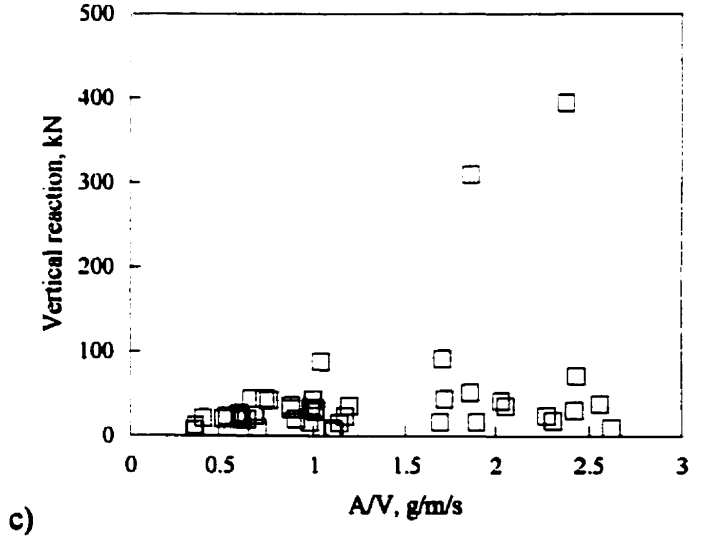

c)

Fig. 4.15 Total vertical dynamic reaction for tower TC3

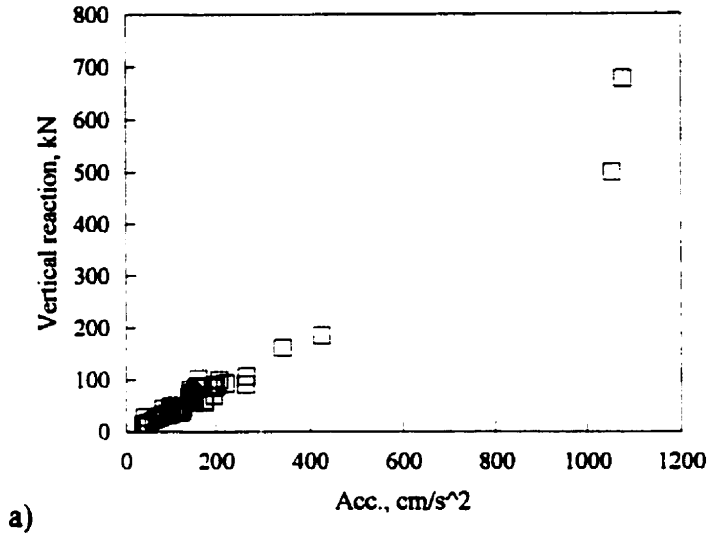

a)

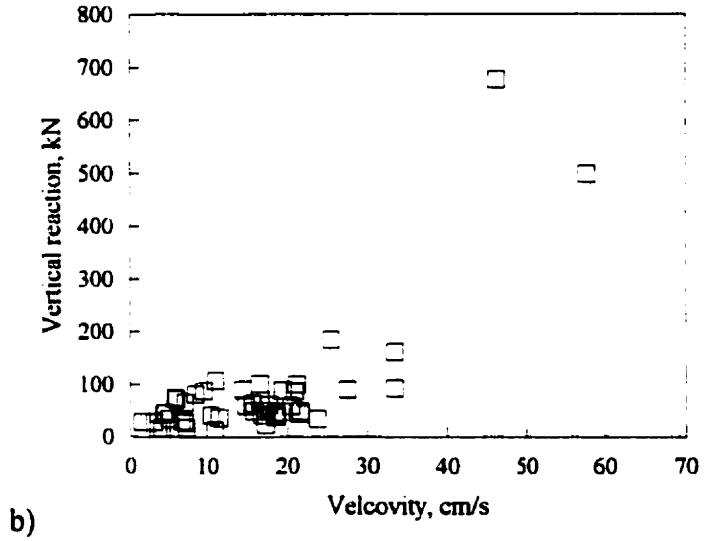

b)

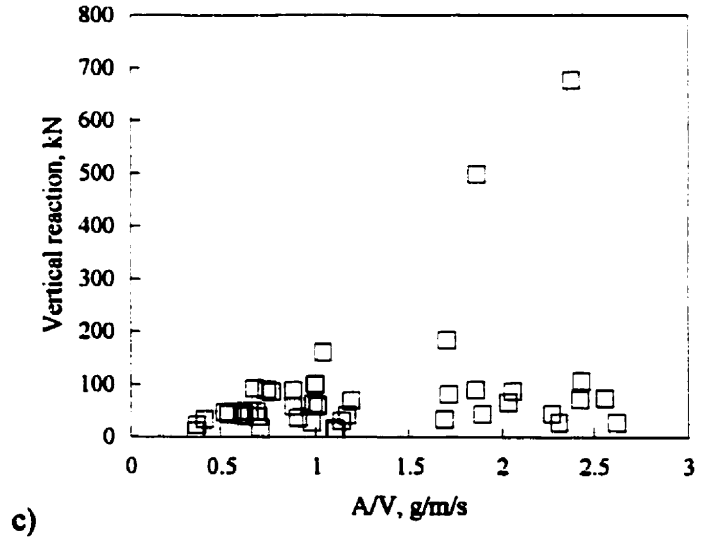

c)

Fig. 4.16 Total vertical dynamic reaction for tower TC4

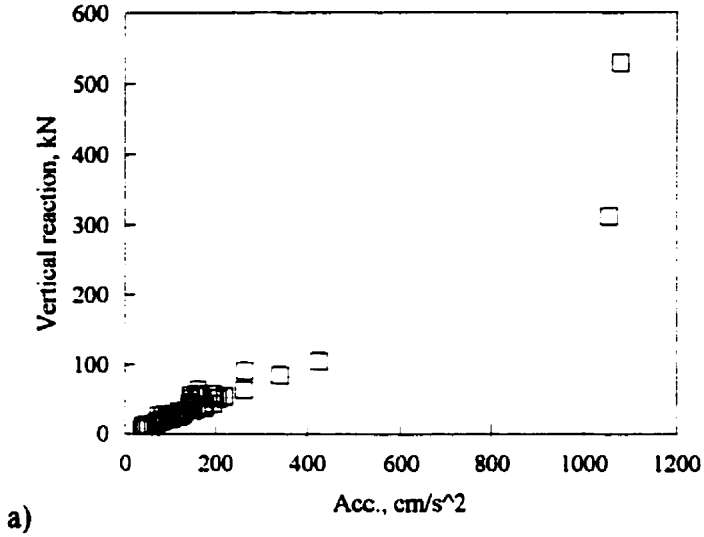

a)

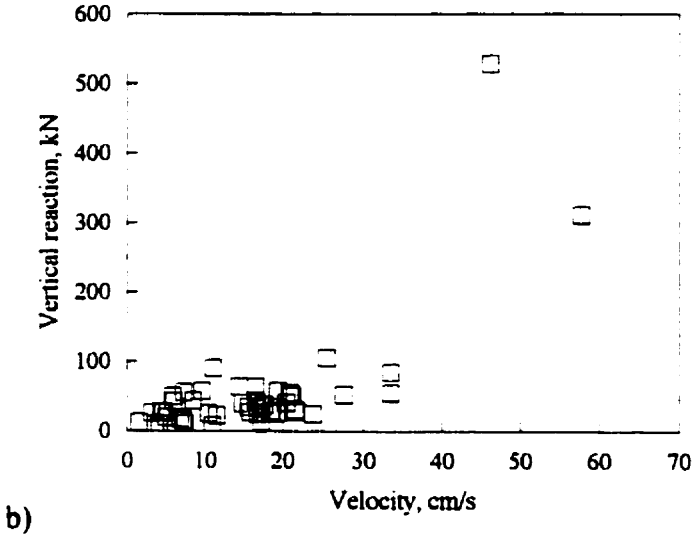

b)

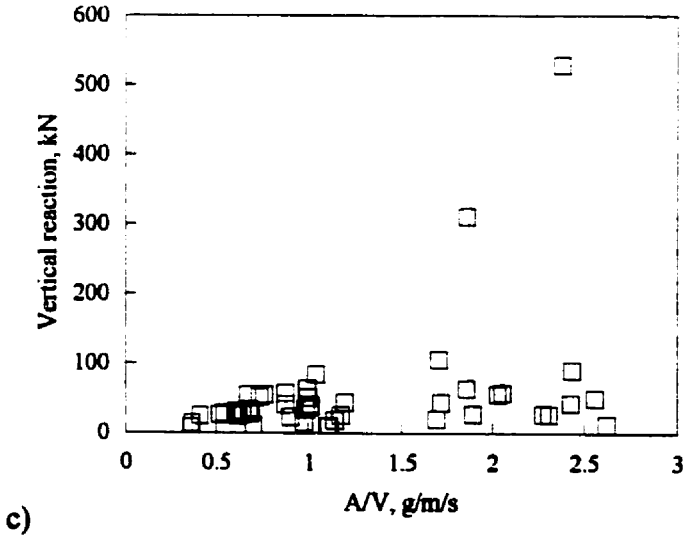

c)

Fig. 4.17 Total vertical dynamic reaction for tower TC5

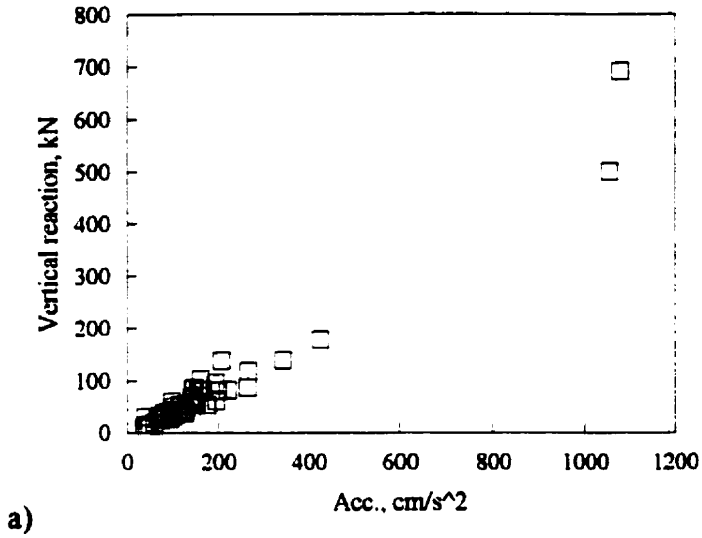

a)

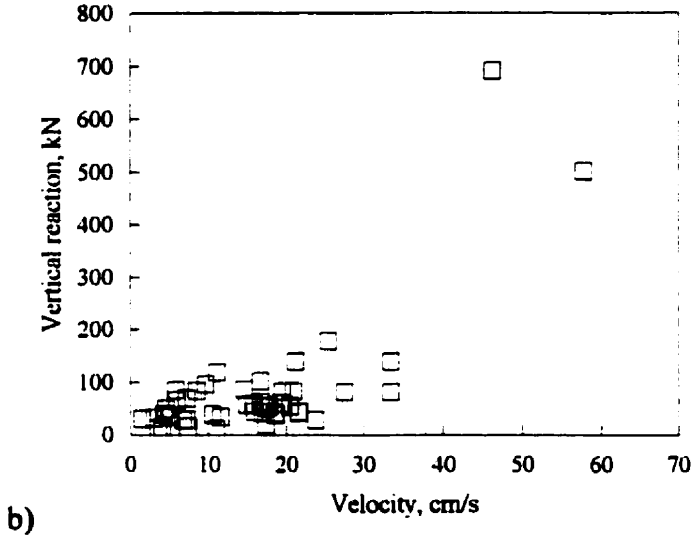

b)

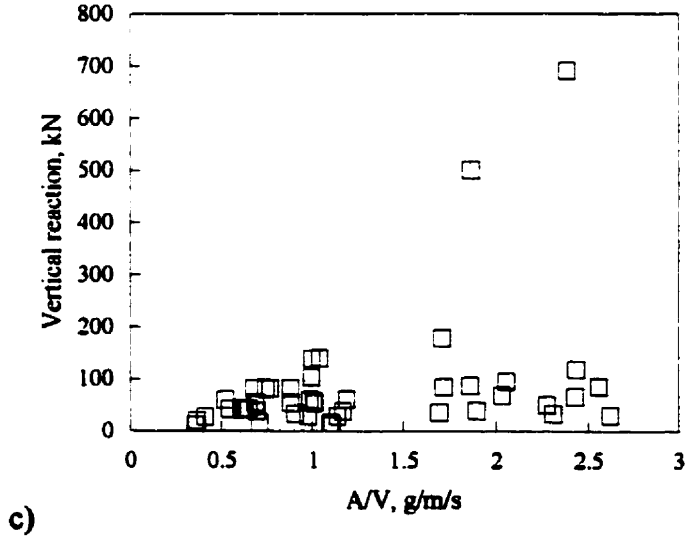

c)

Fig. 4.18 Total vertical dynamic reaction for tower TC6

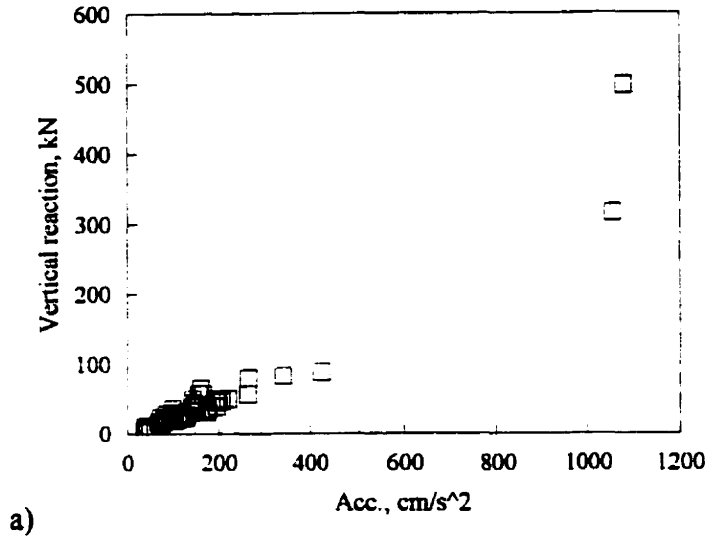

a)

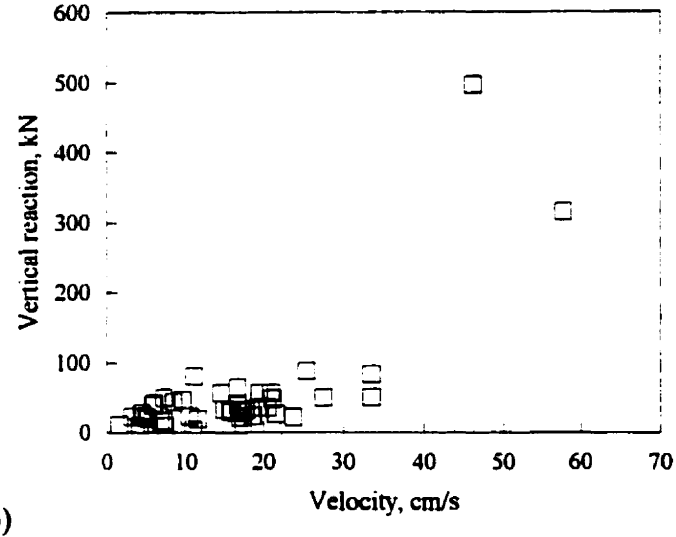

b)

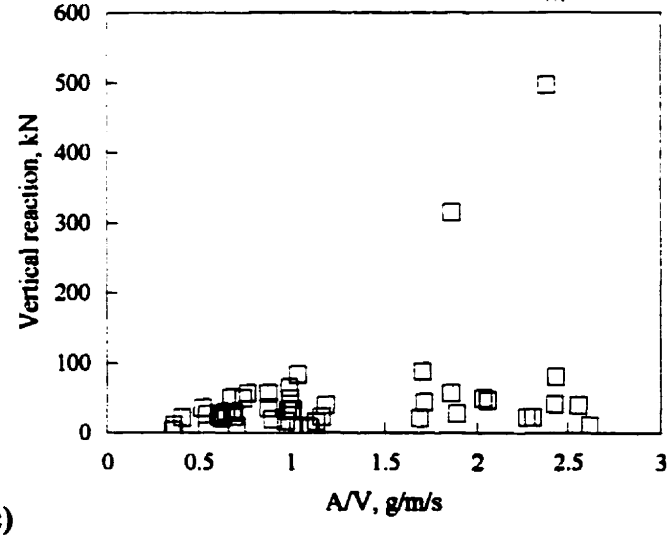

c)

Fig. 4.19 Total vertical dynamic reaction for tower TC7

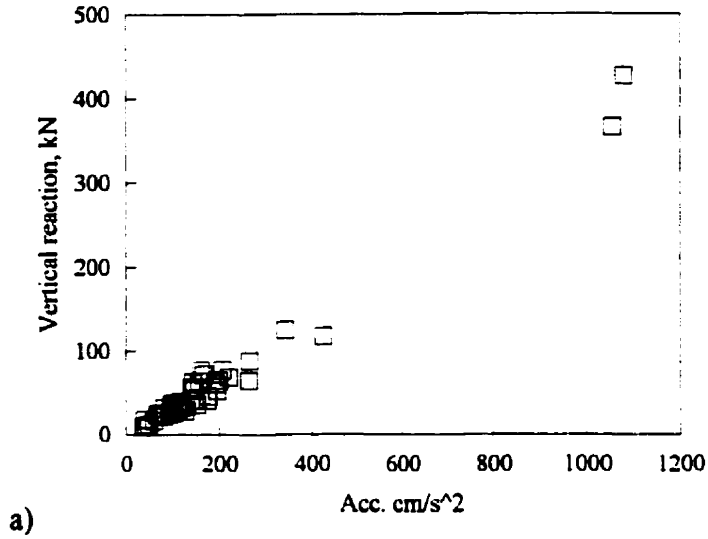

a)

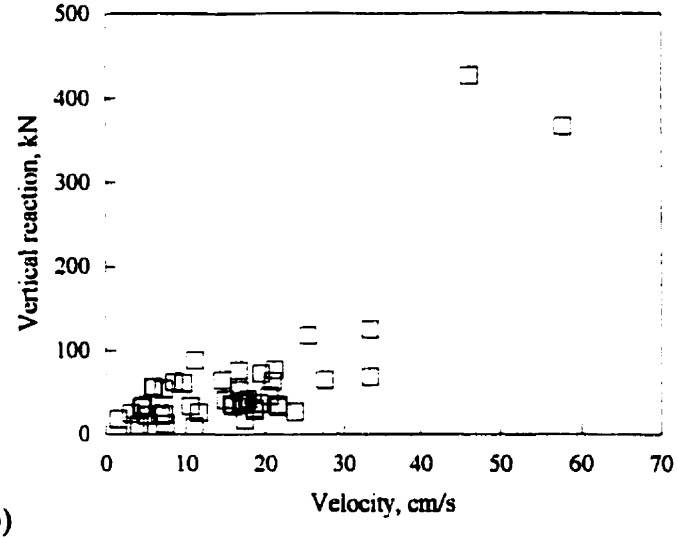

b)

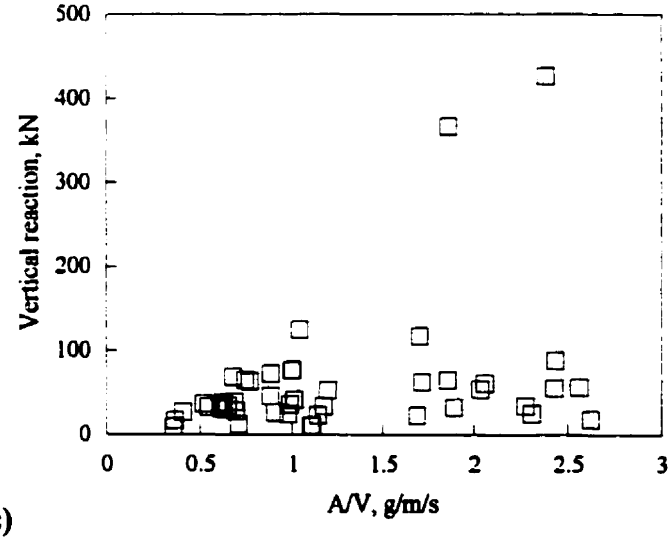

c)

Fig. 4.20 Total vertical dynamic reaction for tower TC8

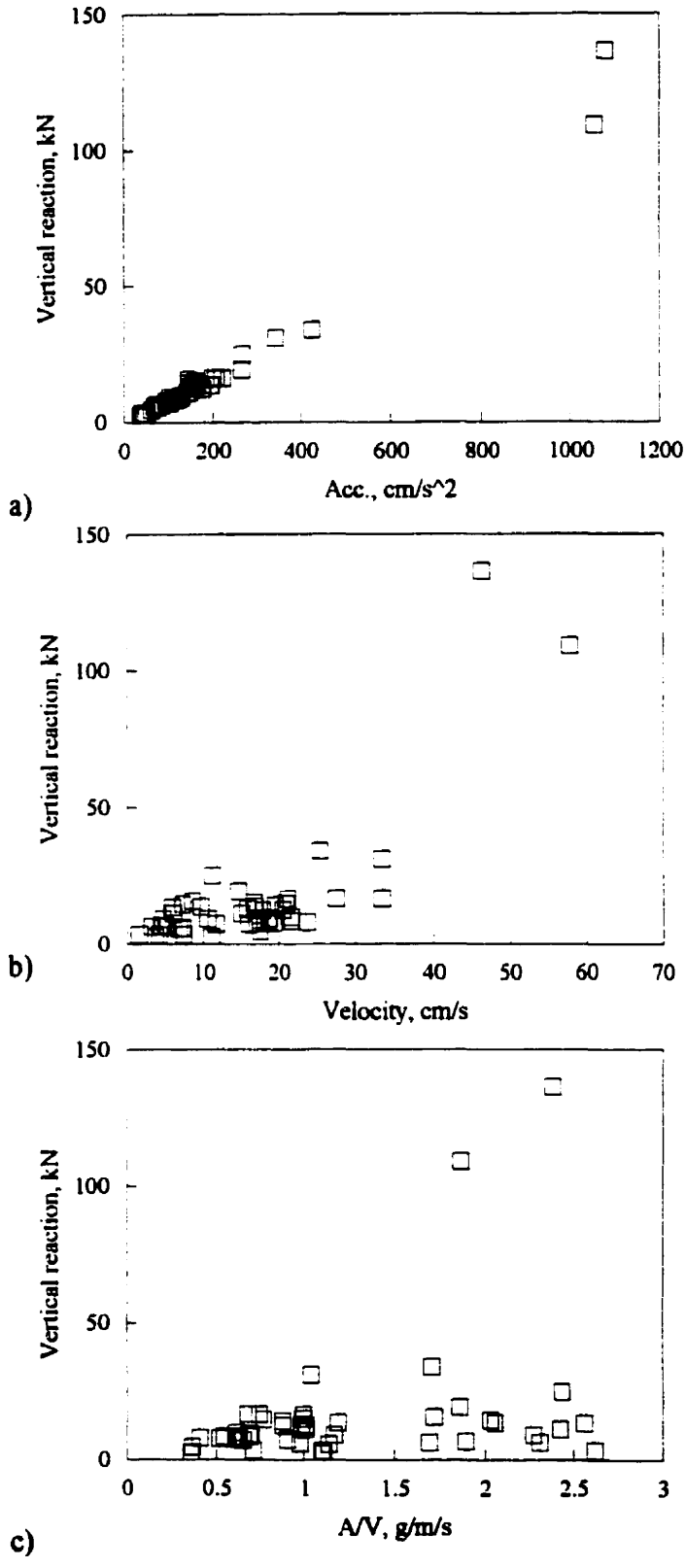

Fig. 4.21 Total vertical dynamic reaction for tower TC9

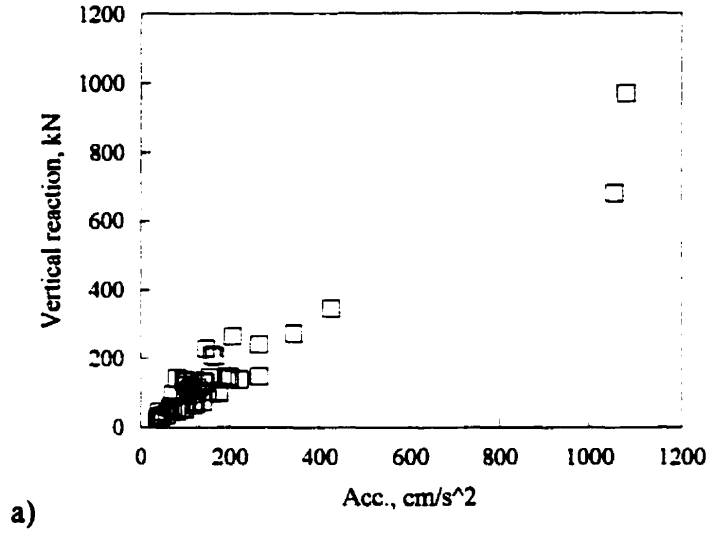

a)

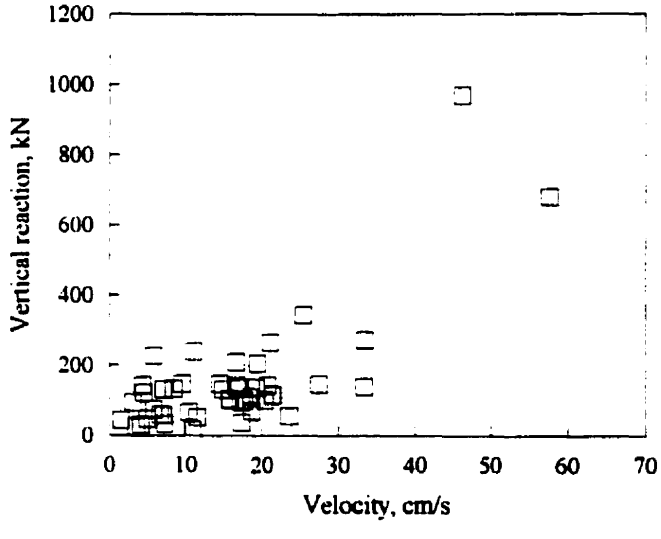

b)

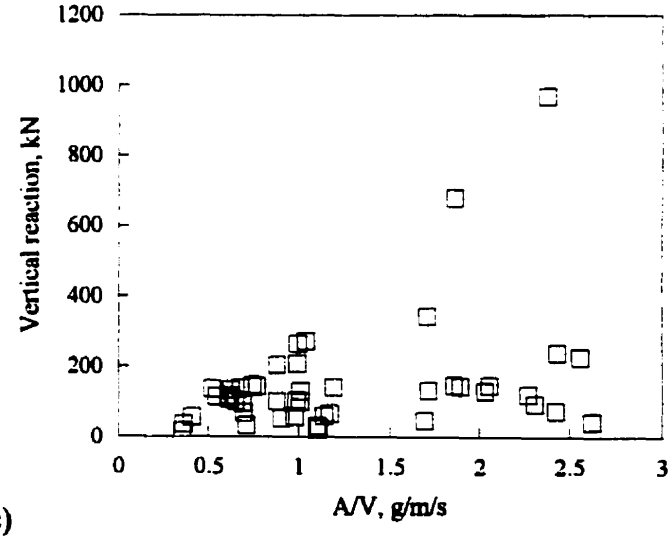

c)

Fig. 4.22 Total vertical dynamic reaction for tower TC10

The vertical force amplification factor is plotted versus the fundamental axial period of the tower, for each of the four earthquake record groups, in Fig. 4.23. Contrary to the maximum base shear response (see Fig. 4.13), the data follows an ascending trend in which the tower with lowest fundamental axial period of vibration has the smallest amplification factor. Linear regression analyses are performed following the same reasoning as in the base shear case, in order to define relations between the vertical force amplification factor and the fundamental axial period of vibration of the tower. After multiplying these factors by the tower mass, M, and the peak ground acceleration, A, the following expressions are obtained for estimating the maximum vertical reaction:

$$V_v = M \times A \times (0.36 + 6.76 \times T_a) \quad \text{for low A/V ratio,} \tag{4.6}$$

$$V_v = M \times A \times (0.31 + 7.58 \times T_a) \quad \text{for intermediate A/V ratio,} \tag{4.7}$$

$$V_v = M \times A \times (0.31 + 7.68 \times T_a) \quad \text{for high A/V ratio and,} \tag{4.8}$$

$$V_v = M \times A \times (0.32 + 7.45 \times T_a) \quad \text{for the entire set} \tag{4.9}$$

where

V_v= total maximum vertical reaction, N

A = peak horizontal ground acceleration in m/s^2

T_a = fundamental axial period of vibration, s.

It should be noted that when applying these expressions to calculate V_v, the peak ground acceleration should not be multiplied by 75% as this constant is already included in the results. A further discussion of these results is presented in section 4.6.

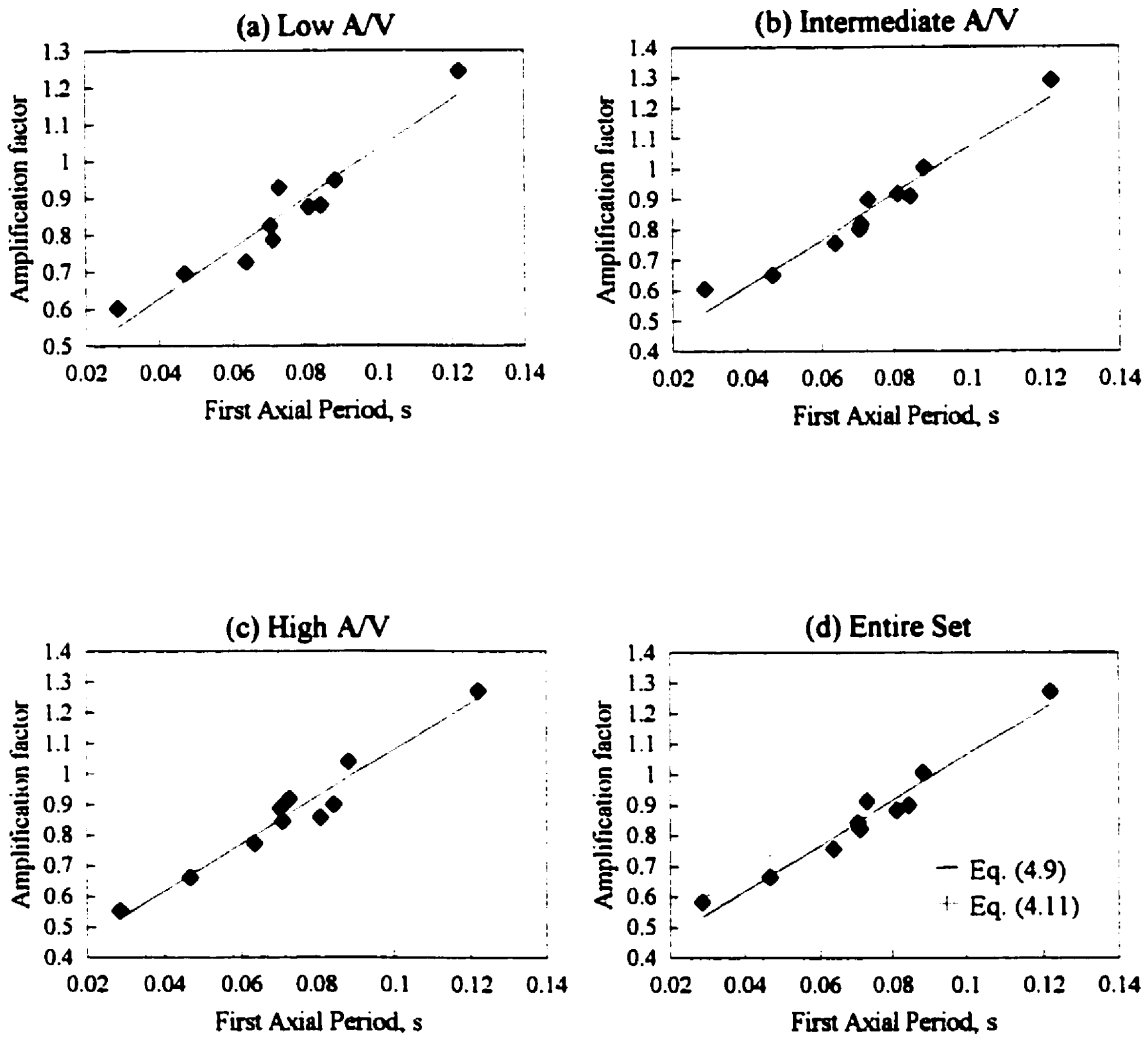

Fig. 4.23 Vertical reaction amplification factors

4.6 Discussion

From the previous results it is seen that dynamic force amplifications follow opposite trends for vertical and horizontal excitations, as a function of fundamental period of vibration. This point is clarified by studying the average acceleration response spectrum evaluated for the four series of records for 3% damping ratio, and normalized with respect to the peak ground acceleration (Fig 4.24). This figure shows three distinct regions. The first one is characterized by increasing spectral accelerations in the short period (high frequency) range of 0.05 to approximately 0.15 s (4 to 20 Hz). The second one covers a range of periods of 0.15 to 0.33 s (3 to 6 Hz) for which the spectral accelerations are maximum and remain more or less constant. Finally, the third region shows decreasing spectral accelerations for longer periods of 0.33 to 1.25 s (lower frequencies 0.8 to 3 Hz). This is in agreement with the findings for the total dynamic vertical reaction resulting from the excitation of the fundamental axial modes of the tower, and the base shear resulting from the fundamental flexural modes of the towers respectively. It should be noted that several design spectra follow the same ascending-descending trends around approximately a period of 0.25 s (4 Hz), as reported by Gupta (1992).

In general, the results indicate that classifying the accelerograms with respect to their A/V ratio does not contribute to improve the accuracy of the estimated values of maximum base shear or vertical reaction. As these expressions are only for estimating the level of the dynamic forces developed in towers due to horizontal and vertical earthquake excitation, it is recommended that only the expressions for the entire set be used. The values of the maximum base shear and total vertical reaction estimated using eqs. (4.5) and (4.9) are drawn in Figs. 4.25 and 4.26, respectively, with the values obtained from

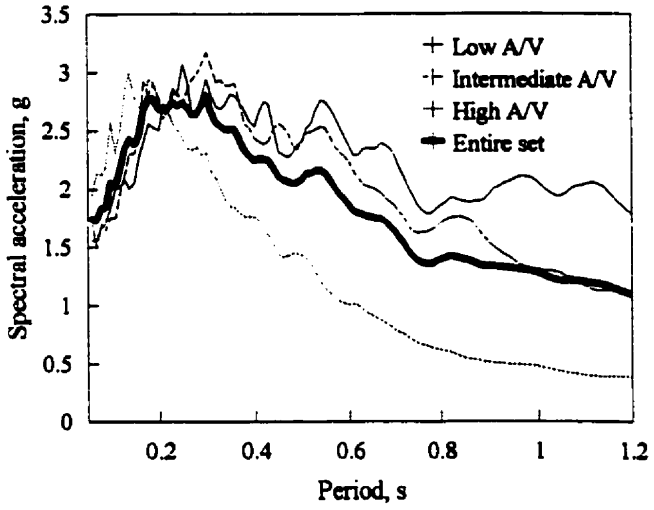

Fig. 4.24 Acceleration response spectra evaluated for 3% damping

detailed dynamic analyses for TC3. Similar graphs are presented in Appendix B for the nine remaining towers. In order to obtain an upper bound to the expected level of dynamic forces, one standard deviation is added to the numerical factors of eqs. (4.5) and (4.9) to yield the following expressions:

$$V_h = M \times A \times (1.91 - 0.66 \times T_f) \tag{4.10}$$

$$V_v = M \times A \times (0.36 + 8.01 \times T_a) \tag{4.11}$$

These upper bound values of the amplification factors obtained are drawn in Figs. 4.25 and 4.26, for comparison with those obtained using the average parameters of the regressions in eqs. (4.5) and (4.9), respectively.

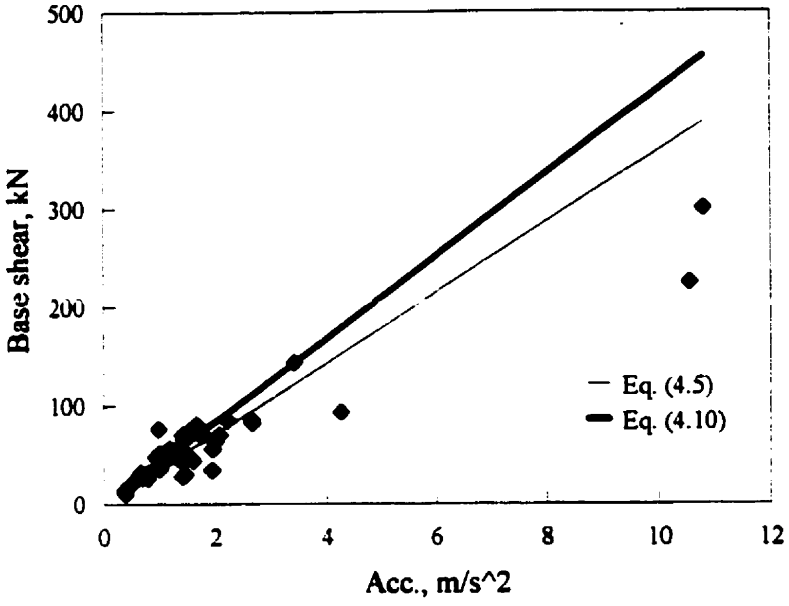

Fig. 4.25 Maximum base shear vs. peak ground acceleration in TC3

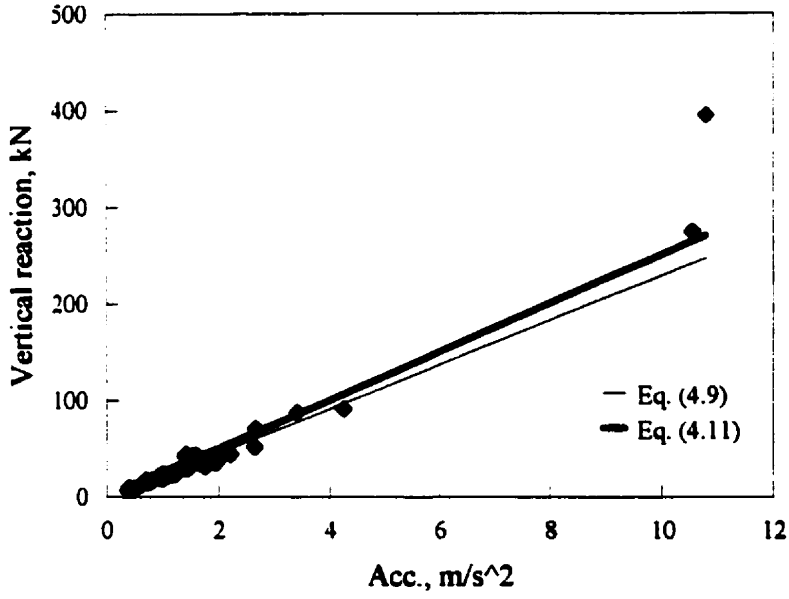

Fig. 4.26 Maximum dynamic vertical reaction vs. peak ground acceleration in TC3

4.7 Conclusions

In this chapter two expressions were proposed to estimate the values of the maximum base shear and total vertical reaction of self-supporting telecommunication lattice towers, based on the tower mass and fundamental periods (lateral and axial) and on the peak horizontal acceleration at the tower site. These expressions are valid for towers with regular geometry and heights up to 120 m. They have not been verified for taller towers but it is expected that the trends should be similar. Furthermore, it is important to realize that these expressions are not proposed for detailed member design purposes but only as an approximate method to assess the seismic sensitivity of towers in the preliminary design phase.

These simple seismic response indicators may help tower designers decide whether dynamic loads are likely to influence the final design and consequently whether more refined analysis (either static or dynamic) is necessary.

As a further step in the seismic analysis of telecommunication towers, the next chapter proposes a simplified equivalent static method of analysis. The method will deal with both horizontal and vertical earthquake excitations.

CHAPTER 5

PROPOSED STATIC METHOD OF ANALYSIS

5.1 Theoretical Background

As was mentioned in Chapter 1, this study is based on the modal analysis method and the response spectrum approach. A quick review of the equation of motion, the response spectrum approach and modal analysis theory is presented hereafter for completeness.

5.1.1 Equation of motion and response spectrum

The equation of motion of a discrete parameter single-degree-of-freedom system (SDOF) under the effect of base excitation is given by:

$$m\ddot{u}(t) + c\dot{u}(t) + ku(t) = -m\ddot{y}_s(t) \tag{5.1}$$

where

$\ddot{y}_s$ = the base acceleration

m = mass

k = stiffness

c = viscous damping constant

$\ddot{u}, \dot{u}$ and u = relative acceleration, velocity and displacement respectively, with respect to the moving base, and are functions of time t.

This equation can be solved using Duhamel's integral, and the solution is given by:

$$u(t) = \frac{1}{m\omega_D} \int_0^t -m\ddot{y}_s(\tau) e^{-\zeta\omega(t-\tau)} \sin\omega_D(t-\tau) d\tau \tag{5.2}$$

where

ξ= is the viscous damping ratio = $\frac{c}{2\omega m}$

ω and ω_D = undamped and damped circular frequency of vibration respectively, in rad/s.

For small damping ratios (ξ<0.10, $\omega_D \simeq \omega$), this equation can be written in the form:

$$u(t) = \frac{1}{\omega}\int_0^t \ddot{y}_s(\tau)e^{-\xi\omega(t-\tau)}\sin\omega(t-\tau)d\tau \tag{5.3}$$

Taking the first derivative of (5.3) with respect to time:

$$\dot{u}(t) = \int_0^t \ddot{y}_s(\tau)e^{-\xi\omega(t-\tau)}\cos\omega(t-\tau)d\tau - \xi\int_0^t \ddot{y}_s(\tau)e^{-\xi\omega(t-\tau)}\sin\omega(t-\tau)d\tau \tag{5.4}$$

Substituting the previous two equations into the forced equation of motion given by:

$$\ddot{u}^t(t) = -2\omega\xi\dot{u}(t) - \omega^2 u(t) \tag{5.5}$$

The expression for the absolute acceleration, $\ddot{u}^t$, is then given as:

$$\begin{aligned}\ddot{u}^t(t) = \omega(2\xi^2 - 1)\int_0^t \ddot{y}_s(\tau)e^{-\xi\omega(t-\tau)}\sin\omega(t-\tau)d\tau - \\ 2\omega\xi\int_0^t \ddot{y}_s(\tau)e^{-\xi\omega(t-\tau)}\cos\omega(t-\tau)d\tau\end{aligned} \tag{5.6}$$

The absolute maximum values of the quantities given by (5.3), (5.4) and (5.6) are the spectral relative displacement $S_d(\xi,T)$, the spectral relative velocity $S_v(\xi,T)$, and the spectral absolute acceleration $S_a(\xi,T)$, respectively. It is now beneficiary to introduce a new spectral value, the spectral pseudo-velocity $S_{pv}(\xi,T)$:

$$S_{pv}(\xi, T) = \left|\int_0^t \ddot{y}_s(\tau)e^{-\xi\omega(t-\tau)}\sin\omega(t-\tau)d\tau\right|_{\max} \tag{5.7}$$

The relative spectral displacement is given by:

$$S_d(\xi, T) = \frac{1}{\omega}S_{pv}(\xi, T) \tag{5.8}$$

For small damping ratios (ξ<0.10) the absolute spectral acceleration can be written in terms of the pseudo-velocity as:

$$S_a(\xi, T) \simeq \omega S_{pv}(\xi, T) \tag{5.9}$$

which is called the pseudo-acceleration and is denoted as $S_{pa}(\xi,T)$. The pseudo-acceleration can be used to estimate the maximum elastic force, f_s, developed during the earthquake using the relation $k = \omega^2 m$:

$$f_s = k S_d(\xi, T) = m S_{pa}(\xi, T) \tag{5.10}$$

5.1.2 Modal analysis

The total displacement, u, of any linear system can be evaluated using the sum of the modal components as follows:

$$u(x,t) = u_1(x,t) + u_2(x,t) + u_3(x,t) + ... \tag{5.11}$$

One can rewrite the previous equation so as to separate the two variables in the following form:

$$u(x,t) = \phi_1(x)y_1(t) + \phi_2(x)y_2(t) + \phi_3(x)y_3(t) + ... \tag{5.12}$$

where $\phi(x)$ is a function of position only, while $y(t)$ is a function of time only. The main objective of this separation of variables is to transform the continuous or the multi-degree-of-freedom (MDOF) system to a set of uncoupled algebraic equations representing SDOF systems. The total response of the system can be obtained by solving these equations using the mode shapes of the total structure. Throughout the course of this work the cantilever models were assumed to be continuous rather than lumped parameter systems which means that the mode shapes and mass distributions are given in closed form expressions. Therefore, it is only necessary to further discuss the seismic response of continuous system.

5.1.3 Seismic response of continuous systems

The equation of motion of a continuous system can be expressed in the following form:

$$f_I(x,t)+f_D(x,t)+f_S(x,t)=0 \tag{5.13}$$

The terms in the previous expression are inertia force, damping force and elastic force respectively. Restricting the displacement of this system to a single shape, mode shape i for instance, as described in section 5.1.2, and applying a virtual displacement of the form:

$$\delta u=\phi_i(x)\delta y \tag{5.14}$$

equation (5.13) is reduced to:

$$f_{I,i}\delta y+f_{D,i}\delta y+f_{S,i}\delta y=0 \tag{5.15}$$

where

$$f_{I,i}=\int_0^1 f_I(x,t)\phi_i(x)dx \tag{5.16}$$

$$f_{D,i}=\int_0^1 f_D(x,t)\phi_i(x)dx \tag{5.17}$$

$$f_{S,i}=\int_0^1 f_S(x,t)\phi_i(x)dx \tag{5.18}$$

are the generalized inertia force, the generalized damping force and the generalized elastic force for mode i respectively. Both damping and elastic forces depend only on the relative motion of the system. However, inertia forces depend on the total acceleration and are given by:

$$f_I(x,t)=m(x)\phi_i(x)\ddot{y}(t)+m(x)\ddot{y}_s(t) \tag{5.19}$$

Substituting (5.19) into (5.16) the generalized inertia forces can be expressed as follows:

$$f_{I,i}=\ddot{y}(t)\int_0^1\phi_i(x)m(x)\phi_i(x)dx+\ddot{y}_s(t)\int_0^1 m(x)\phi_i(x)dx=\ddot{y}(t)M_i+\ddot{y}_s(t)L_i \tag{5.20}$$

in which M_i and L_i are the generalized mass and the excitation factor for mode i. The expressions for the generalized damping force and generalized elastic force can be written in the following forms:

$$f_{D,i} = C_i \dot{y} \tag{5.21}$$

$$f_{S,i} = K_i y \tag{5.22}$$

where

C_i= generalized damping of mode i

K_i= generalized stiffness of mode i.

Substituting (5.20), (5.21) and (5.22) into (5.15), the equation of motion of the generalized SDOF representing mode i can be expressed as:

$$M_i \ddot{y}(t) + C_i \dot{y}(t) + K_i y(t) = -L_i \ddot{y}_s(t) \tag{5.23}$$

dividing by M_i, substituting $C_i = 2\omega_i \xi_i M_i$ and neglecting the sign of the right-hand side, the equation of motion of the SDOF system can be written in the following form:

$$\ddot{y}(t) + 2\omega_i \xi_i \dot{y}(t) + \omega_i^2 y(t) = \frac{L_i}{M_i} \ddot{y}_s(t) \tag{5.24}$$

Using the response spectrum technique, the maximum acceleration profile of mode i is given by:

$$\ddot{u}_{i\max}(x) = \phi_i(x) \frac{L_i}{M_i} S_{pa}(\xi_i, T_i) \tag{5.25}$$

and the contribution of mode i to the maximum elastic force acting on the structure is given by:

$$f_{S,i\max}(x) = m(x)\, \phi_i(x) \frac{L_i}{M_i} S_{pa}(\xi_i, T_i) \tag{5.26}$$

It should be noted that the previous discussion is true for both discrete and continuous systems with adjustments in definitions. For discrete systems the mass, stiffness, and mode

shapes are given in matrix and vector forms, while in continuous systems they are expressed as functions of the coordinate system used.

For continuous cantilevers, the modal shear force (V_i) and bending moment (M_{fi}) at any relative position x are given by:

$$V_i(x) = \int_1^x m(x)\, \phi_i(x)\, \frac{L_i}{Mi}\, S_{pa}(\xi_i, T_i)\, dx \tag{5.27}$$

and

$$M_{fi}(x) = \int_1^x m(x)\, \phi_i(x)\, \frac{L_i}{Mi}\, S_{pa}(\xi_i, T_i)\, x\, dx \tag{5.28}$$

These modal contributions can be combined using the SRSS method to yield an estimate of the total maximum response. Considering the three lowest flexural modes, the total response can be expressed as follows:

$$V(x) \simeq \sqrt{\Sigma_{i=1}^{3} V_i(x)^2} \tag{5.29}$$

and

$$M_f(x) \simeq \sqrt{\Sigma_{i=1}^{3} M_{fi}(x)^2} \tag{5.30}$$

where

$V(x)$ = internal shear force

$M_f(x)$= internal bending moment.

5.2 Proposed Method for Horizontal Earthquake Excitation

The proposed method is based on the definition of a horizontal acceleration profile that can give the same value of shear or bending moment at each tower section as the value obtained from the SRSS combination of the three lowest flexural modes. Fig. 5.1 is a schematic representation of the concept of the proposed method.

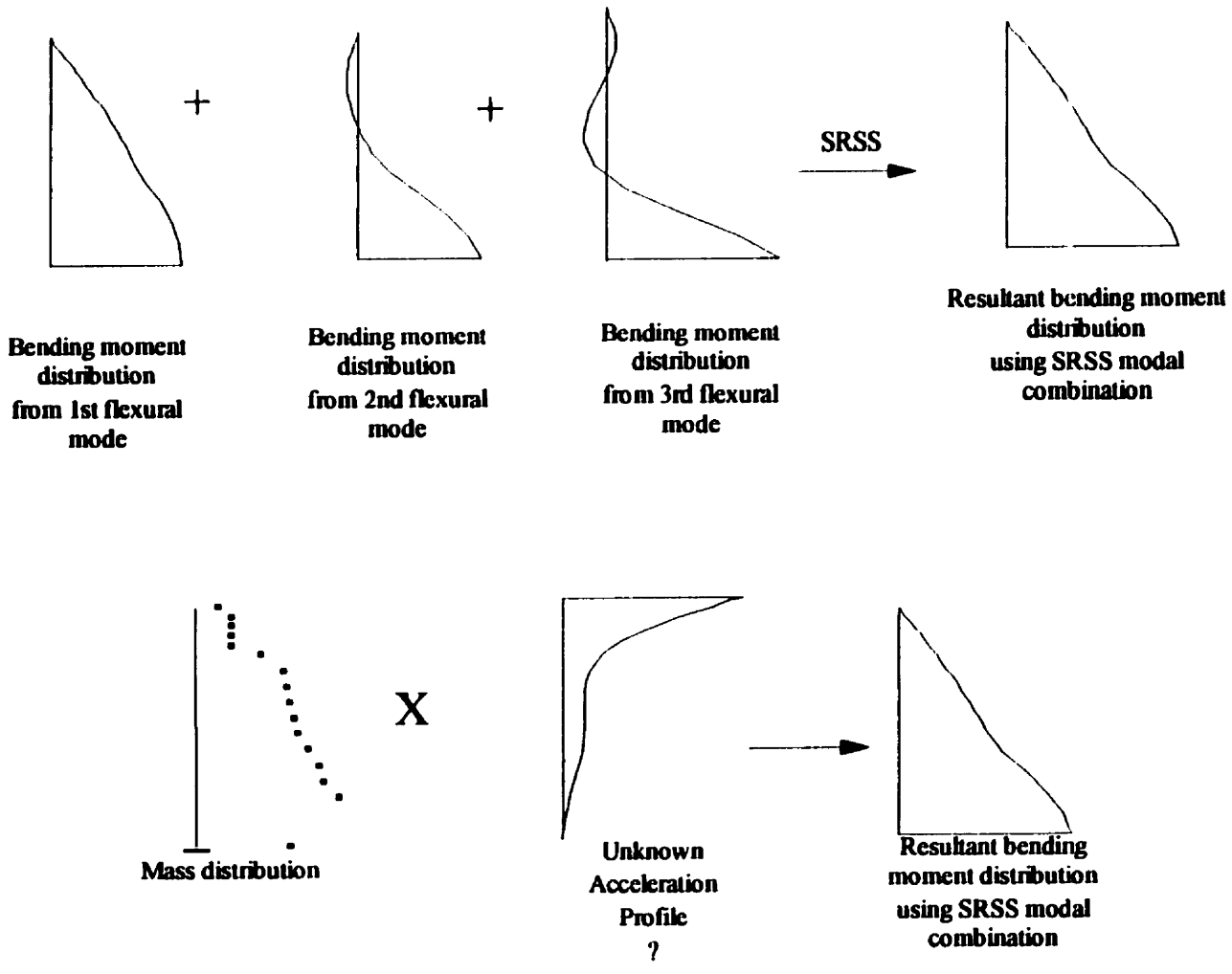

Fig. 5.1 Concept of the proposed method

For the evaluation of the acceleration profile, the self-supporting tower is assumed to be a continuous prismatic cantilever system with rigid base. The mass profile and the lowest three flexural modes of the tower are therefore assumed to be known in closed form. The prediction of the flexural mode shapes and the mass profile is presented in the work done by Sackmann (1996).

Using eqs. (5.29) and (5.30) the transverse shear and the bending moment can be written in the form:

$$V(x) = \int_1^x a(x)\, m(x)\, dx = \sqrt{\Sigma_{i=1}^{3} \left(\int_1^x m(x)\, \phi_i(x)\, \frac{L_i}{Mi}\, S_{pa}(\xi_i, T_i)\, dx\right)^2} \qquad (5.31)$$

and

$$M_f(x) = \int_1^x a(x)\, m(x)\, x\, dx = \sqrt{\Sigma_{i=1}^{3} \left(\int_1^x m(x)\, \phi_i(x)\, \frac{Li}{M_i}\, S_{pa}(\xi_i, T_i)\, x\, dx\right)^2} \qquad (5.32)$$

from which the expression for the acceleration profile $a(x)$ can be extracted. After investigating several towers, it was found that using the acceleration profile obtained from matching values of the bending moment, eq. (5.32), rather than the shear force, eq. (5.31). gives better predictions for the leg member forces. However, eq. (5.31) is more accurate for diagonals and horizontals. Since the seismic forces developed in horizontals and diagonals are usually low and therefore not likely to govern their design, it was decided to use $a(x)$ obtained from eq. (5.32). Accordingly, the expression for the acceleration profile $a(x)$ is given by:

$$a(x) = \frac{a_1 S_{pa1}^2 + a_2 S_{pa2}^2 + a_3 S_{pa3}^2}{\sqrt{a_4 S_{pa1}^2 + a_5 S_{pa2}^2 + a_6 S_{pa3}^2}} \qquad (5.33)$$

where the coefficients a_1 to a_6 depend on the lowest three flexural mode shapes and the mass profile of the tower. The values suggested for these coefficients are discussed in detail later.

In order to demonstrate the potential of the proposed method, results obtained for Tower TC9 are reported hereafter. It should be noted that the coefficients a_1 to a_6 of eq. (5.33) were calculated using the actual mode shapes and mass profile of the tower.

The tower is analyzed using three different earthquake accelerograms acting horizontally along one principal direction. The earthquake records used are San Fernando (1971) N61W for low A/V ratio, California (1952) S69E for intermediate A/V ratio, and Parkfield (1966) N65W for high A/V ratio. The tower was first analyzed using the software SAP90 utilizing the response spectrum option and including the lowest three flexural modes of vibration.

The acceleration profiles were then calculated using eq. (5.33) for each earthquake record and are given in Fig. 5.2. An examination of this figure shows that the resulting acceleration profiles do not have the same shape for all accelerograms. For the San Fernando and California earthquakes (low and intermediate A/V ratio) the acceleration profile does not change sign along the tower height. However, the acceleration profile of the Parkfield earthquake (high A/V ratio) is characterized by a change in sign. The values of the equivalent lateral forces are obtained by multiplying the mass and the acceleration profiles. The tower is then analyzed statically under the effect of these lateral forces. A comparison between the member forces obtained using response spectrum analysis and the proposed method is given in Fig. 5.3. It should be noted that for Tower TC9, members 63 through 69 are leg members. Other members are typical horizontals and diagonals.

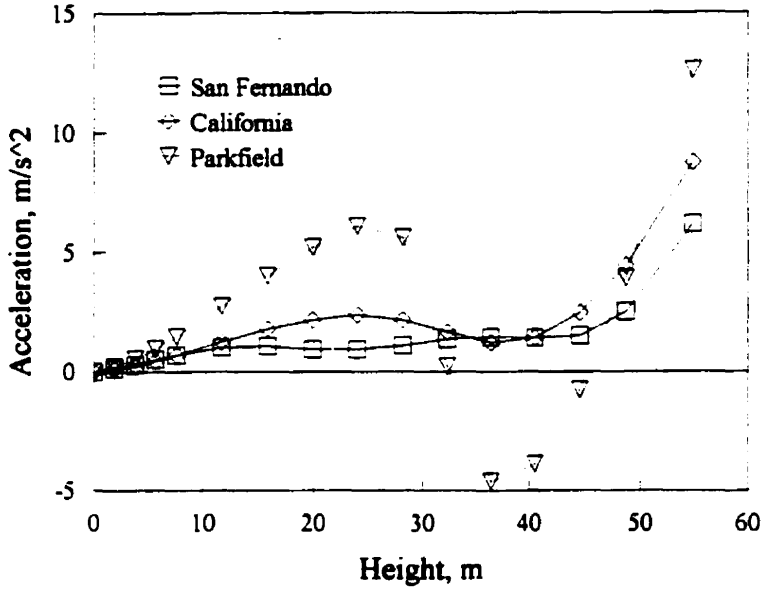

Fig. 5.2 Acceleration profiles for tower TC9

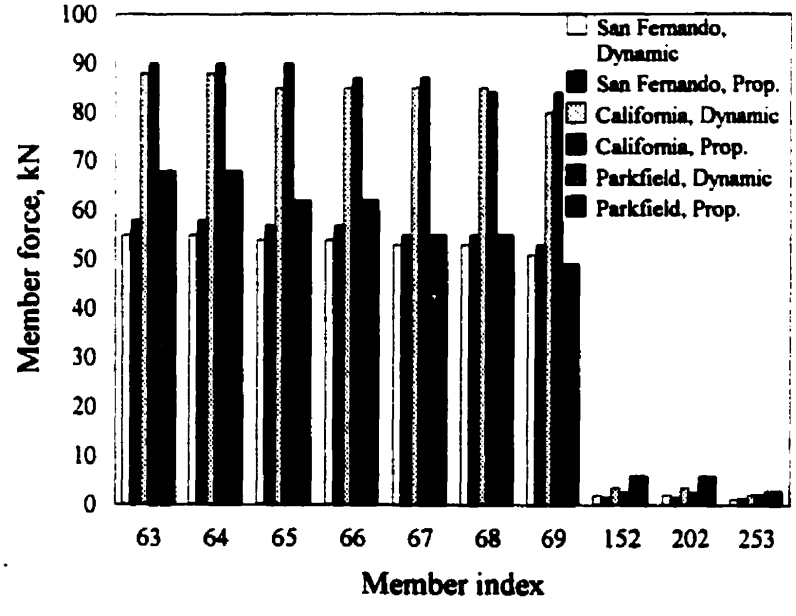

Fig. 5.3 Comparison between member forces obtained from dynamic analysis and the proposed method

These results show that the forces predicted in the main legs by the proposed method are in agreement with those obtained using dynamic analysis. For some of the lightly loaded members (other than the leg members) the difference in the two sets of predicted forces is as high as 30%. However, the design of these members is not likely to be governed by this load.

To generalize the procedure, the coefficients a_1 to a_6, which are functions of both the mode shapes and the mass distribution of the tower, should be assigned values based on the general configuration of the towers. To do so, it is suggested that the mode shapes proposed by Sackmann (1996) for the different tower categories be used in calculating these coefficients, except that some modifications are made to the lowest flexural mode. These changes are made because of the fact that Sackmann (1996) used the same prediction for the lowest flexural mode of the three groups. In order to obtain the maximum possible accuracy it was found beneficiary to use a different prediction for each group, which is still within the bounds suggested by Sackmann (1996). The lowest flexural mode of the three categories defined in Tables 3.2 and 3.3 is as follows:

$$\phi(x) = x^{2.0} \text{ for group A1} \tag{5.34}$$

$$\phi(x) = x^{2.3} \text{ for group A2} \tag{5.35}$$

$$\phi(x) = x^{2.0} \text{for group B} \tag{5.36}$$

A closed-form expression for the mass distribution is also necessary to evaluate the a_i coefficients for each category. The mass distribution profiles are found from curve fitting the mass distributions of the ten towers used in this study taking into account only

the shape of the mass distribution, i.e. using normalized functions. The following expressions are used to evaluate the a_i coefficients:

$$m(x) = 1 - 1.24\,x + 0.37\,x^2 \text{ for group A1} \tag{5.37}$$

$$m(x) = 1 - 1.54\,x + 0.87\,x^2 \text{ for group A2} \tag{5.38}$$

$$m(x) = 1 - 0.94\,x + 0.24\,x^2 \text{ for group B} \tag{5.39}$$

Figs. 5.4 to 5.6 show the lowest three flexural modes of the three categories on the left ordinate while the mass distribution used in the analysis is plotted versus the right ordinate. The abscissa represents the relative height x (considering total height equals unity).

Using the above expressions and equating the bending moment, $M_i(x)$ of eq. (5.32), at different levels of the cantilever model, the a_i coefficients were evaluated using the Mathematica software. The coefficients are plotted in Figs. 5.7 to 5.9.

In summary the following seven steps are suggested to find the equivalent member forces:

1. Calculate the lowest three flexural periods of vibration of the tower.
2. Evaluate the mass distribution along the tower's height and lump the mass at leg joints.
3. Define a design spectrum suitable for the tower site.
4. Determine the corresponding pseudo-acceleration values for each of the three lowest flexural natural periods and damping ratio (S_{pa1}, S_{pa2} and S_{pa3}).
5. Calculate the acceleration profile $a(x)$ using eq. (5.33) and the appropriate a_i coefficients using Figs. 5.7 to 5.9.

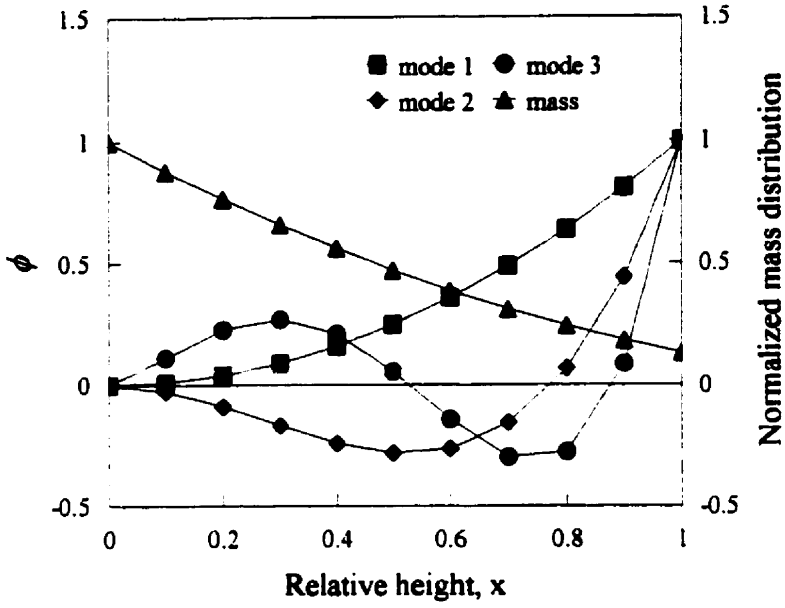

Fig. 5.4 Lateral mode shapes and mass distribution for Group A1

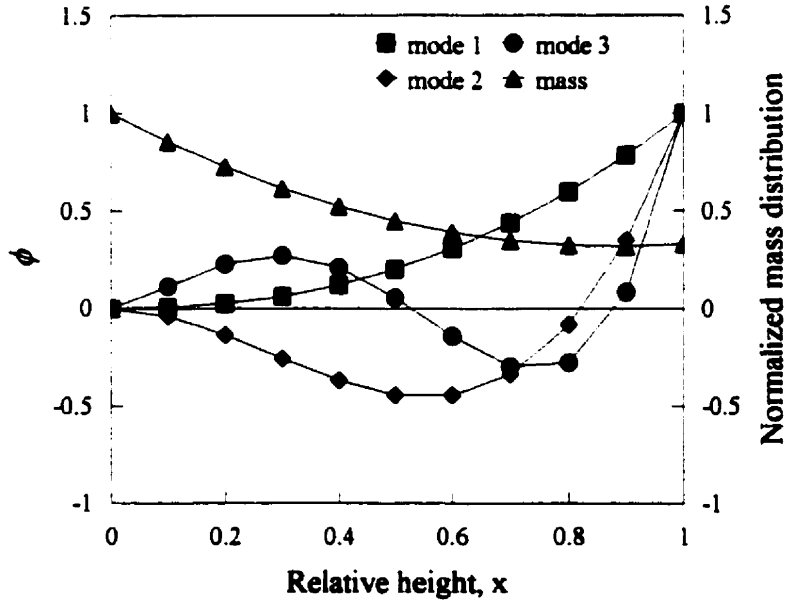

Fig. 5.5 Lateral mode shapes and mass distribution for Group A2

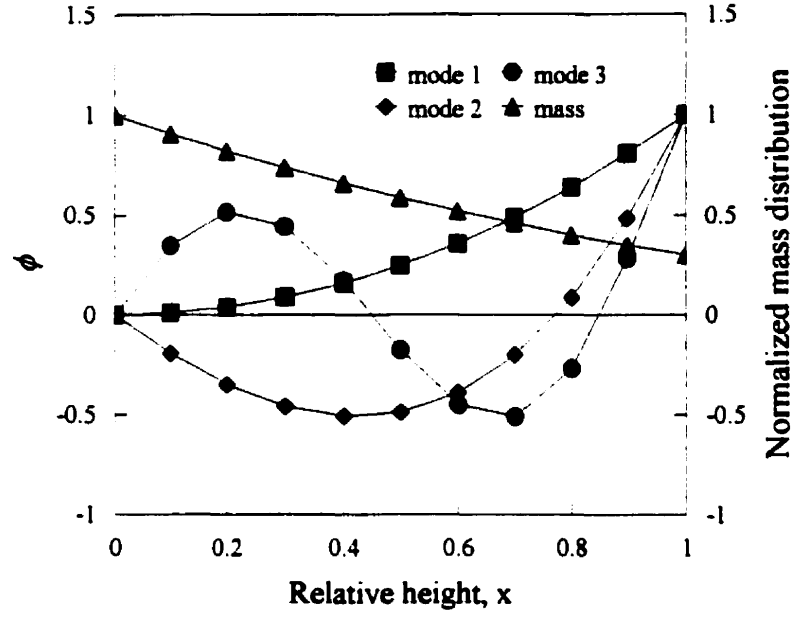

Fig. 5.6 Lateral mode shapes and mass distribution for Group B

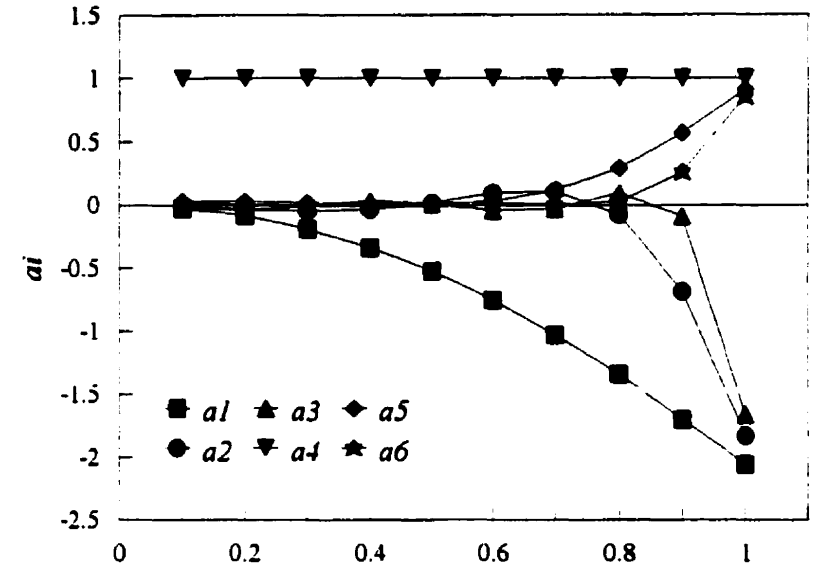

a)

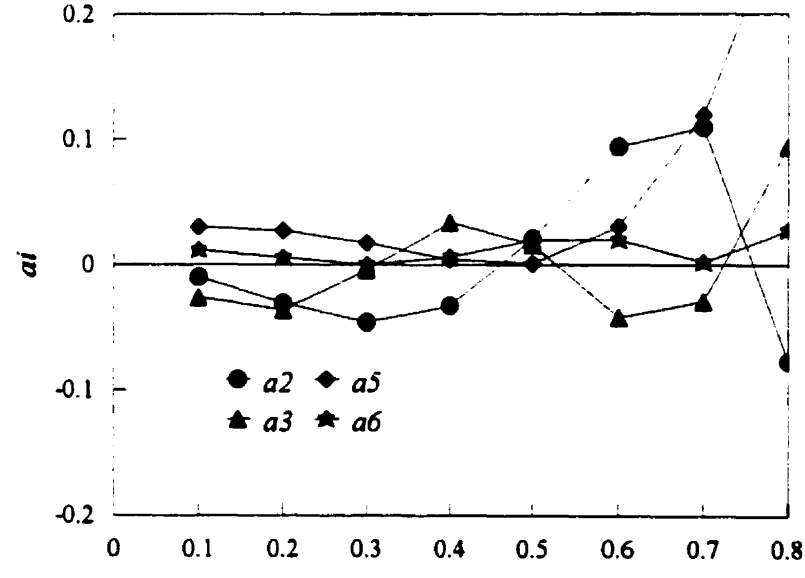

b)

Fig. 5.7 The a_i coefficients for Group A1

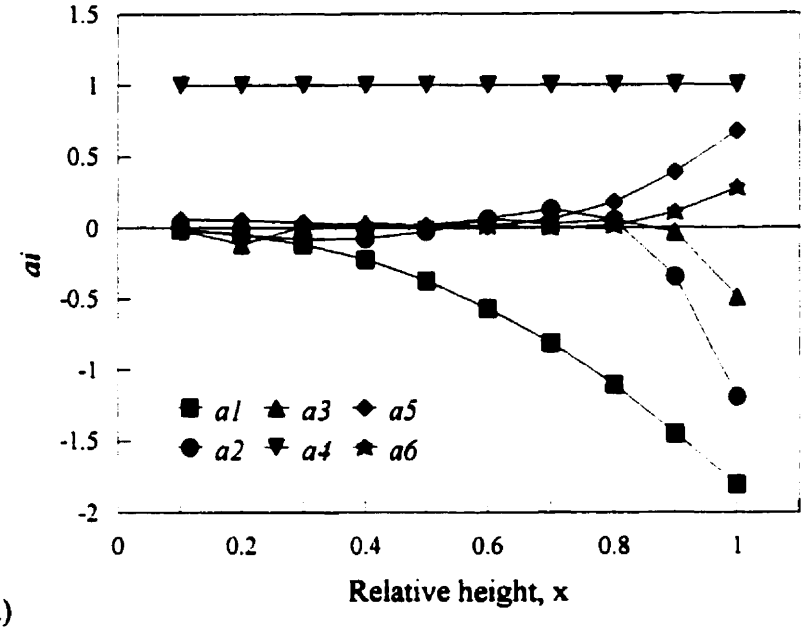

a)

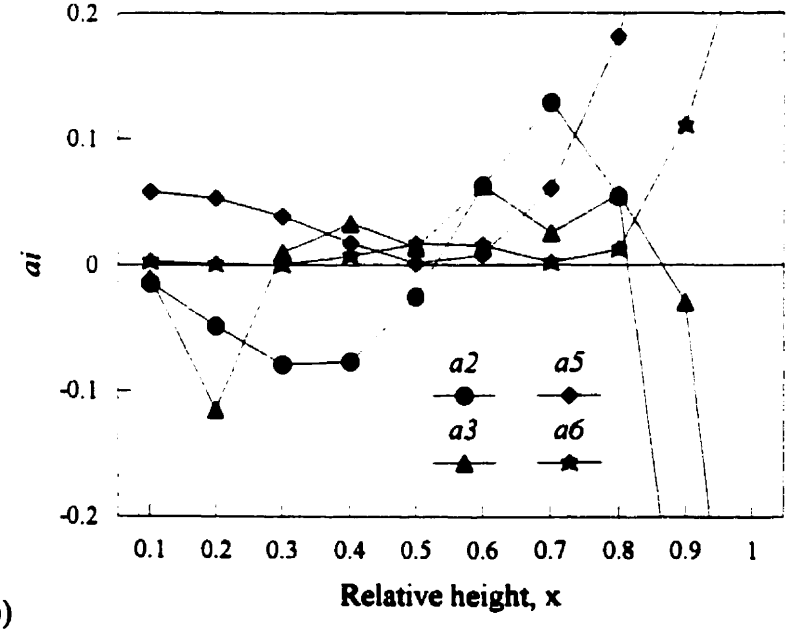

b)

Fig. 5.8 The a_i coefficients for Group A2

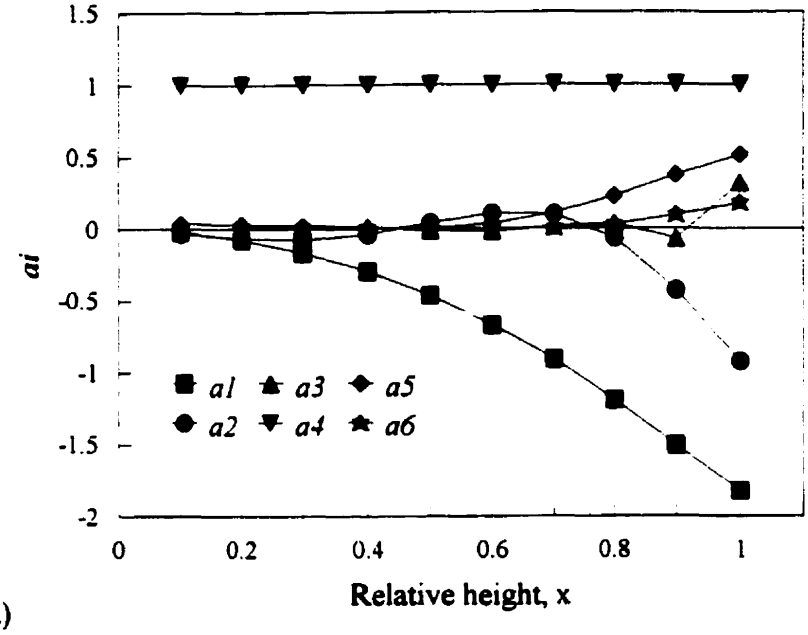

a)

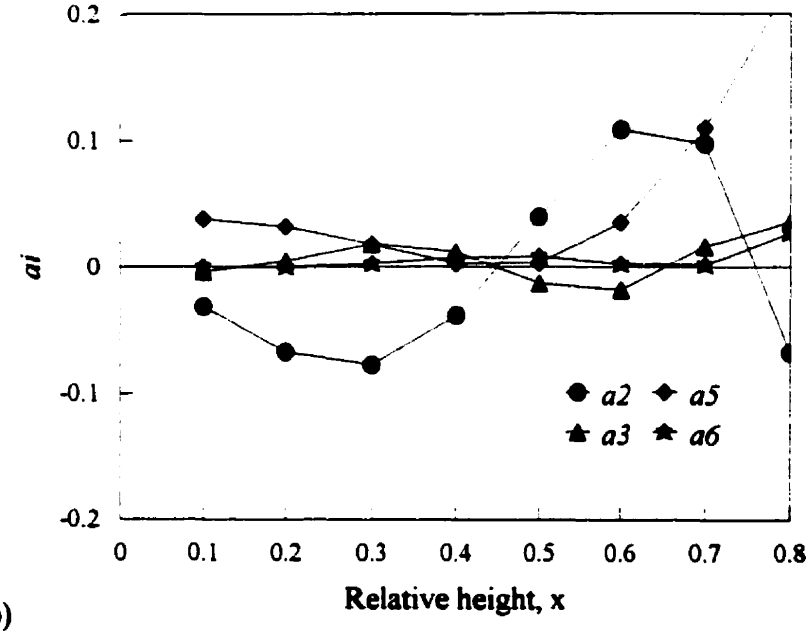

b)

Fig. 5.9 The a_i coefficients for Group B

6. Multiply the lumped mass at each level by the corresponding horizontal acceleration value to find the equivalent lateral inertia force profile.
7. Analyze the structure statically using these lateral inertia forces as external loading.

5.3 Verification of the Proposed Method

The ten towers used in the study are used to verify the proposed simplified method. This is achieved using response spectrum analyses performed on the towers under the effect of the 45 earthquake records separately. The computer program SAP90 is used in this part implementing the option SPEC. The earthquakes are assumed to act along one of the principal horizontal directions.

Each tower is classified into groups A1, A2 or B and the corresponding set of a_i coefficients is chosen. The spectral acceleration values corresponding to the lowest three flexural periods of the tower under investigation are obtained from the response spectrum of the earthquake record used. A set of horizontal forces is then calculated following steps 5 to 7. The internal forces obtained from the equivalent static analysis are then compared with those obtained using the SPEC option in SAP90. Fig. 5.10 shows a comparison between the results obtained from both analyses and the percentage of error for each leg member force. These results are for tower TC1 subjected to three selected earthquakes namely: Michoacan, Mexico 1985, N00E component (L14), Kern County, California 1952, N21E component (N3) and San Fernando, California 1971, S74W component (H8). It should be noted that these records are selected to represent the three

A/V categories namely low, intermediate and high. Similar groups of figures are presented for the other towers in Appendix D.

As it can be seen from these figures, for the same tower, the percentage of error differs from one earthquake record to another. For the same earthquake record, the percentage of error differs from one tower to another. Using different earthquake records for the same tower resulted in error due to the use of different spectral acceleration values for the lowest three flexural modes. It was noticed that as the spectral acceleration values corresponding to the second and third flexural periods increases in comparison to that of the first flexural period, the percentage of error also increases which is usually the case for records with high A/V ratio. This is due to the fact that each of the lowest three flexural modes contribute to the final inertia force profile, hence the tower response and the degree of this contribution depends on the spectral acceleration values assigned to each of these modes. As the accuracy in predicting the second and third mode shapes is less than that of the lowest flexural mode, assigning the former two modes higher spectral acceleration values will result in an increase in the percentage of error. For the same earthquake, the difference in the percentage of error from one tower to the other is due to percentage of error between the tower actual mode shapes and the mode shapes predicted for its category, the latter having been used in evaluating the a_i coefficients.

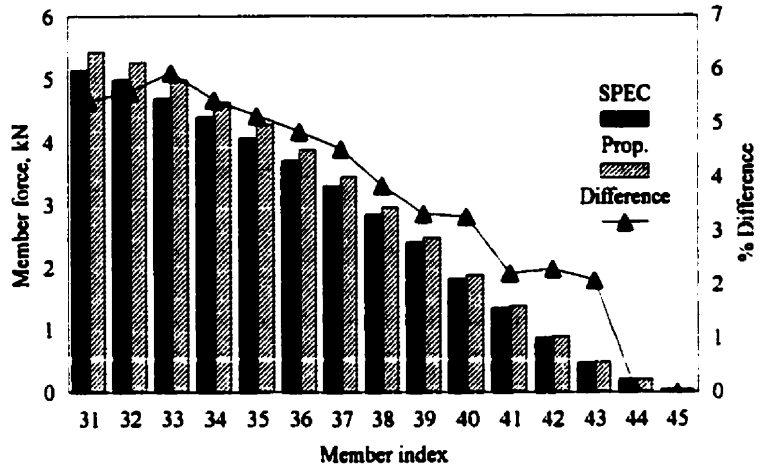

a) Earthquake record L14

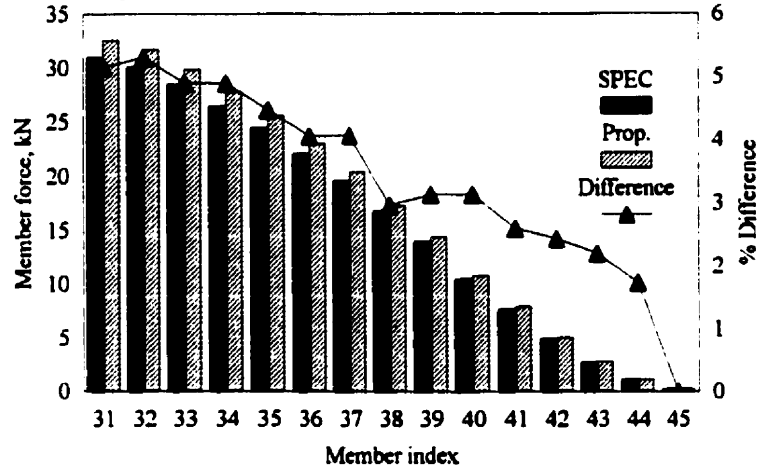

b) Earthquake record N3

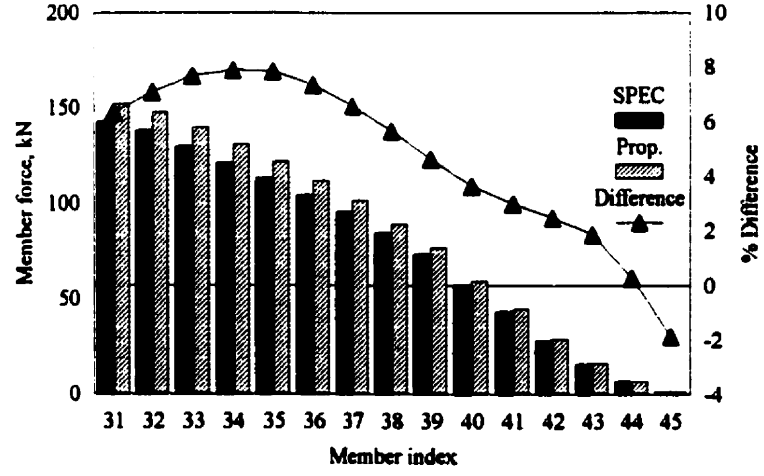

c) Earthquake record H8

Fig. 5.10 Member forces for tower TC1

Another source of error is the mass distribution used in evaluating the a_i coefficients. As it can be seen from Figs. 5.4 to 5.7, the mass distribution along the tower height is approximated as a smooth average curve. However, the actual mass distribution is rather discontinuous with height, with discontinuities at the location of horizontal panels.

As the percentage of error varies from one earthquake to another and from one tower to another, it was found beneficiary to investigate the percentage of error when considering a smoothed response spectrum. To this end, the NBCC 1995 response spectrum was used in the analysis. Each of the towers used in the study was analyzed assuming the three regions defined in the code, namely $Z_a<Z_v$, $Z_a=Z_v$ and $Z_a>Z_v$. The towers were analyzed using the response spectrum method and the proposed static method of analysis, and the member forces were evaluated. A comparison between the forces calculated using both methods was made in Fig. 5.11 for tower TC1. The results obtained for other towers are presented in Appendix D. From this comparison it is concluded that the maximum expected error using the proposed static method with a smoothed response spectrum similar to the one used in NBCC will not exceed 25% in the extreme cases, and the average error is ±7% (Figs D.9 to D.16). The maximum error was found to be with tower TC9, this difference is due to the fact that this tower has a mass distribution which is not typical of the other towers studied.

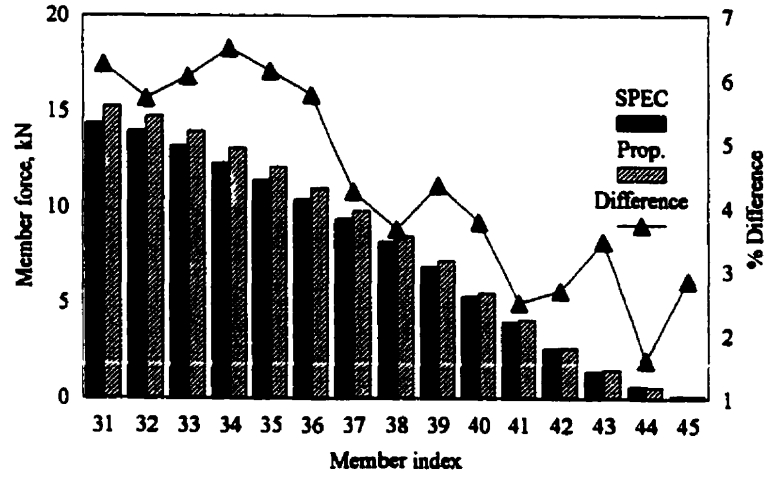

a) Za<Zv

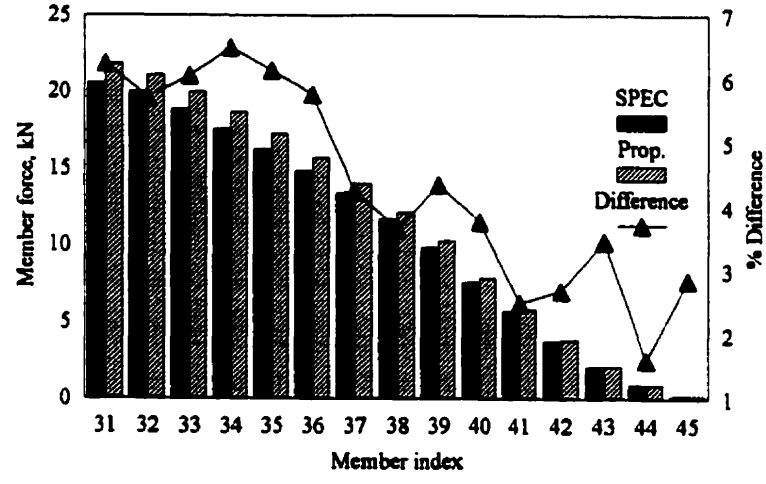

b) Za=Zv

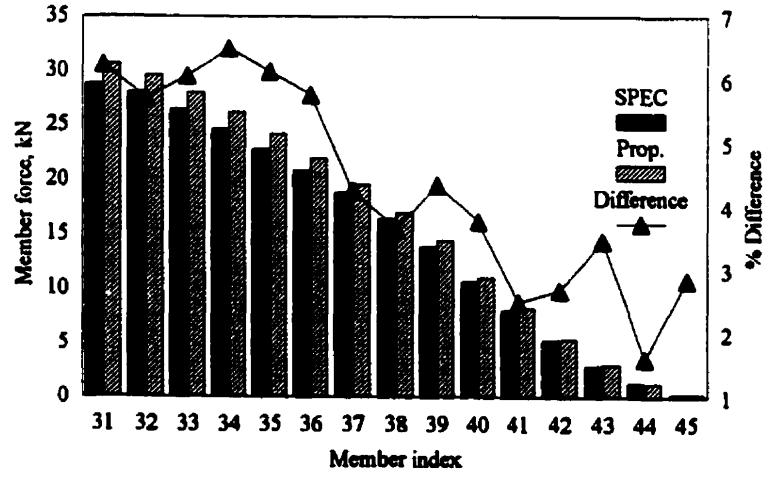

c) Za>Zv

Fig. 5.11 Member forces in tower TC1 using NBCC spectrum

5.4 Vertical Earthquake Excitation

In a preliminary study performed by Mikus (1994), it was concluded that the tower's axial modes of vibration are not likely to be excited and that vertical earthquake accelerations have little effect on the tower's response. In that study, however, the towers used were subjected to only three earthquake records. It was decided therefore to reexamine these findings with the towers used in this research and the set of 45 earthquake records after scaling them to ¾ of their original values as mentioned in Chapter 4. From these simulations it was found that although vertical earthquake accelerations do not produce forces of the same order of magnitude as those due to horizontal accelerations, the additional induced forces in the main legs ranged form 0.8 to 2.4 times the forces due to the tower self-weight.

From this study it was also found that only the first axial mode of vibration is likely to be excited by vertical earthquake accelerations, at least for the range of frequency content of the accelerograms considered.

The modal method of analysis and the response spectrum techniques are also used for the study of the vertical earthquake excitation. A vertical acceleration profile is proposed which depends on the tower's first axial mode and mass distribution.

The fundamental axial mode shapes of the towers used in this study are found to be very close to each other. Therefore an average function was selected, from curve fitting, to represent the mode shape. The lowest axial mode is then given by the following expression:

$$\phi(x) = 1.4x + 0.48x^2 - 1.16x^3 + 0.28x^4 \qquad (5.40)$$

where

ϕ = first axial mode shape

x = dimensionless coordinate measured from tower base.

An average profile for the mass distribution of the towers used in this study was also adopted to represent the mass distribution of typical towers. The following is the expression used:

$$m(x) = 1 - 1.11x - 0.21x^2 + 0.57x^3 \tag{5.41}$$

where

$m(x)$ = mass at position x.

It should be noted that contrary to the study of horizontal earthquake excitation, the towers were not divided into three groups. This is due to the fact that the fundamental axial mode shape of the towers were found to be very close to each other. Hence, eq. (5.41) is simply an average for the mass distributions of the towers used in the study.

The excitation factor and generalized mass defined in eq. (5.20) for the first axial mode were calculated, using the previous two expressions, and found to be L = 0.25 and M = 0.17.

The vertical acceleration profile for the tower is then evaluated using eq. (5.25) with the value of the generalized mass and excitation factor for i=1 only. The resulting vertical acceleration profile is given by:

$$a(x) = S_a \times (2.05x + 0.70x^2 - 1.70x^3 + 0.41x^4) \tag{5.42}$$

where

$a(x)$ = vertical acceleration at position x

S_a = spectral acceleration value.

Fig. 5.12 shows the vertical acceleration profile evaluated for a unit value of S_a.

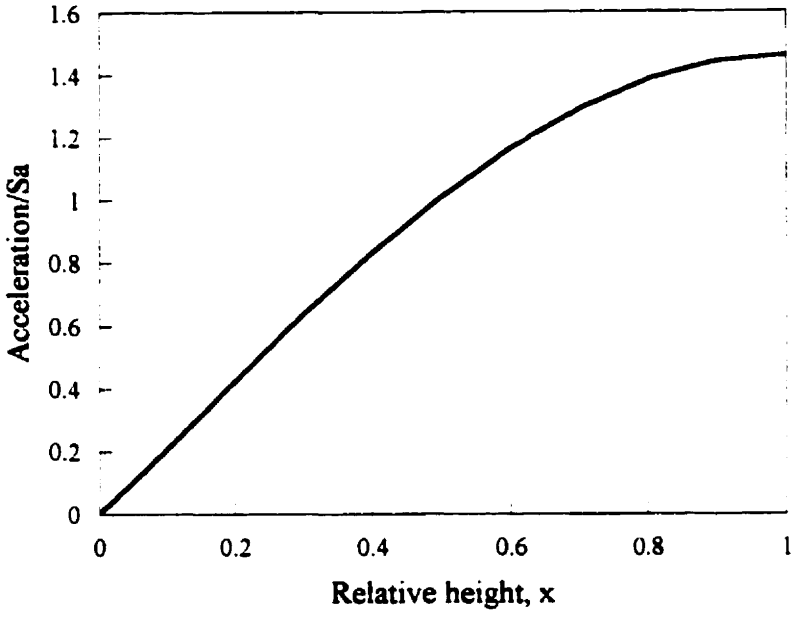

Fig. 5.12 Proposed vertical acceleration profile

The vertical acceleration profile takes the shape of the fundamental axial mode multiplied by 1.47 (the ratio of the excitation factor to the generalized mass) as implied in its derivation. If in the future vertical design spectra and peak vertical ground accelerations are included in design codes, this acceleration profile should be verified as more axial modes may be significantly excited.

The solution steps for the vertical earthquake excitation do not differ much from the horizontal case, however they are presented here for completeness:

1. Calculate the fundamental axial period of vibration of the tower.

2. Evaluate the mass distribution along the tower's height and lump the mass at leg joints.
3. Determine the corresponding pseudo-acceleration value (S_a) for the natural period evaluated at step 1 and the appropriate damping ratio.
4. Calculate the vertical acceleration profile $a(x)$ using eq. (5.42) or Fig. 5.12.
5. Multiply the lumped mass at each level by the corresponding vertical acceleration value to find the equivalent inertia force profile, acting in the vertical direction.
6. Analyze the structure statically using these vertical inertia forces as external loading.

5.5 Verification of the Proposed Vertical Acceleration Profile

To verify the proposed acceleration profile, the towers used in the study were first analyzed dynamically considering the lowest axial mode of vibration and assuming a constant spectral acceleration value equal to unity. Then the towers were analyzed again using the proposed static method of analysis and considering the spectral acceleration equal to unity. This procedure was chosen since only the lowest axial mode is considered. Therefore, the response of the towers to different earthquake records can simply be equal to the response resulting from the unit spectral acceleration multiplied by the corresponding spectral acceleration of the earthquake record.

A comparison between the forces developed in the main leg members for tower TC1 using both methods is presented in Fig. 5.13; similar figures are presented in Appendix D for the rest of the towers. From these figures it is seen that the proposed acceleration

profile yields excellent results for all the towers with a maximum difference of ±10% and an average error of 2% only.

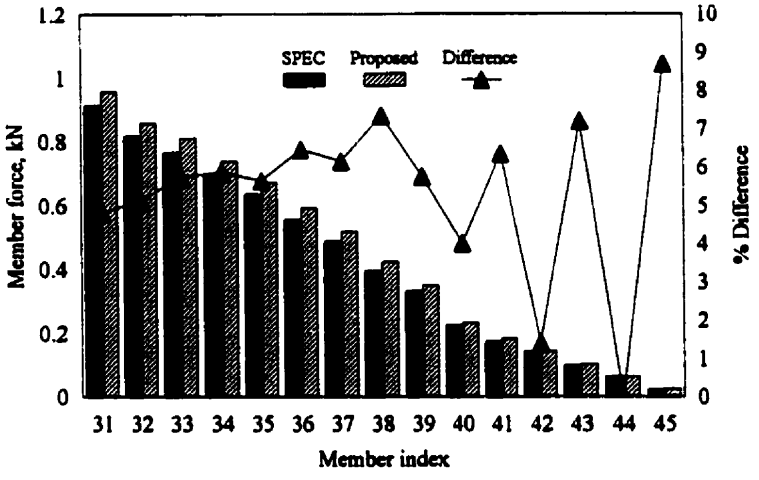

Fig. 5.13 Member forces in tower TC1 under vertical excitation

5.6 Effect of Concentrated Mass of Antennae

The results presented in the previous sections were evaluated considering the bare towers without accounting for the effects of antenna clusters. The coefficients a_1 to a_6 presented for the horizontal earthquake excitation as well as the expression for the vertical acceleration profile, eq. (5.42), were obtained using the mode shapes of the bare towers. This approach was justified due to the fact that the arrangement, position, weight and number of antennae vary significantly from one tower to another. As the mode shapes and

mass distribution will change to various degrees with the addition of a new antenna it was found impractical to consider all the possibilities and include them in the proposed method. Therefore another approach was adopted to account for the presence of antennae in the analysis. It is proposed to use the a_i coefficients (or eq. (5.42) for vertical excitations) defined for bare towers and account for the presence of the antennae by simply multiplying its mass by the corresponding acceleration while taking its eccentricity into consideration.

After including the antennae masses, the telecommunication towers were analyzed using the proposed approach. The member forces evaluated for towers TC3 (shown in Fig. 5.14 with antennae arrangements) are shown in Figs. 5.15 and 5.16 using the NBCC 1995 spectrum for $Z_a<Z_v$ in the horizontal and vertical directions respectively. These figures show agreement between the forces evaluated using the two approaches with a difference of 7% in average in the case of horizontal excitation and only 3% in the case of vertical excitation. It was found that using the same approach for towers with heavy antennae, specially if the antennae are located at the top of the tower, will result in overly conservative results. This is due to the fact that the mode shapes and mass distributions used in evaluating the a_i coefficients and eq. (5.42) will change significantly. However, this concern should have less and less importance in the future as antennae used in modern digital transmission have a very small diameter and are lightweight compared to conventional microwave drums.

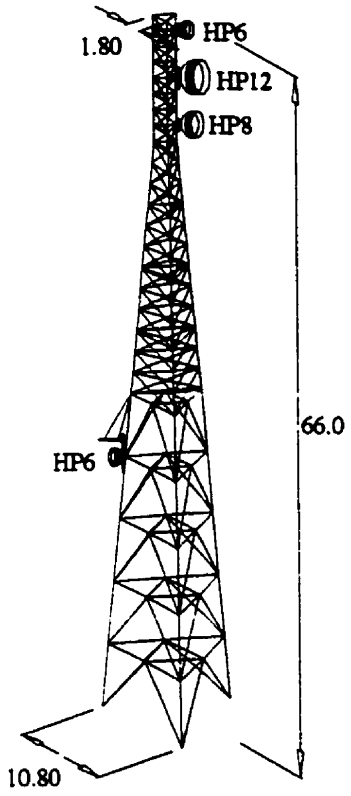

Fig. 5.14 Tower TC3 with antennae

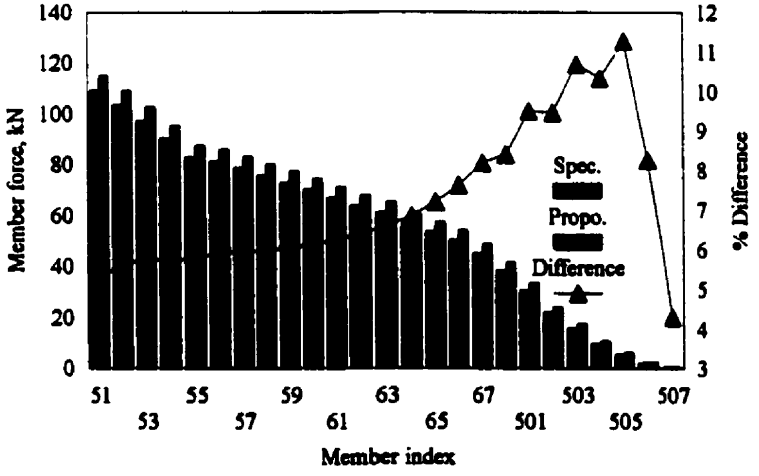

Fig. 5.15 Member forces including the effect of antenna mass for tower TC3 using NBCC 1995 for Z_a<Z_v ratio in the horizontal direction

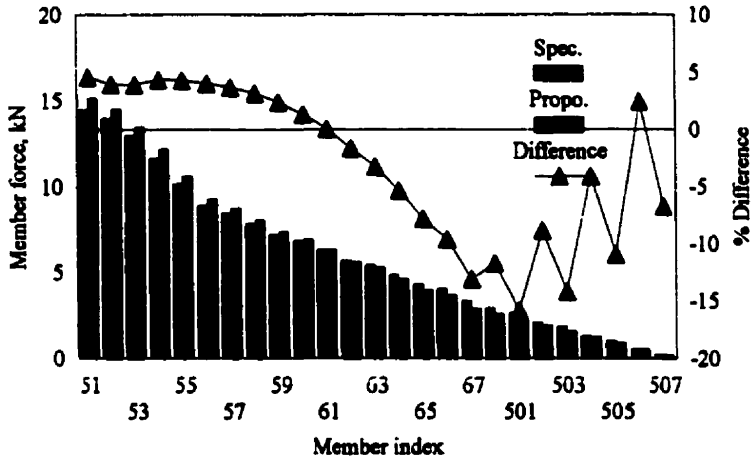

Fig. 5.16 Member forces including the effect of antenna mass for tower TC3 using NBCC 1995 for $Z_a<Z_v$ ratio in the vertical direction

At this point it was found necessary to further study the change in member forces and base shear due to horizontal earthquake excitations when adding heavy antennae. As was mentioned earlier, the location, orientation and mass of these antennae depend on the importance and the main function of the tower. Two approaches were used to account for the presence of these antennae. The first approach is by lumping an eccentric mass with a value ranging from 5% to 10% of the tower's total mass at the tip of the tower. The second approach involves distributing 10% of the tower's total mass evenly on one leg of the tower's top prismatic part. The eccentricities of these added masses will allow to study torsional effects. The NBCC 1995 design spectrum with its three regions was used again in these analyses. To this end, the four cases studied are as follows:

1. The bare tower

2. The tower with a lumped mass at the top equal to 5% of its total mass

3. The tower with a lumped mass at the top equal to 10% of its total mass

4. The tower with a mass equal to 10% of its total mass distributed along the top prismatic part.

For each of these four cases the base shear values, the main leg forces and the forces in selected diagonal and horizontal members are calculated. A comparison between these results and those corresponding to the bare tower case was then performed. Figs. 5.17 to 5.25 show the results obtained using the NBCC spectrum for $Z_a<Z_v$.

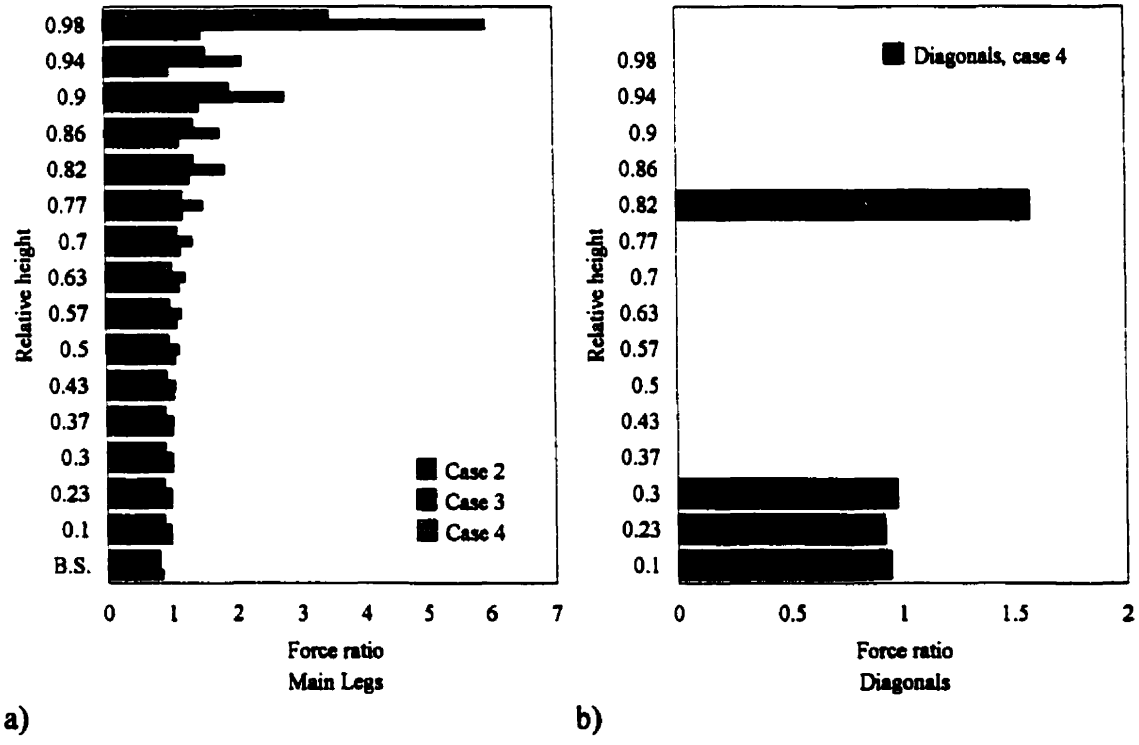

Fig. 5.17 Effect of including heavy antennae on tower TC1

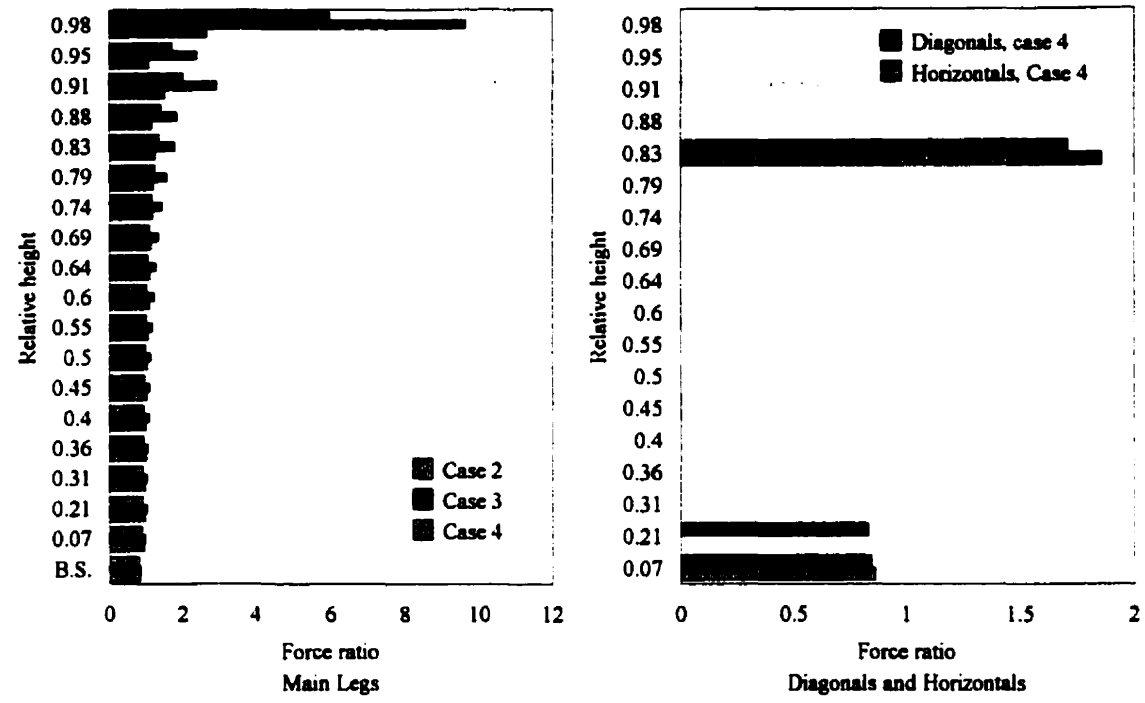

a) b)

Fig. 5.18 Effect of including heavy antennae on tower TC2

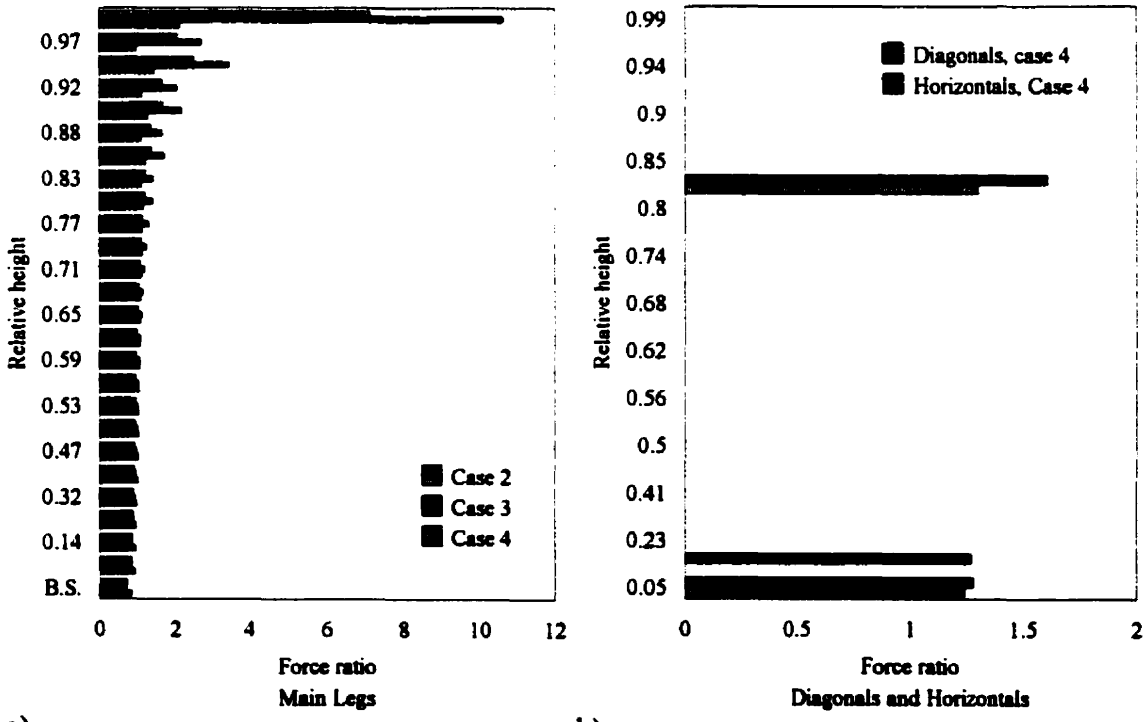

a) b)

Fig. 5.19 Effect of including heavy antennae on tower TC3

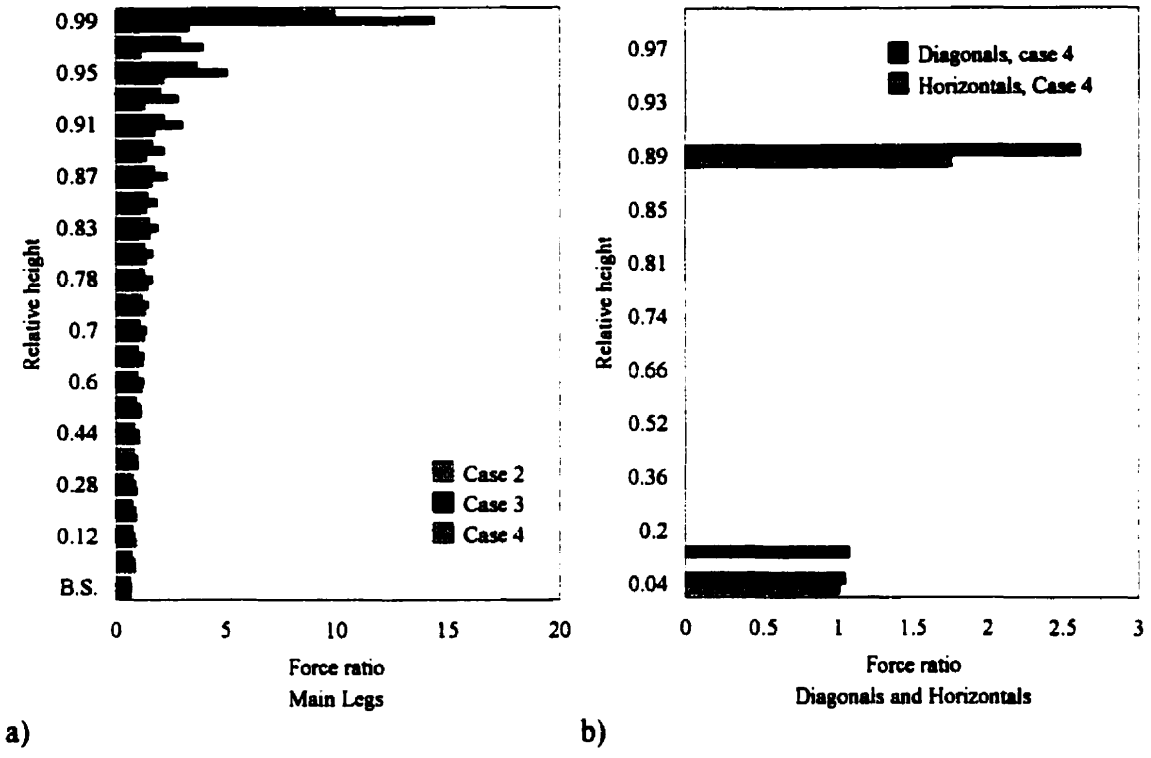

Fig. 5.20 Effect of including heavy antennae on tower TC5

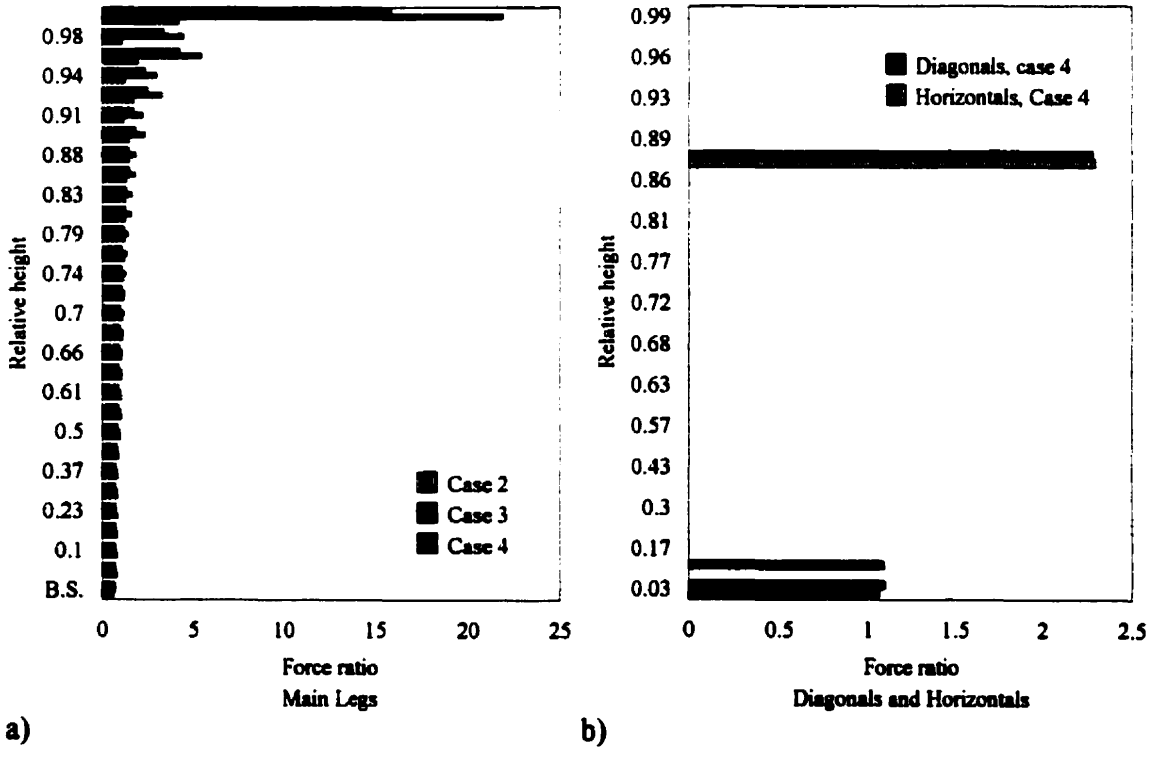

Fig. 5.21 Effect of including heavy antennae on tower TC6

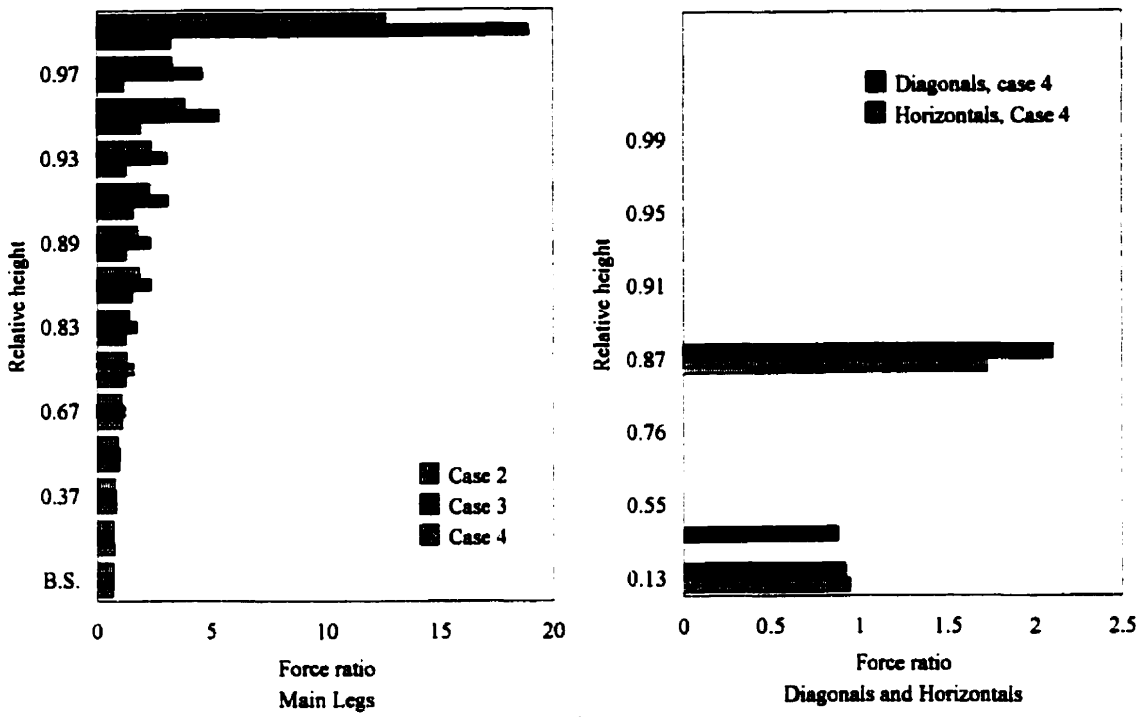

Fig. 5.22 Effect of including heavy antennae on tower TC7

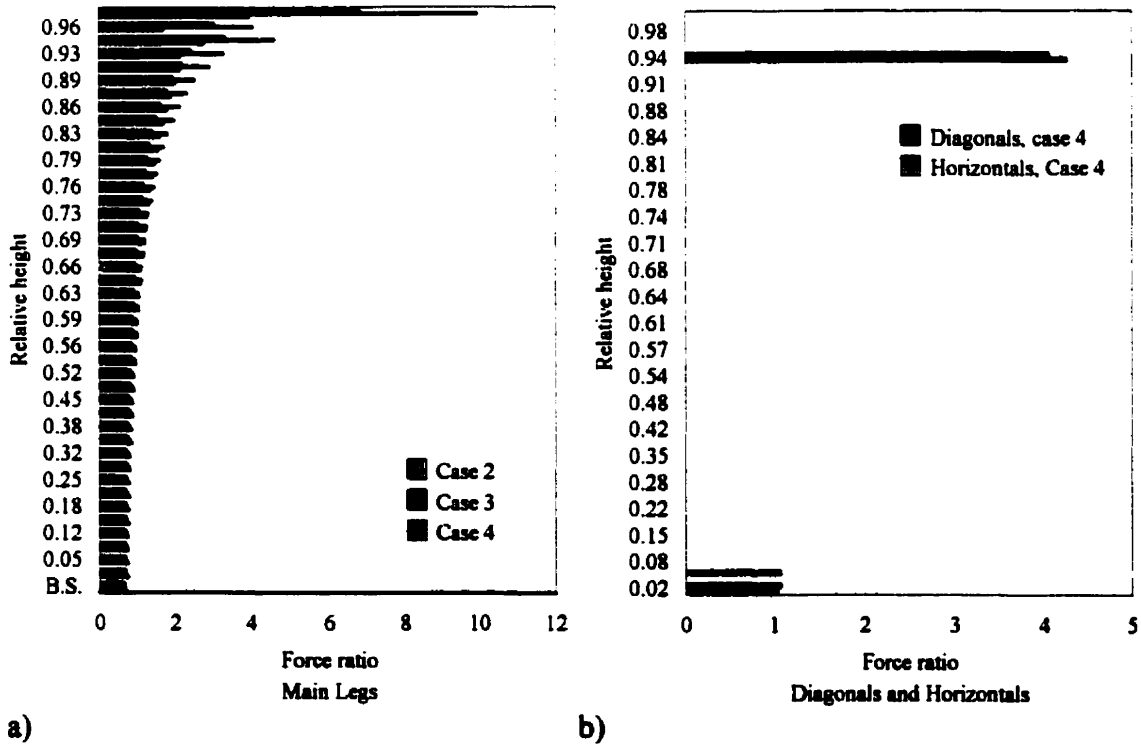

Fig. 5.23 Effect of including heavy antennae on tower TC8

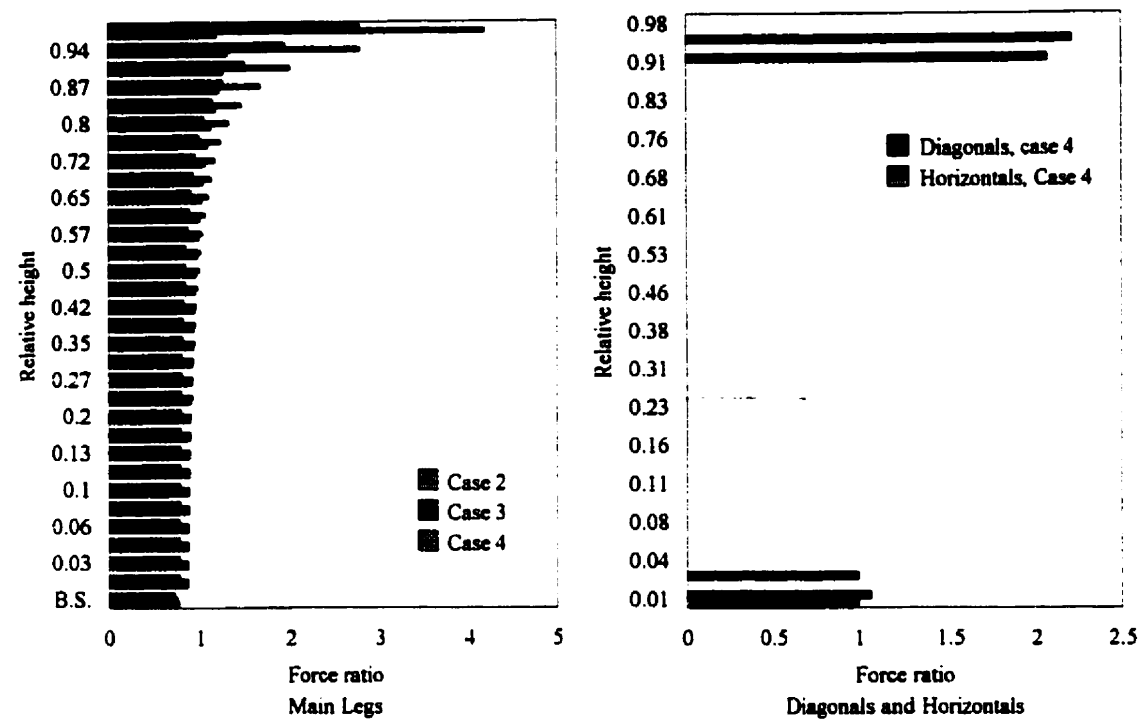

Fig. 5.24 Effect of including heavy antennae on tower TC9

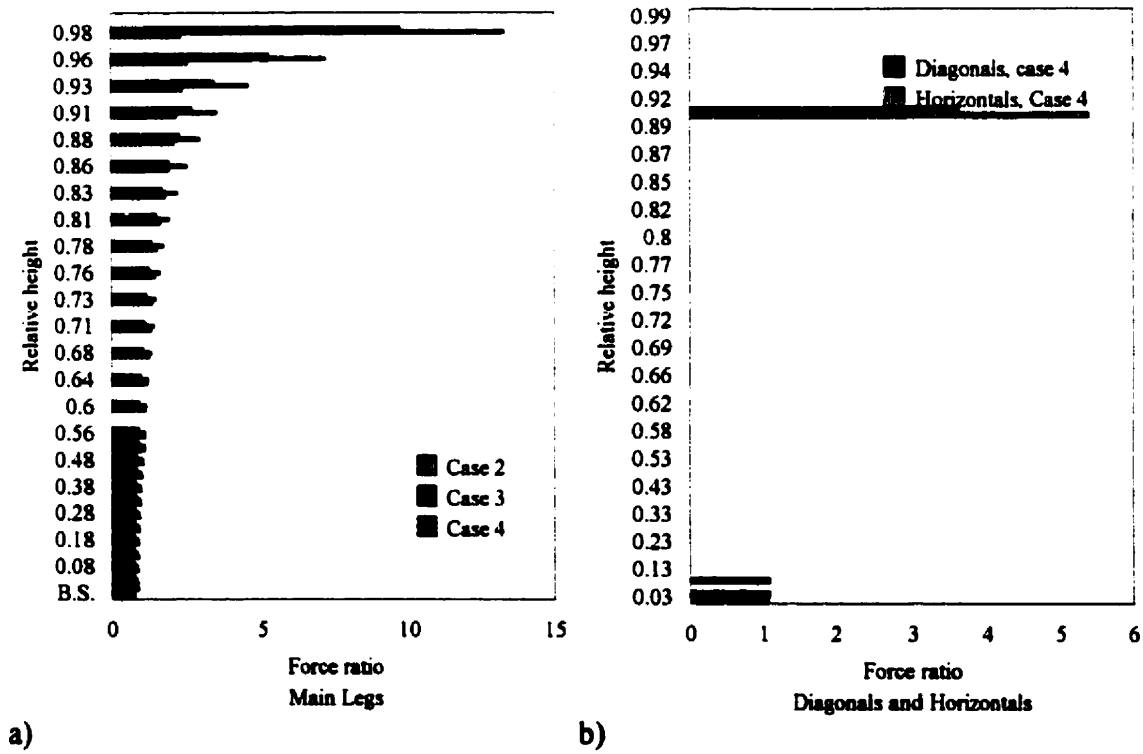

Fig. 5.25 Effect of including heavy antennae on tower TC10

From this study it was concluded that adding the equivalent of antennae masses of up to 10% of the tower's total mass consistently reduces the maximum base shear value as a global response indicator. The average reduction is about 20% when compared to the corresponding bare tower case. This finding is contrary to the intuitive belief (and misconception) that adding mass will necessarily increase the inertia forces and hence the base shear. The explanation for this reduction is that the addition of significant masses to the tower, and especially near its top, will tend to increase the natural period of the tower which in turn will reduce the spectral acceleration values corresponding to these modified periods, as it can be seen on the NBCC 1995 spectrum in Fig. 4.1. When comparing leg member forces (Figs. 5.17a to 5.25a), it is found that members near the base carry smaller forces than the bare tower case. This reduction in leg axial forces near the base was found to be 15% on average. However, this reduction becomes less significant when moving up towards the tower's prismatic part near the location of the antennae. At some elevation, from 0.5 to 0.7 of the height, the members start carrying larger forces than in the bare case. At the top level for case 3 (a lumped mass of 10% of the tower's mass) the leg members carry as much as 20 times the force calculated in case 1. The same comparison was carried out considering some diagonal and horizontal members (Figs. 5.17b to 5.25b) but no clear trend could be identified in the results near the base, except that the maximum change never exceeded ±10% when compared to the bare tower case. It is emphasized that the increase in the forces developed in the diagonal and horizontal members adjacent to the location of the antennae is very significant.

From the previous discussion it follows that including extremely heavy antennae (up to 10% of the tower self-weight) to the top prismatic part of telecommunication

towers has two effects: from a global perspective, it consistently reduces the base shear values of the tower, but it increases the member forces locally near the antenna positions and this increase tends to propagate downwards with the increase in the lumped mass value.

The previous study shows that the proposed horizontal acceleration profile will work well for towers having lightweight antennae, of mass of 5% or less of the tower mass. However, for towers with heavy antennae (above 5%) a corrected evaluation of the lowest three flexural modes, mass distribution and acceleration profile should take place prior to the application of the proposed equivalent static method.

This study was not extended to cover the effects of heavy antennae clusters under vertical excitation. The conclusions of such a case can be drawn from the information available about the fundamental axial period of the towers used and the NBCC 1995 response spectrum presented in Fig. 4.1. From Table 3.1 it is seen that the fundamental axial period of the towers used ranges between 0.03 and 0.12 s, which corresponds to the horizontal part of the NBCC 1995 spectrum (up to 0.2 s). This means that shifting the fundamental axial period within that range will not result in a change in the corresponding spectral acceleration value. Therefore, adding antennae to the tower and hence increasing the total mass will result in a proportional increase in the total vertical reaction of the tower. In addition, there will be a proportional increase in the forces developed in leg members along the tower's height as well as in diagonals and horizontals near the locations of mass concentration.

CHAPTER 6

SEISMIC CONSIDERATIONS FOR TRANSMISSION TOWERS

6.1 Introduction

Transmission tower designers lack simplified methods for seismic analysis. However, before such simplified design methods are proposed, a better understanding of the dynamic behavior of the coupled tower-cable system should be achieved. To gain more insight into the dynamic response of a transmission line system and to be able to simplify its response it was found important to perform frequency analysis on such systems. As presented in Chapter 2, most of the few published works in this area are devoted to the response of the cables only. This study, however, is also devoted to the response of the towers in the tower-cable system. The objective is to evaluate the feasibility of simplifying the analysis of the tower-cable system by replacing the cables by an equivalent mass and stiffness.

6.2 Mathematical Modeling

The line model used in this study consists of six spans of cables attached to five suspension towers. Towers TR2 and TR6 are first used in this type of analysis in order to investigate the possibility of simplifying the analysis, other towers will be used in the verification stage if successful. Two types of cables are included: the conductors and the overhead ground wires, the latter being directly anchored to the tower at its peak while the conductors are suspended to the tower cross arms with insulator strings. The length of the insulator strings varies in accordance with the voltage of the line, typically between 1.4

to 4.0 m for voltage of 120 to 735 kV, respectively. The cable ends which are not attached to the suspension tower in the end spans are assumed to be fixed. Fig. 6.1 shows the typical components of a transmission line segment used in this study. The following two paragraphs address in more details some modeling considerations for both the towers and the cables.

6.2.1 Modeling of towers

The transmission towers are modeled as three-dimensional structures in which the main legs are three-dimensional frame elements, while truss elements are used for modeling all the other horizontal and diagonal members. This choice of elements is used to simulate, as closely as possible, the actual behavior of the towers. It should also be noted that the model used in the analysis of the coupled tower-cable system is, in fact, a simplified reduced model of the tower for which a detailed three-dimensional model was constructed. The insulator strings are modeled using two-node truss elements.

6.2.2 Modeling of cables

The cables in each span are modeled using 20 two-node tension-only truss elements with initial prestress. The cross section of each cable is assumed constant. The material used for the cable elements is assumed linear elastic tension-only. The choice of the number of truss elements to be used in the finite element mesh is based on a convergence test of the lowest modes of vibrations of a single span cable; this approach was used by McClure and Tinawi (1987). Fig. 6.2 shows a comparison between the results obtained for the lowest transverse mode using different numbers of elements, and sufficient accuracy is obtained with 20 elements.

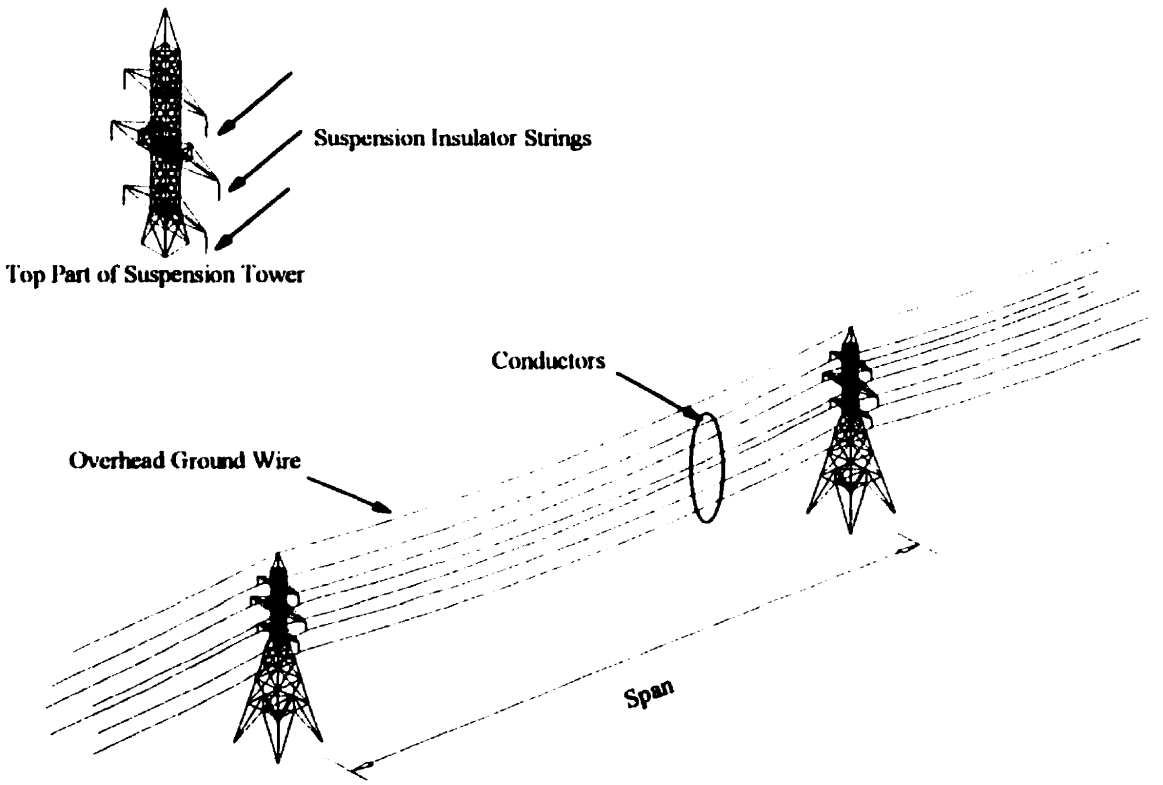

Fig. 6.1 Components of transmission line section on double-circuit lattice towers

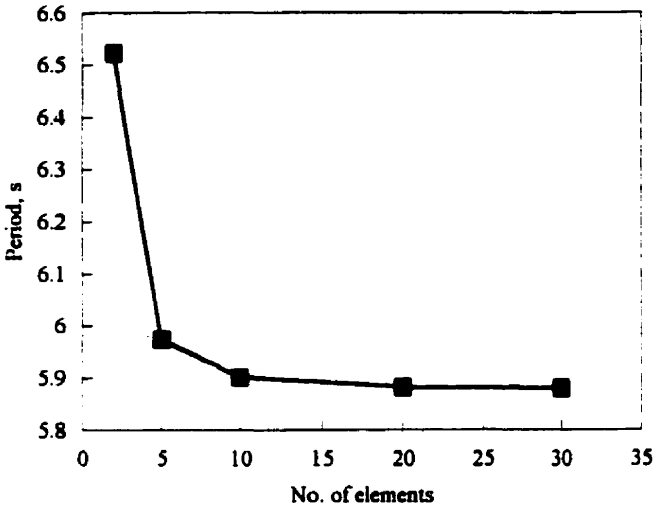

Fig. 6.2 Mesh convergence for the lowest transversal mode

Three types of conductors were used in the parameteric study performed namely, CONDOR 54/7 ACSR (Aluminum Conductor Steel Reinforced), CURLEW 54/7 ACSR and BERSFORT 48/7 ACSR. Table 6.1 contains some characteristics of these conductors in addition to those of the overhead ground wire (O.H.G.W.). The horizontal tensions used were 10, 15, 20 and 25 kN for CONDOR , 25, 30, 35 and 40 kN for both CURLEW and BERSFORT. These values are specified at 0°C. For the overhead ground wire the horizontal tension, $H_{O.H.G.W.}$, was calculated using the following relation:

$$H_{O.H.G.W.} = H_{cond.} \times \frac{w_{O.H.G.W.}}{w_{cond}} \tag{6.1}$$

where

H_{cond} = conductor horizontal tension

$w_{O.H.G.W.}$ = overhead ground wire weight per unit length

$w_{cond.}$ = conductor's weight per unit length.

Table 6.1 - Cable data

Cable	Diameter, mm	E composite, MPa	Weight, N/m	Cross sectional area, mm^2	Rated tensile strength, kN
CONDOR	27.7	67,225	14.93	455	127
CURLEW	31.6	68,325	19.38	592	165
BERSFORT	35.6	67,600	23.23	747	180
O.H.G.W.	12.7	172,400	7.44	97	114

6.3 Methods of Analysis

The computer program ADINA (Automatic Dynamic Incremental Nonlinear Analysis) ADINA R&D (1997), is used in the analysis of transmission line systems. SAP90 could not be used as it can only perform linear analysis. In order to achieve the goal of this study two types of analysis are performed, which are:

1. A non linear static analysis under self weight to obtain the static equilibrium position of the cables.
2. A frequency analysis in the initial configuration, to obtain the lowest flexural modes of the towers and those of the entire cable-tower system.

more details on these analyses follow.

6.3.1 Nonlinear static analysis

In this part of the simulation, the model comprises five towers with six spans of cables, and is analyzed under the action of self weight. Due to the geometrically nonlinear response of the suspended cables, the kinematics formulation used to obtain the stiffness matrix of the system is that of large displacements and small strains. The iteration method used to solve the nonlinear problem is the full-Newton with reformulation of the stiffness matrix at each iteration. The convergence criterion selected is based on the displacement

vector norm. The tolerance used was 1.0^{-5}. The time function used to apply the gravitational load is linear with 100 time increments of 0.01 such that at time t=1.0 the initial equilibrium configuration of the line is reached.

6.3.2 Frequency analysis

After obtaining the cable equilibrium configuration, the natural periods and mode shapes of the towers in the tower-cable system are calculated. To determine the number of modes sufficient to capture the significant response of the towers, a linear dynamic analysis of the six towers (without cables) used in the study was performed using three selected horizontal earthquake records each having a different A/V ratio. From this preliminary investigation, it was concluded that only the lowest two flexural modes are participating in the response. It is noted that these towers are generally more rigid than telecommunication towers for which the third flexural mode of vibration was also found significant. Therefore, it was concluded that only the lowest two flexural modes in each of the two main orthogonal directions (longitudinal and transverse) should be obtained for the coupled tower-cable system. The method used in frequency analysis is the subspace iteration. To obtain the required eigenvalues, a small frequency interval around the corresponding bare tower frequency was specified in order to reduce the calculation effort.

6.4 Parametric Study

Eighteen cases were considered in performing the frequency analyses, as summarized in Table 6.2, in which the following parameters are studied: span, cable

tension and conductor type. The cable span (distance between towers) varied from 300 to 400 m, the cable tension varied from 10 to 40 kN and three conductor types were used in the simulations. The type of the overhead ground wire was kept the same, i.e. Grade 180 galvanized steel 12.7 mm in diameter, and its tension was calculated using eq. 6.1.

Table 6.2 - Cases used in the parametric study

Case no.	Conductor type	Area m^2	E MPa	Span m	Sag m	Tension kN	Initial strain ε
1				350	22.99	10	3.3E-04
2				350	15.28	15	4.9E-04
3	Condor	4.6E-04	6.7E+10	350	11.45	20	6.5E-04
4				350	9.15	25	8.2E-04
5				300	11.22	15	4.9E-04
6				400	19.97	15	4.9E-04
7				350	11.89	25	6.2E-04
8				350	9.9	30	7.4E-04
9	Curlew	5.9E-04	6.8E+10	350	8.49	35	8.7E-04
10				350	7.42	40	9.9E-04
11				300	7.27	30	7.4E-04
12				400	12.94	30	7.4E-04
13				350	14.26	25	5.0E-04
14				350	11.88	30	5.9E-04
15	Bersfort	7.5E-04	6.8E+10	350	10.17	35	6.9E-04
16				350	8.9	40	7.9E-04
17				300	8.72	30	5.9E-04
18				400	15.52	30	5.9E-04

As was mentioned earlier only towers TR2 and TR6 are used in the frequency analysis. All 18 cases are studied for tower TR2 while only the first 12 (i.e. Condor and Curlew) cases are used for tower TR6. The lowest two flexural periods of vibration in both the longitudinal and transverse directions are obtained and compared to the corresponding periods of the bare suspension tower.

For each conductor type the results are pooled in two groups: the first group for a given tension but with different spans (Figs. 6.3a to 6.7a), and the second group for a given span but with different tensions (Figs. 6.3b to 6.7b). These figures show the ratio of the natural periods calculated in the coupled tower-cable system to the corresponding values calculated for bare towers. It is seen from Figs. 6.3b to 6.7b that for a given span length changing the cable tension (in the range considered) has no significant effect on the natural period of the system. This can be explained as the towers considered in the study are suspension towers with balanced longitudinal loads. Since the conductors are attached to the towers' cross arms with insulator strings that can rotate freely, the change in the conductor's tension is not directly felt by the tower. Only the change in the tension of the overhead ground wire is affecting slightly the periods of the system.

However, varying the span length while keeping the cable tension constant resulted in a significant change in the periods, as shown in Figs. 6.3a to 6.7a. The period increased (in most of the cases) with the increase in span, but this effect did not follow a predictable trend. Another observation is that for a given span length there is no change in the calculated natural periods from one type of conductor to another. This observation may not be generalized since the physical characteristics (stiffness and mass) of the conductors used in the simulations are of the same order, and only equal and level spans are considered. The lowest two longitudinal mode shapes of tower TR6 in the coupled system are shown in Fig. 6.8 where it can be observed that the insulator strings suspending the conductors to the tower rotate while the conductors' position does not change. This means that the mass of the conductors does not participate in the longitudinal mode shapes. This observation, however, is not true when examining the transverse modes.

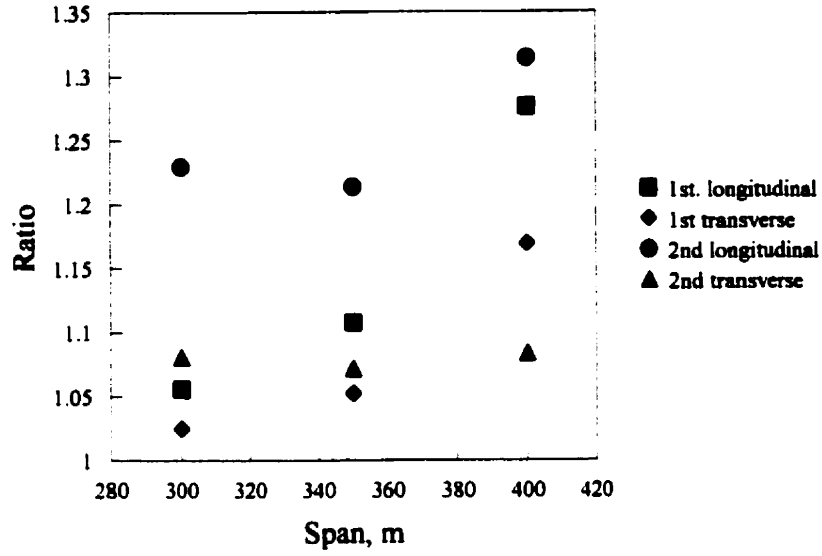

a) Initial tension = 15 kN

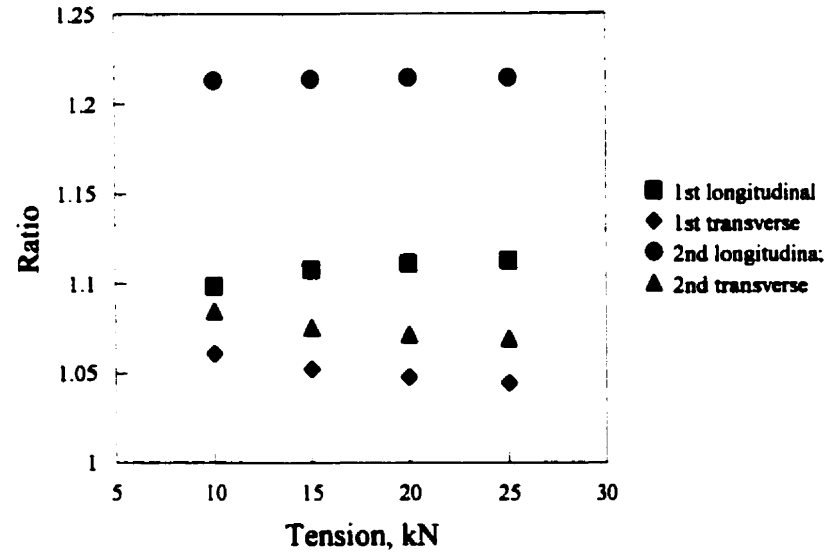

b) Span length = 350 m

Fig. 6.3 Ratio between calculated natural periods of the coupled line system and the bare tower for tower TR2 with Condor

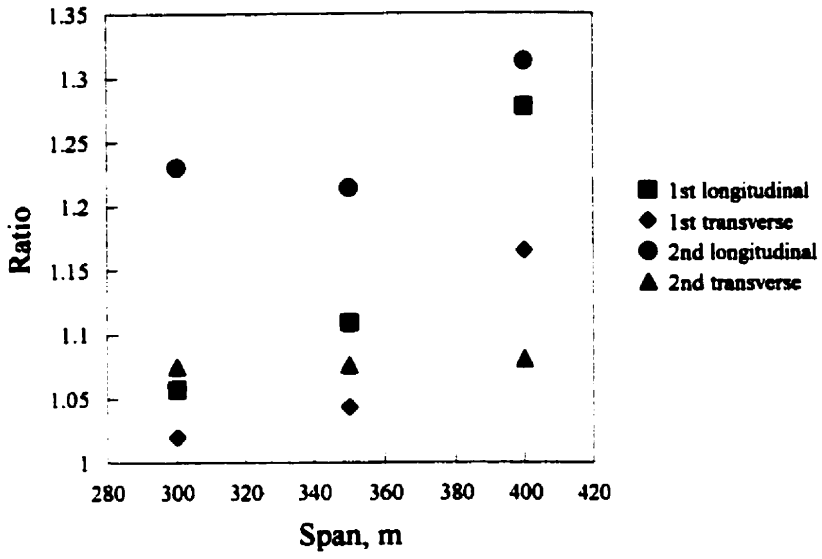

a) Initial tension = 30 kN

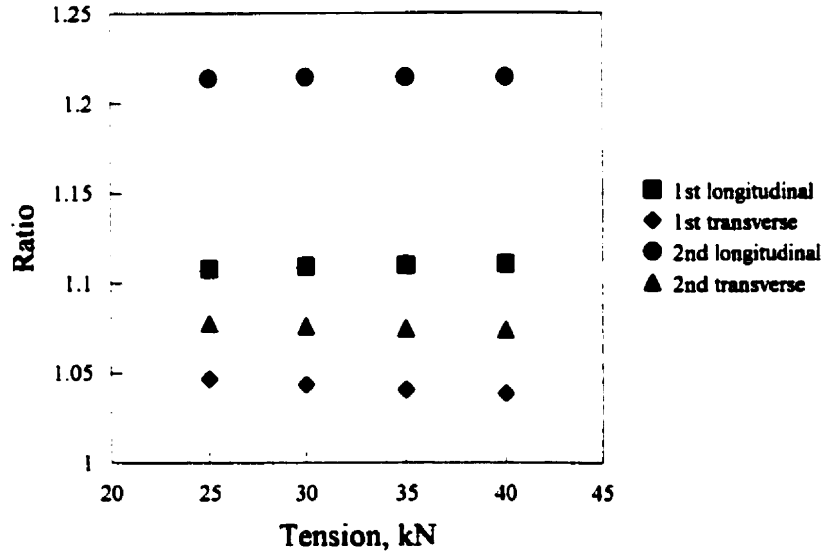

b) Span length = 350 m

Fig. 6.4 Ratio between calculated natural periods of the coupled line system and the bare tower for tower TR2 with Curlew

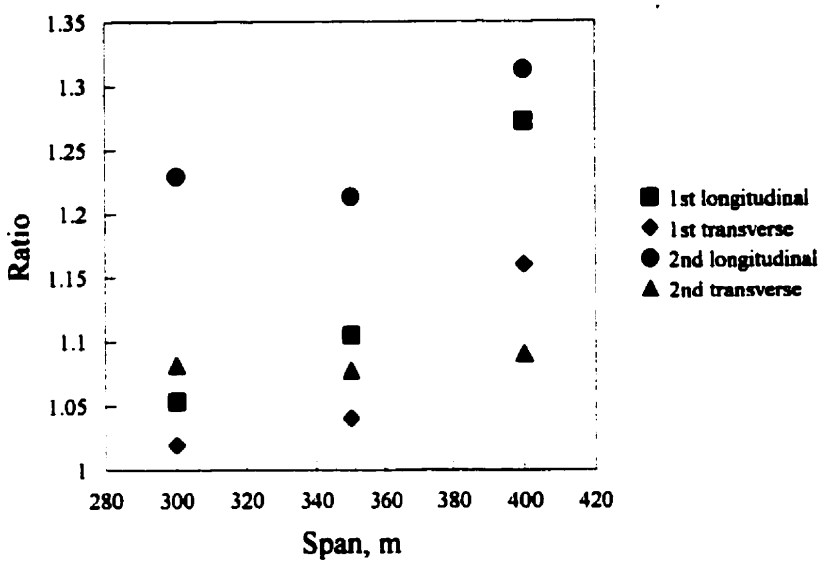

a) Initial tension = 30 kN

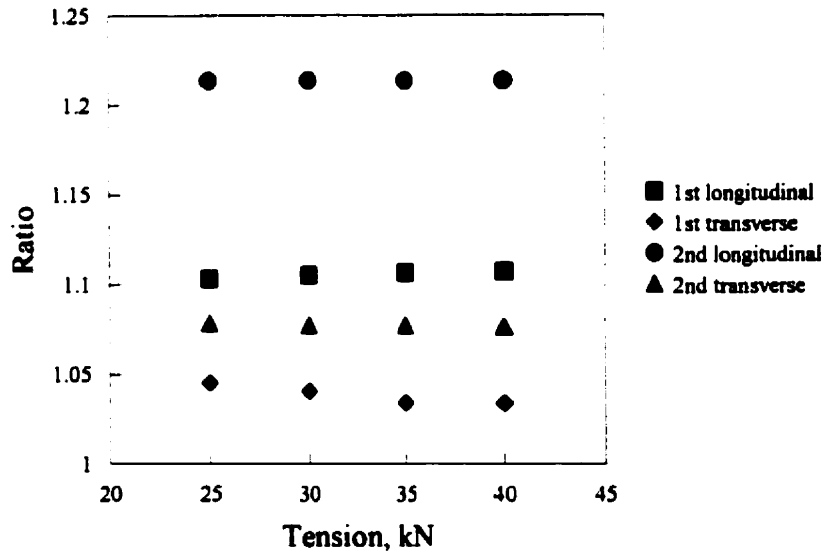

b) Span length = 350 m

Fig. 6.5 Ratio between calculated natural periods of the coupled line system and the bare tower for tower TR2 with Bersfort

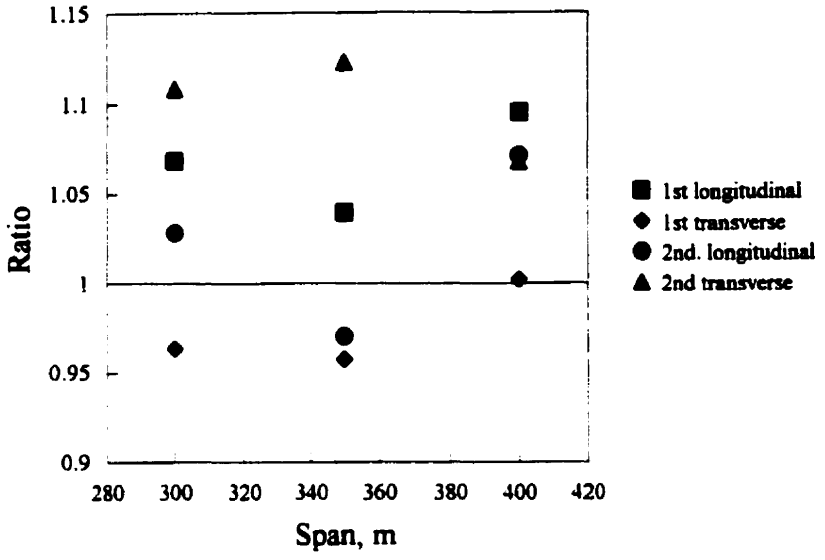

a) Initial tension = 15 kN

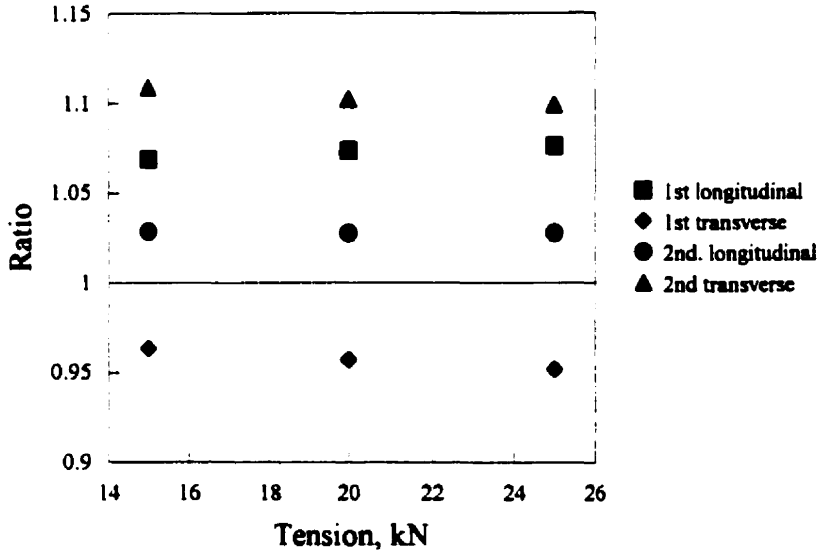

b) Span length = 350 m

Fig. 6.6 Ratio between calculated natural periods of the coupled line system and the bare tower for tower TR6 with Condor

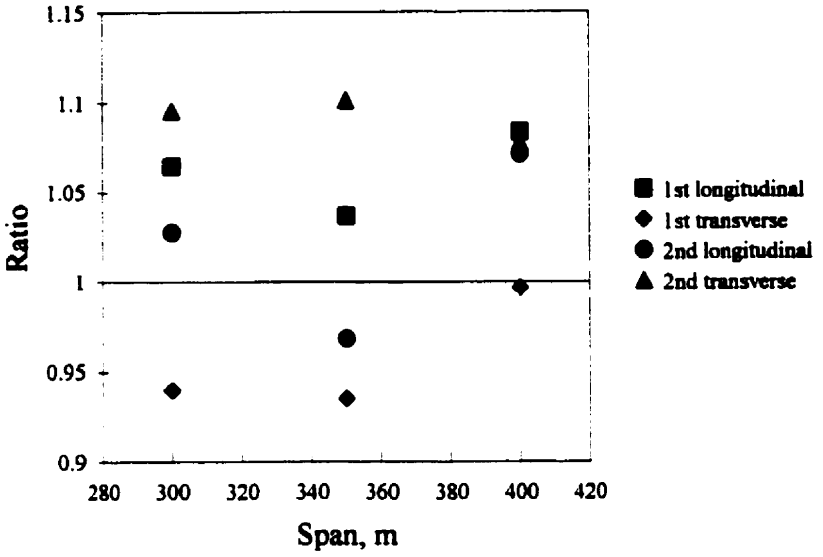

a) Initial tension = 30 kN

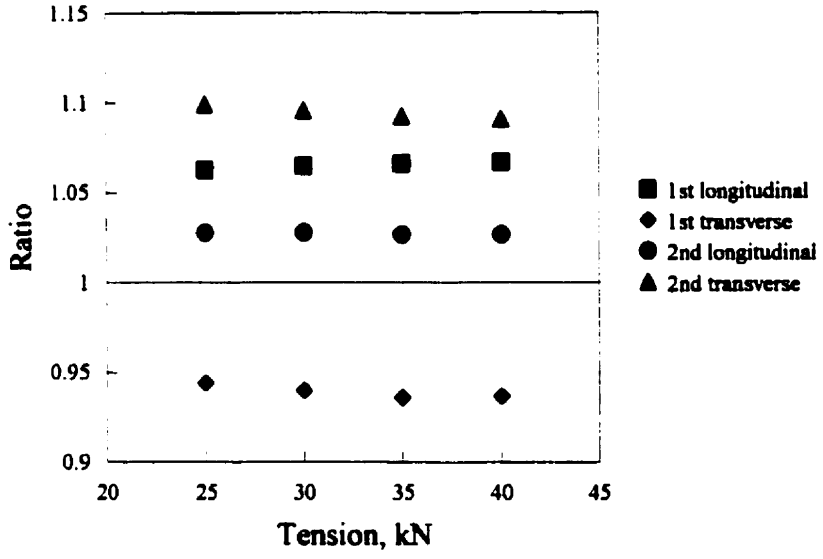

b) Span length = 350 m

Fig. 6.7 Ratio between calculated natural periods of the coupled line system and the bare tower for tower TR6 with Curlew

a)

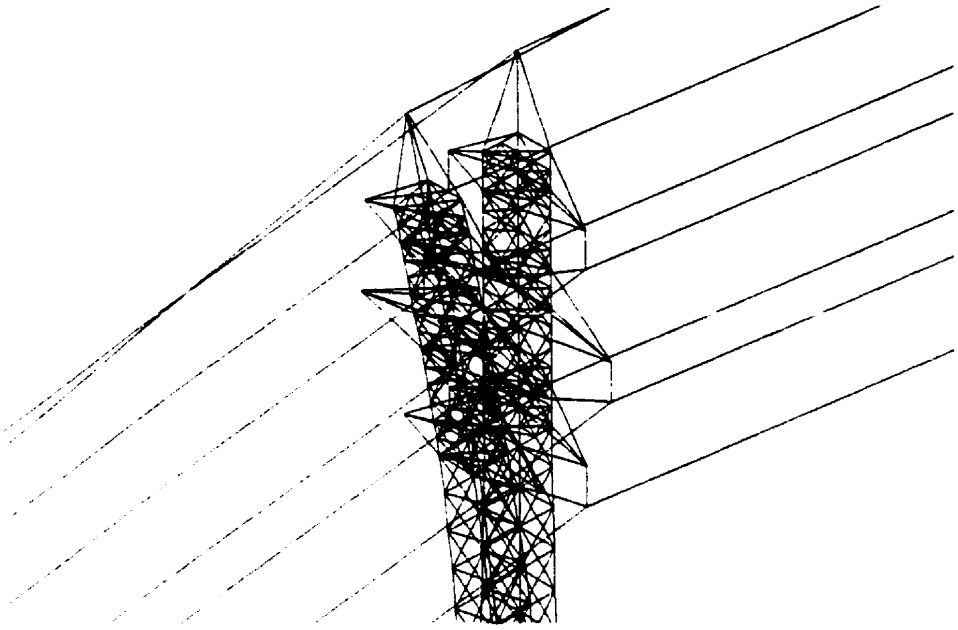

b)

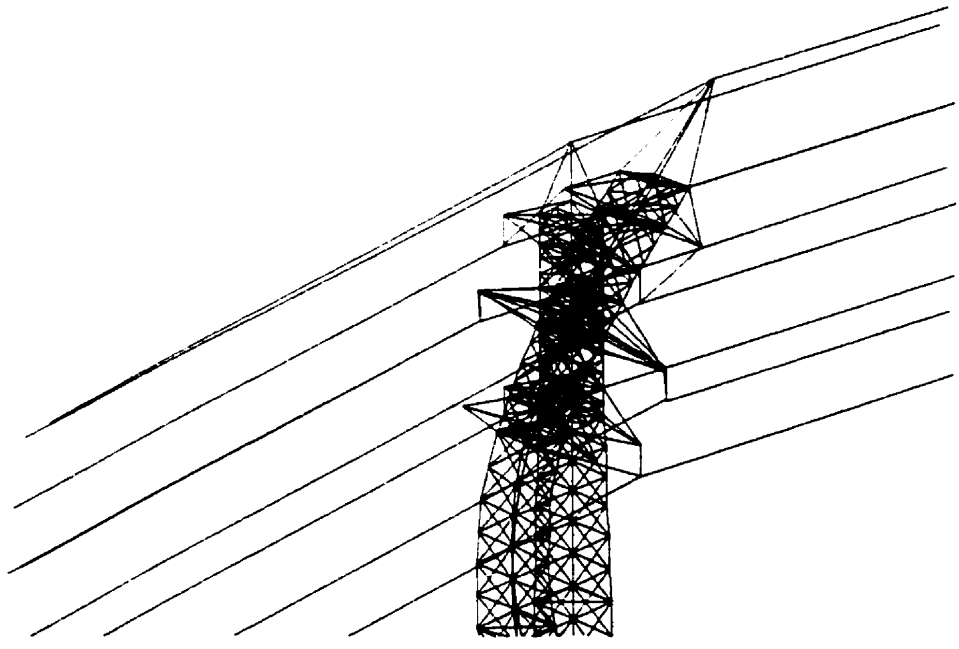

Fig. 6.8 The lowest two calculated longitudinal modes of tower TR6

This conclusion cannot be generalized to angle or anchor towers where the conductors are directly connected to the tower. For the transverse direction there is no clear explanation to the behavior of the system. Therefore, it is believed that at this preliminary stage only the response in the longitudinal direction can be simplified.

6.5 Equivalent Mass

From the previous discussion, it is concluded that only the mass of the overhead ground wire affects the longitudinal modes of the suspension towers. However, Figs. 6.3 to 6.7 indicate that the trend followed by the lowest two longitudinal modes is not linear. Therefore, a single value for the participating mass will not satisfy all the cases and an average should be obtained. The approach followed to obtain this equivalent cable mass for the lowest longitudinal mode can be summarized in the following steps:

1. Obtain the bare tower mode shape for the lowest longitudinal mode

2. Assuming that the mode shape of the tower is not affected by the presence of suspended cables and knowing the mass distribution and frequency of the bare tower, calculate the generalized stiffness of the tower using the following relation:

$$\omega = \sqrt{\frac{k^*}{m^*}} \tag{6.2}$$

where

k^* = generalized stiffness

m^* = generalized mass, eq. (5.20).

3. Assuming that the generalized stiffness of the tower in the system is unchanged and knowing the new frequency of the system in the same longitudinal mode, calculate the generalized mass of the tower in the system.

4. Knowing the generalized mass and the period, calculate the participating mass of the overhead ground wire using eq. (6.2).

This approach was applied to the 30 cases considered in the parametric study, 18 for tower TR2 and 12 for TR6, from which it was concluded that about 25 to 35 % of the overhead ground wire mass is participating in the longitudinal direction. Performing a frequency analysis of the tower alone after replacing the overhead ground wire by 25 to 35% of its mass and neglecting the presence of the conductors showed that for all the cases considered this percentage range yielded acceptable results specially for the lowest mode.

6.6 Conclusions

For the cases studied it can be seen that for suspension towers with level and equal spans the change in the cable tension had no significant effects on the period of the system. It is also seen that only the mass of the overhead ground wire affects the longitudinal modes of vibration of the tower. It is found that 25 to 35% of the overhead ground wire mass contributes in the longitudinal modes of the system. In the transverse direction, however, there is no trend followed that can enable us to assess the contribution of the cables' mass to the transverse modes of the system.

At this point it was concluded that the response of the coupled tower-cable system cannot be simplified in such a manner that would allow the extension of the proposed simplified method for self-supporting telecommunication towers to transmission line towers.

It should be noted that these conclusions do not mean that the system is uncoupled or has only little coupling. Therefore, in the case of seismic effects it could be true that there is only little coupling between the cables and the towers if the tower displacements are small, however, this need to be qualified in another study.

CHAPTER 7

SUMMARY AND CONCLUSIONS

7.1 Summary

The aim of this study was to provide tower designers with suitable tools to evaluate the overall seismic response of self-supporting lattice telecommunication towers without performing detailed dynamic analysis. Ten existing three-legged self-supporting steel telecommunication towers with height ranging from 30 to 120 m were used, which cover the usual range of such towers erected in Canada. A set of 45 earthquake records categorized with respect to their maximum A/V (peak ground acceleration / peak ground velocity) ratio in three categories namely: low, intermediate and high was used as horizontal seismic input. The same set of records was also used as vertical input after reducing its amplitudes to ¾ when studying the vertical response of telecommunication towers. The main findings and contributions can be summarized in the following points:

- Seismic amplification factors for base shear, eq. (4.10), and total vertical reaction, eq. (4.11), for self-supporting lattice telecommunication towers are proposed in a closed form.
- A simplified equivalent static method is proposed to estimate tower member forces due to horizontal and vertical earthquake excitation.
- The effect of including heavy antenna clusters on the base shear and member forces in self-supporting telecommunication towers is investigated.

- An investigation of the frequency characteristics of transmission line towers is carried out. The objective was to investigate the feasibility of simplifying the response of transmission towers in the coupled tower-cable system and then to extend the proposed simplified quasi-static method of analysis to cover this application. Several observations are made from this study, but the main conclusion is that the natural frequencies of the towers could not be simplified in a manner suitable for the direct application of the proposed equivalent static method to transmission line towers.

The following sections recapitulate in some detail the major findings and contributions of this research. Suggestions of future work and a statement of originality are also presented.

7.2 Earthquake Amplification Factors

It is demonstrated that the seismic behavior of self-supporting lattice telecommunication towers differs significantly from that of buildings. This is illustrated through a comparison between the maximum base shear values obtained using the NBCC 1995 static approach and those obtained using the response spectrum method with the NBCC earthquake spectrum. The building code static approach consistently overestimates the base shear values.

New simple expressions are proposed to estimate the maximum base shear, eq. (4.10), and vertical reaction, eq. (4.11), due to horizontal and vertical earthquake excitations. These expressions are based on the total mass of the tower, the lowest flexural

(or axial, as appropriate) period of the tower and the peak ground acceleration specified for the tower site. The base reactions obtained from these expressions are not meant to be redistributed along the tower height, as in the building code static approach. They are seismic response parameters that should indicate whether or not earthquake effects may govern the design. If seismic effects are likely to be significant based on these maximum base reactions, a more detailed, yet still simple method is proposed to approximate these effects on member forces.

7.3 Simplified Methods of Analysis

The research resulted in proposing two simple equivalent static methods for seismic analysis of self-supporting lattice telecommunication towers subjected to base excitations in the horizontal and vertical directions.

In the first method, a horizontal acceleration profile is defined based on both the response spectrum approach and modal analysis method, including the effect of the lowest three flexural modes of vibration of the tower. The main idea is to define an acceleration profile which will produce the same effect on the tower as the combined effect of the lowest three flexural modes. The proposed acceleration profile has yielded very good results in estimating member forces with an average error of ±7% and a maximum error of ±25% when compared to results obtained from response spectrum analysis.

In the second method, a vertical acceleration profile is proposed which only includes the lowest axial mode of vibration of the tower. The use of this acceleration profile has also produced very good results with a maximum error of only ±10% and an average error of ±2% only.

The effects of the presence of heavy antenna clusters near the top of the towers are also investigated both locally, on individual member forces, and globally on base reactions. The main findings are as follows:

- Added mass consistently reduces the base shear (within the range of values considered) with an average reduction of 22% compared to the corresponding bare tower case.
- Leg member forces near the base are also reduced by 15% on average.
- At relative heights of 0.5 to 0.7, force amplifications begin to appear in the leg members.
- Diagonal and horizontal members close to the antenna attachments experience very large force amplifications. A factor of 20 is calculated when 10% of the tower mass (a very large value meant to be an upper bound) was lumped at the top.
- Diagonals and horizontals near the base experience a change in internal force which does not exceed ±10% when compared to the bare tower case.

The proposed equivalent static method was verified on bare towers with height ranging from 30 to 120 m. It is suitable for towers with lightweight antennae (less than 5% of tower self-weight), however, towers with heavy antennae (mass > 5% of tower mass) cannot be analyzed using this method without modifications to the a_i coefficients.

7.4 Analysis of Transmission Line Towers

The following conclusions were drawn for suspension towers and cannot be generalized to cover other types of transmission towers or line parameters:

- The change in the cable tension had no significant effect on the fundamental periods of the system.
- Only the mass of the overhead ground wire has an effect on the frequency characteristics of the tower-cable system. The replacement of the overhead ground wire by 25% to 35% of its mass produced satisfactory results specially for the lowest longitudinal flexural period.
- The response in the transverse direction could not be simplified in the same manner. This is due to the fact that there is no clear trend in the results that could enable us to assess the contribution of the cables' mass to the transverse modes of the system.
- The response of the tower-cable system could not be simplified in a way permitting the application of the proposed equivalent static method for seismic response to transmission line towers.

7.5 Recommendations for Future Work

The work presented in this thesis has covered several aspects related to the simplification of the seismic analysis of self-supporting lattice telecommunication towers, but more research is still needed to further investigate the following topics:

1) The effect of including heavy antennae and accessories on the prediction of the mode shapes and natural frequencies of vibration of telecommunication towers.
2) The effect of including the torsionsal modes of vibrations on the seismic response of telecommunication towers.

3) The effect of foundation flexibility on the seismic response of telecommunication towers.

4) The applicability of the proposed method to four-legged towers.

5) A comprehensive study on the seismic analysis of transmission line towers.

Statement of Originality

To the best of author's knowledge, this work constitutes the first comprehensive research on the simplified seismic analysis of self-supporting telecommunication towers. The following summarize the three main original contributions of the thesis:

1) Two simple seismic response indicators are proposed which can be used by tower designers to estimate the maximum base shear and the total vertical reaction of self-supporting telecommunication towers due to earthquake excitations.

2) A simplified equivalent static method is proposed for the prediction of member forces in self-supporting telecommunication towers due to horizontal and vertical earthquake excitations. The originality of the method lies in the definition of an acceleration profile adapted to the essential dynamic characteristics (natural frequencies and mode shapes) of the towers.

3) A better understanding of the effect of heavy antenna clusters on the seismic response of telecommunication towers.

REFERENCES

ADINA R&D, Inc. (1997). 'ADINA (Automatic Dynamic Incremental Nonlinear Analysis) Theory and Modelling Guide', Report ARD 97-8, Watertown, MA., U.S.A.

Anagnostopoulos, S. A. (1982). 'Wave and Earthquake Response of Offshore Structures: Evaluation of Modal Solutions', *Journal of the Structural Division*, ASCE, Vol. 108, No. ST10, 2175-2191.

ASCE Standard (1986). 'Seismic Analysis of Safety-Related Nuclear Structures', *American Society of Civil Engineers*, ASCE 4-86.

Australia Standards AS 3995 (1994). 'Design of Steel Lattice Towers and Masts', *Standards Australia.*

Bathe, K. J. (1982). 'Finite Element Procedures in Engineering Analysis', Prentice-Hall, Englewood Cliffs, NJ.

Baenziger, M.A., James, W.D., Wouters, B., and Li, L. (1994). 'Dynamic Loads on Transmission Line Structures Due to Galloping Conductors', *IEEE Transaction on Power Delivery*, Vol. 9, No. 1, 40-47.

CAN/CSA - S37, (1994). 'Antennas, Towers, and Antenna-Supporting Structures', *Canadian Standards Association.*

Chan, H. S. (1994). 'Earthquake Response Spectrum Analysis of Offshore Platforms', *Engineering Structures*, Vol. 9, No. 10, 272-276, October.

Chiu, A.N.L. and Taoka, G.T. (1973). 'Tower Response to Actual and Simulated Wind Forces', *Journal of The Structural Division*, ASCE, Vol. 99, No. ST9, 1911-1929.

Chopra, A. K. and Goyal, A. (1991). 'Simplified Earthquake Analysis of Intake Outlet Towers', *Journal of Structural Engineering*, ASCE, Vol. 117, No. 3, 767-788.

Clough, R. W. and Penzien, J. (1993). 'Dynamics of Structures', McGraw-Hill, New York.

European Prestandard ENV 1998-3 (1995). 'Design Provisions for Earthquake Resistance of Structures, Part 3: Towers, Masts and Chimneys', Brussels.

Gálvez, C. and McClure, G. (1995). 'A Simplified Method for Aseismic Design of Self-Supporting Lattice Telecommunication Towers', *Proc. of the 7th Canadian Conference on Earthquake Engineering*, Montreal, 5-7 June, 541-548.

Gálvez, C. (1995). 'Static Method For Aseismic Design of Self-Supporting Towers', M.Eng. Project Report G95-08, Department of Civil Engineering and Applied Mechanics, McGill University.

Gupta, A. K. (1992). 'Response Spectrum Method in Seismic Analysis and Design of Structures', CRC Press, Boca Raton.

Holmes, J. D. (1994). 'Along-Wind Response of Lattice Towers: Part I - Derivation of Expressions for Gust Response Factors', *Engineering Structures*, Vol. 16, No. 4, 287-292.

_____ (1996). 'Along-Wind Response of Lattice Towers: Part II - Aerodynamic Damping and Deflections', *Engineering Structures*, Vol. 18, No. 7, 483-488.

_____ (1996). 'Along-Wind Response of Lattice Towers: Part III - Effective Load Distributions', *Engineering Structures*, Vol. 18, No. 7, 489-494.

Jamaleddine, A., McClure, G., Rousselet, J., and Beauchemin, R. (1993), 'Simulation of Ice-Shedding on Electrical Transmission Lines Using ADINA', *Computers and Structures*, Vol. 47, No. 4/5, 523-536.

Kempner, L. draft (1996). TS 13 Nonbuilding Structures, US NEHRP.

Khedr, M. A. (1997). 'Seismic Analysis of Lattice Towers - Literature Review', Structural Engineering Report, No. 97-9, Department of Civil Engineering and Applied Mechanics, McGill University.

Khedr, M. A. and McClure, G. (1997). 'A Quasi-Static Method for the Seismic Analysis of Self-supporting Latticed Telecommunication Towers', *Proceedings of the 25th Annual Conference of the Canadian Society for Civil Engineering*, Sherbrooke, Quebec, Canada, Vol. 6, pp 327-336.

Khedr, M. A. and McClure, G. (1998). 'Earthquake Amplification Factors for Self-supporting Telecommunication Towers', *The Canadian Journal of Civil Engineering* (accepted for publication).

Konno, T. and Kimura, E. (1973). 'Earthquake Effects on Steel Tower Structures Atop Building', *World Conference of Earthquake Engineering*, Vol. 1, 184-193.

Kotsubo, S., Takanishi, T., Uno, K., and Sonoda, T.(1985). 'Dynamic Tests and Seismic Analyses of High Steel Towers of Electrical Transmission Line', *Transactions of JSCE*, Vol. 15, 72-75.

Li, H., Wang, S., Lu, M., and Wang, Q. (1991). 'Aseismic Calculations for Transmission Towers', *Lifeline Earthquake Engineering, Proceedings of the Third US Conference*, August 22-23, 275-284, ASCE, New York.

Li, H-N., Swarez L. E. and Singh, M. P. (1994). 'Seismic Effects on High-Voltage Transmission Tower and Cable Systems', *Proceedings of the Fifth US National Conference on Earthquake Engineering*, Earthquake Engineering Research Institute, Oakland, California, Vol. IV, 819-827.

Long, L.W. (1974). 'Analysis of Seismic Effects on Transmission Structures', *IEEE Transactions on Power Apparatus and Systems*, Vol. 93, No 1, 248-254.

McClure, G. and Tinawi, R. (1987). 'Mathematical Modeling of the Transient Response of Electric Transmission Lines Due to Conductor Breakage', *Computers and Structures*, Vol. 26, No. 1/2, 41-56.

Mikus, J. (1994). 'Seismic Analysis of Self-Supporting Telecommunication Towers', M. Eng. Project Report G94-10, Department of Civil Engineering and Applied Mechanics, McGill University.

National Research Council of Canada (1995). *National Building Code of Canada 1995*, 11th edition, Ottawa.

Ozono, S. and Maeda, J. (1992). 'In-Plane Dynamic Interaction Between a Tower and Conductors at Lower Frequencies', *Engineering Structures*, Vol. 14, No. 4, 210-216.

Ozono, S., Maeda, J. and Makino, M.(1988). 'Characteristics of In-Plane Free Vibration of Transmission Line Systems', *Engineering Structures*, Vol. 10, No. 10, 272-280.

Paz, M. (1994). 'International Handbook of Earthquake Engineering: Codes, Programs, and Examples', Champan & Hall, New York.

Pierre, J. R. (1995). 'Damage Caused by the Hanshin-Awaji (Kobe-Japan) Earthquake to the Electrical and Telecommunications Networks and its Impact on the Implementation of Emergency Measures', RE-GEN-95-40, Hydro-Québec.

Penzien, J. and Kaul, M. K. (1972). 'Response of Offshore Towers to Strong Motion Earthquakes', *Earthquake Engineering and Structural Dynamics*, Vol. 1, 55-68.

Sackmann, V. (1996). ' Prediction of Natural Frequencies and Mode Shapes of Self-Supporting Lattice Telecommunication Towers', Diplomarbeit-Nr. 76, Technische Universität

München, Lehrstuhl Für Baumechanik & Department of Civil Engineering and Applied Mechanics, McGill University.

Tso, W. K., Zhu, T. J. and Heidebrecht, A. C. (1992). 'Engineering implication of ground motion A/V ratio', *Soil Dynamics and Earthquake Engineering*, Vol. 11, No. 3, 133-144.

Valliappan, S., White, W., Germanis, E. and Jagger, A.C. (1980). 'Analysis of Earthquake Effects on the Intake Tower of Mangrove Creek Dam', *Proceedings of the International Conference on Engineering for Protection from Natural Disasters*, Bangkok, January 1980, 85-98.

Venkateswarlu, B., Harikrishna, P., Rajan S., and Kumar, M. (1994). 'Stochastic Gust Response of Microwave Lattice Towers', *Computers and Structures*, Vol. 52, No. 5, 1031-1041.

Wilson, E.L. and Habibullah, A. (1988). 'SAP90 User's Manual', Computers and Structures, Inc. Berkely, California.

Wolfram, S. (1996). 'The Mathematica Book, Third Edition'. Wolfram Media, Inc. and Cambridge University Press.

APPENDIX A

EARTHQUAKE RECORDS

A1: EARTHQUAKE RECORDS WITH LOW A/V RATIO

A2: EARTHQUAKE RECORDS WITH INTERMEDIATE A/V RATIO

A3: EARTHQUAKE RECORDS WITH HIGH A/V RATIO

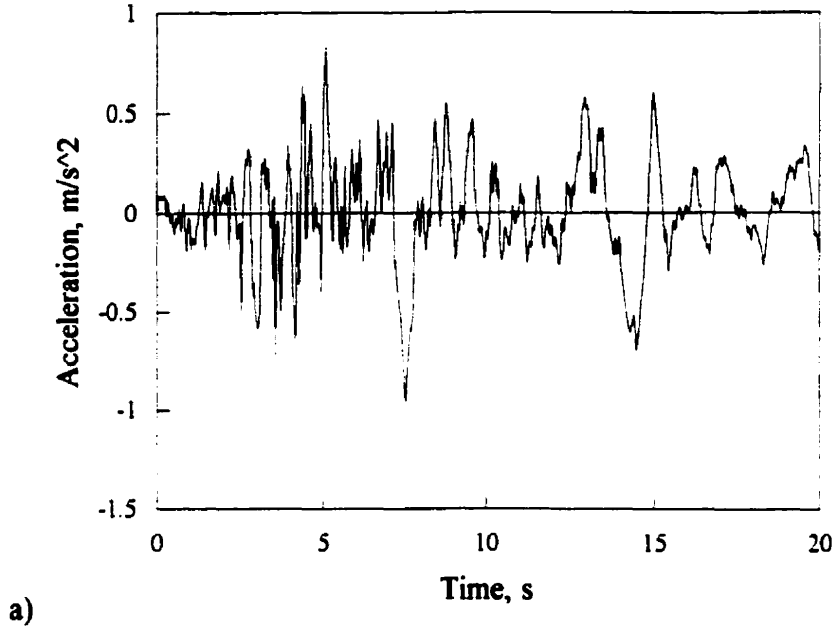

a)

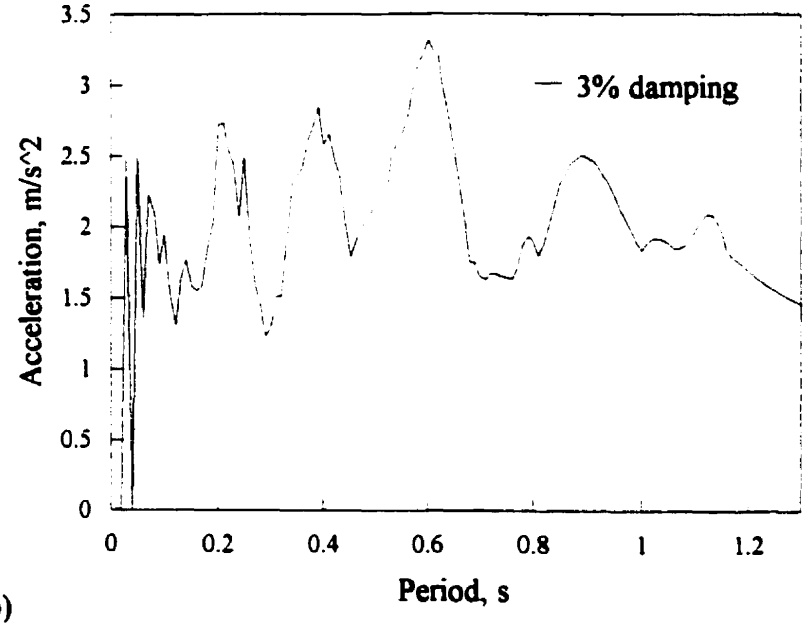

b)

Fig. A1.1 Earthquake record Long Beach, N51W (L1)

Event: Long Beach earthquake
Compnent: N51W
Station: L.A. Subway Terminal, Los Angeles, Cal..
Peak Acceleration: 95.63460 cm/s^2 at 7.50 s
Peak Velocity: -23.68613 cm/s at 13.62 s

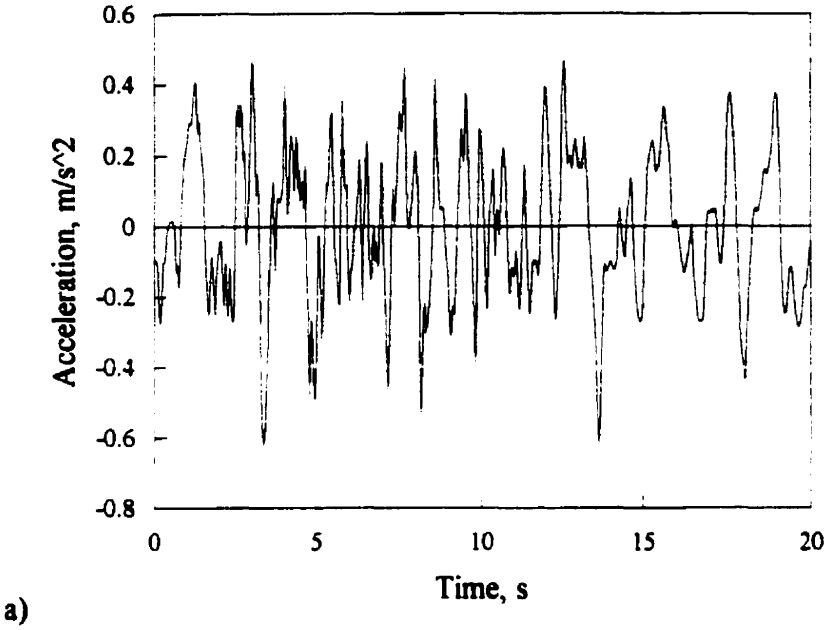

a)

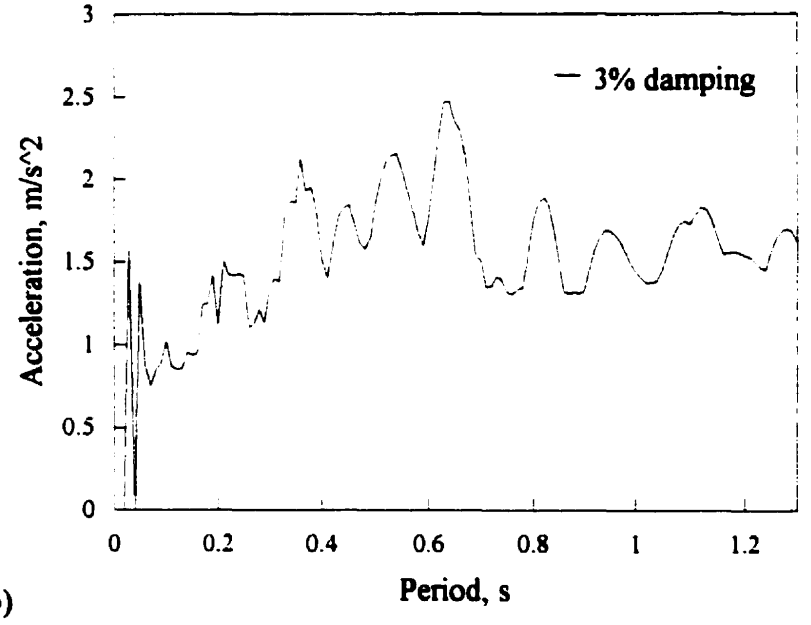

b)

Fig. A1.2 Earthquake record Long Beach N39E (L2)

Event: Long Beach earthquake
Compnent: N39E
Station: L.A. Subway Terminal, LOS Angeles, Cal.
Peak Acceleration: 62.32811 cm/s^2 at 3.36 s
Peak Velocity: -17.34293 cm/s at 13.32 s

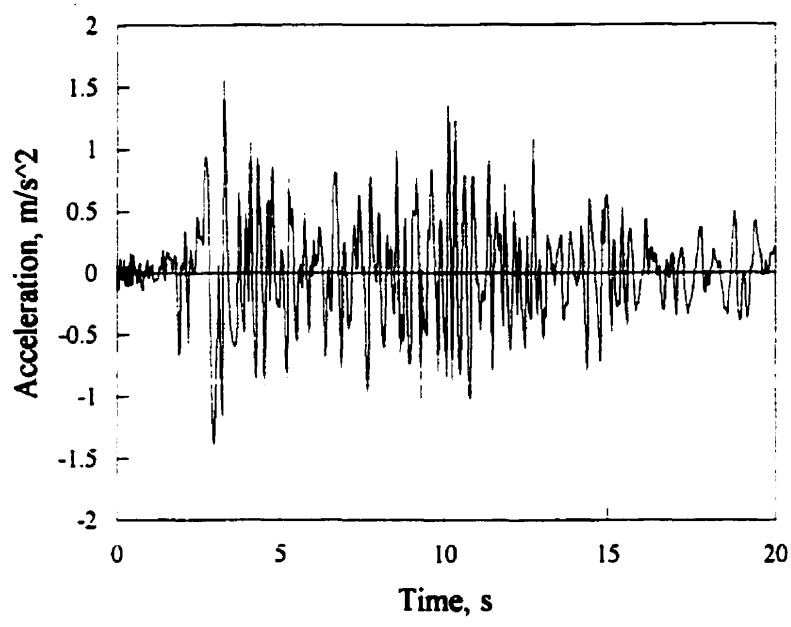

a)

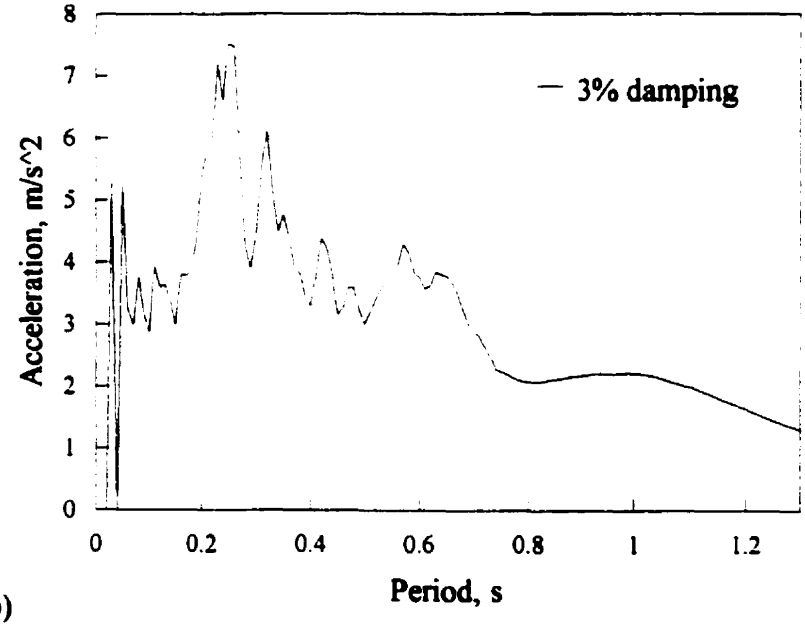

b)

Fig. A1.3 Earthquake record Lower California S00W (L3)

Event: Lower California earthquake
Compnent: S00W
Station: EL Centro Imperial Valley
Peak Acceleration: -156.82112 cm/s^2 at 3.32 s
Peak Velocity: -20.85573 cm/s at 2.90 s

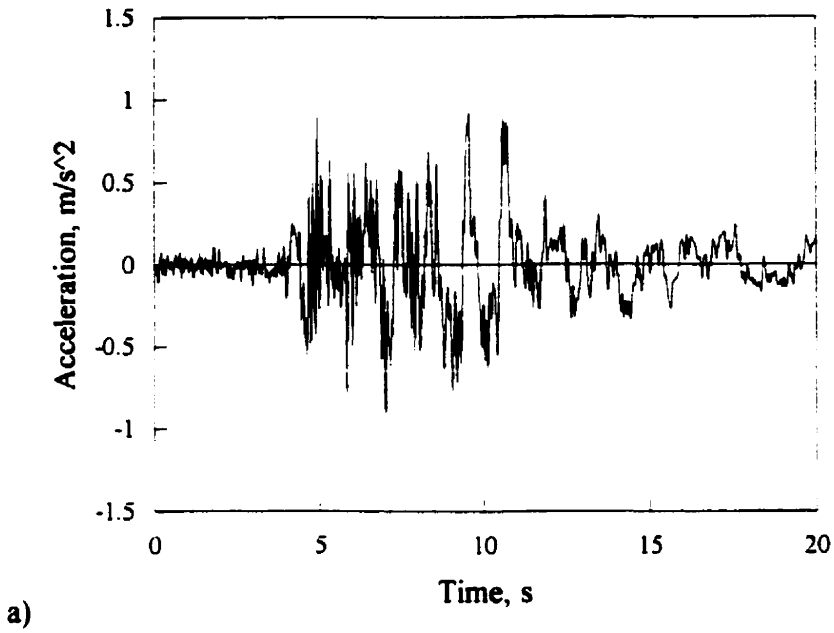

a)

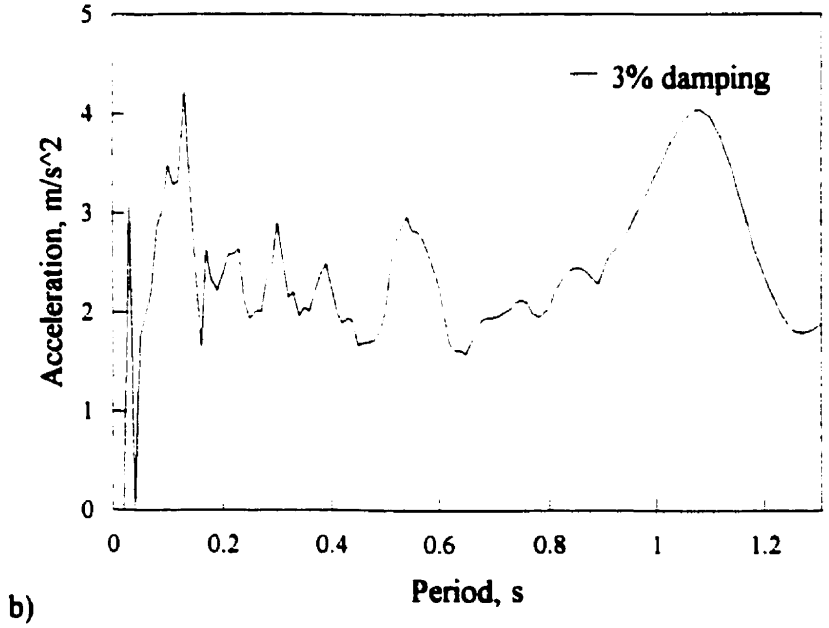

b)

Fig.A1.4 Earthquake record San Fernando N61W (L4)

Event : San Fernando earthquake
Component: N61W
Station: 2500 Wilshire Blvd., Basement, Los Angeles, Cal.
Peak Acceleration: 98.74722 cm/s^2
Peak Velocity: 19.30336 cm/s

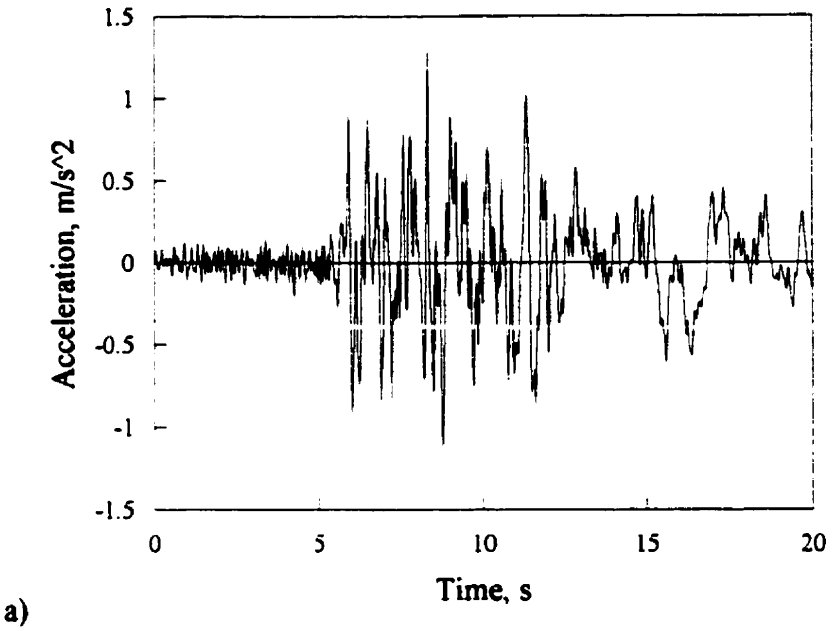

a)

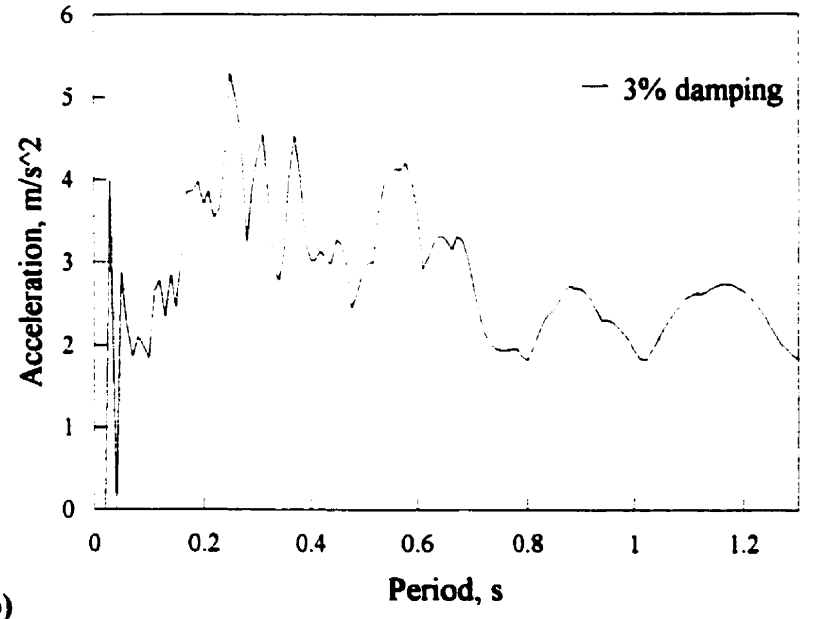

b)

Fig. A1.5 Earthquake record San Fernando West (L5)

Event: San Fernando earthquake
Component: West
Station: 3550 Wilshire Blvd., Basement, Los Angeles, Cal.
Peak Acceleration: -129.81620 cm/s^2
Peak Velocity: 21.58354 cm

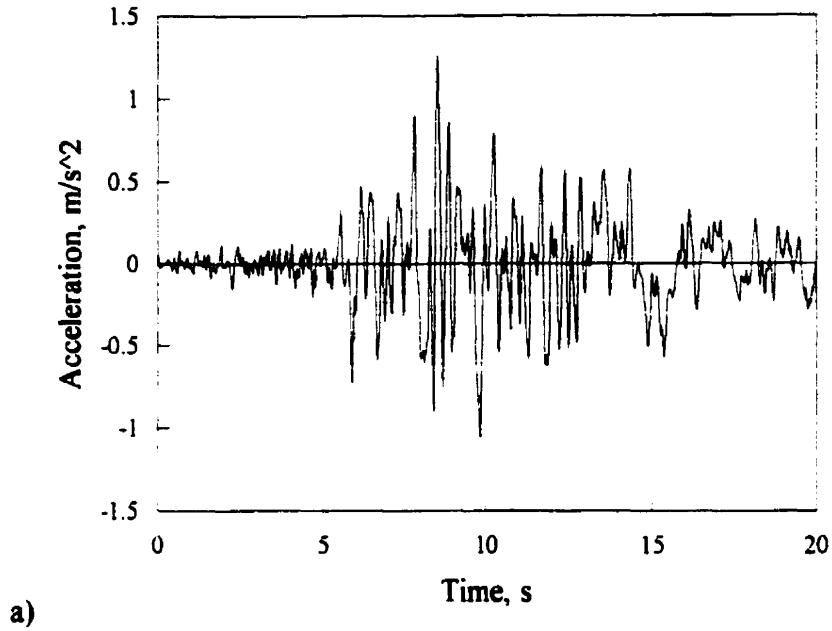

a)

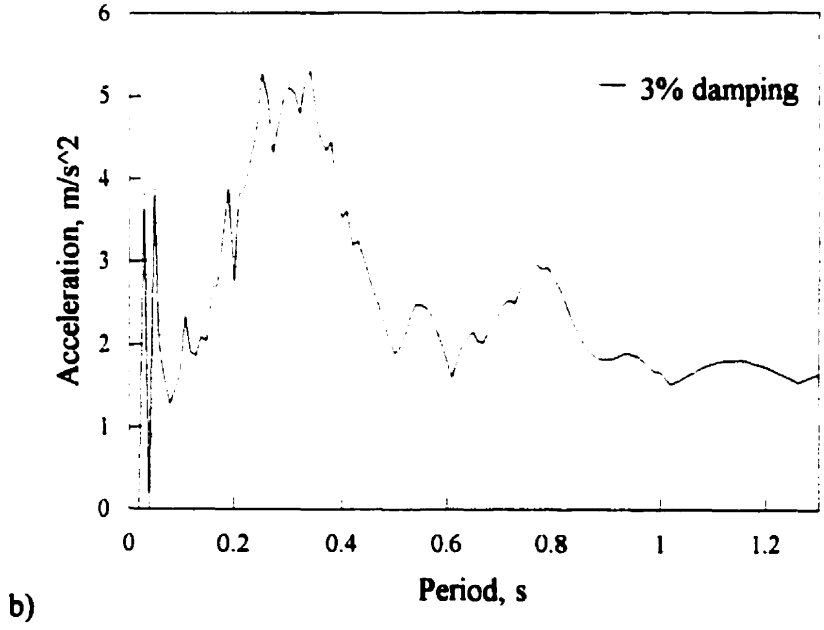

b)

Fig. A1.6 Earthquake record San Fernando S37W (L6)

Event: San Fernando earthquake
Component: S37W
Station: 222 Figueroa Street, 1st. floor, Los Angeles, Cal.
Peak Acceleration: -126.88940 cm/s^2
Peak Velocity: -18.63307 cm

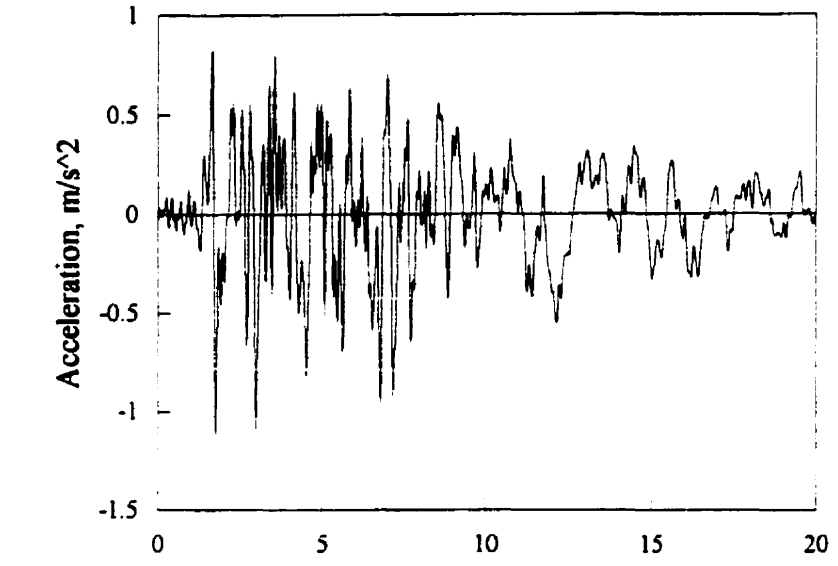

a)

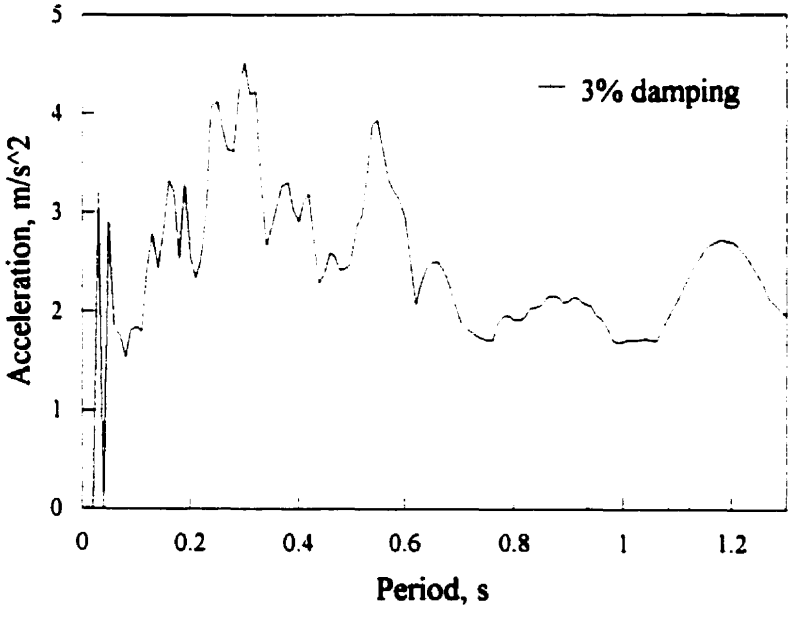

b)

Fig. A1.7 Earthquake record San Fernando S90W (L7)

Event: San Fernando earthquake
Component: S90W
Station: 3470 Wilshire Blvd., Sub-basment, Los Angeles, Cal.
Peak Acceleration: 111.84380 cm/s^2
Peak Velocity: 18.56407 cm/s

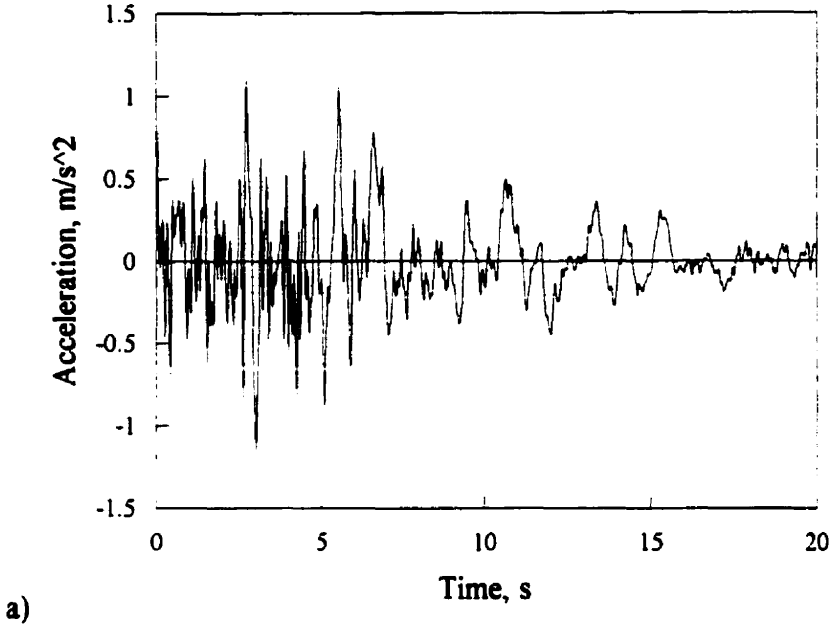

a)

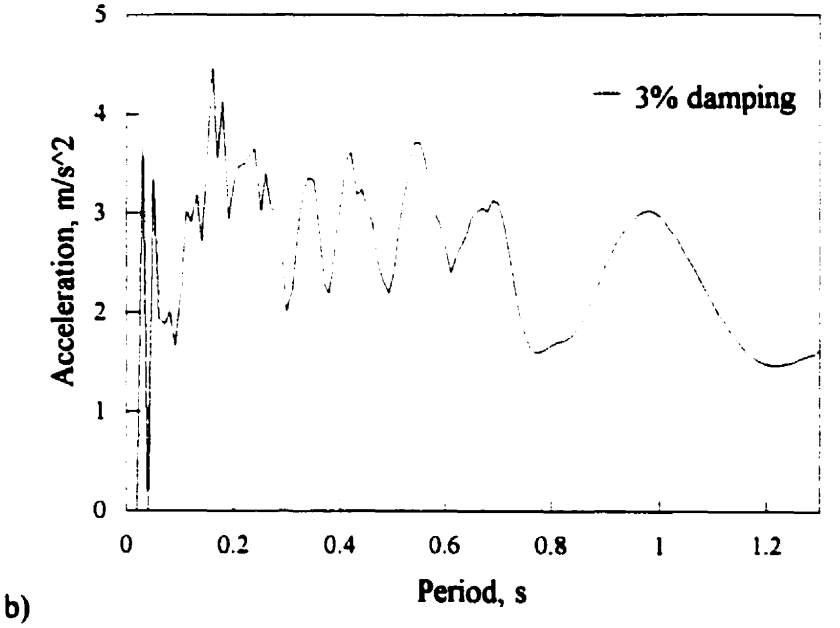

b)

Fig. A1.8 Earthquake record San Fernando N15E (L8)

Event: San Fernando earthquake
Component: N15E
Station: 4680 Wilshire Blvd., Basement, Los Angeles, Cal.
Peak Acceleration: 114.97610 cm/s^2
Peak Velocity: 21.53514 cm

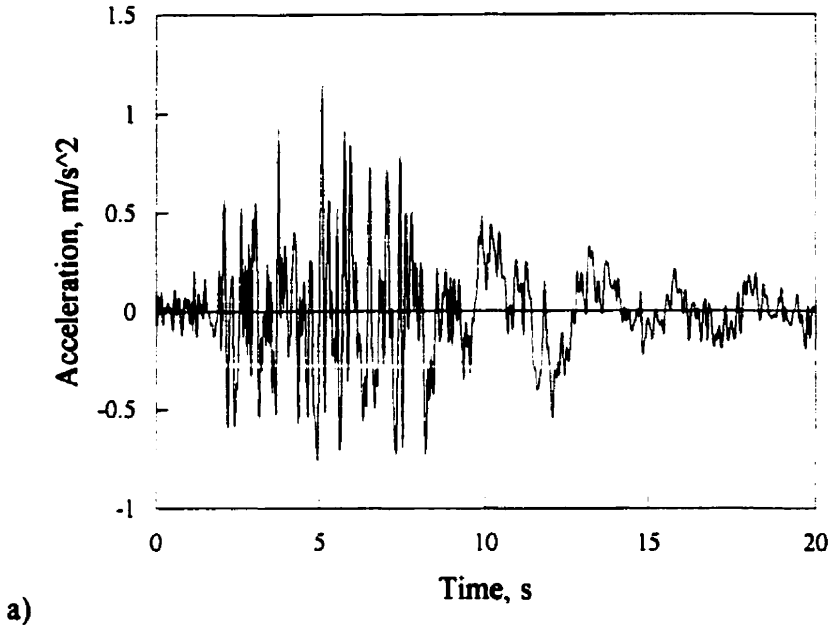

a)

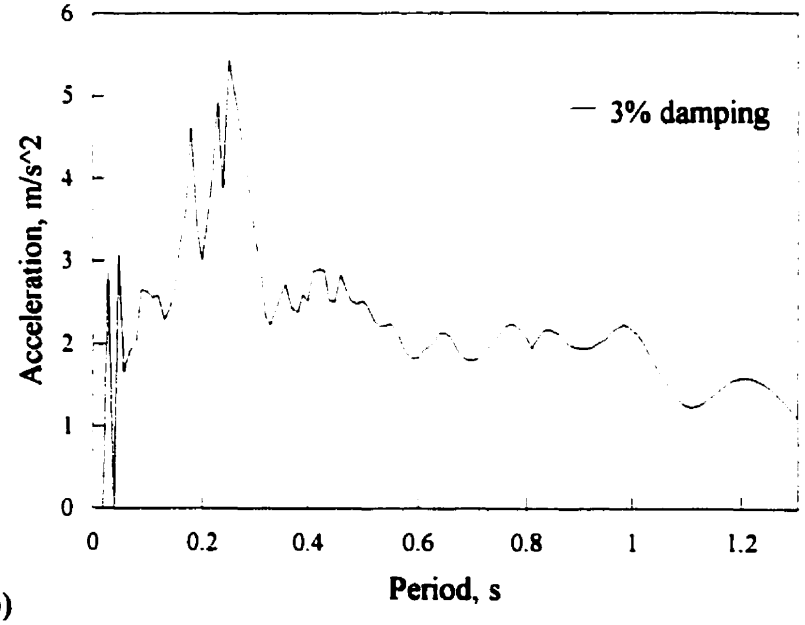

b)

Fig. A1.9 Earthquake record San Fernando S38W (L9)

Event: San Fernando earthquake
Component: S38W
Station: 445 Figueroa Street, Sub-basement, Los Angeles, Cal.
Peak Acceleration: -116.96350 cm/s^2
Peak Velocity: -17.31090 cm

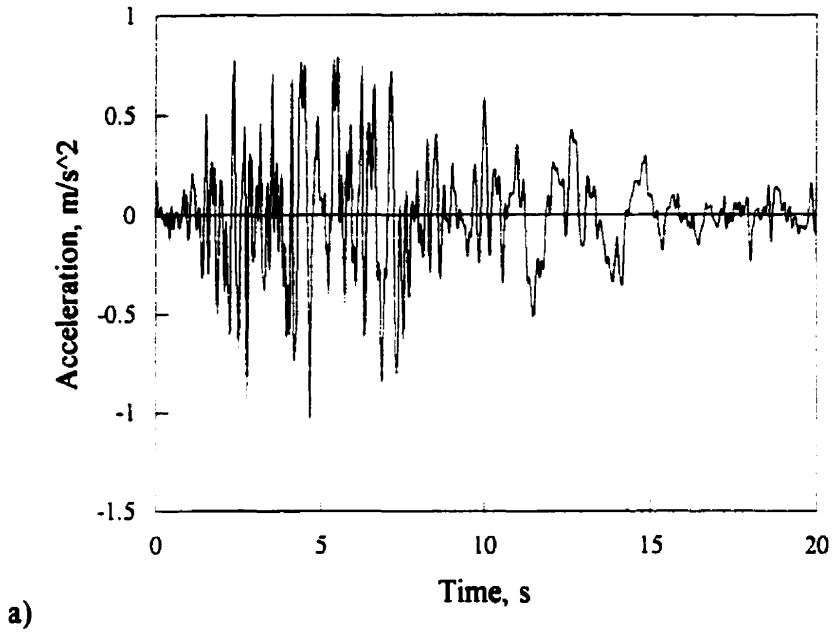

a)

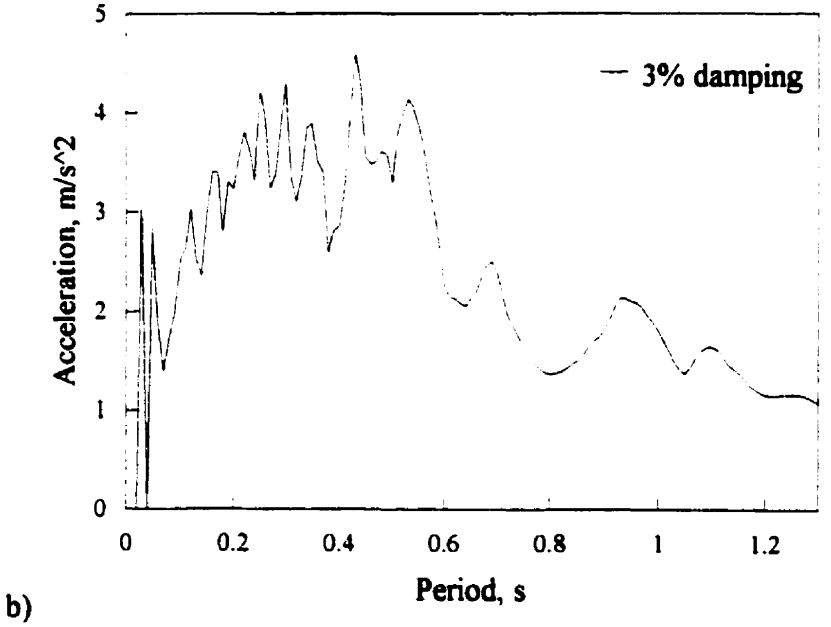

b)

Fig. A1.10 Earthquake record San Fernando S00W (L10)

Event: San Fernando earthquake
Component: S00W
Station: Hollywood Storage, Basement, Los Angeles, Cal.
Peak Acceleration: 103.78419 cm/s^2
Peak Velocity -16.96477 cm/s

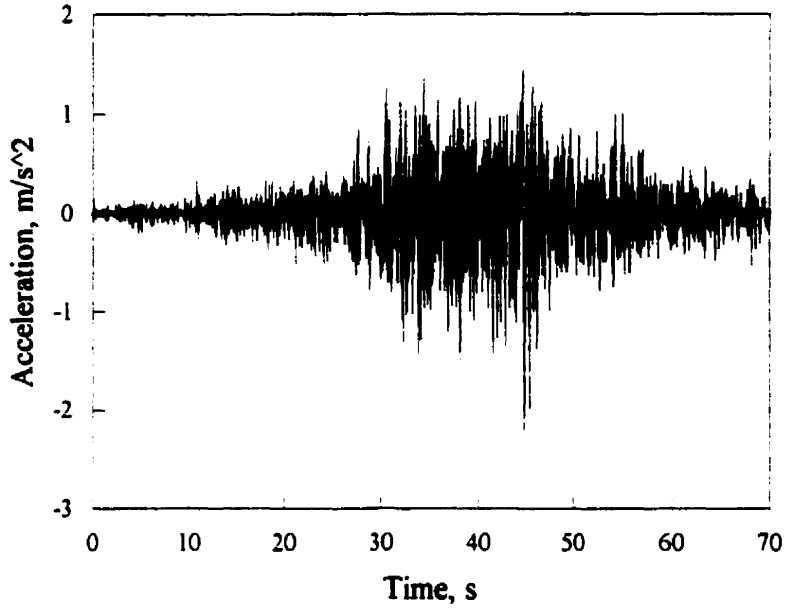

a)

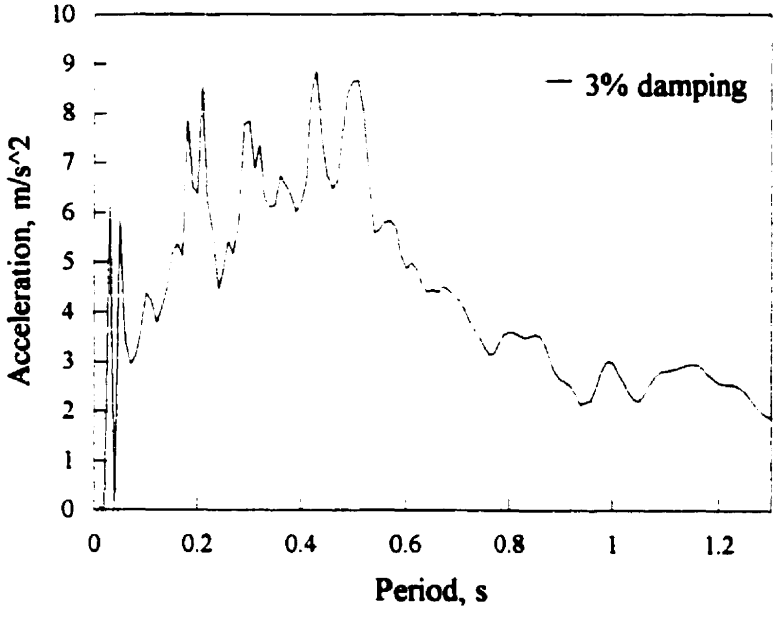

b)

Fig. A1.11 Earthquake record Near E. Cost of Honshu NS (L11)

Event: Near E. Cost of Honshu earthquake
Component: NS
Station: HK003
Peak Acceleration: -221.50 cm/s^2
Peak Velocity: 33.40 cm/s

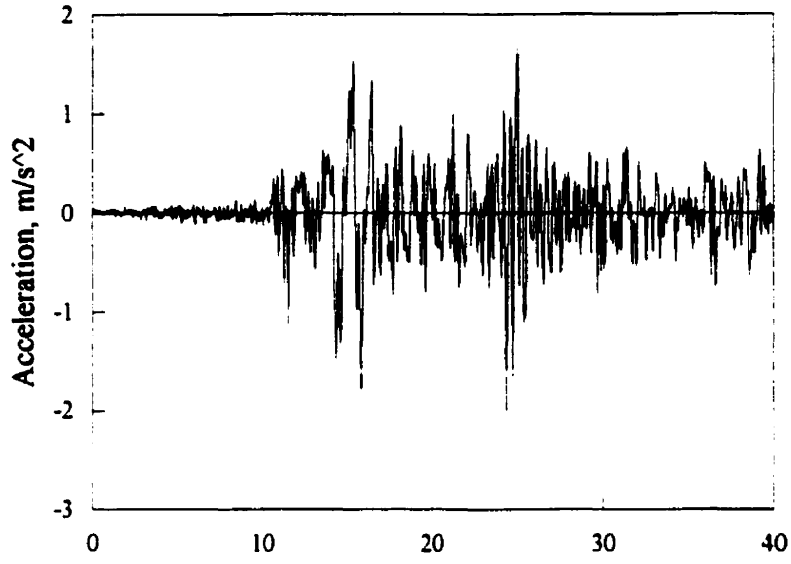

a)

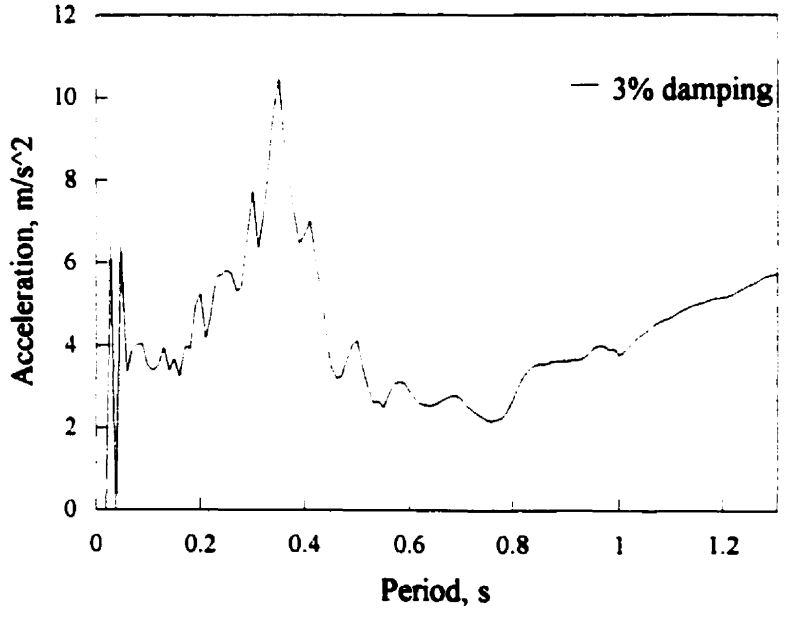

b)

Fig. A1.12 Earthquake record Near E. Coast of Honshu (L12)

Event: Near E. Coast of Honshu earthquake
Component: NS
Station: HK004
Peak Acceleration: -200.9 cm/s^2
Peak Velocity: 27.5 cm/s

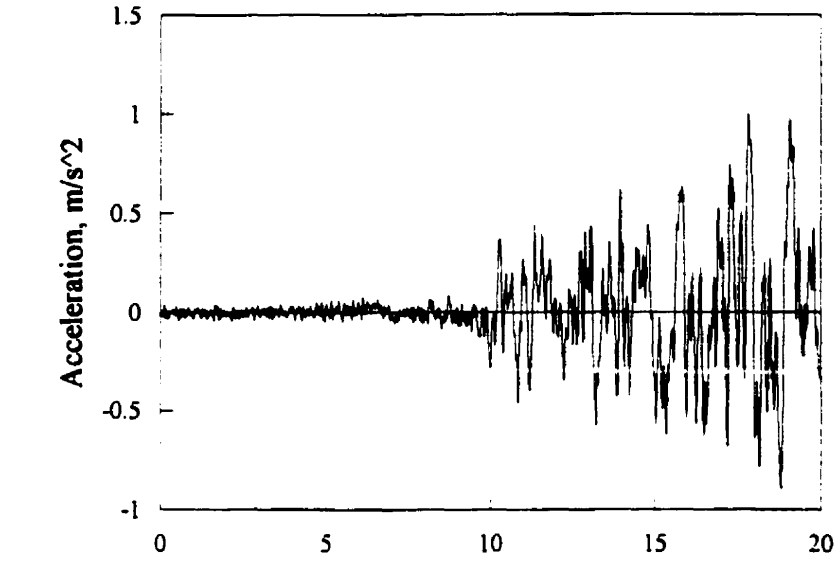

a)

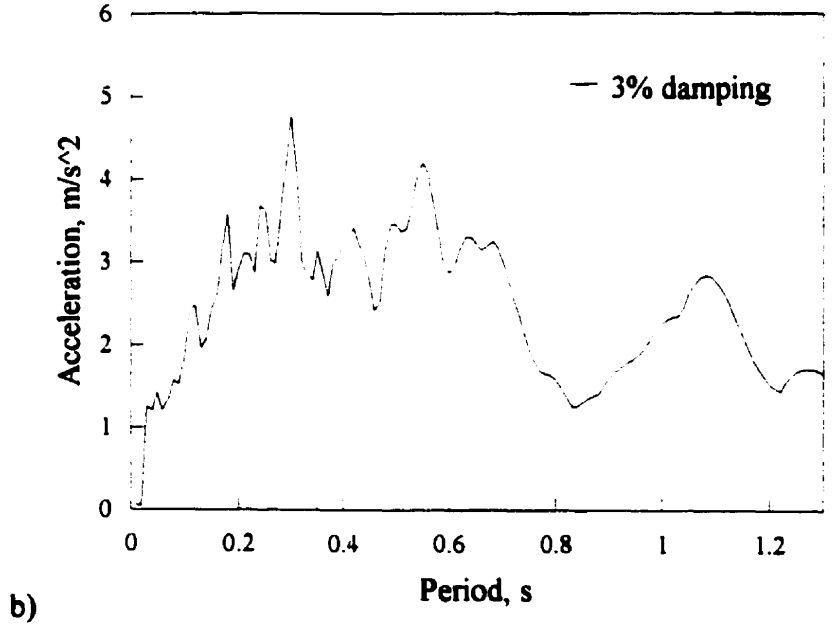

b)

Fig. A1.13 Earthquake record Michoacan S00E (L13)

Event: Michoacan earthquake
Component: S00E
Station: AZIH
Peak Acceleration: 101.30 cm/s^2
Peak Velocity: -15.86 cm/s

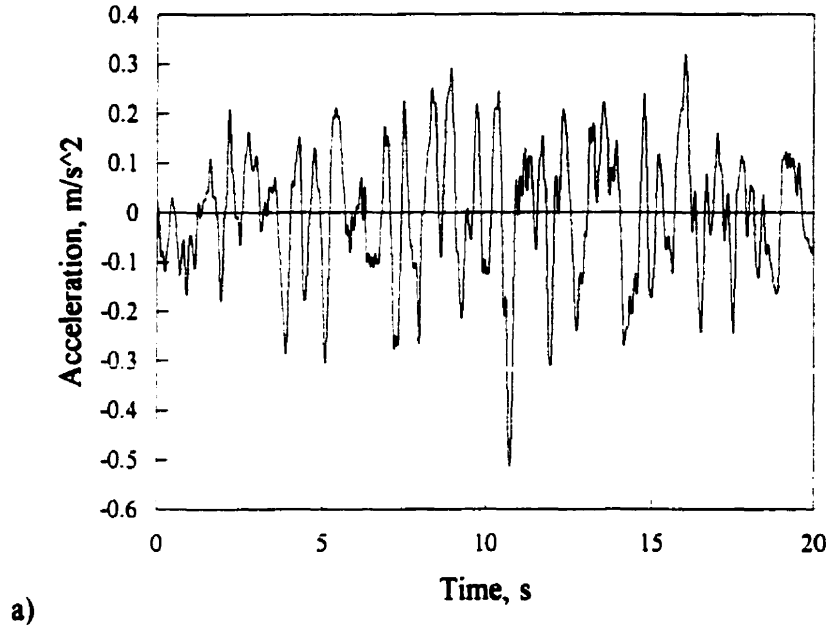

a)

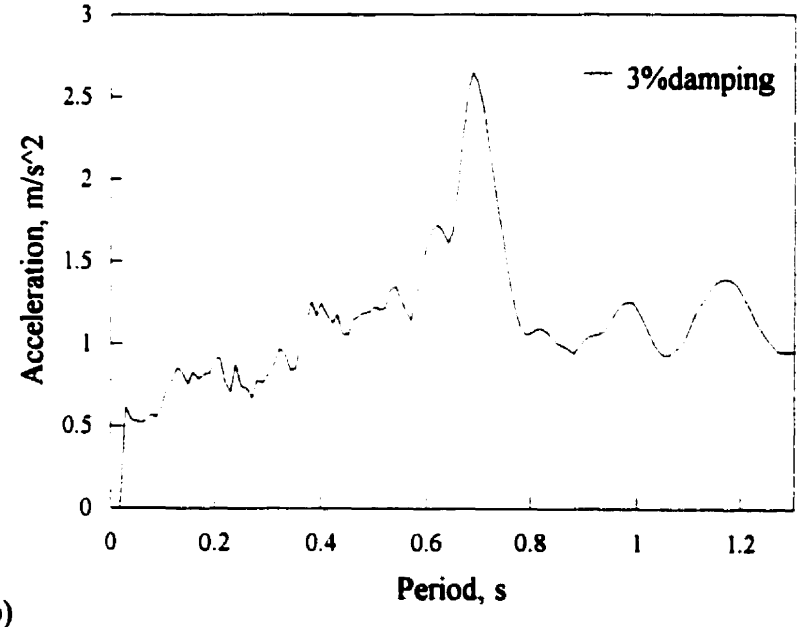

b)

Fig. A1.14 Earthquake record Michoacan N00E (L14)

Record: Michoacan earthquake
Component: N00E
Station: TEAC
Peak Acceleration: -51.30 cm/s^2
Peak Velocity: 7.38 m/s

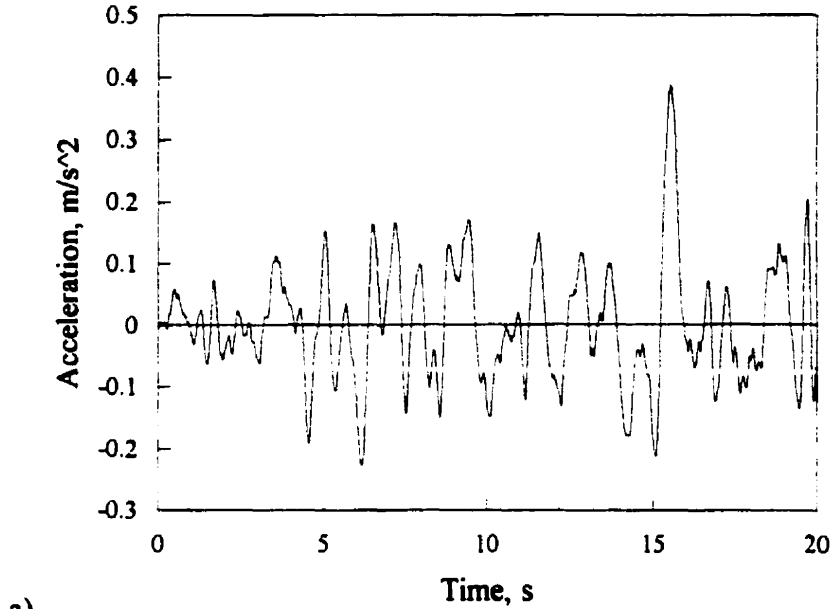

a)

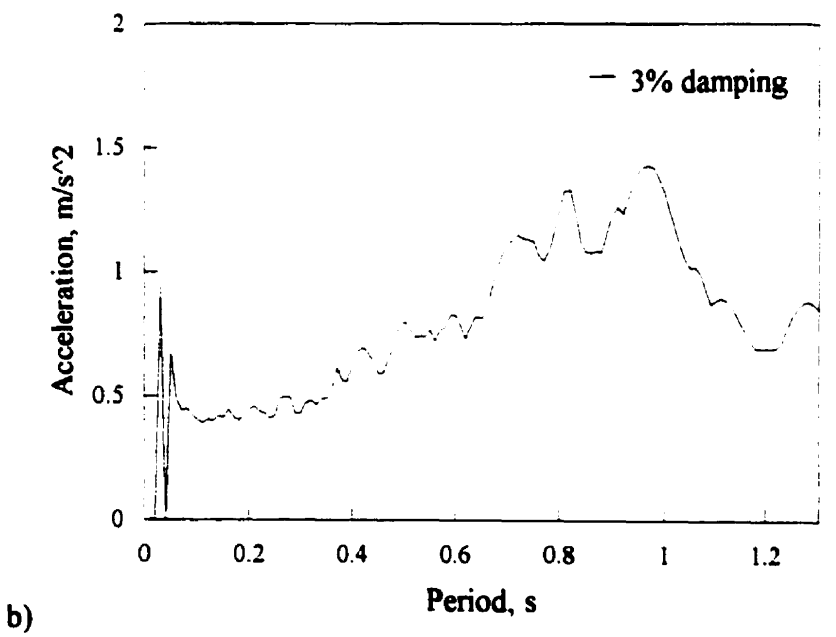

b)

Fig. A1.15 Earthquake record Michoacan N90W (L15)

Event: Michoacan earthquake
Component: N90W
Station: CUMV
Peak Acceleration: 38.83 m/s^2
Peak Velocity: -11.01 m/s

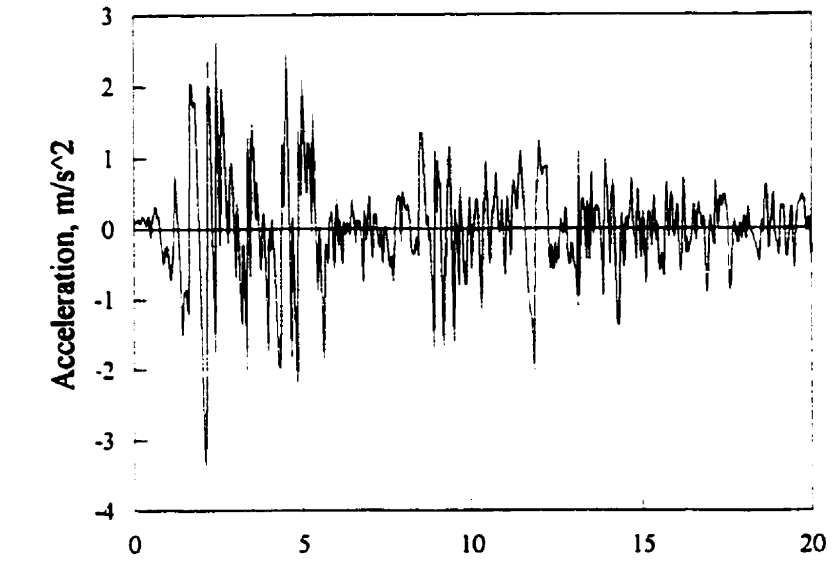

a)

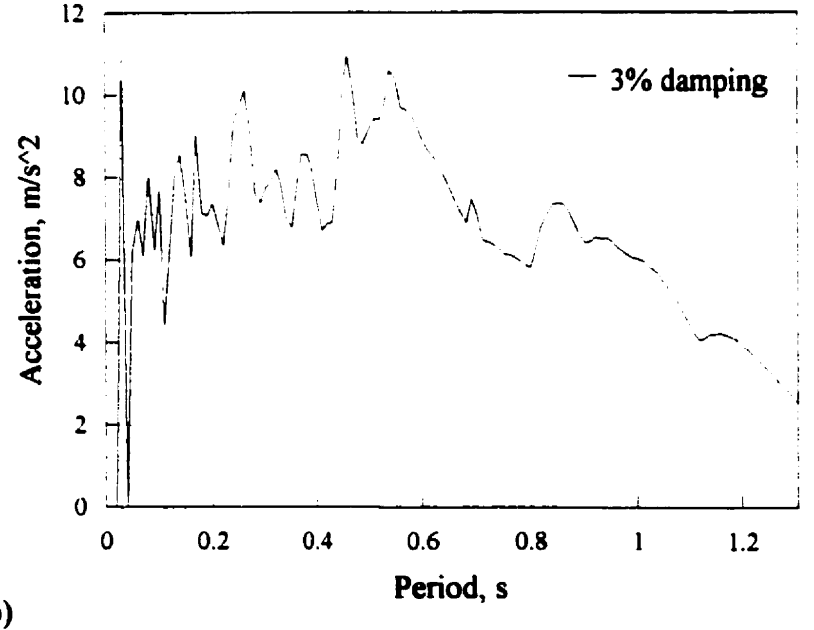

b)

Fig. A2.1 Earthquake record Imperial Valley S00E (N1)

Event: Imperial Valley earthquake
Component: S00W
Station:El Centro site Imperial Valley Irrigation District
Peak Acceleration: 341.70508 cm/s^2
Peak Velocity: 33.44281 cm/s

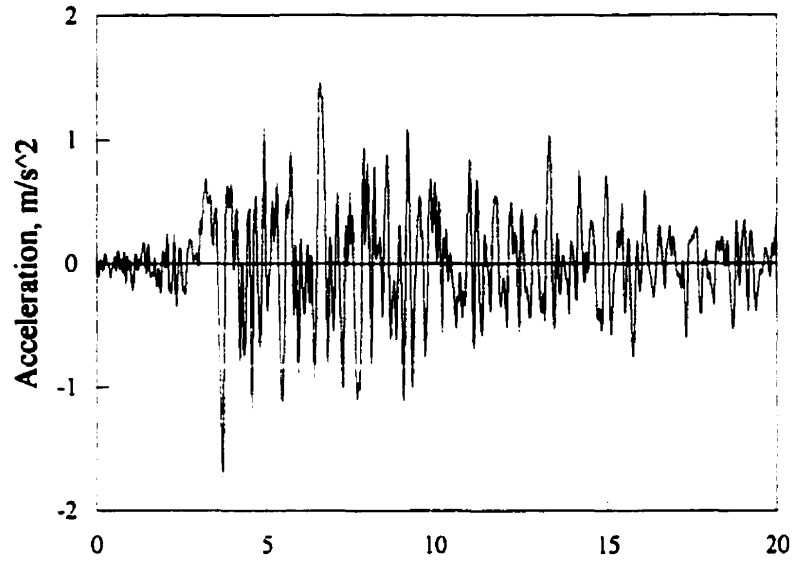

a)

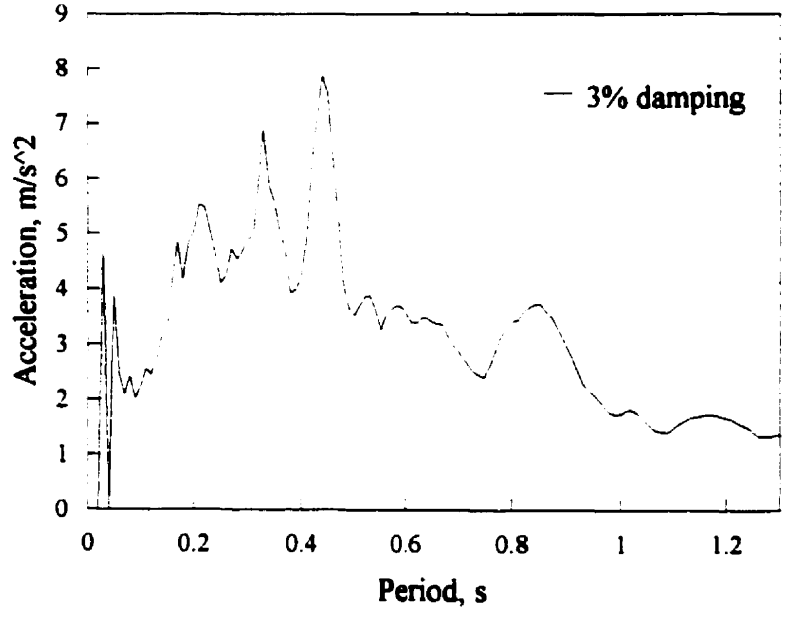

b)

Fig. A2.2 Earthquake record Kern County S69E (N2)

Event: Kern County earthquake
Component: S69E
Site: Taft Lincoln school tunnel
Peak Accelration: 175.9404 cm/s^2
Peak Velocity: -17.72147 cm/s

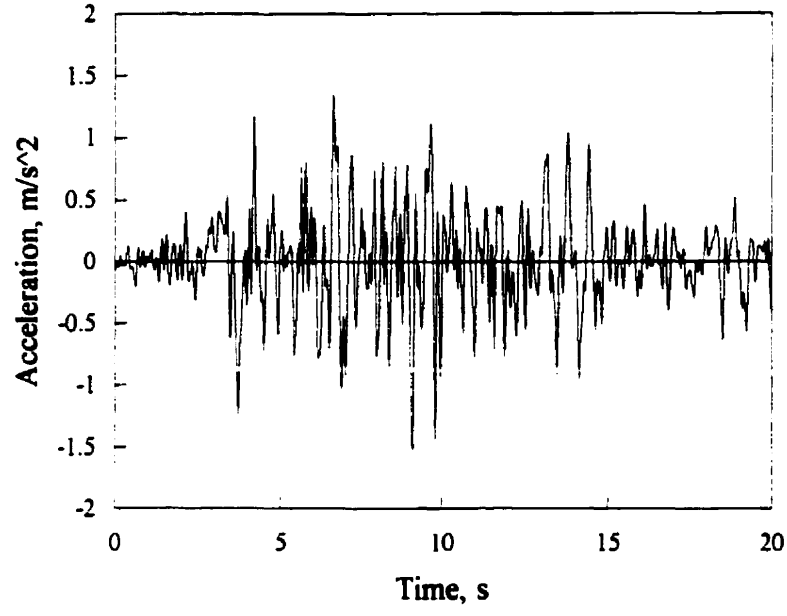

a)

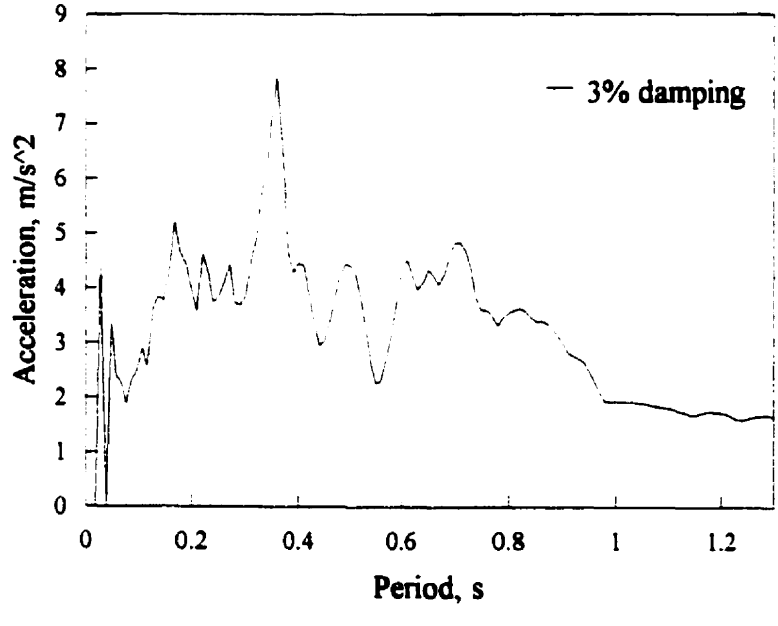

b)

Fig. A2.3 Earthquake record Kern County N21E (N3)

Event: Kern County earthquake
Component: N21E
Station: No. 095
Peak Acceleration: 152.70538 cm/s^2
Peak Velocity: -15.7254 cm/s

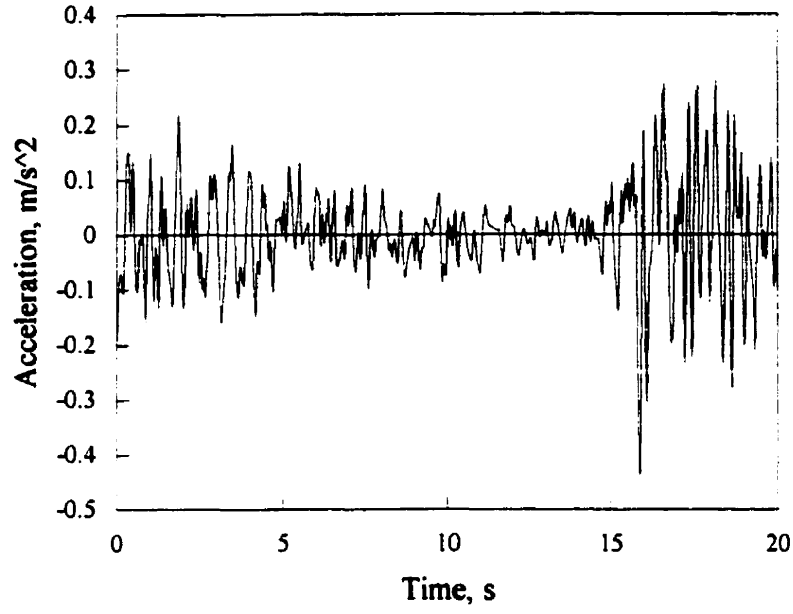

a)

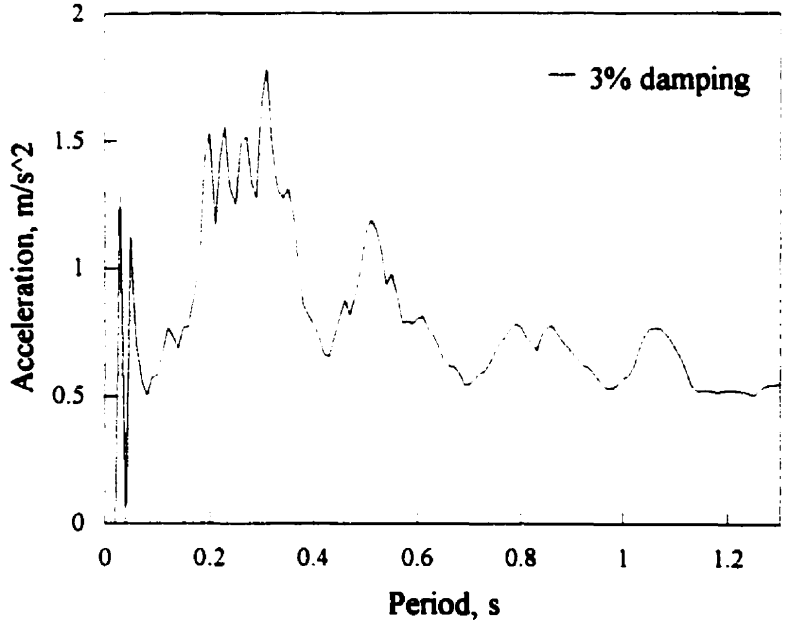

b)

Fig. A2.4 Earthquake record Borrego Mountain N57W (N4)

Event: Borrego Mountain earthquake
Component: N57W
Station: San Onofre power plant
Peak Acceleration: -45.53455 cm/s^2
Peak Velocity: -4.20186 cm/s

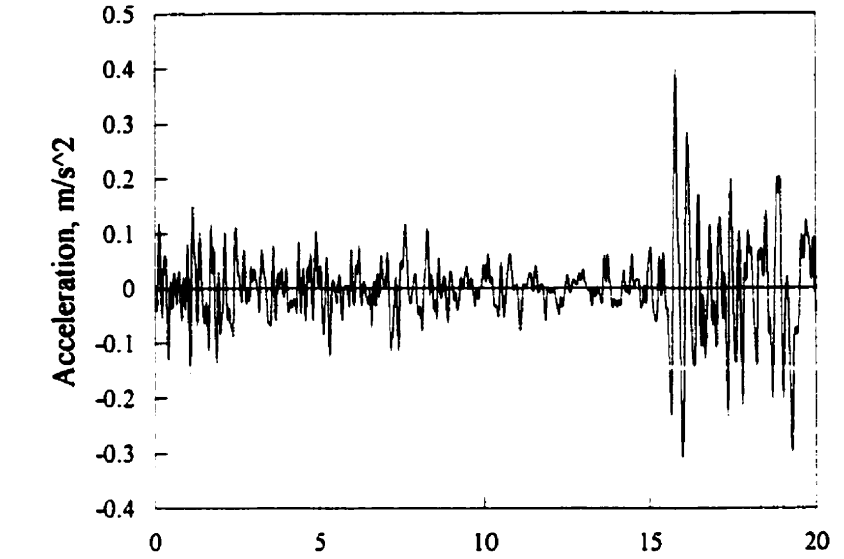

a)

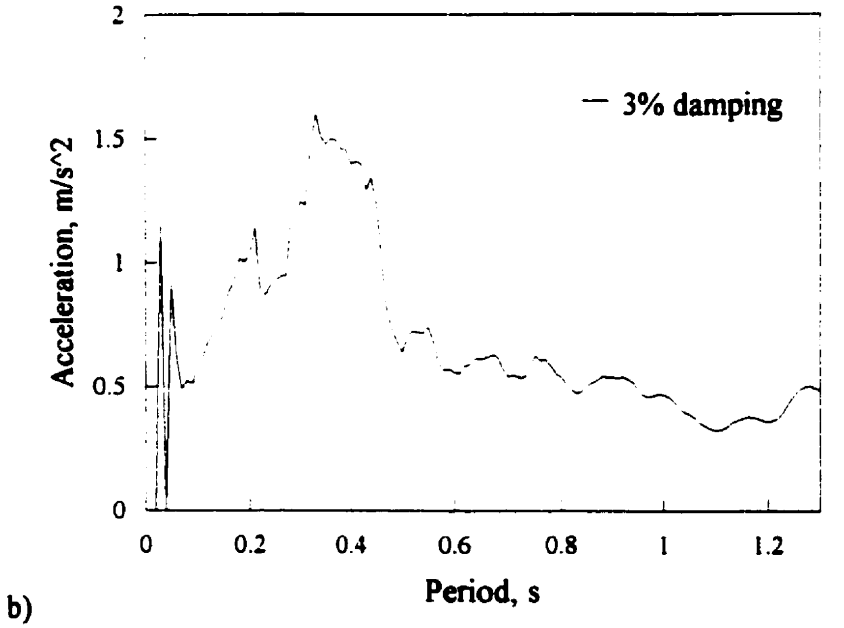

b)

Fig. A2.5 Earthquake record Borrego Mountain N33E (N5)

Event: Borrego Mountain earthquake
Component: N33E
Station: 280, 33 22 05N, 117 33 17W
Peak Acceleration: 40.02722 cm/s^2
Peak Velocity: -3.67305 cm/s

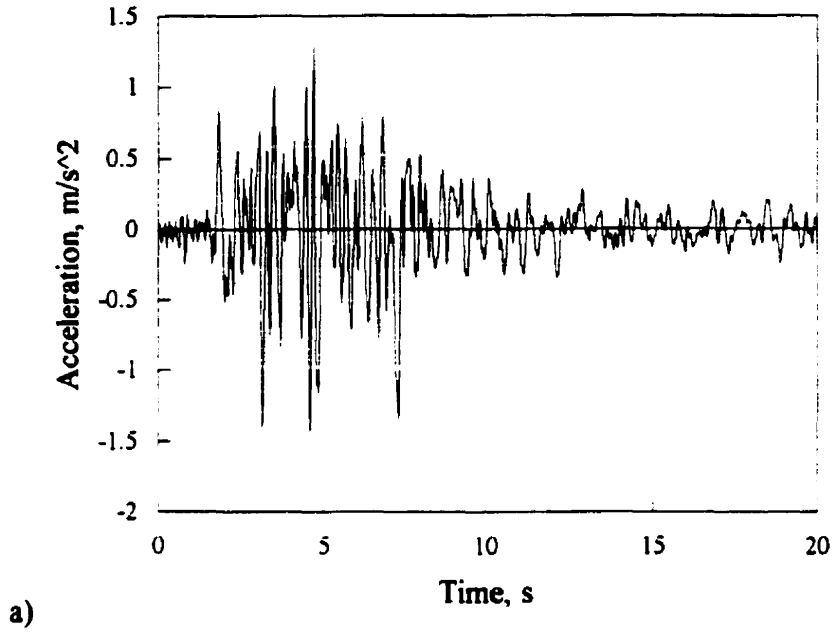

a)

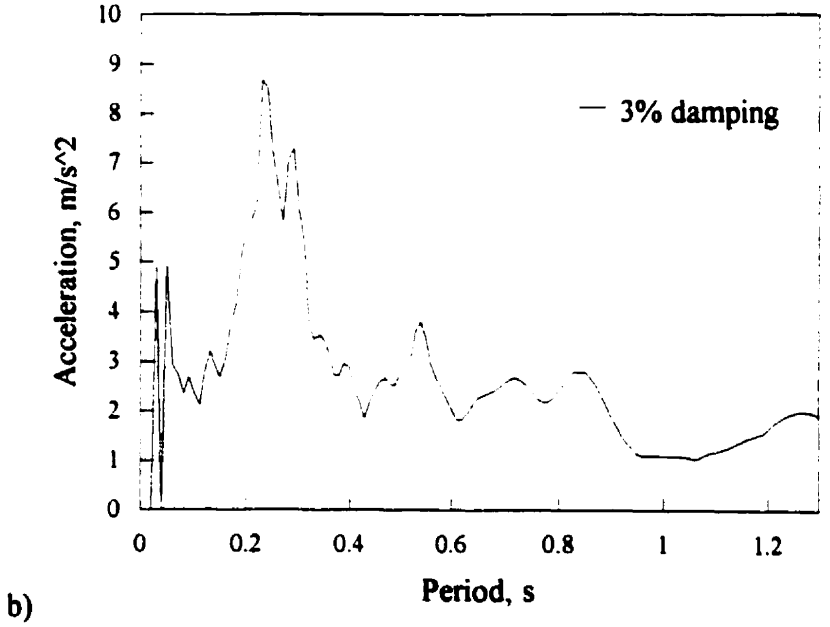

b)

Fig. A2.6 Earthquake record San Fernando S90W (N6)

Event: San Fernando earthquake
Component: S90W
Station: 3838 Lankershim Blvd., basement, Los Angeles, Cal.
Peak Acceleration: 147.6254 cm/s^2
Peak Velocity: 14.87841 cm/s

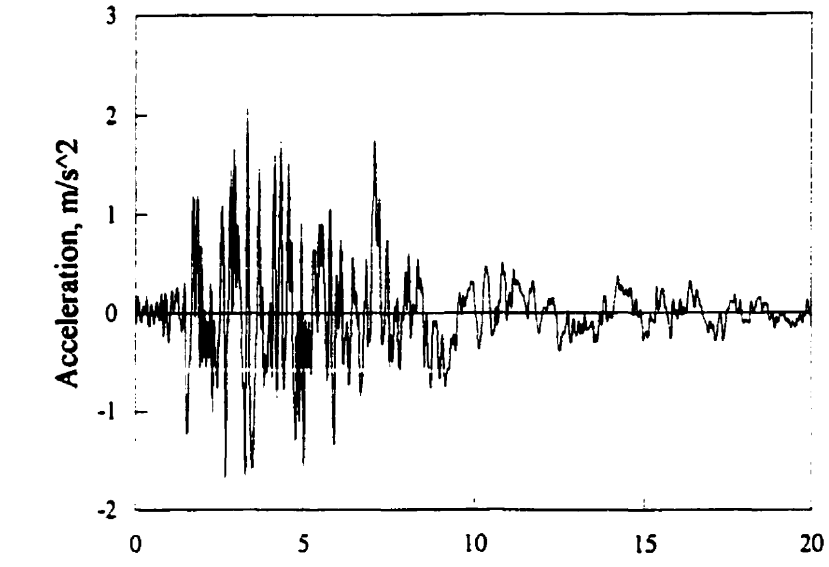

a)

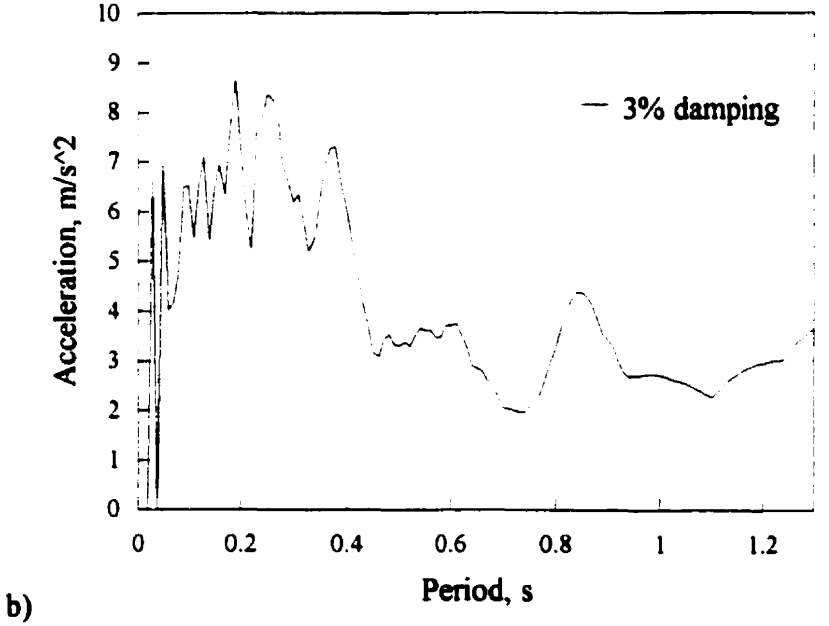

b)

Fig. A2.7 Earthquake record San Fernando N90E (N7)

Event: San Fernando earthquake
Component: N90E
Station: Hollywood Storage P.E. Lot, Los Angeles, Cal.
Peak Acceleration: -206.99030 cm/s^2
Peak Velocity: -21.13652 cm/s

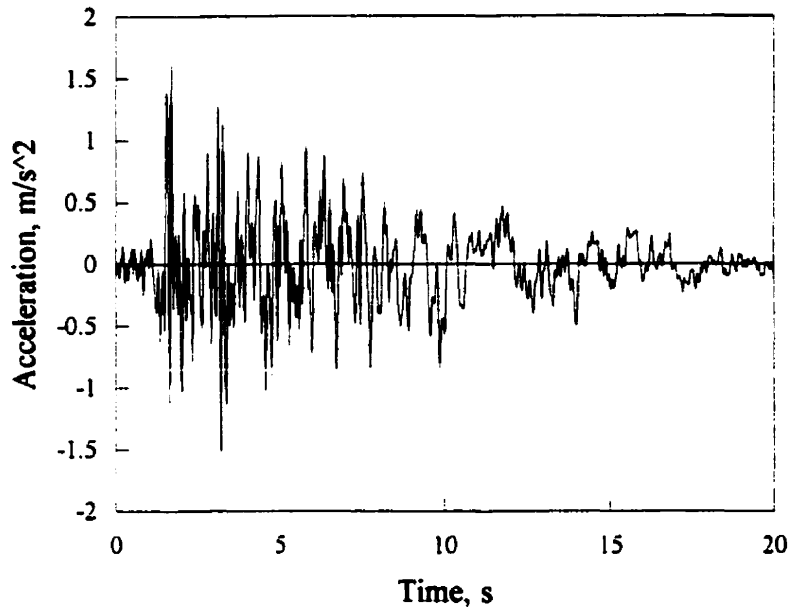

a)

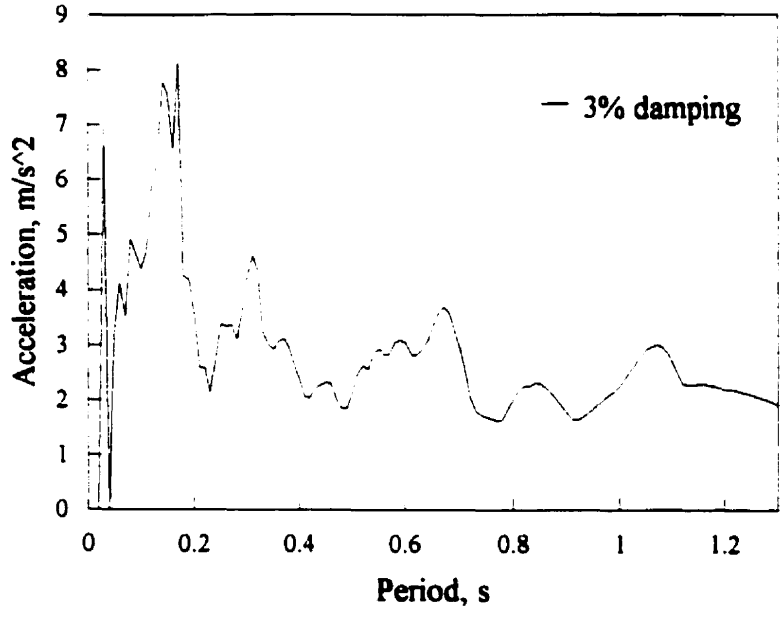

b)

Fig. A2.8 Earthquake record San Fernando N90E (N8)

Event: San Fernando earthquake
Component: N90E
Station: 3407 6th Street, basement, Los Angeles, Cal.
Peak Acceleration: -161.94800 cm/s^2
Peak Velocity: -16.59729 cm/s

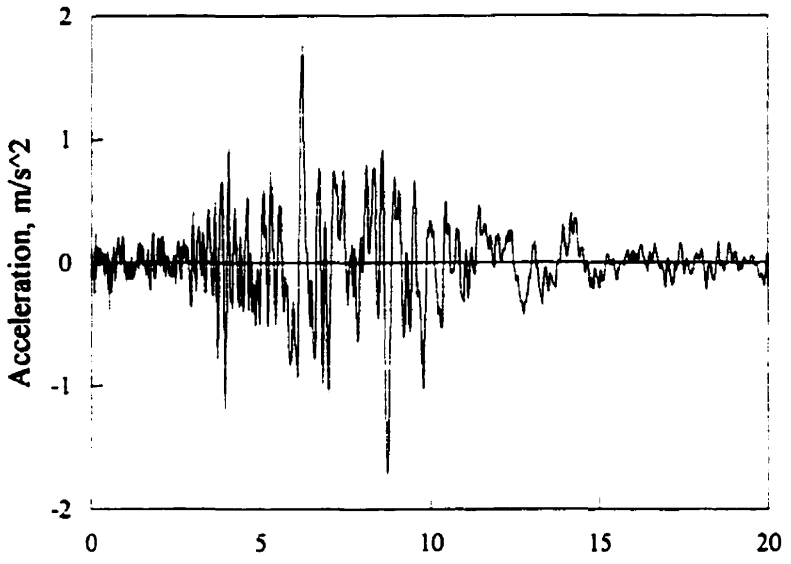

a)

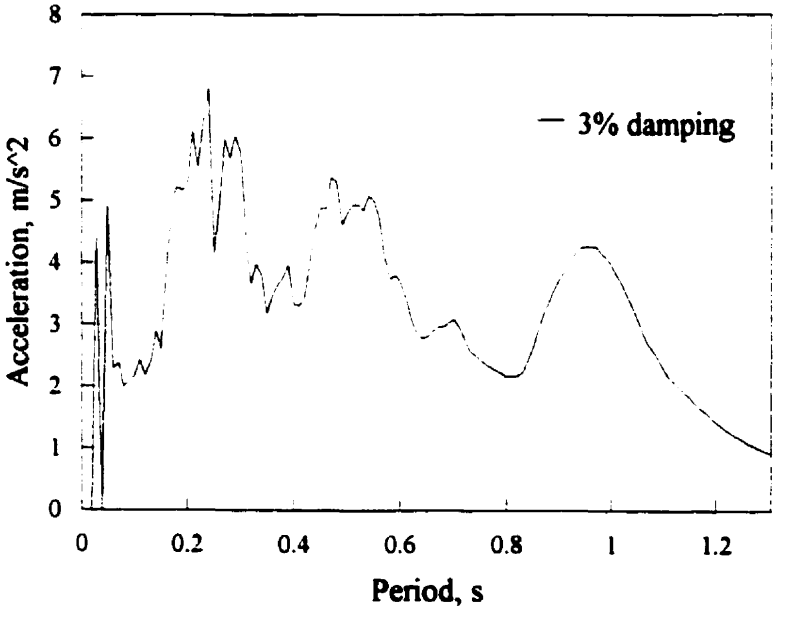

b)

Fig. A2.9 Earthquake record San Fernando S00W (N9)

Evevnt: San Fernando earthquake
Component: S00W
Station: Griffith Park Observatory, moon room, Los Angeles, Cal.
Peak Acceleration: -176.89980 cm/s^2
Peak Velocity: -20.48128 cm/s

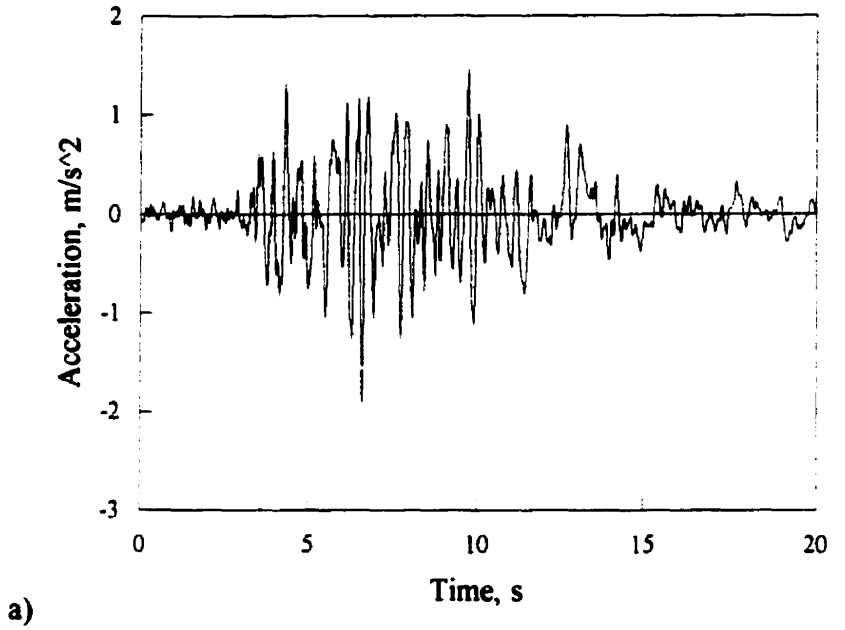

a)

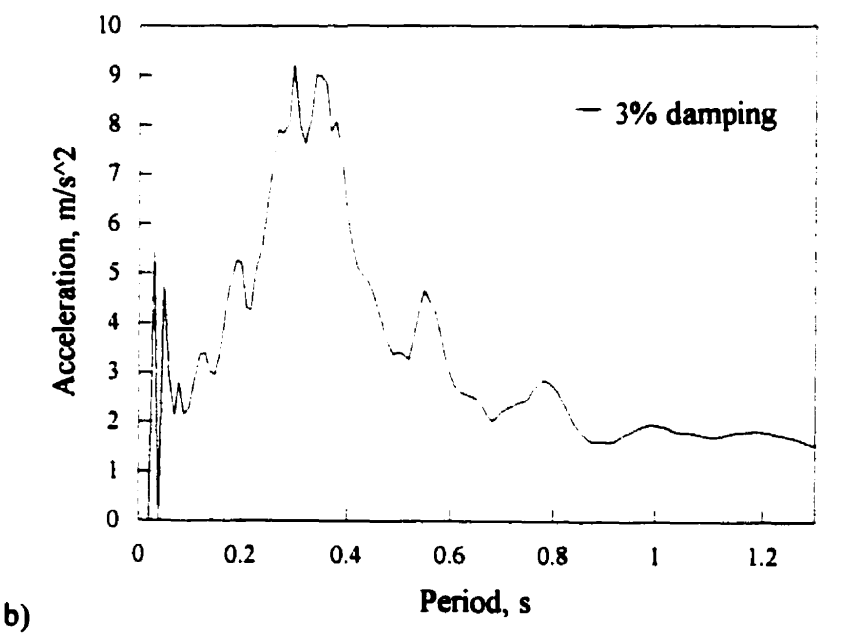

b)

Fig. A2.10 Earthquake record San Fernando N37E (N10)

Event: San Fernando earthquake
Component: N37E
Station: 234 Figueroa Street, basement, Los Angeles, Cal.
Peak Acceleration: 195.65120 cm/s^2
Peak Velocity: 16.72186 cm/s

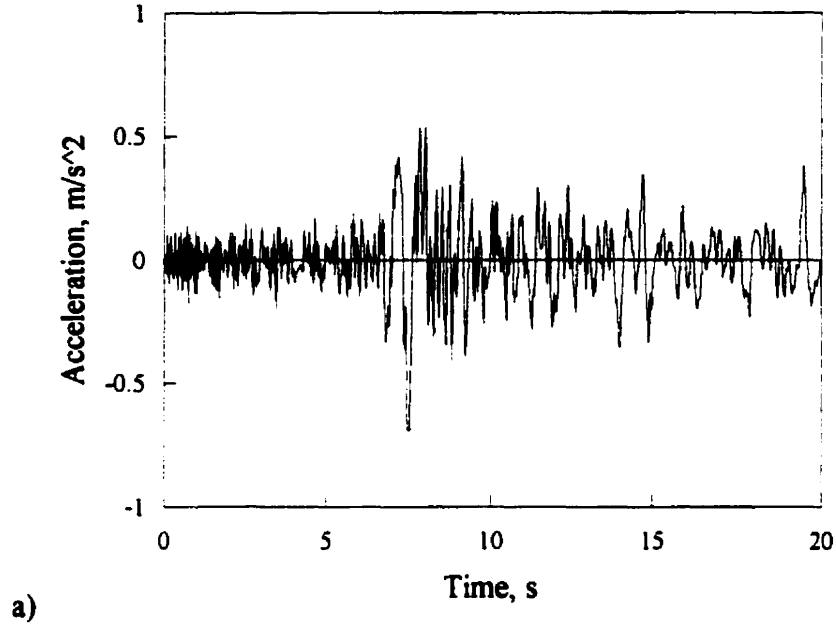

a)

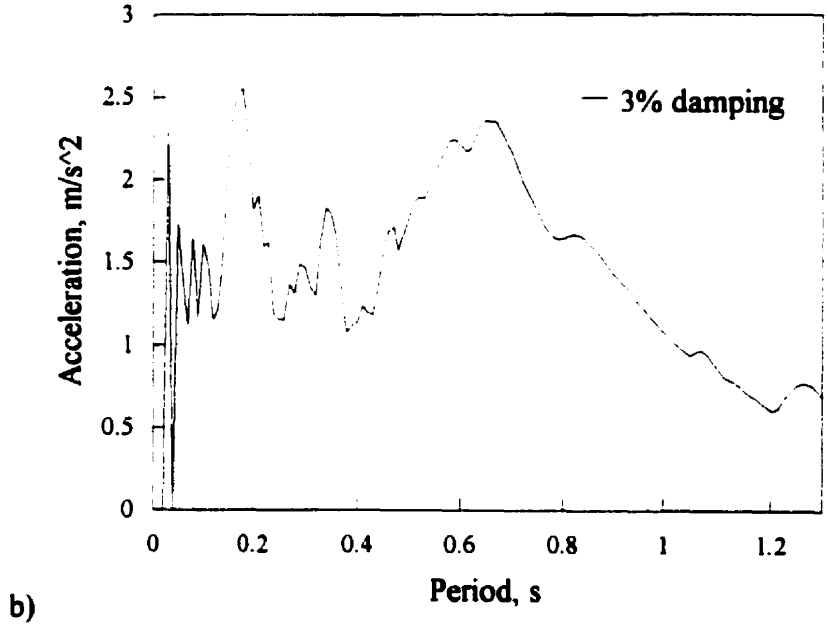

b)

Fig. A2.11 Earthquake record Near E. Coast of Honshu NS (N11)

Evevnt: Near E. Coast of Honshu earthquake
Component: NS
Station: KT036
Peak Acceleration: -69.1 cm/s^2
Peak Velocity: -7.2 cm/s

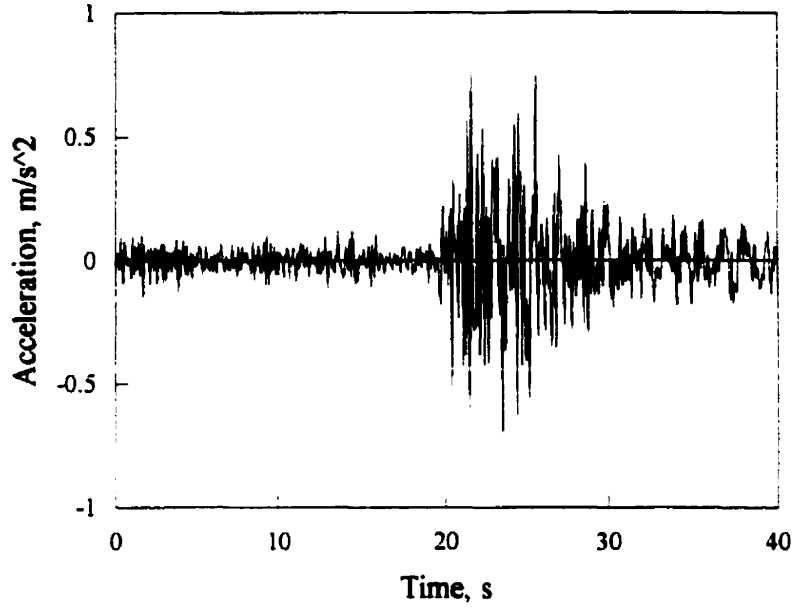

a)

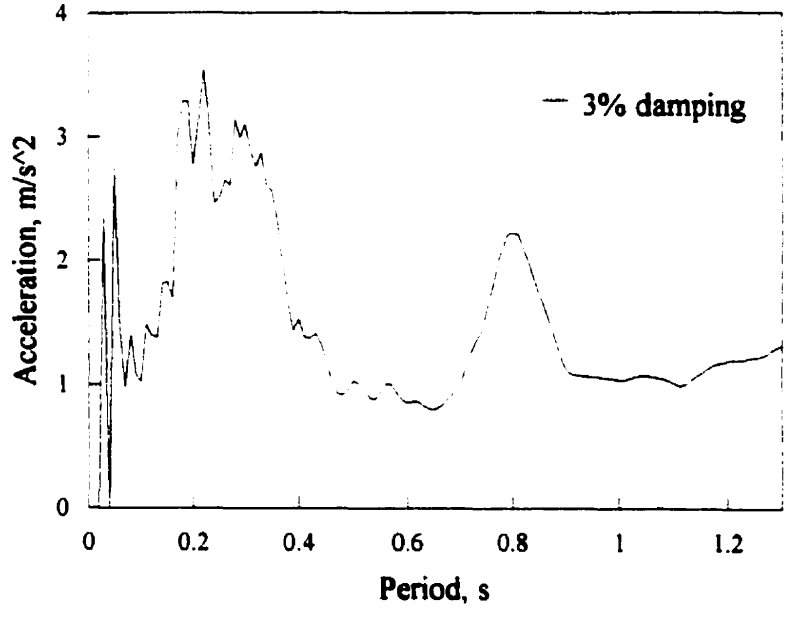

b)

Fig. A2.12 Earthquake record Near S. Coast of Honshu EW (N12)

Event: Near S. Coast of Honshu earthquake
Component: EW
Station: HK004
Peak Acceleration: 76.1 cm/s^2
Peak Velocity: 6.8 cm/s

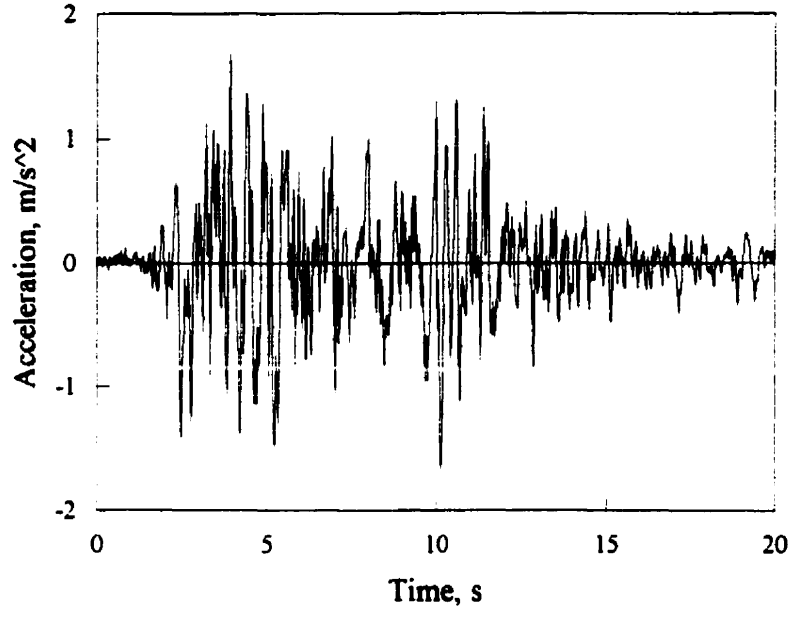

a)

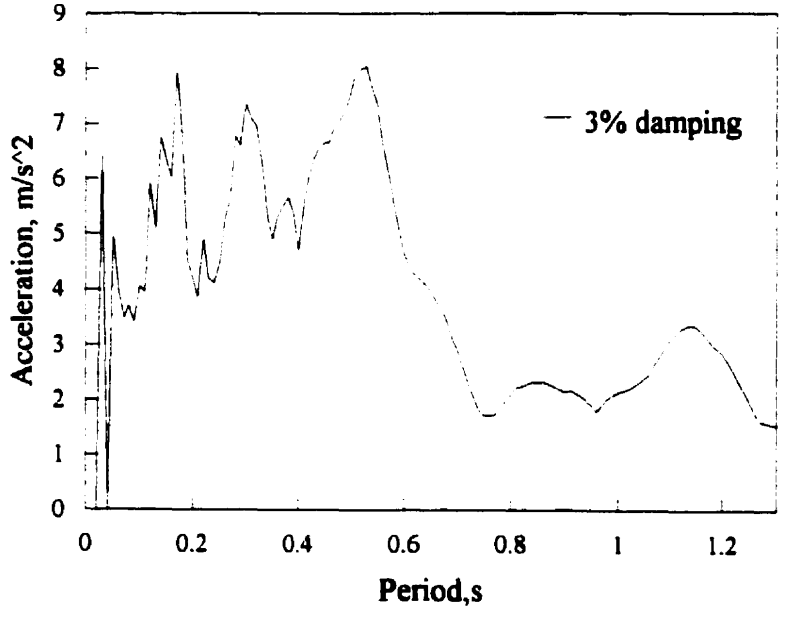

b)

Fig. A2.13 Earthquake record Monte Negro N00W (N13)

Event: Monte Negro earthquake
Component: N00W
Peak Acceleration: 170.0 cm/s^2
Peak Velocity: 19.4 cm/s

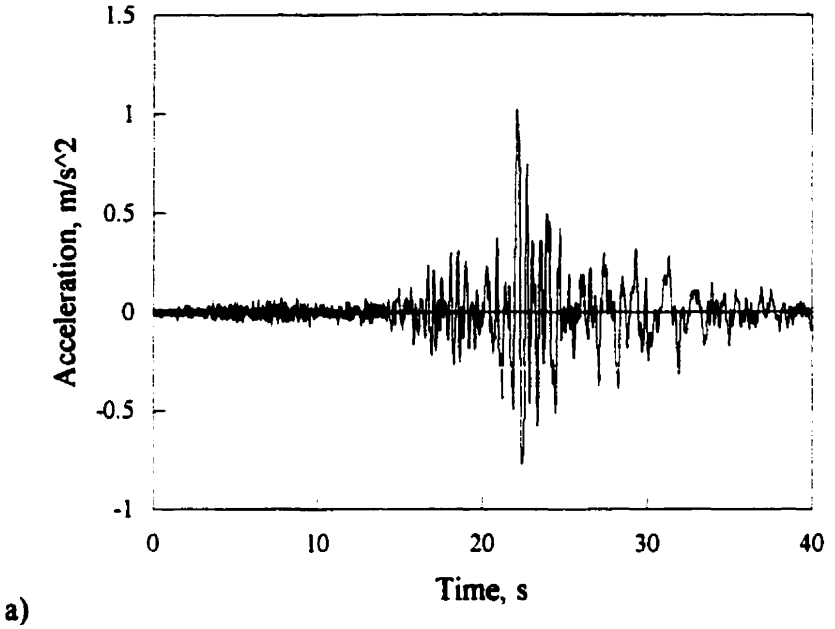

a)

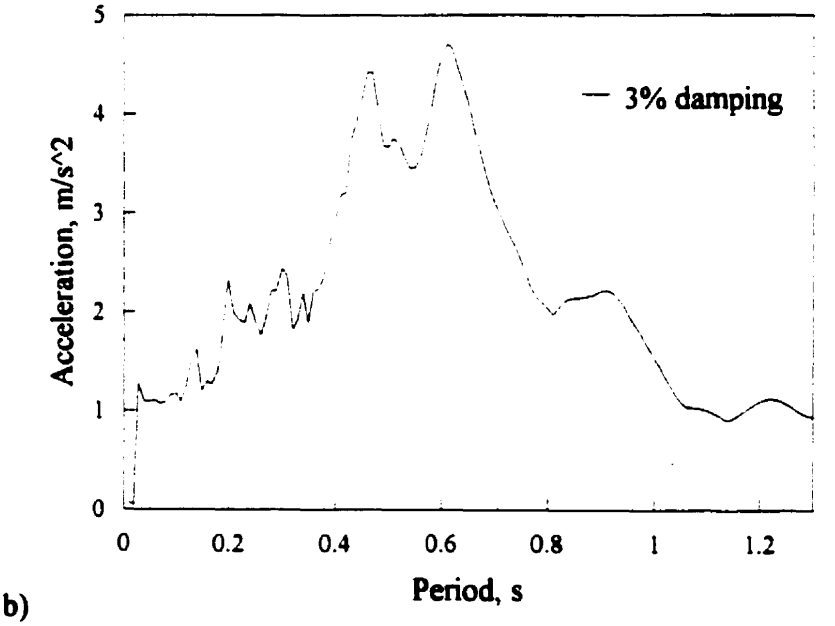

b)

Fig. A2.14 Earthquake record Michoacan S00E (N14)

Event: Michoacan earthquake
Component: S00E
Station: SUCH
Peak Acceleration: 103.12 cm/s^2
Peak Velocity: -11.61 cm/s

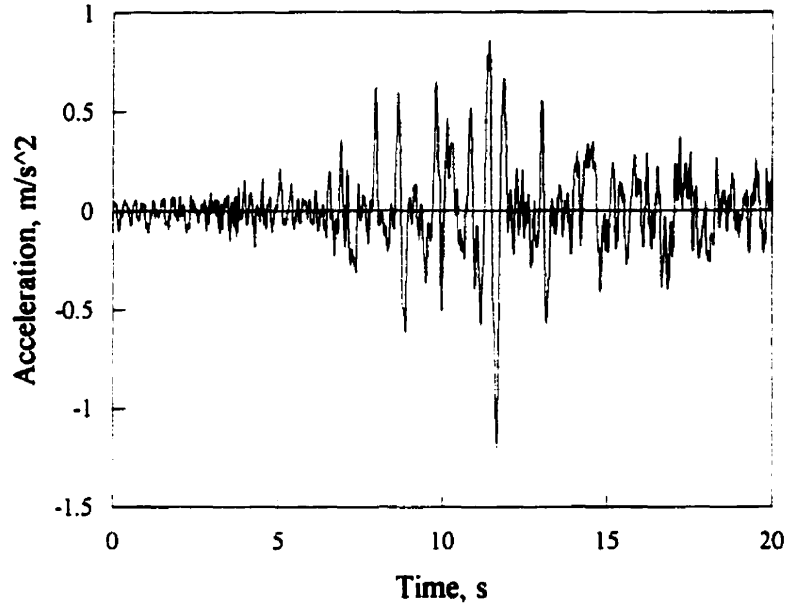

a)

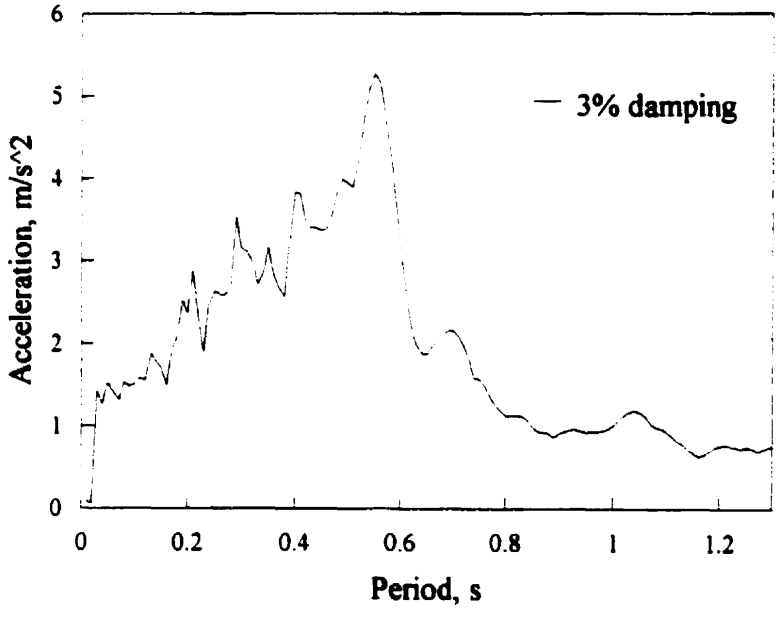

b)

Fig. A2.15 Earthquake record Michoacan N90E (N15)

Event: Michoacan earthquake
Component: N90E
Station: VILE
Peak Acceleration: -120.87 cm/s^2
Peak Velocity: 10.51 cm/s

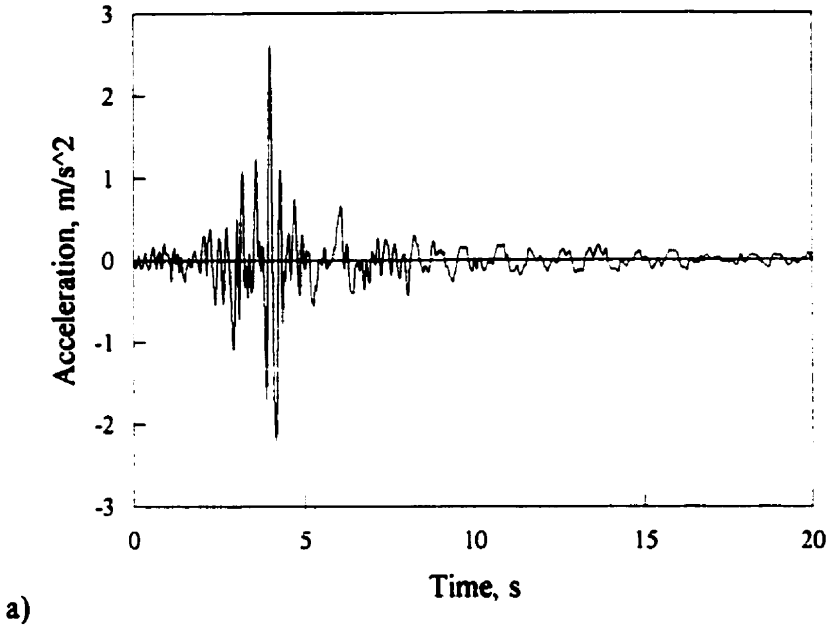

a)

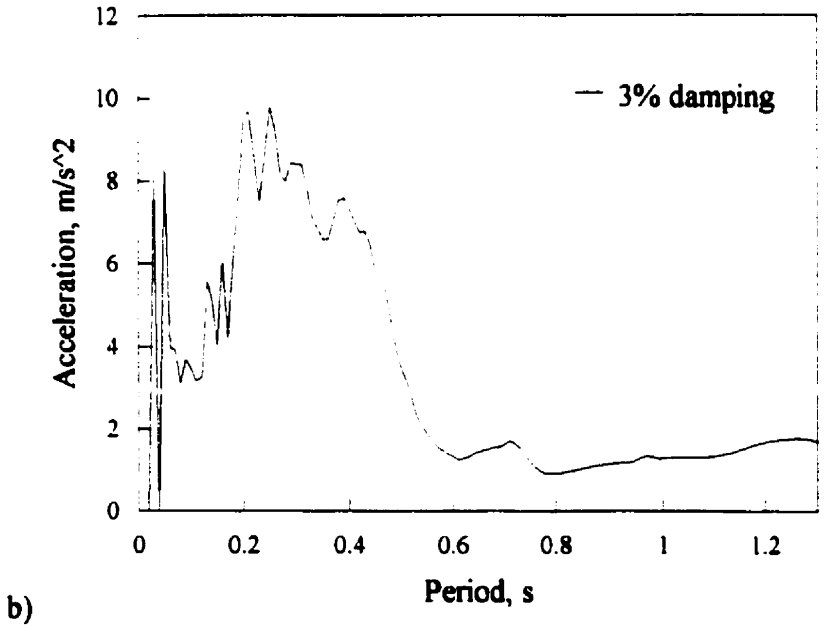

b)

Fig. A3.1 Earthquake record Parkfield N65W (H1)

Event: Parkfield earthquake
Component: N65W
Station: Temblor, California No. 2
Peak Acceleration: -264.35 cm/s^2
Peak Velocity: -14.51 cm/s

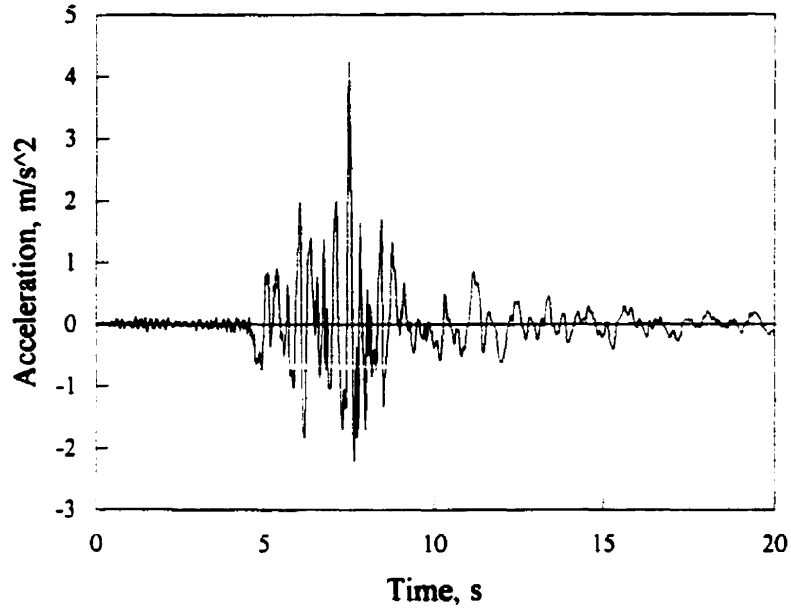

a)

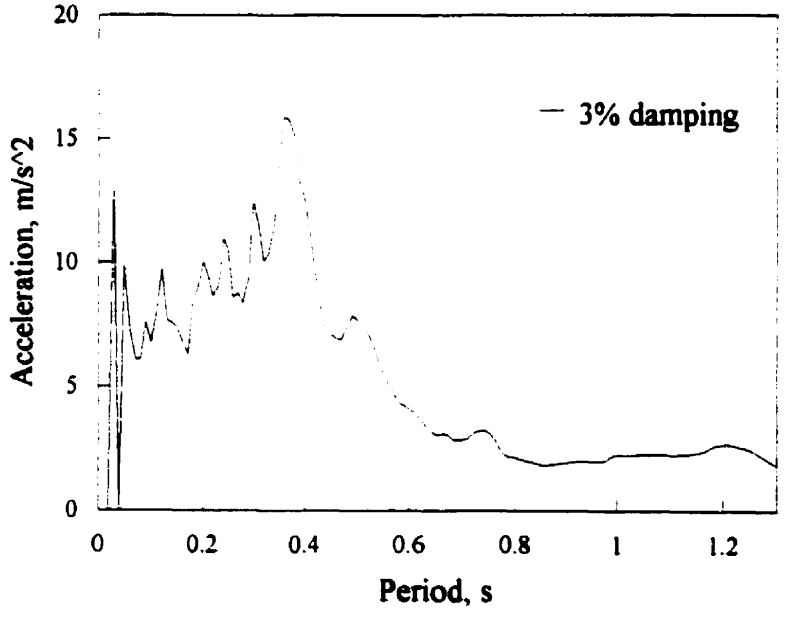

b)

Fig. A3.2 Earthquake record Parkfield N85E (H2)

Event: Parkfield earthquake
Component: N85E
Station: Tholame, Shandon, California Array No. 5
Peak Acceleration: -425.68 cm/s^2
Peak Velocity: - cm/s

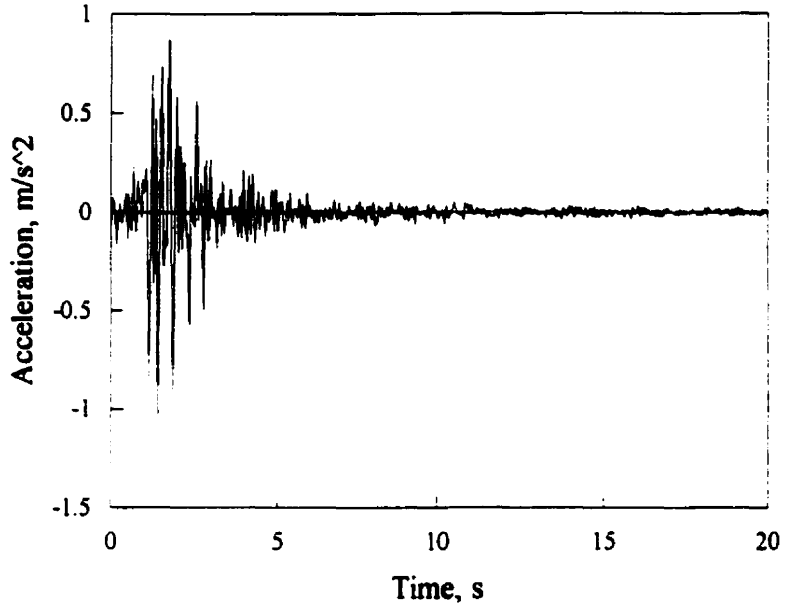

a)

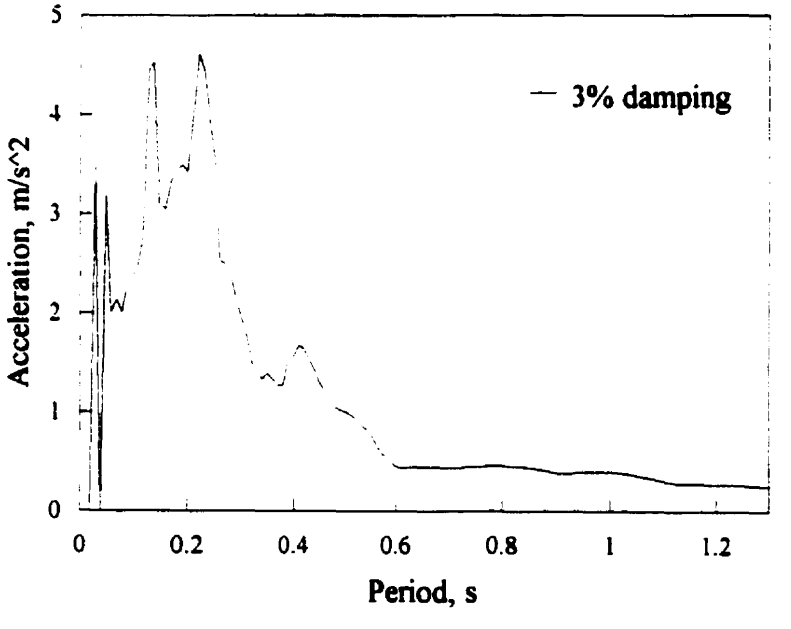

b)

Fig. A3.3 Earthquake record San Francisco S80E (H3)

Event: San Francisco earthquake
Component: S80E
Station: San Francisco Golden Gate park
Peak Acceleration: -102.80 cm/s^2
Peak Velocity: -4.61 cm/s

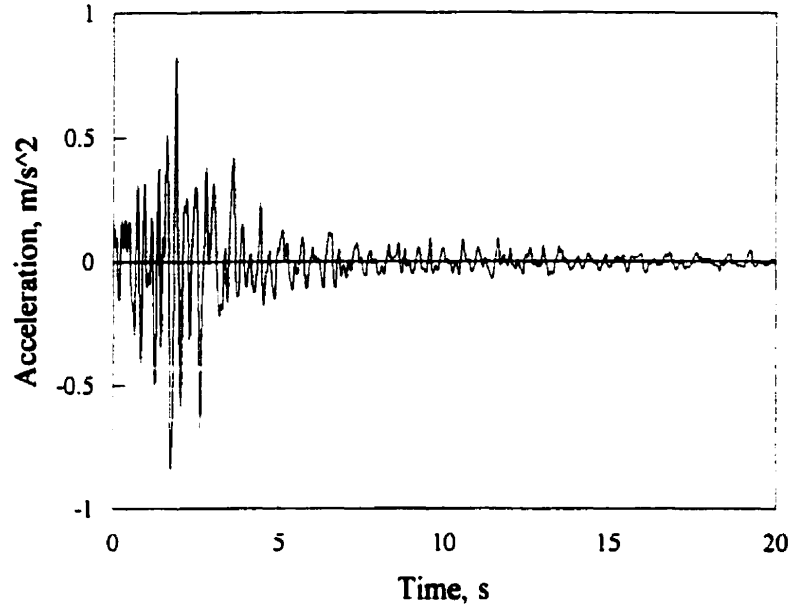

a)

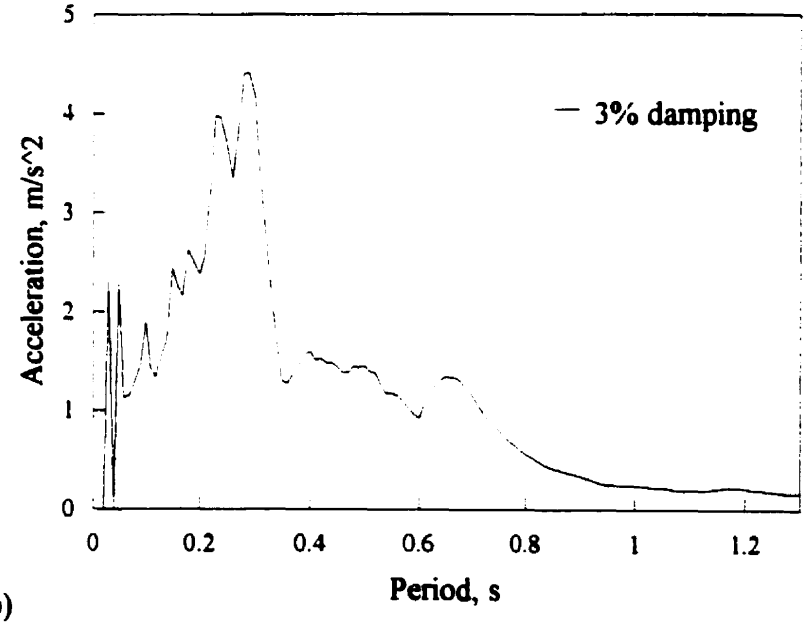

b)

Fig. A3.4 Earthquake record San Francisco S09E (H4)

Event: San Francisco earthquake
Component: S09E
Station: San Francisco State building, basement
Peak Acceleration: -83.81 cm/s^2
Peak Velocity: -5.05 cm/s

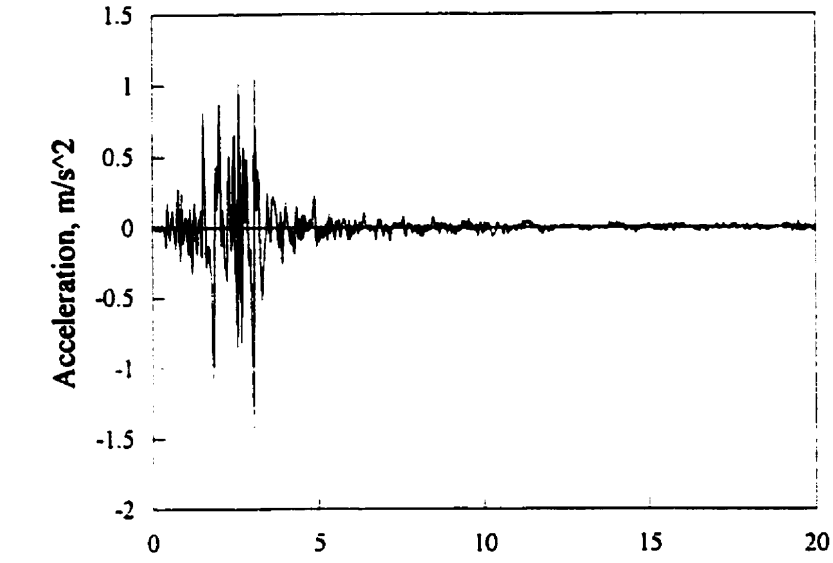

a)

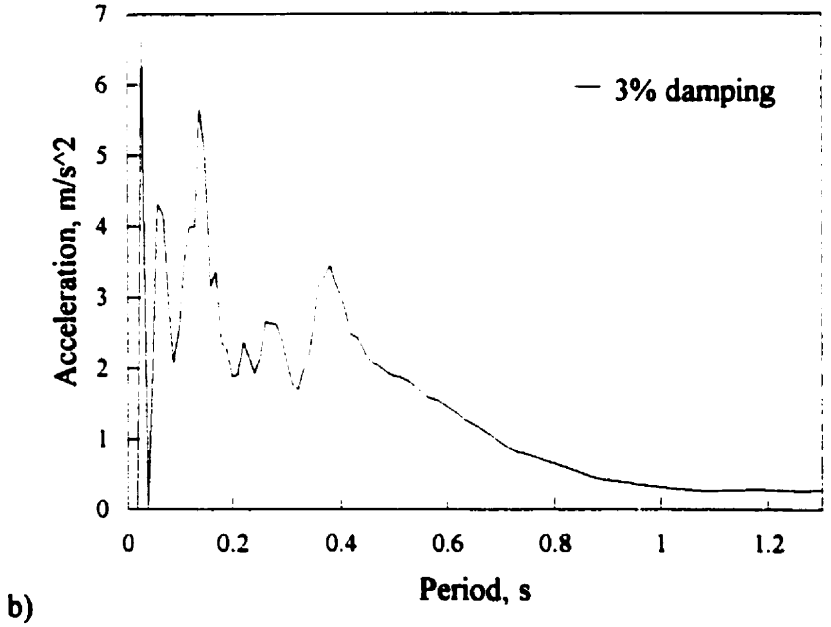

b)

Fig. A3.5 Earthquake record Helena Montana S00W (H5)

Event: Helena Montana earthquake
Component: S00W
Station: Helena, Montana Carroll college
Peak Acceleration: 143.71 cm/s^2
Peak velocity: 7.21 cm/s

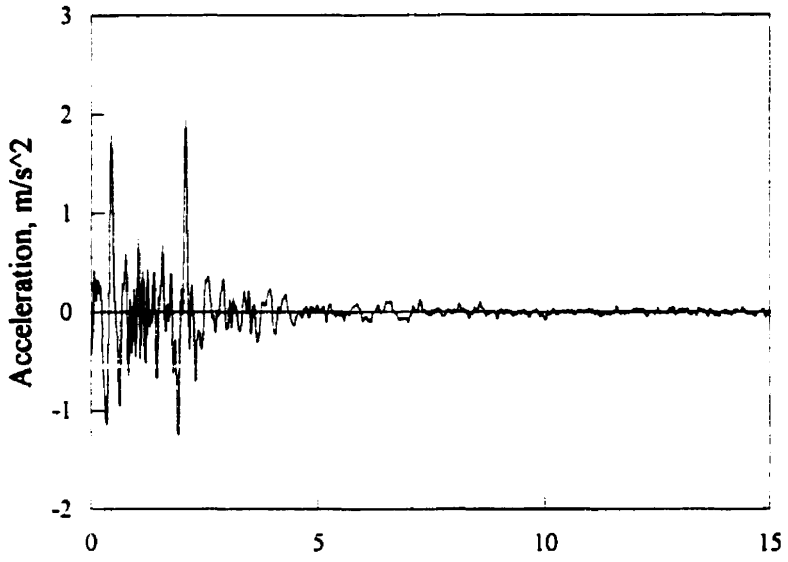

a)

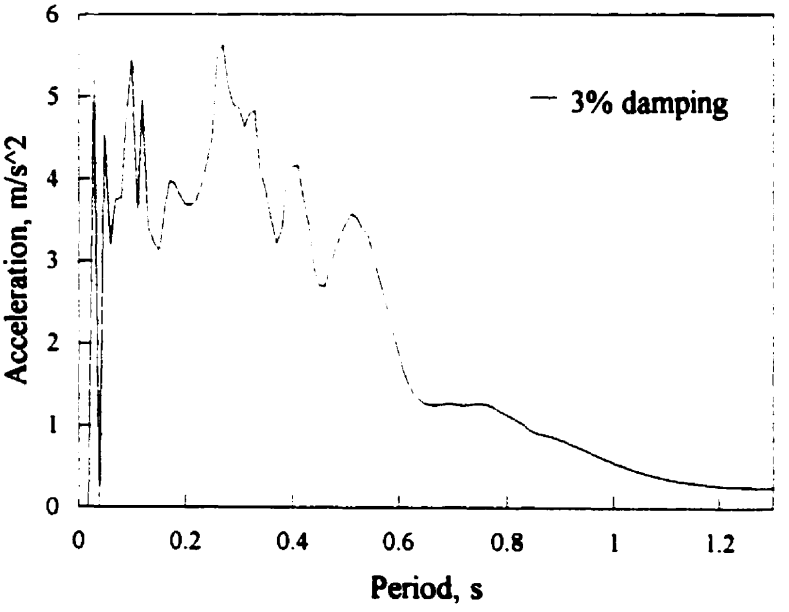

b)

Fig. A3.6 Earthquake record Lytle Creek S25W (H6)

Event: Lytle Creek earthquake
Component: S25W
Station: N/A
Peak Acceleration: 194.41 cm/s^2
Peak velocity: -9.64 cm/s

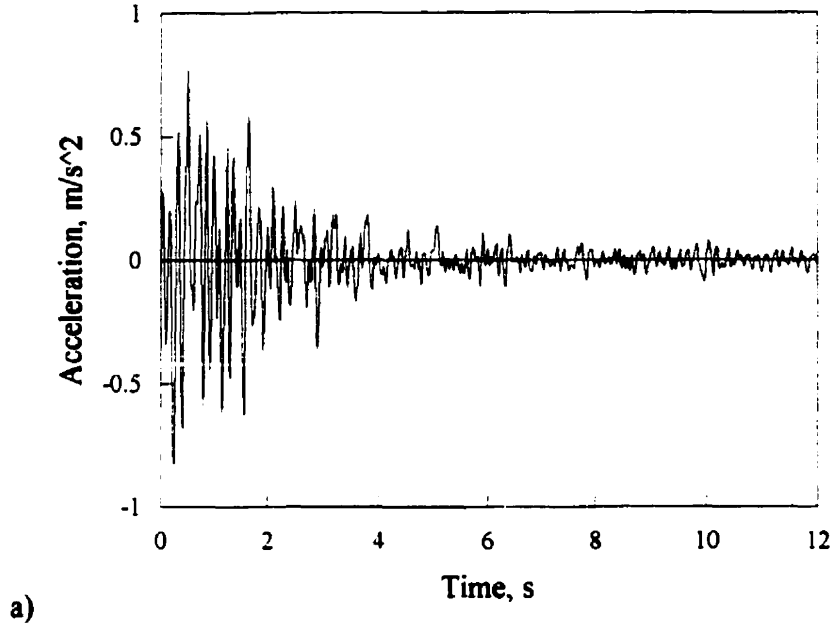

a)

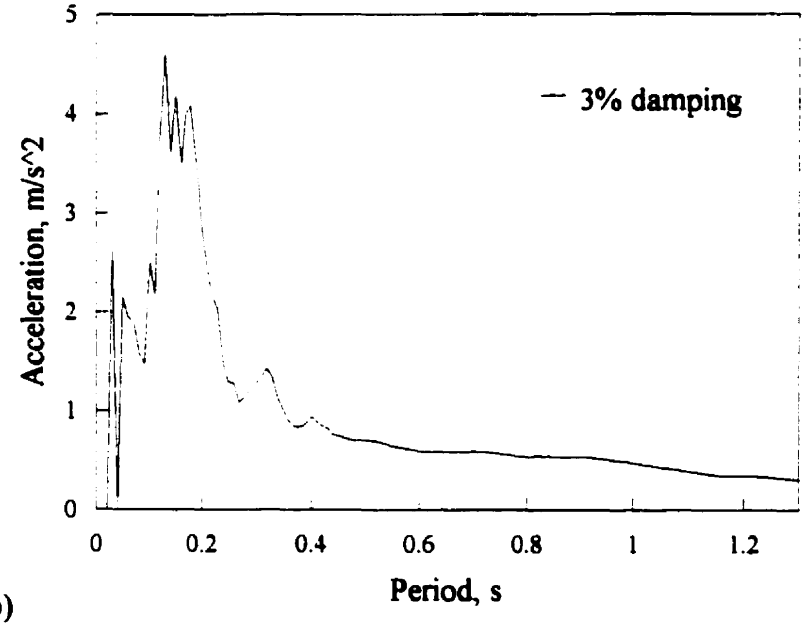

b)

Fig. A3.7 Earthquake record Oroville N53W (H7)

Event: Oroville earthquake
Component: N53W
Station: Oroville Dam, California, Seismograph station, ground level
Peak Acceleration: -82.5 cm/s^2
Peak Velocity: -4.44 cm/s

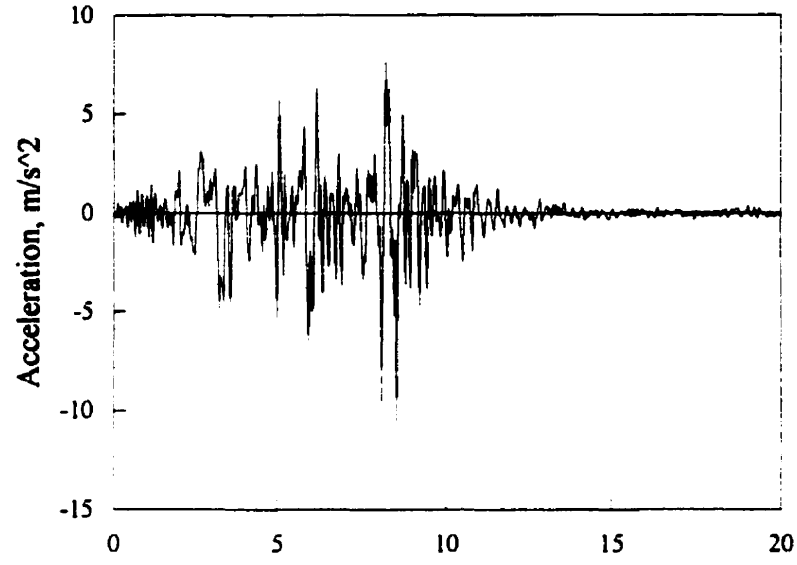

a)

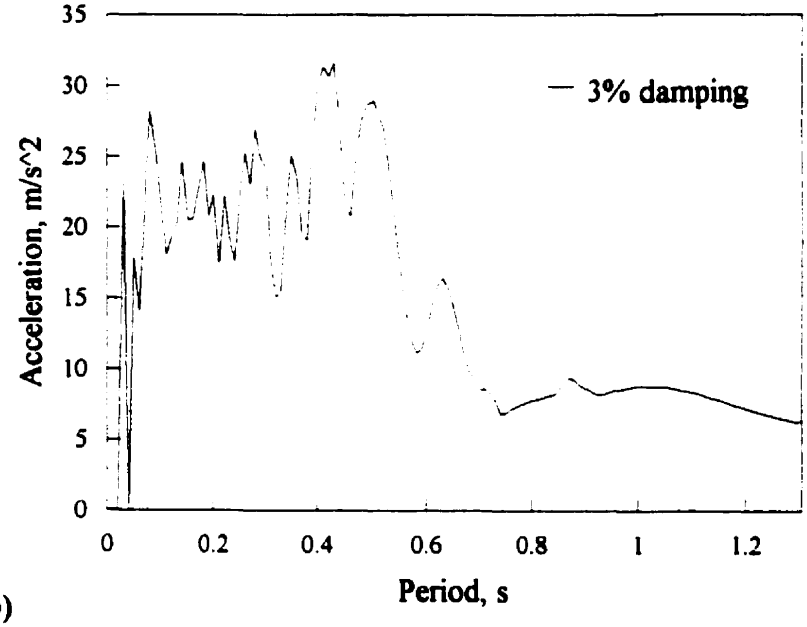

b)

Fig. A3.8 Earthquake record San Fernando S74W (H8)

Event: San Fernando earthquake
Component: S74W
Station: Pacoima Dam, California
Peak Acceleration: 1054.95 cm/s^2
Peak Velocity: -57.74 cm/s

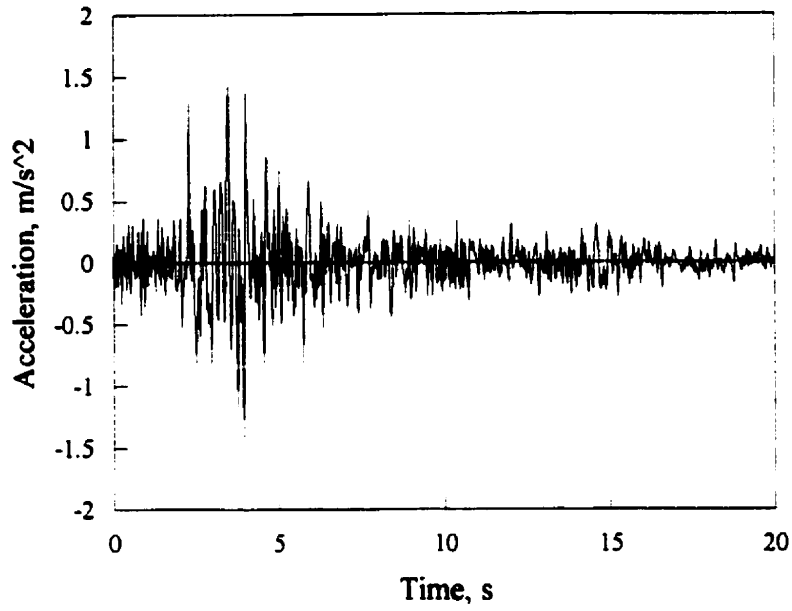

a)

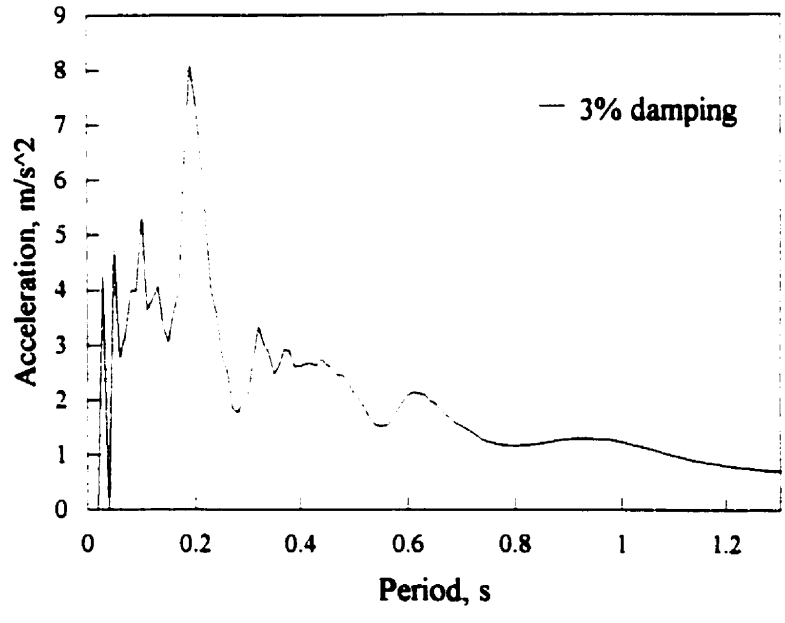

b)

Fig. A3.9 Earthquake record San Fernando S21W (H9)

Event: San Fernando earthquake
Component: S21W
Station: Lake Hughes, Array station 4, California
Peak Acceleration: -143.51 cm/s^2
Peak Velocity: -8.53 cm/s

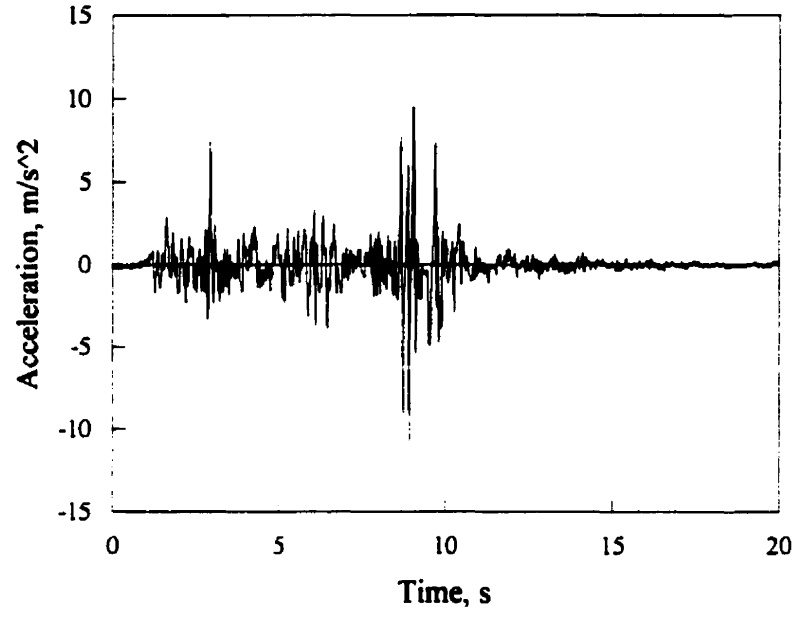

a)

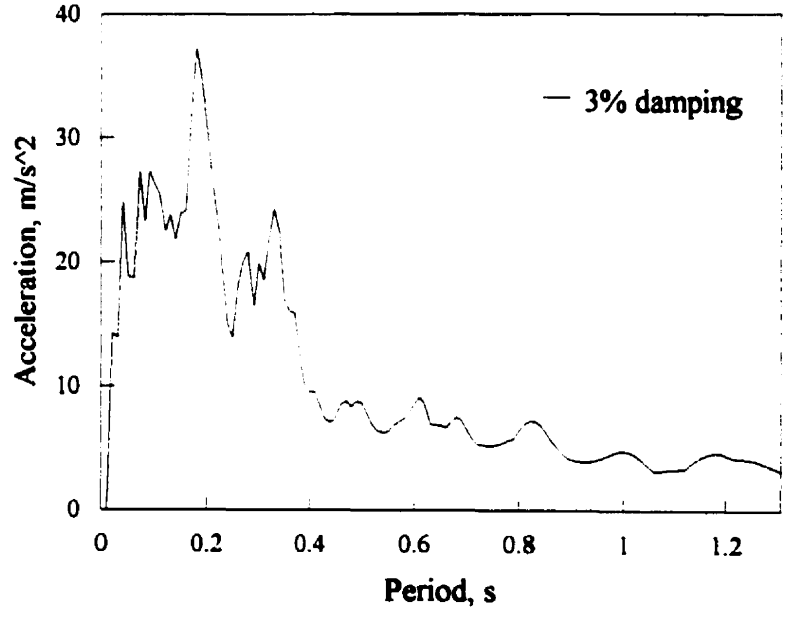

b)

Fig. A3.10 Earthquake record Nahanni Longitudinal (H10)

Event: Nahanni earthquake
Component: Longitudinal
Station:
Peak Acceleration: 1100.0 cm/s^2
Peak Velocity: 46.2 cm/s

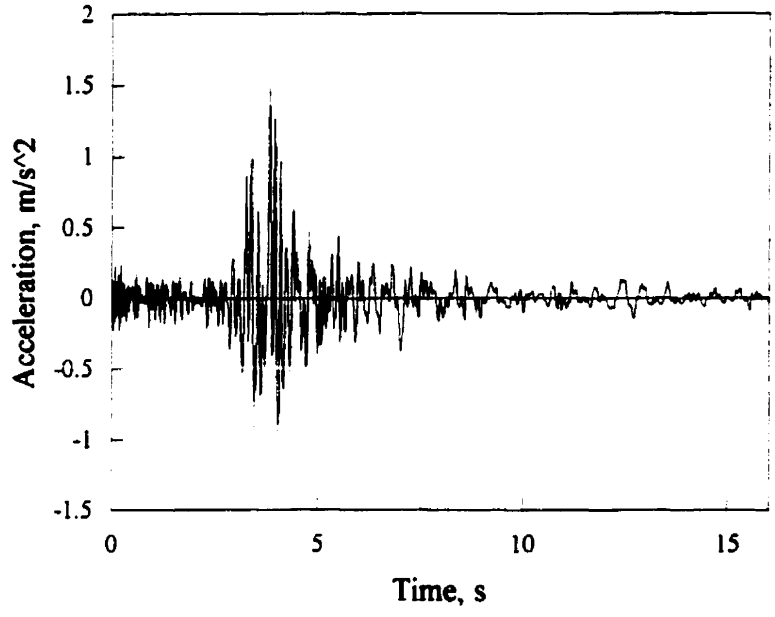

a)

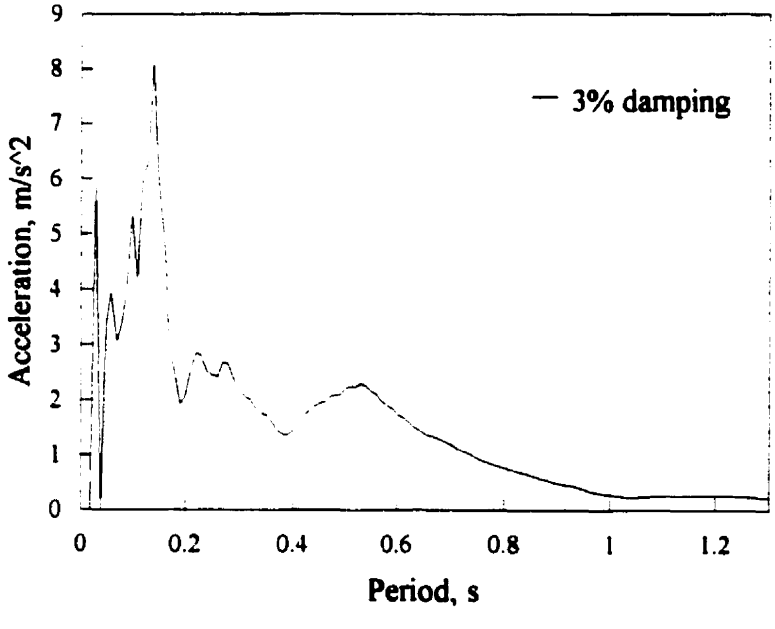

b)

Fig. A3.11 Earthquake record Centeral Honshu TR (H11)

Event: Centeral Honshu earthquake
Component: TR
Station: CB030
Peak Acceleration: 148.10 cm/s^2
Peak Velocity: 5.9 cm/s

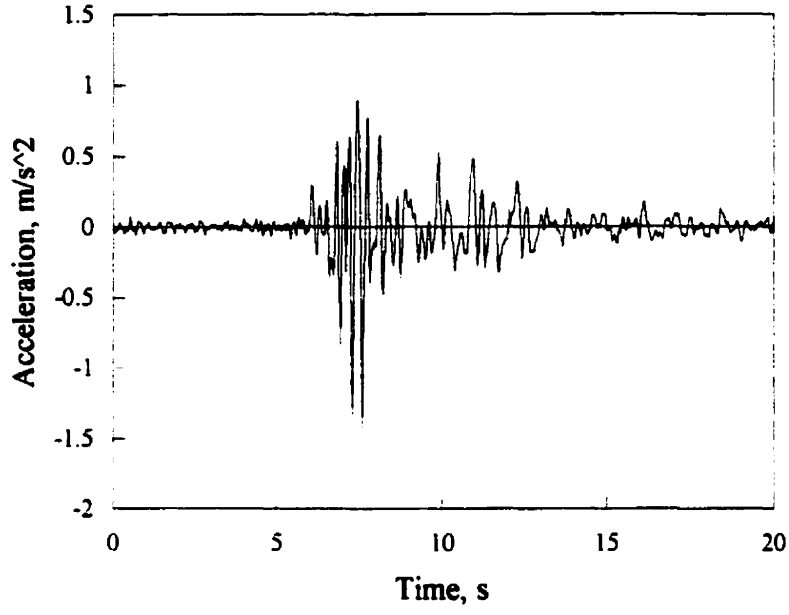

a)

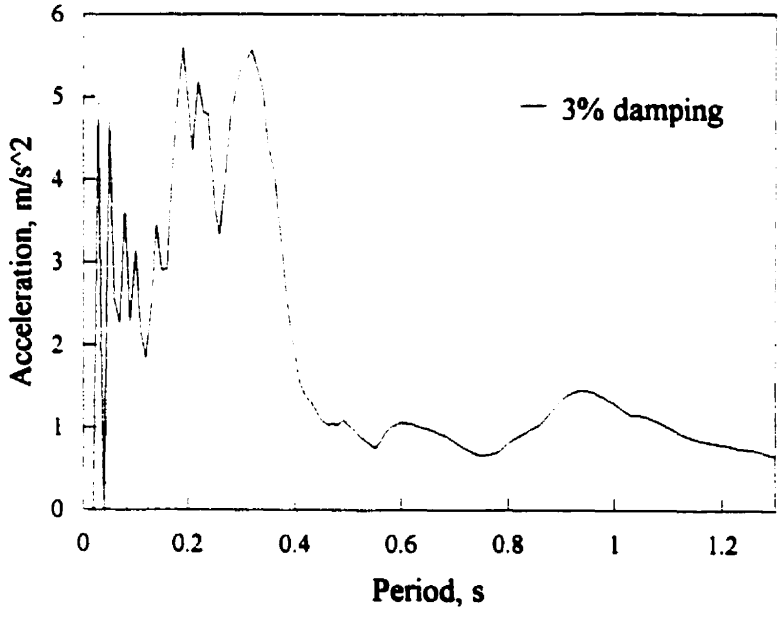

b)

Fig. A3.12 Earthquake record Near E. Coast of Honshu NS (H12)

Evevnt: Near E. Coast of Honshu earthquake
Component: NS
Station: HK004
Peak Acceleration: -142.8 cm/s^2
Peak Velocity: 6.0 cm/s

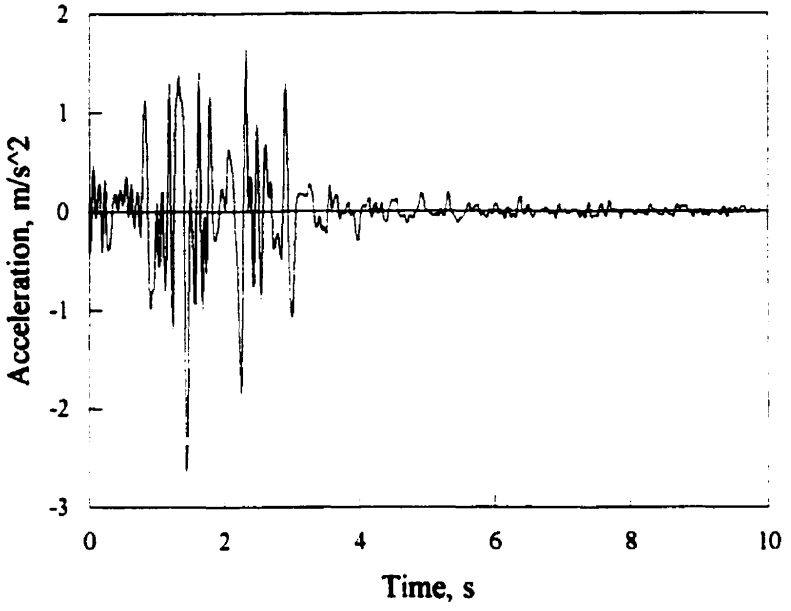

a)

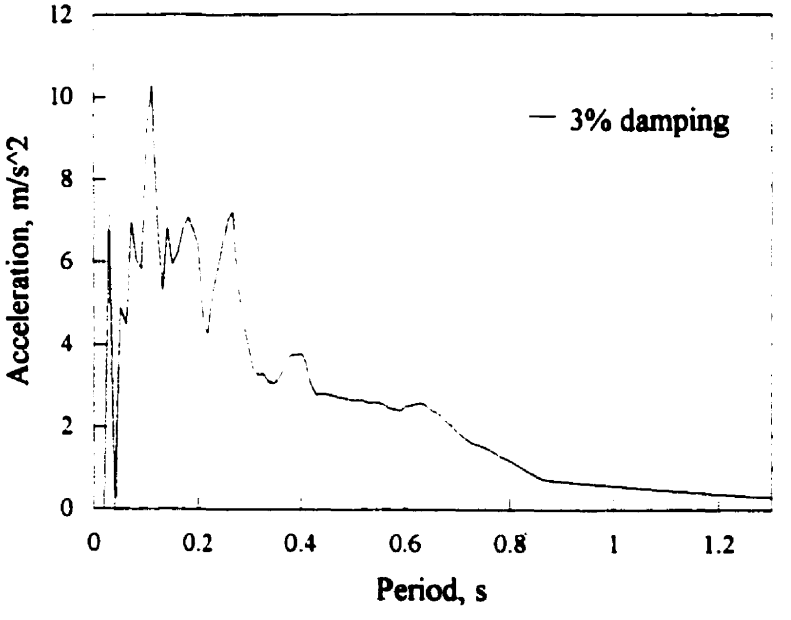

b)

Fig. A3.13 Earthquake record Honshu NS (H13)

Event: Honshu earthquake
Component: NS
Station: No. 2
Peak Acceleration: -265.0 cm/s^2
Peak Velocity: 11.1 cm/s

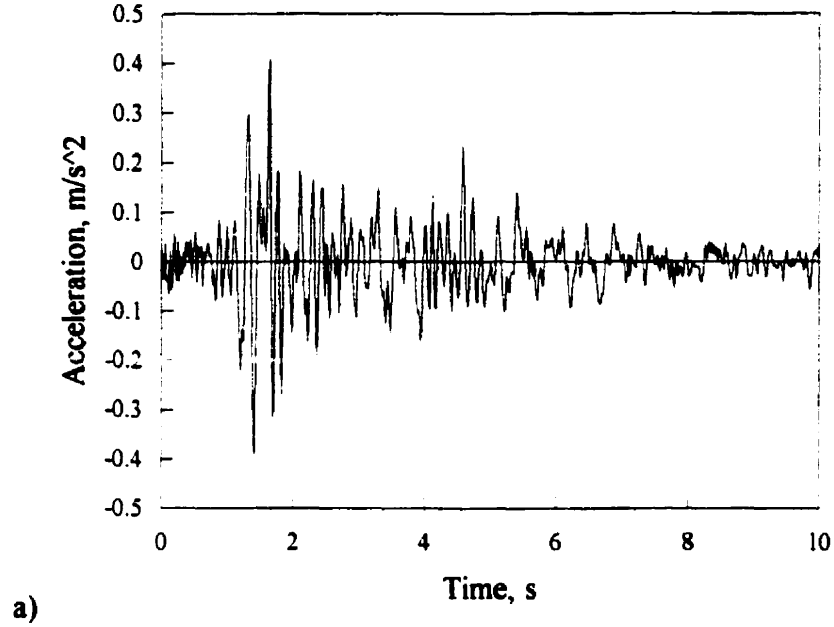

a)

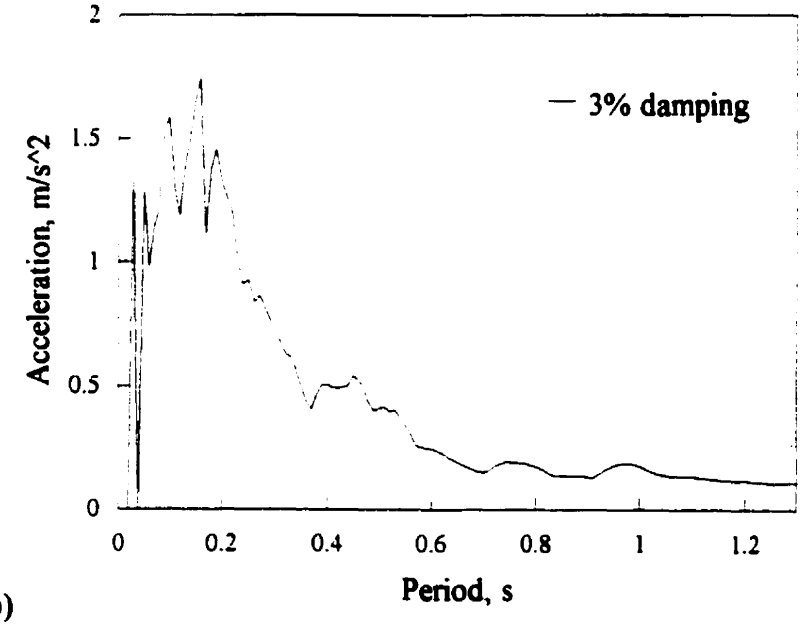

b)

Fig. A3.14 Earthquake record Monte Negro N00W (H14)

Event: Monte Negro earthquake
Component: N00W
Station: Albatros Hotel, basement
Peak Acceleration: 42.0 cm/s^2
Peak Velocity: 1.6 cm/s

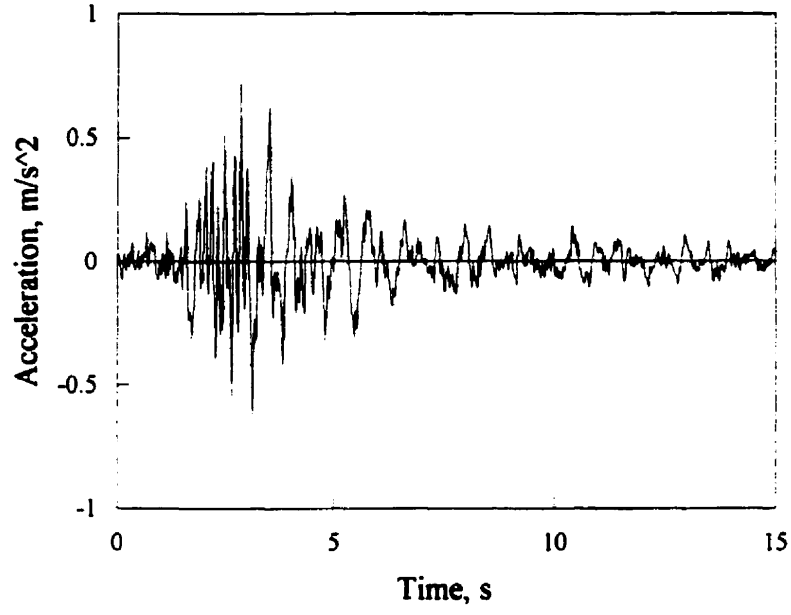

a)

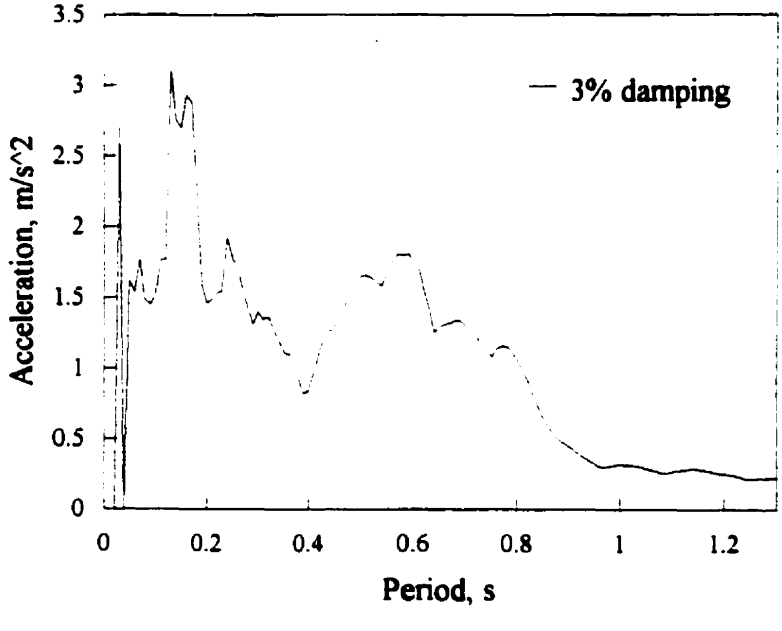

b)

Fig. A3.15 Earthquake record Banja Luka N90W (H15)

Event: Banja Luka earthquake
Component: N90W
Station: Banja Luka-4 seismological station
Paek Acceleration: 73.0 cm/s^2
Peak Velocity: 3.2 cm/s

APPENDIX B

VERIFICATION OF THE PROPOSED EXPRESSIONS FOR THE EARTHQUAKE AMPLIFICATION FACTORS

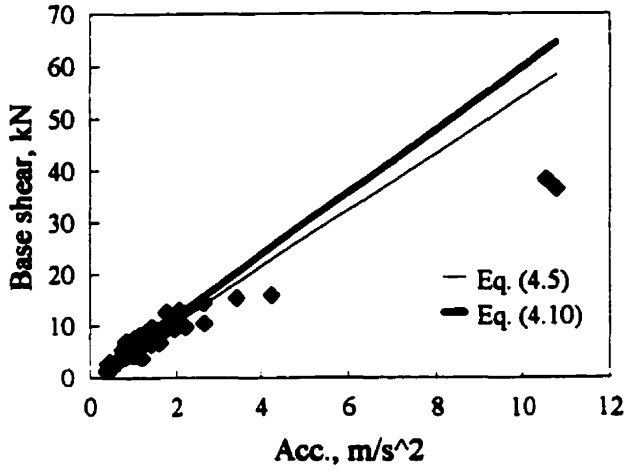

Fig. B.1 Maximum base shear vs. peak ground acceleration in TC1

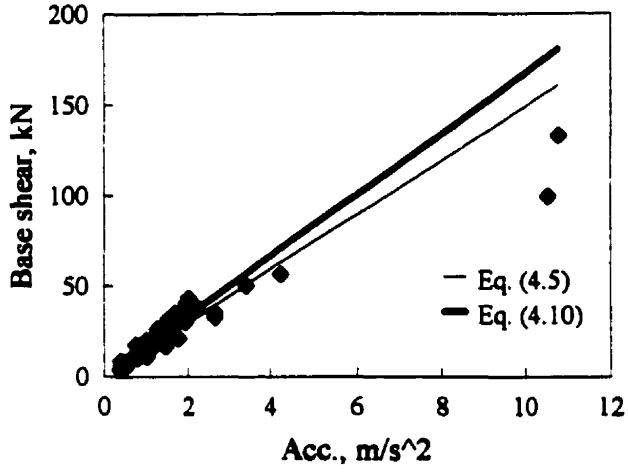

Fig. B.2 Maximum base shear vs. peak ground acceleration in TC2

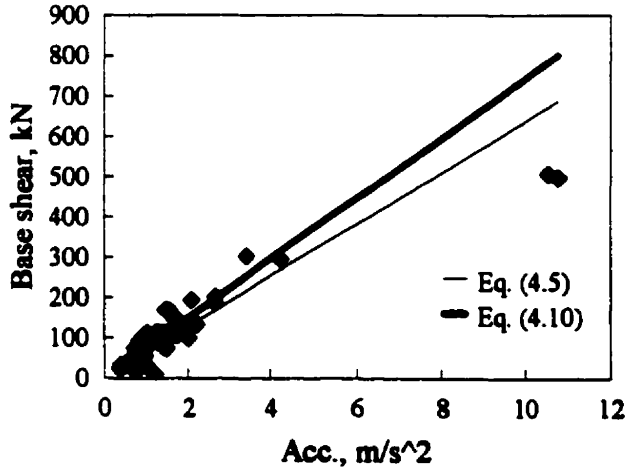

Fig. B.3 Maximum base shear vs. peak ground acceleration in TC4

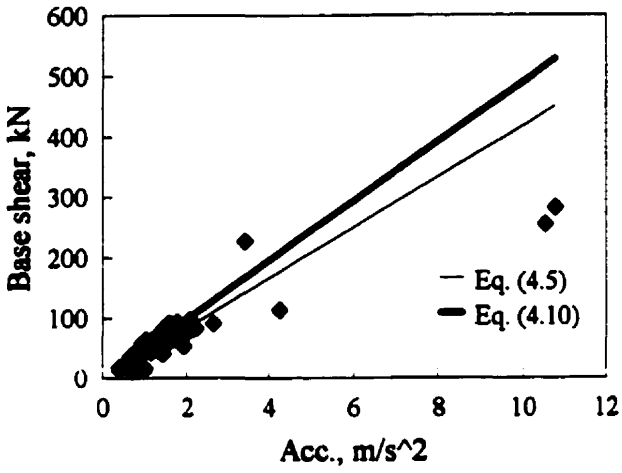

Fig. B.4 Maximum base shear vs. peak ground acceleration in TC5

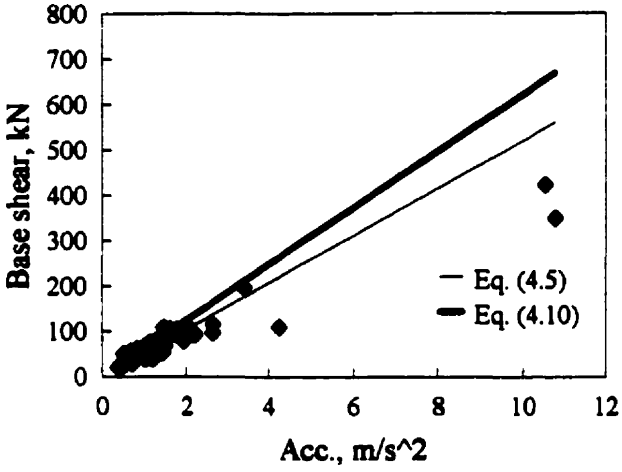

Fig. B.5 Maximum base shear vs. peak ground acceleration in TC6

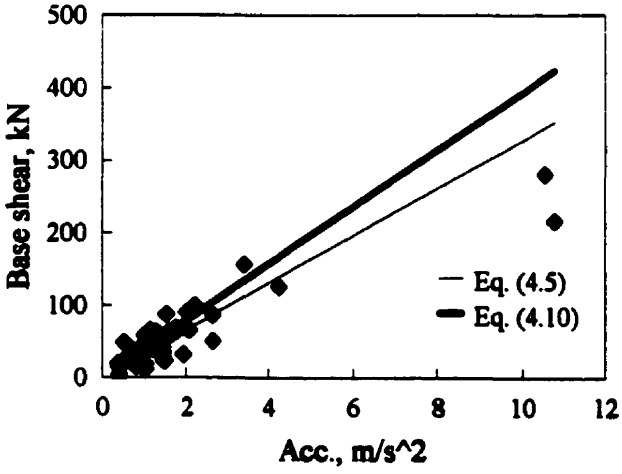

Fig. B.6 Maximum base shear vs. peak ground acceleration in TC7

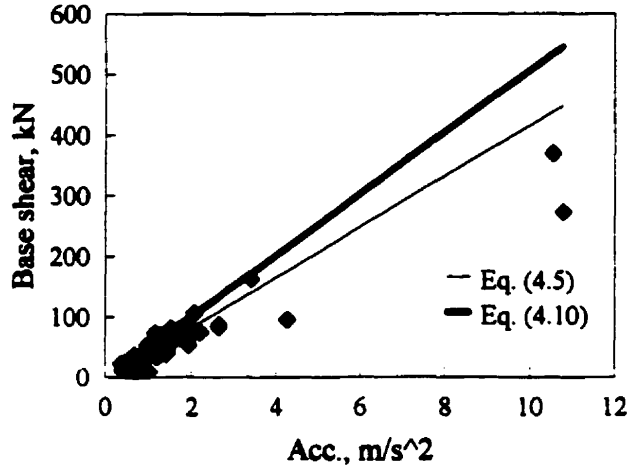

Fig. B.7 Maximum base shear vs. peak ground acceleration in TC8

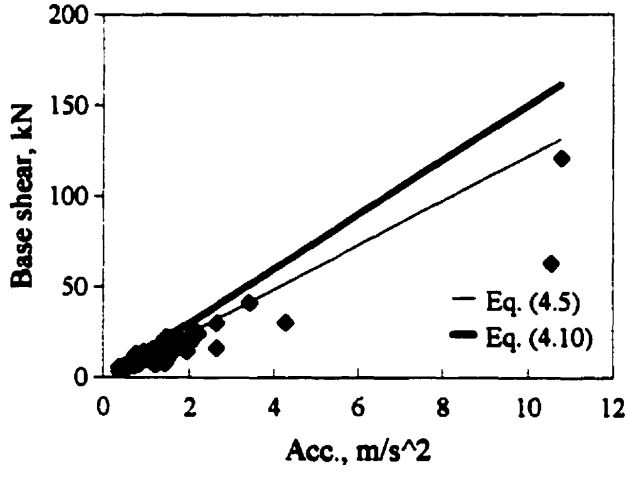

Fig. B.8 Maximum base shear vs. peak ground acceleration in TC9

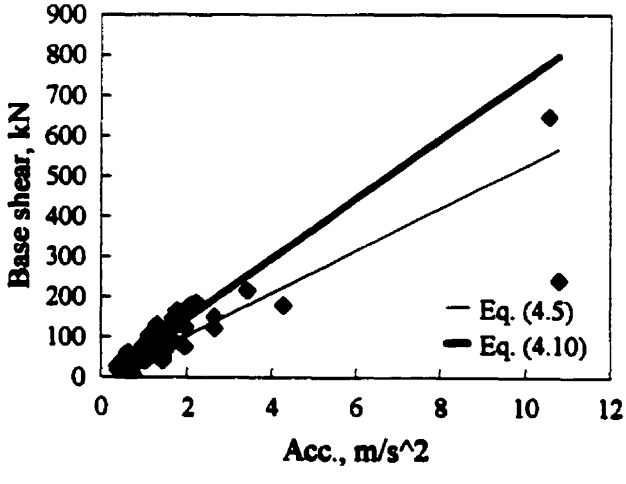

Fig. B.9 Maximum base shear vs. peak ground acceleration in TC10

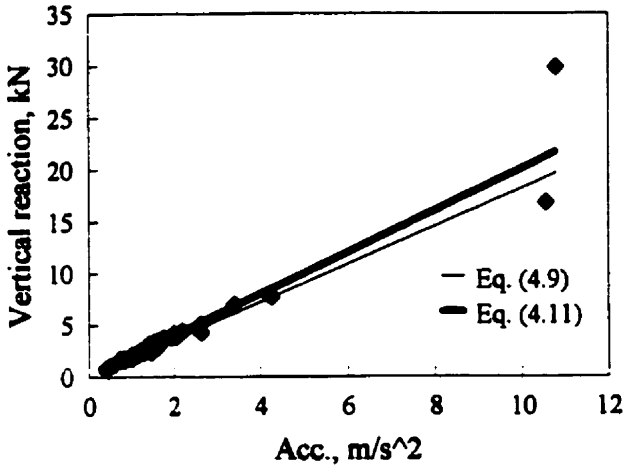

Fig. B.10 Maximum dynamic vertical reaction vs. peak ground acceleration in TC1

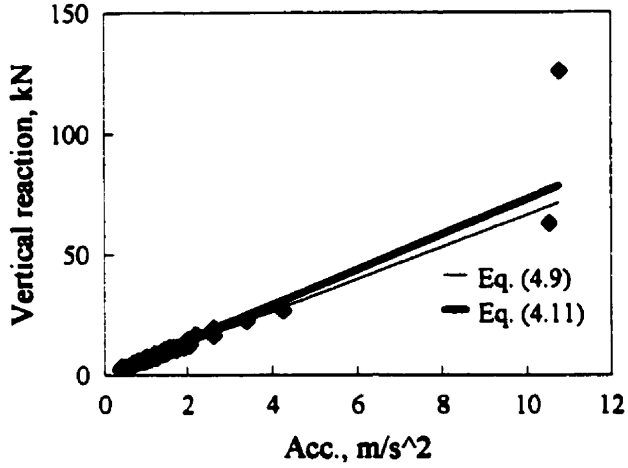

Fig. B.11 Maximum dynamic vertical reaction vs. peak ground acceleration in TC2

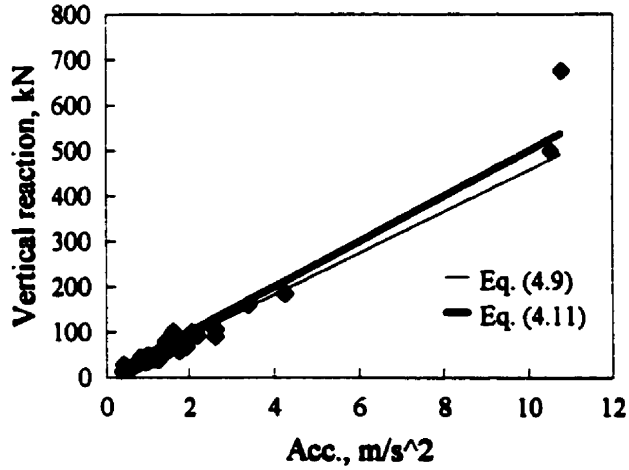

Fig. B.12 Maximum dynamic vertical reaction vs. peak ground acceleration in TC4

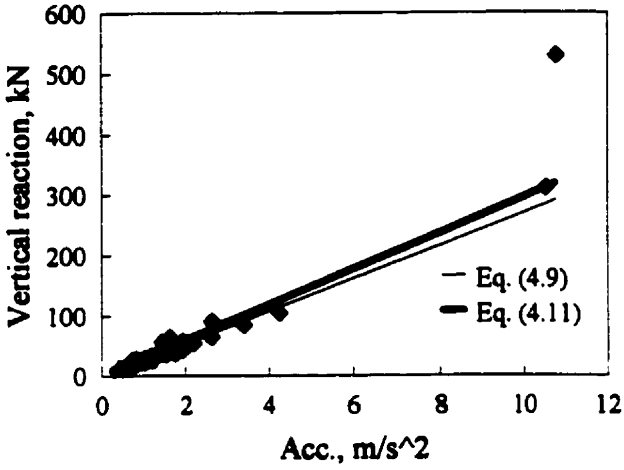

Fig. B.13 Maximum dynamic vertical reaction vs. peak ground acceleration in TC5

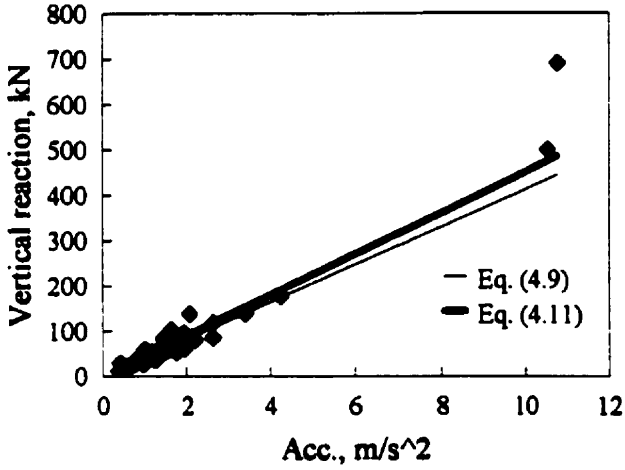

Fig. B.14 Maximum dynamic vertical reaction vs. peak ground acceleration in TC6

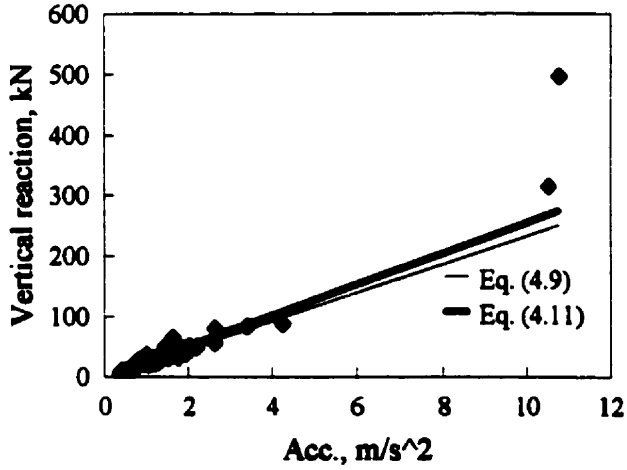

Fig. B.15 Maximum dynamic vertical reaction vs. peak ground acceleration in TC7

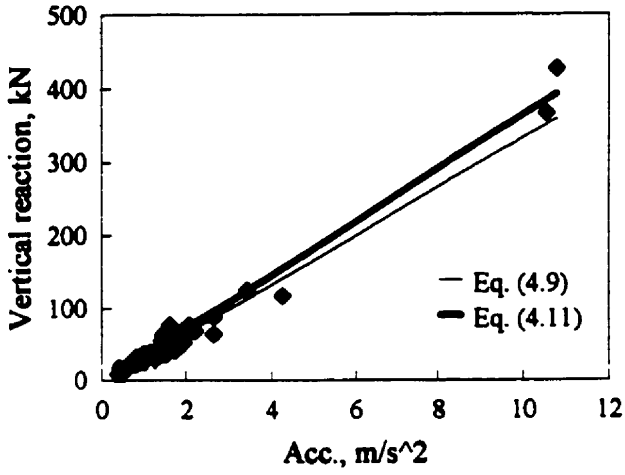

Fig. B.16 Maximum dynamic vertical reaction vs. peak ground acceleration in TC8

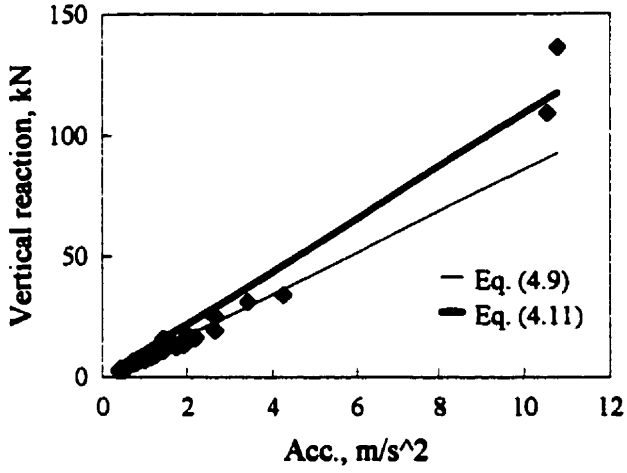

Fig. B.17 Maximum dynamic vertical reaction vs. peak ground acceleration in TC9

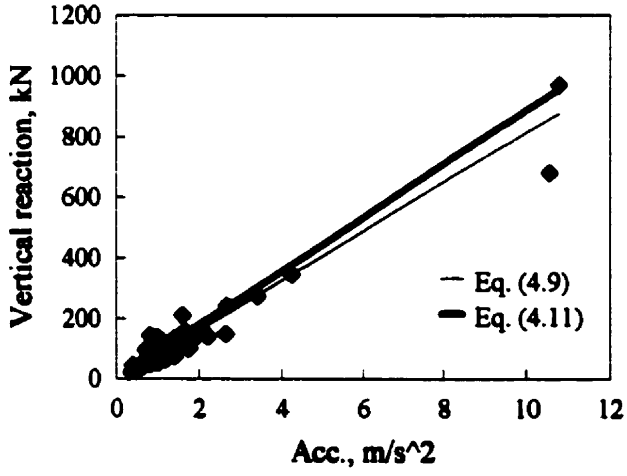

Fig. B.18 Maximum dynamic vertical reaction vs. peak ground acceleration in TC10

APPENDIX C

VERTICAL EARTHQUAKE AMPLIFICATION FACTORS FOR TELECOMMUNICATION TOWERS

C. 1 Introduction

Earthquake amplification factors for both base shear and vertical reaction of self-supporting telecommunication towers were presented in Chapter 4. These vertical amplification factors were obtained by reducing the horizontal accelerograms to 75% of their original values and then used as vertical input. This approach was chosen as most building codes do not contain specific information on the peak vertical ground accelerations.

It was also found useful to present expressions for estimating the vertical earthquake amplification factors using vertical earthquake records. The motivation for presenting these expressions is the fact that vertical earthquake records generally have high frequency content when compared to the horizontal records. The expressions presented in this appendix should replace the expressions presented in Chapter 4, Eqs. (4.9) and (4.11), when information about the peak vertical ground accelerations is included in codes or otherwise available.

C.2 Vertical Earthquake Records

In the present study, as not all the corresponding vertical components of the previous set of horizontal accelerograms were available, a distinct set of 55 vertical earthquake records collected from 17 different events were also considered. The majority of these events were included in the study performed by Tso et al. (1992). Table C.1 lists the events name, magnitude, number of components and date. It should be noted that contrary to the horizontal earthquake records, these records were not classified in accordance to their A/V ratios.

Table C.1 - Earthquake records used as vertical input

Earthquake	Magnitude	No. of records	Date
Long Beach, California	6.4	1	10/03/1933
Lower California	5.6	1	30/12/1934
Helena, Montana	6	1	31/10/1935
Imperial Valley, California	6.6	1	18/05/1940
Santa Barbara, California	5.5	1	30/06/1941
Borrego Valley, California	6.6	1	21/10/1942
Imperial Valley, California	5.8	1	23/01/1951
Kern County, California	7.5	4	21/07/1952
San Francisco, California	5.3	5	22/03/1957
Park Field, California	6.1	5	27/06/1966
Borrego Mountain, California	6.5	12	8/04/1968
Lytle Creek, California	5.3	7	12/09/1970
San Fernando, California	6.6	9	9/02/1971
Oroville, California	5.7	1	1/08/1975
Michoacan, Mexico	8.1	2	19/09/1985
Nahanni, N.W.T., Canada	6.9	1	23/12/1985
Elmore Ranch	6.2	2	24/11/1987

C.3 Vertical Earthquake Excitation

The towers are also analyzed considering the vertical earthquake set acting in the vertical direction. The values of maximum vertical reaction at the tower base are plotted versus the peak ground acceleration. Figs. C.1 to C.10 show the results obtained for the ten towers used in the study as a function of peak vertical ground acceleration.

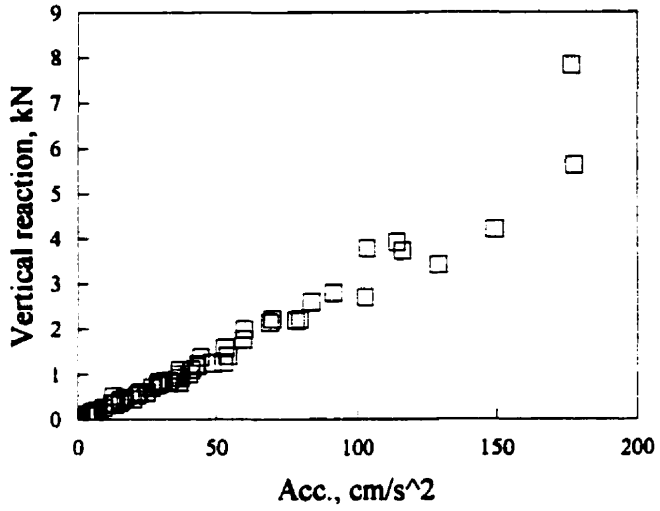

Fig. C.1 Total vertical dynamic reaction for tower TC1

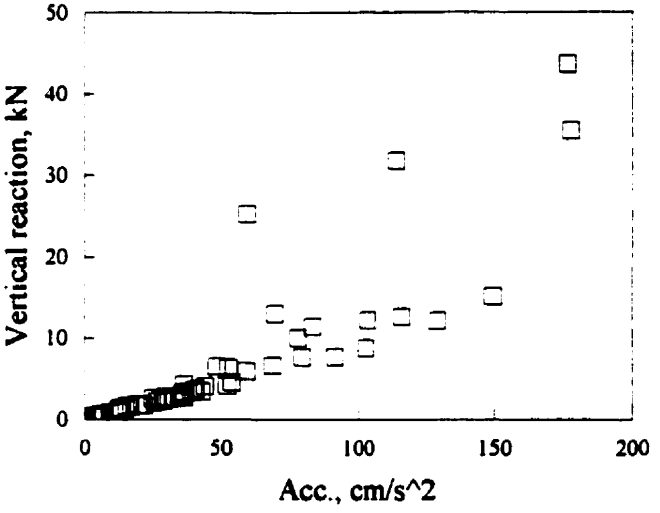

Fig. C.2 Total vertical dynamic reaction for tower TC2

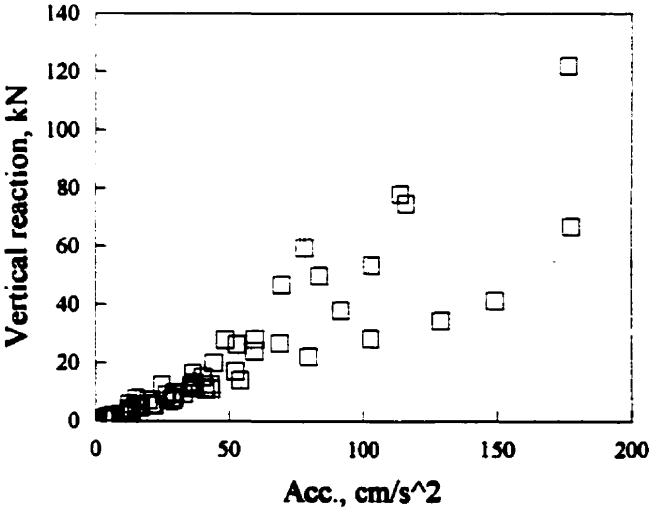

Fig. C.3 Total vertical dynamic reaction for tower TC3

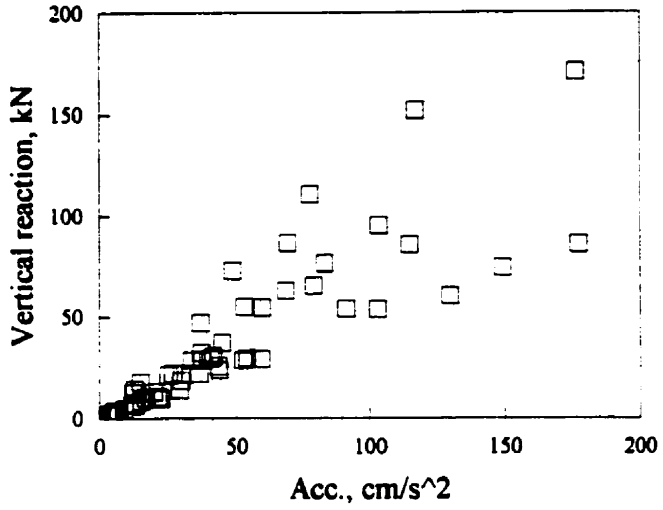

Fig. C.4 Total vertical dynamic reaction for tower TC4

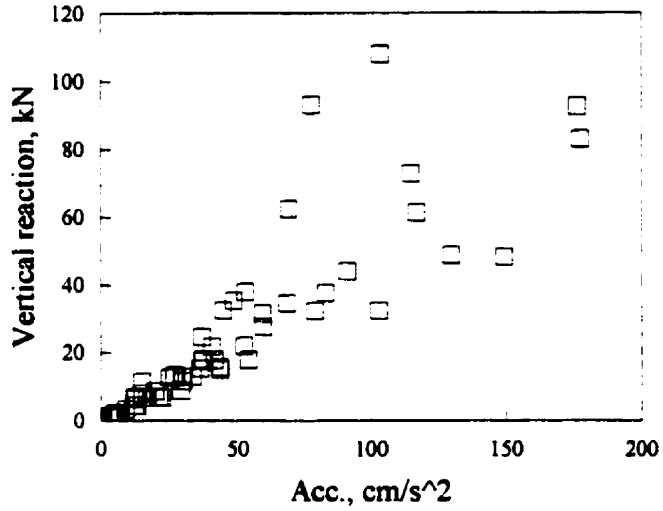

Fig. C.5 Total vertical dynamic reaction for tower TC5

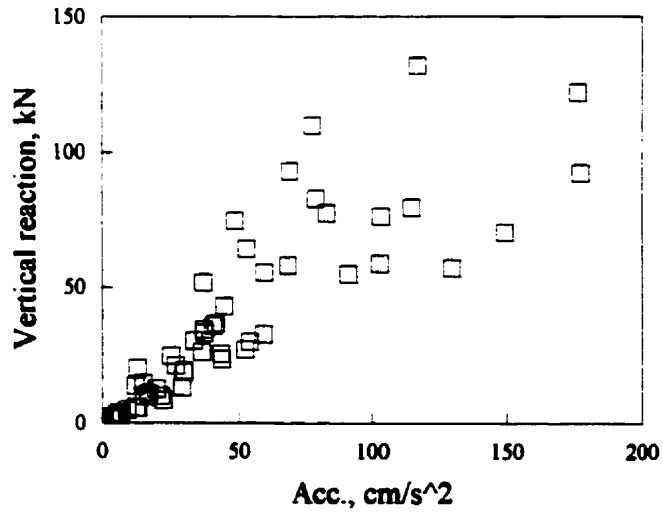

Fig. C.6 Total vertical dynamic reaction for tower TC6

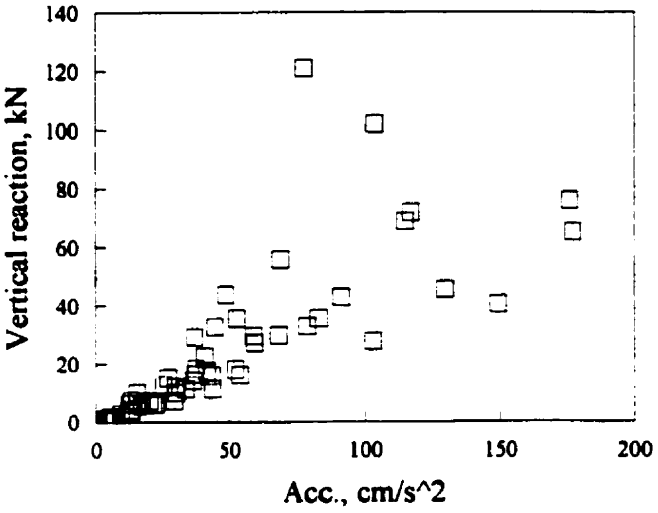

Fig. C.7 Total vertical dynamic reaction for tower TC7

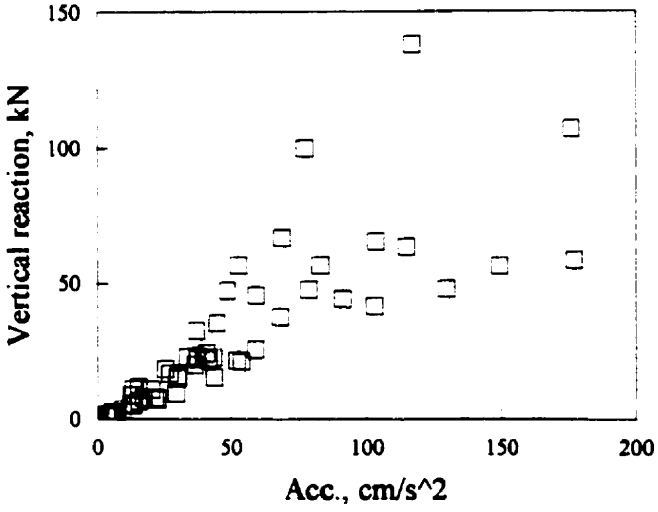

Fig. C.8 Total vertical dynamic reaction for tower TC8

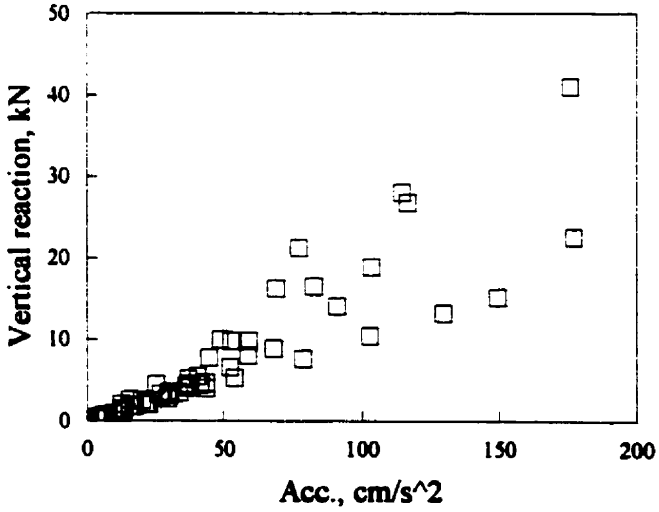

Fig. C.9 Total vertical dynamic reaction for tower TC9

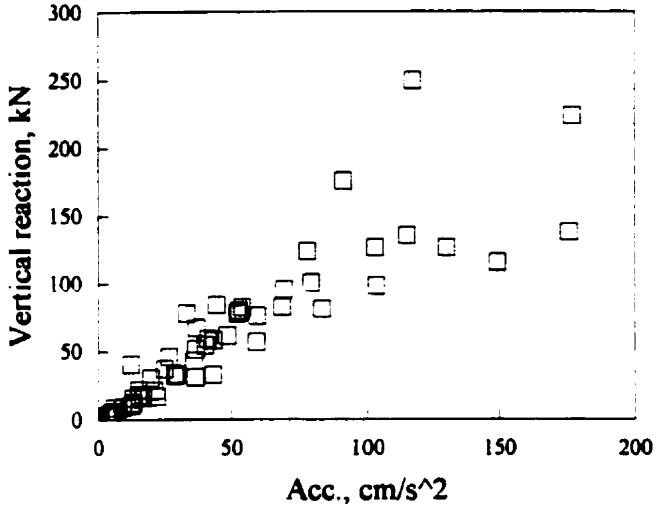

Fig. C.10 Total vertical dynamic reaction for tower TC10

As seen from these figures, the relation between the maximum vertical reaction and the peak vertical ground acceleration follows a linear trend. Therefore, linear regression analyses are performed to correlate the total vertical reaction to the peak ground acceleration and the results are summarized in Table C.2 for the ten towers.

Table C.2 - Linear regression analysis for the total vertical reaction

Tower	Slope	R^2
TC1	0.94	0.92
TC2	1.29	0.73
TC3	1.65	0.77
TC4	1.63	0.78
TC5	1.47	0.78
TC6	1.73	0.76
TC7	1.69	0.60
TC8	1.66	0.71
TC9	1.45	0.79
TC10	1.81	0.73

R: Coefficient of correlation

In keeping with the procedure followed in Chapter 4, the maximum vertical reaction, V_v, is divided by the tower mass and peak ground vertical acceleration, $M \times A_v$, in order to yield a dimensionless factor. These factors are then plotted versus the fundamental axial period of the tower for each earthquake record (Fig. C.11). Contrary to the maximum base shear response, the data follows an ascending trend in which the tower with lowest fundamental axial period of vibration has the smallest amplification factor. Linear regression analyses are performed on the entire set and the following expression is obtained for estimating the maximum vertical reaction:

$$V_v = M \times A_v \times (0.85 + 9.37 \times T_a) \qquad \text{(C.1)}$$

where

V_v = total maximum vertical reaction, N

A_v = peak vertical ground acceleration, m/s^2

T_a = fundamental axial period of vibration, s.

The values of the maximum total vertical reaction estimated using Eq. (C.1) are shown in Figs. C.12 and C.13 , for towers TC3 and TC10, respectively. In order to obtain an upper bound to the expected level of maximum vertical reaction, one standard deviation is added to the numerical factors of eq. (C.1) to yield the following expression:

$$V_v = M \times A_v \times (0.97 + 10.97 \times T_a) \qquad \text{(C.2)}$$

This upper bound expression for the maximum vertical reaction values is shown in Fig. C.11 for comparison with eq. (C.1).

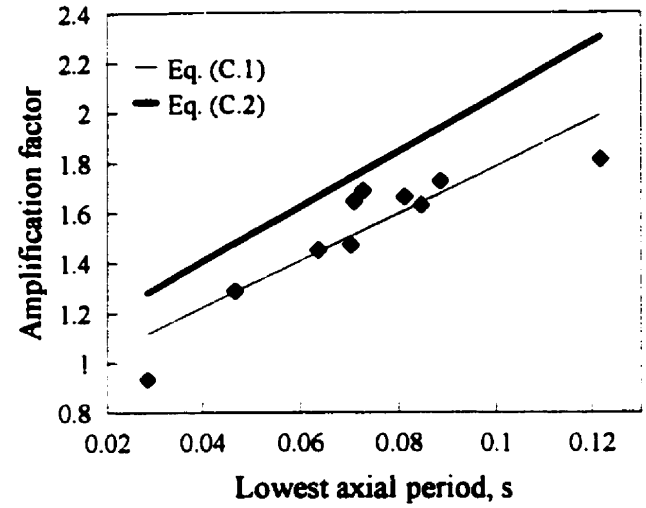

Fig. C.11 Vertical reaction amplification factors

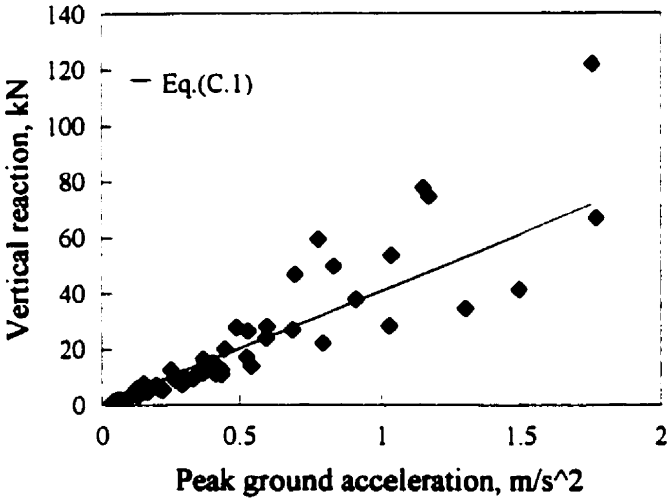

Fig. C.12 Maximum dynamic vertical reaction vs. peak ground acceleration in TC3

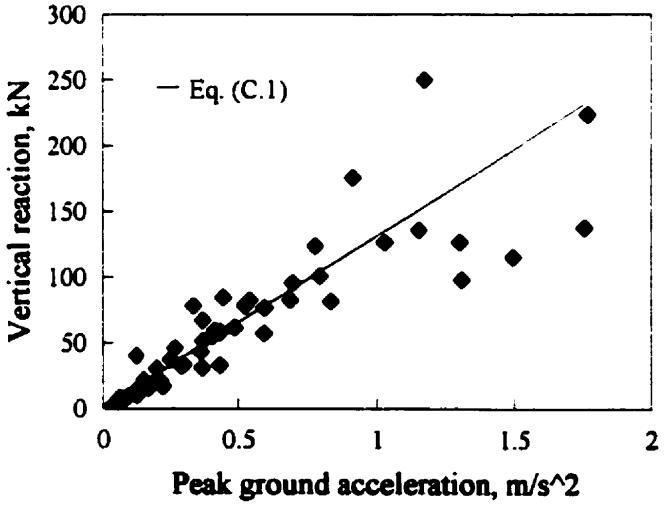

Fig. C.13 Maximum dynamic vertical reaction vs. peak ground acceleration in TC10

C.4 Discussion

Two expressions for the evaluation of the vertical reaction of telecommunication towers under vertical seismic excitations are included in this appendix. Fig. C.14 shows a comparison between these expressions and eqs. (4.9) and (4.11) after multiplying them by 4/3. This was done as eqs. (4.9) and (4.11) were originally evaluated after reducing the peak ground acceleration to 3/4 of the original value. From this figure it is seen that amplification factors predicted by eqs. (C.1) and (C.2) exceed those predicted by eqs. (4.9) and (4.11) by about 40%. This was expected as actual vertical earthquake record possess higher frequency content and therefore will result in more amplification.

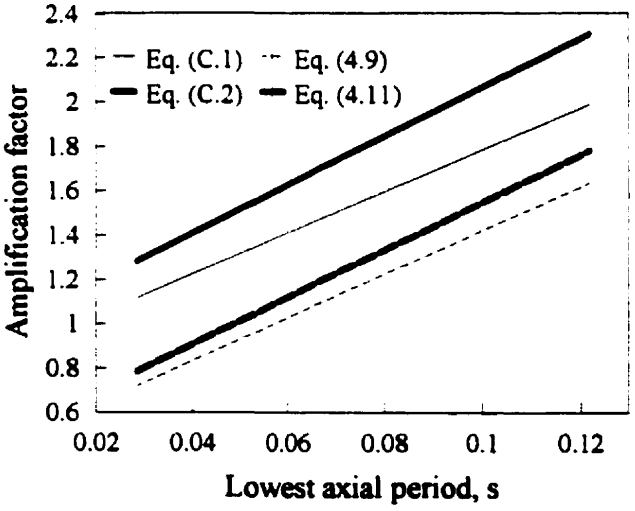

Fig. C.14 Comparison between the expressions for vertical amplification factor

It should be noted that the use of 3/4 of the peak ground acceleration in the vertical direction greatly overestimates the expected peak vertical ground acceleration which is

usually with lower intensities. Therefore, even though the expressions presented in Chapter 4 underestimate the level of dynamic amplification, they are used with higher intensities of ground acceleration than the actual vertical earthquakes possess.

APPENDIX D

VERIFICATION OF THE PROPOSED STATIC METHOD

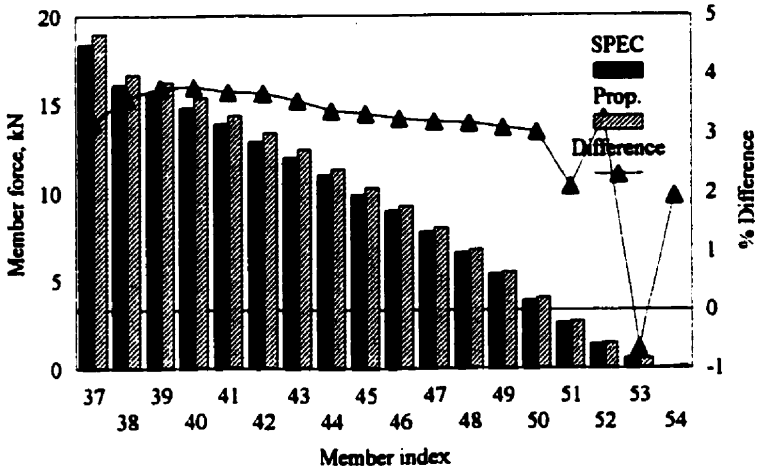

a) Earthquake record L14

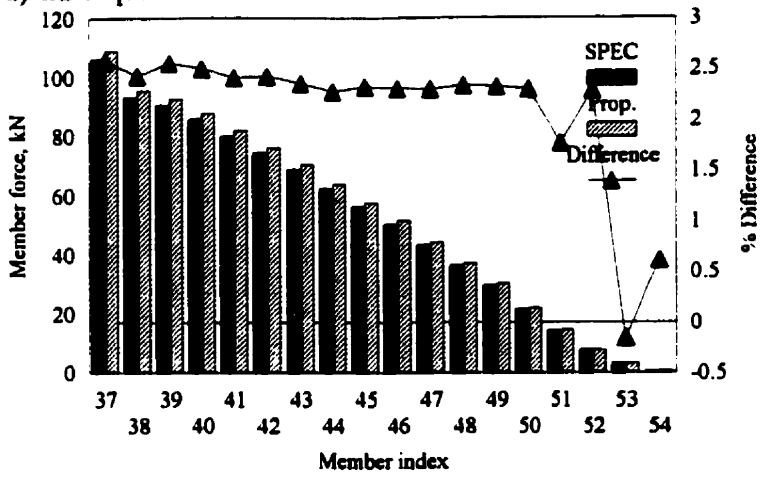

b) Earthquake record N3

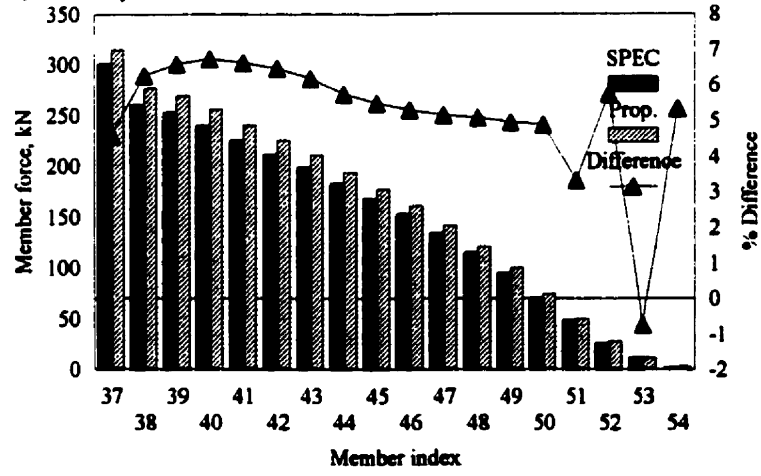

c) Earthquake record H8

Fig. D.1 Member forces in tower TC2

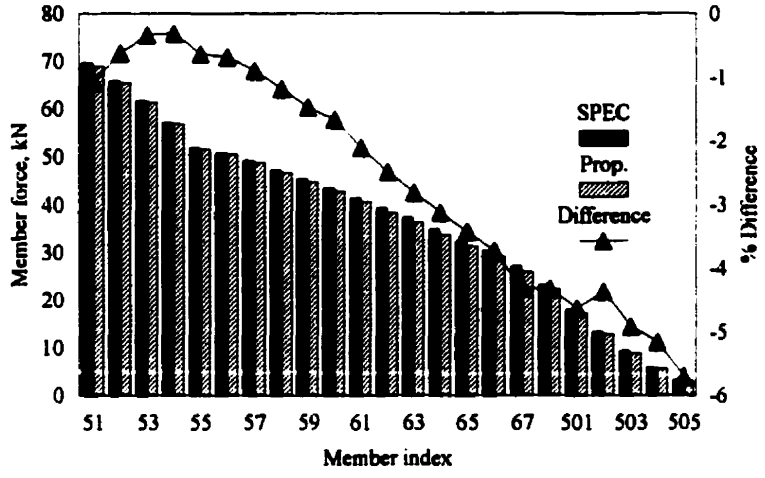

a) Earthquake record L14

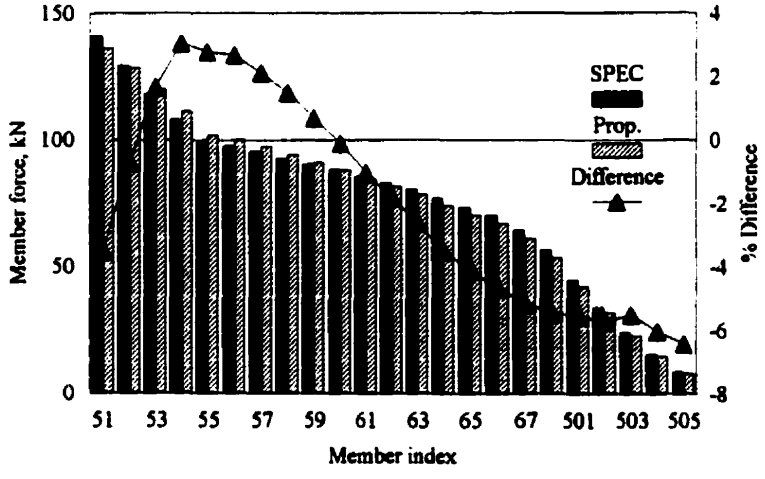

b) Earthquake record N3

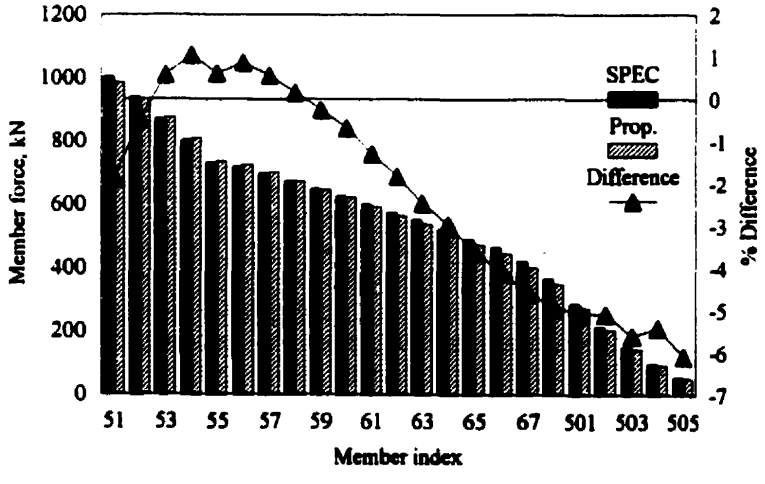

c) Earthquake record H8

Fig. D.2 Member forces in tower TC3

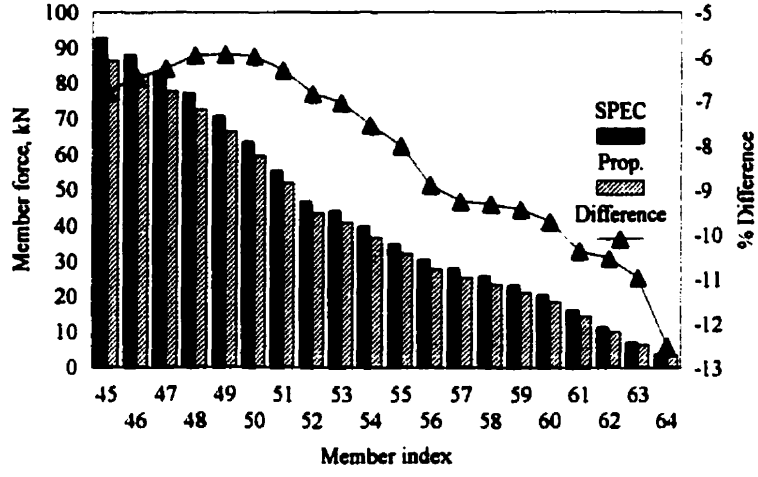

a) Earthquake record L14

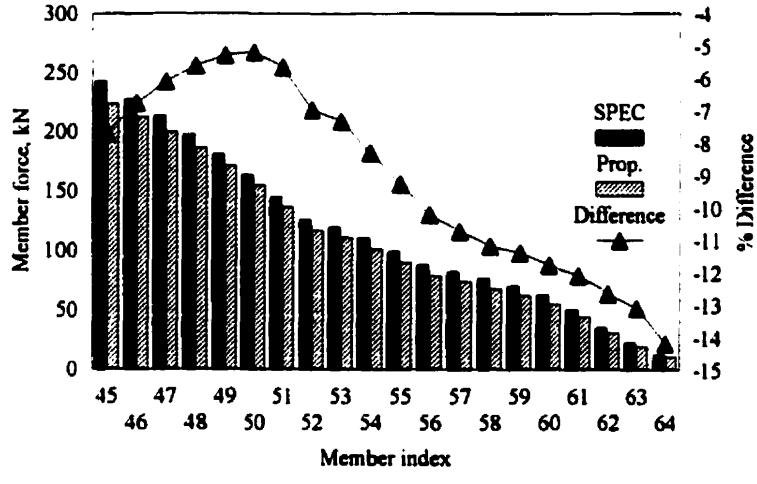

b) Earthquake record N3

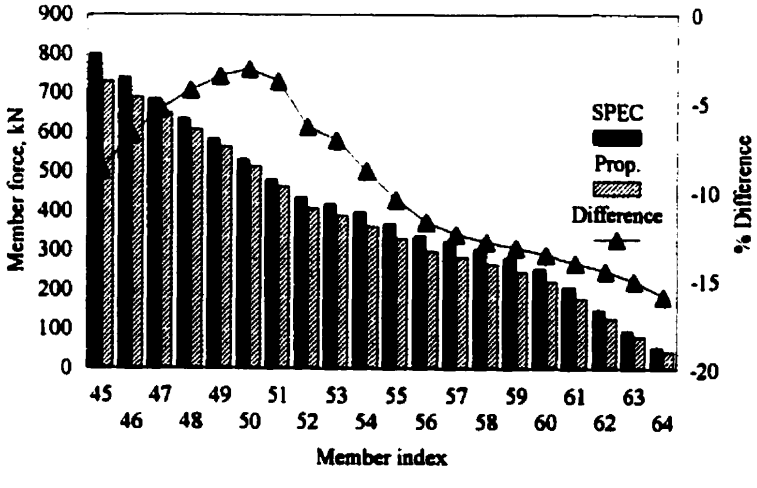

c) Earthquake record H8

Fig. D.3 Member forces in tower TC5

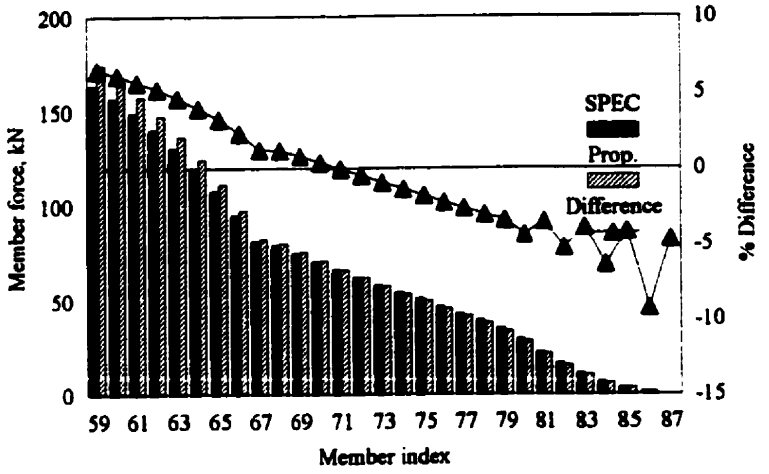

a) Earthquake record L14

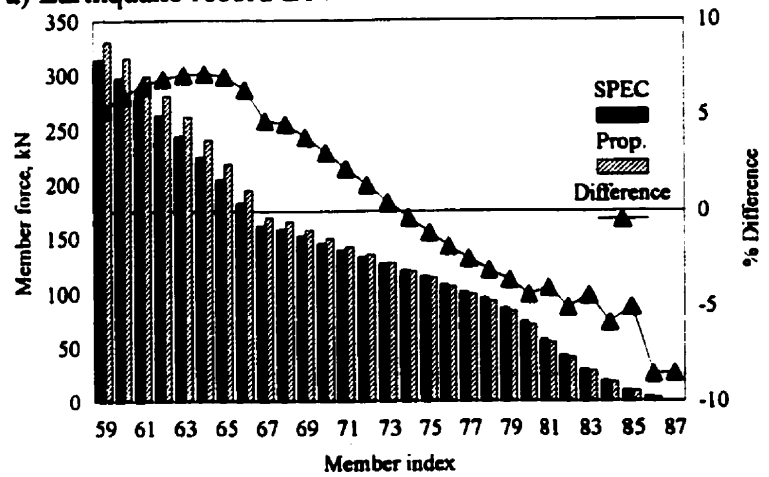

b) Earthquake record N3

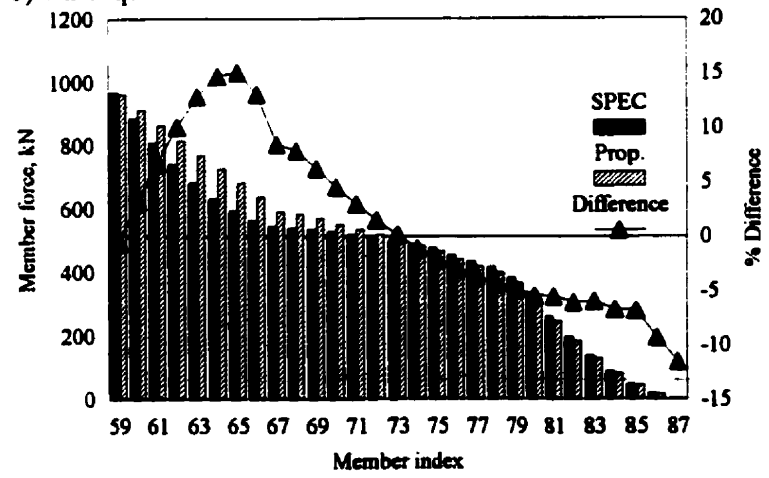

c) Earthquake record H8

Fig. D.4 Member forces in for tower TC6

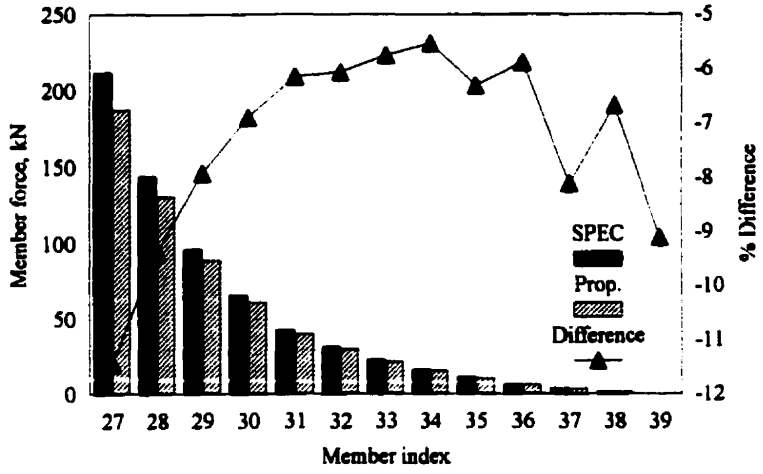

a) Earthquake record L14

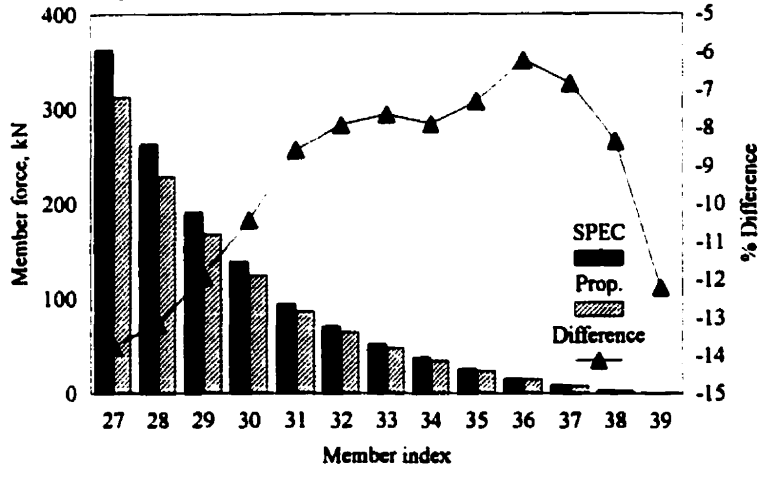

b) Earthquake record N3

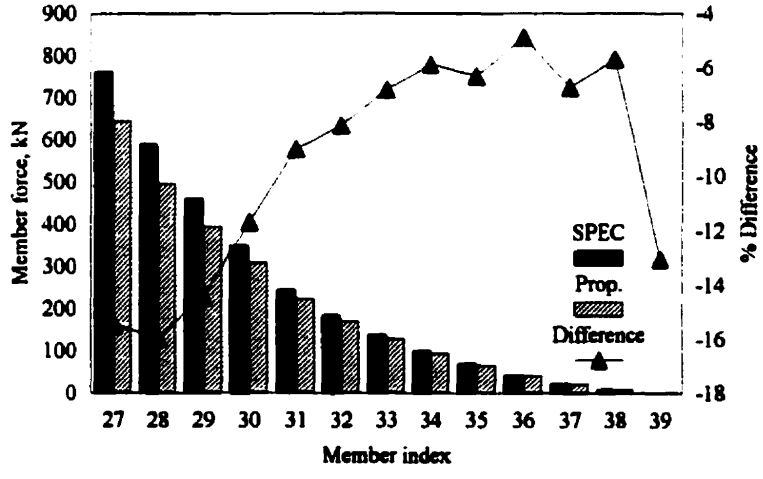

c) Earthquake record H8

Fig. D.5 Member forces in tower TC7

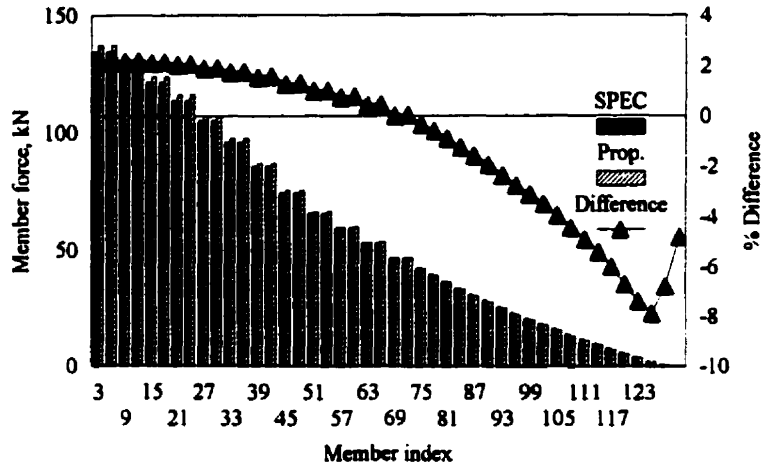

a) Earthquake record L14

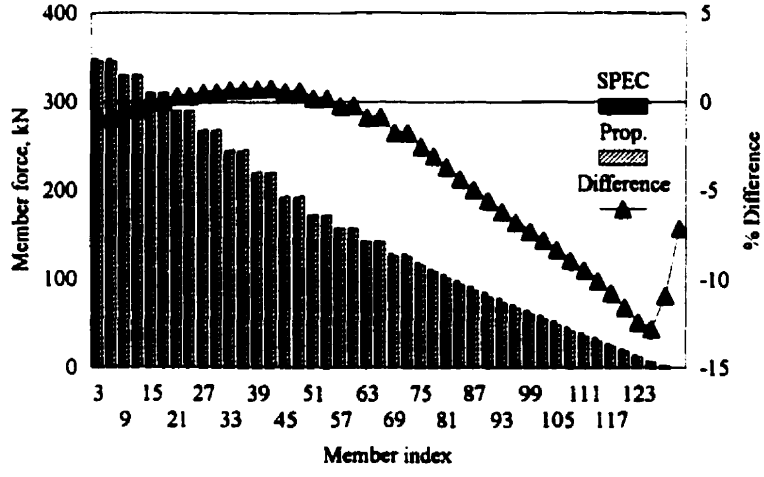

b) Earthquake record N3

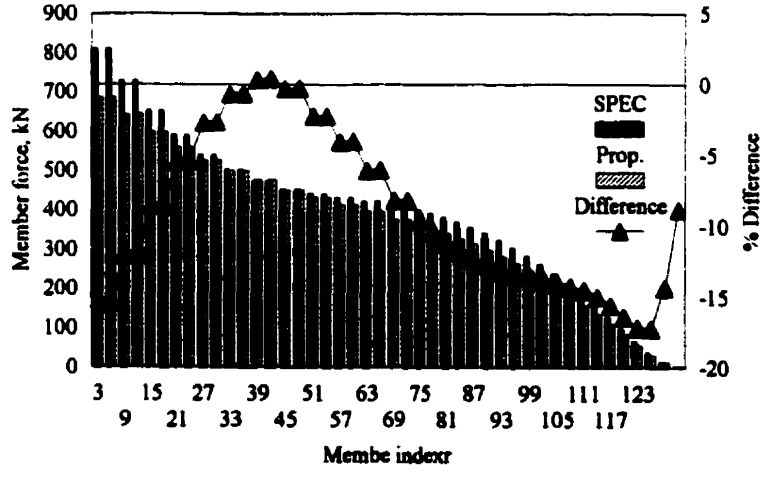

c) Earthquake record H8

Fig. D.6 Member forces in for tower TC8

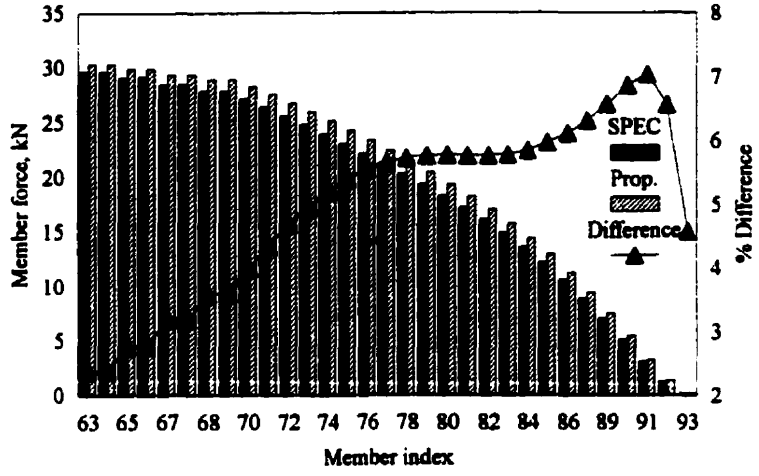

a) Earthquake record L14

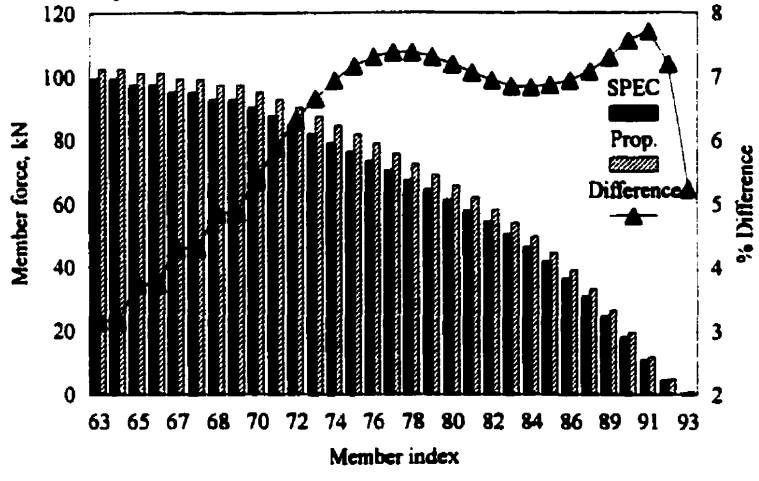

b) Earthquake record N3

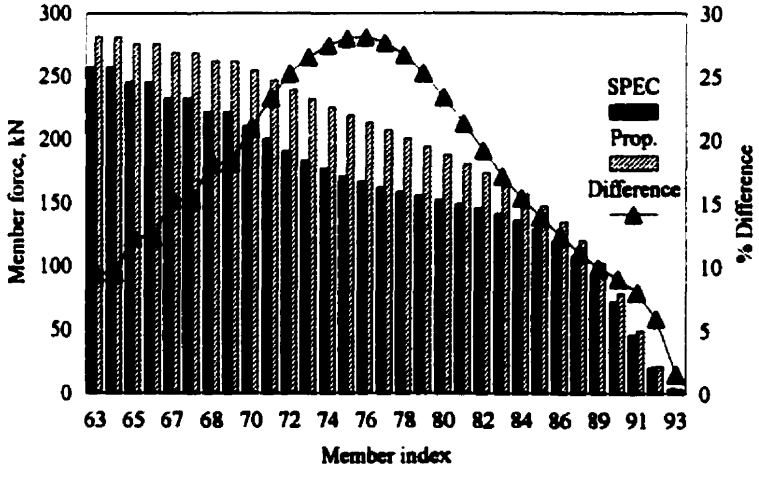

c) Earthquake record H8

Fig. D.7 Member forces in tower TC9

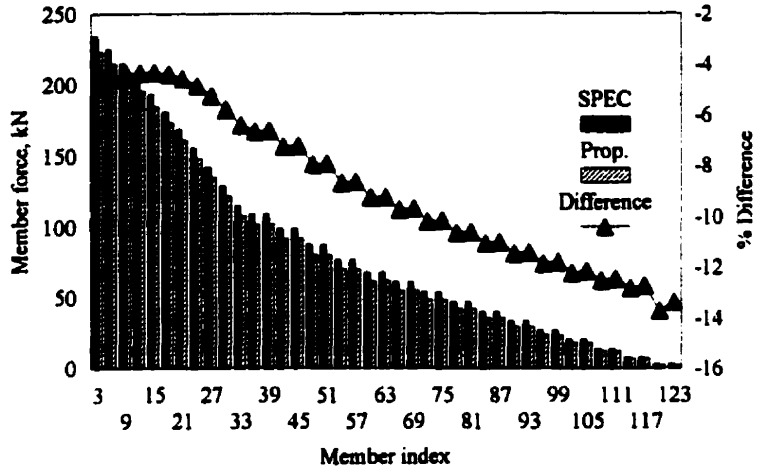

a) Earthquake record L14

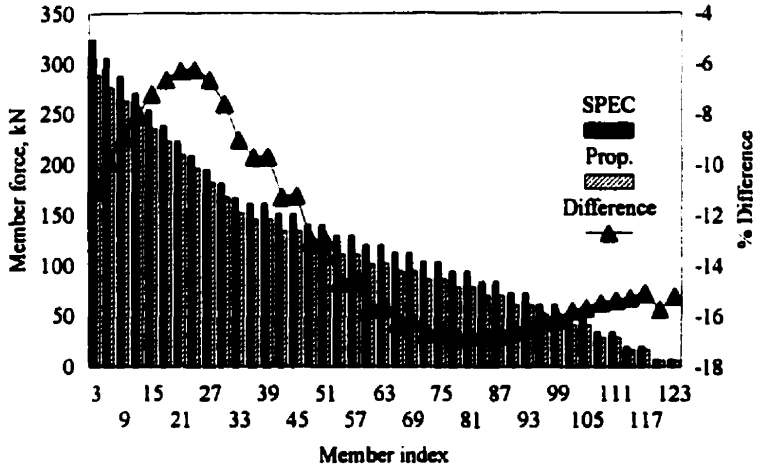

b) Earthquake record N3

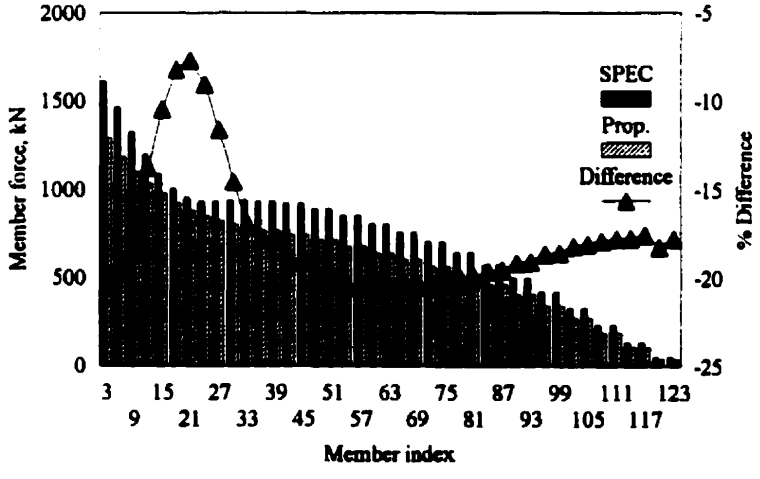

c) Earthquake record H8

Fig. D.8 Member forces in tower TC10

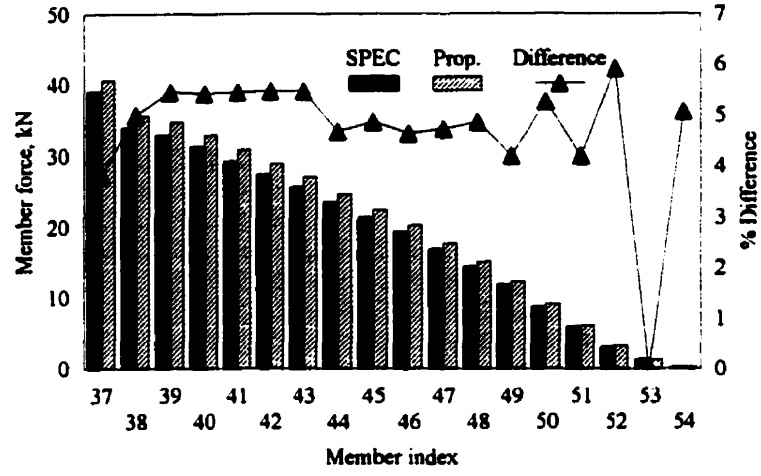

a) Za<Zv

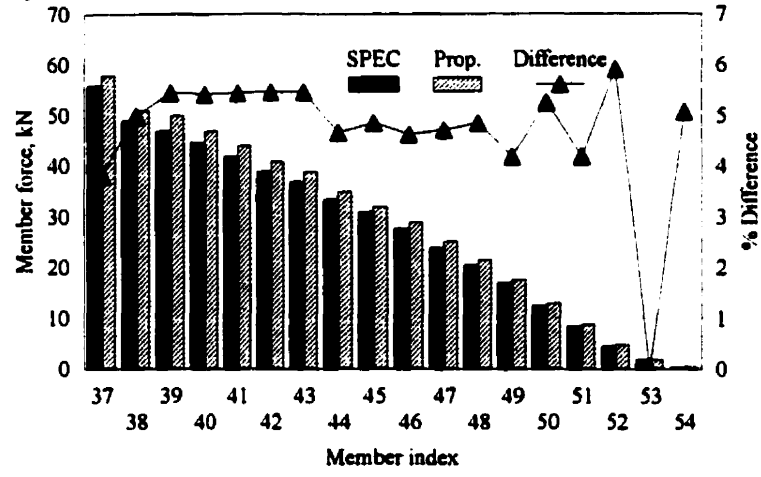

b) Za=Zv

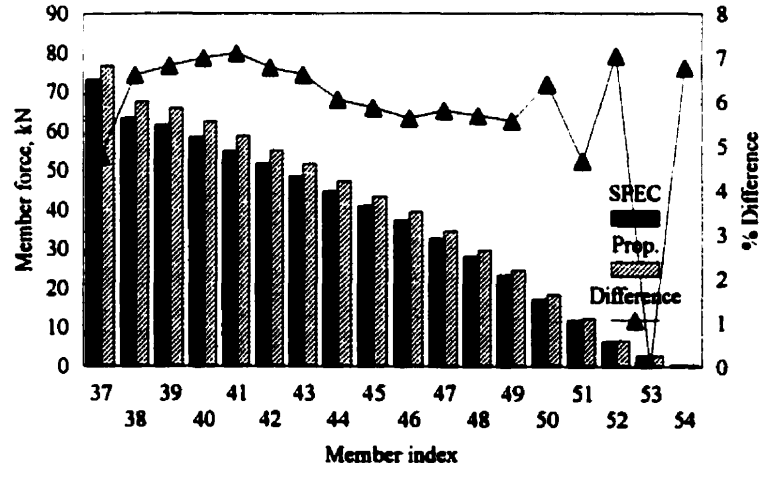

c) Za>Zv

Fig. D.9 Member forces in tower TC2 using NBCC spectrum

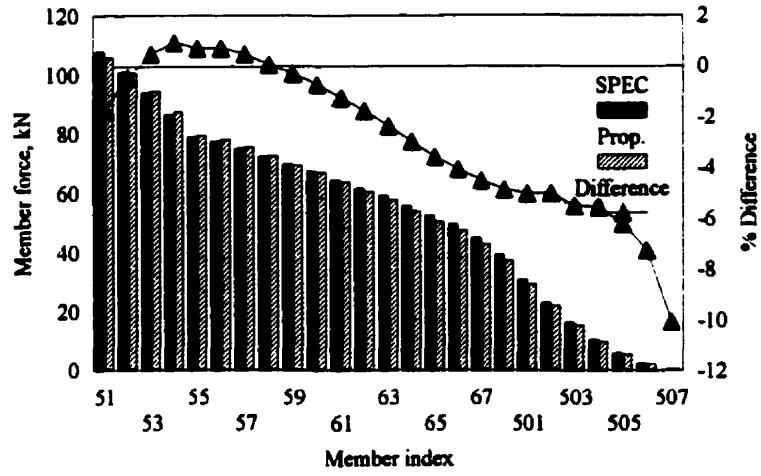

a) Za<Zv

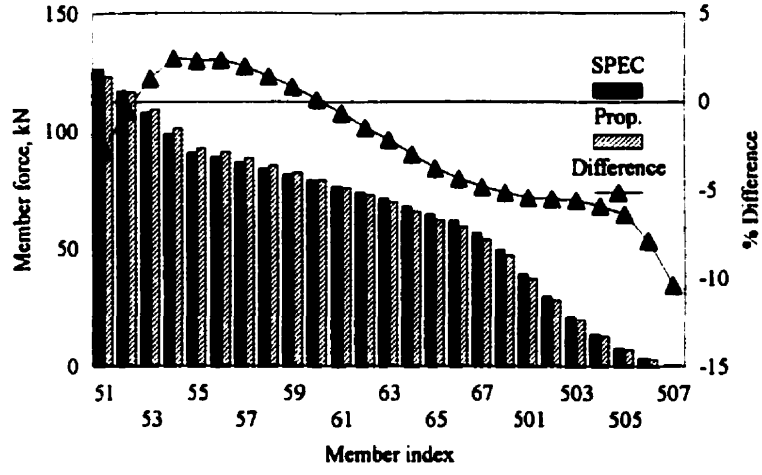

b) Za=Zv

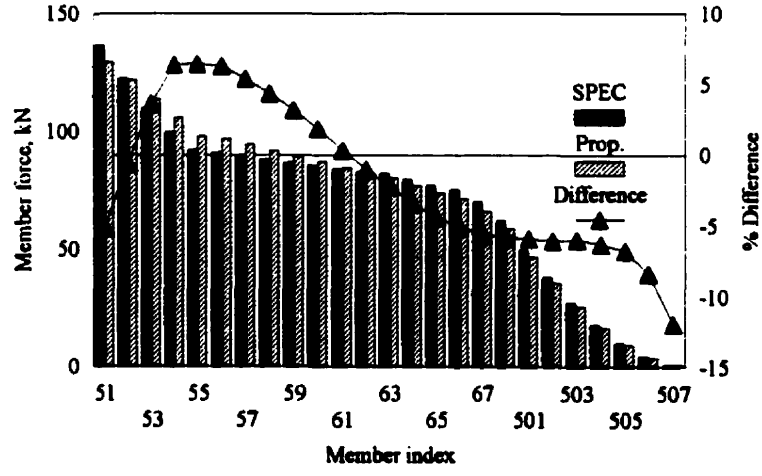

c) Za>Zv

Fig. D.10 Member forces in tower TC3 using NBCC spectrum

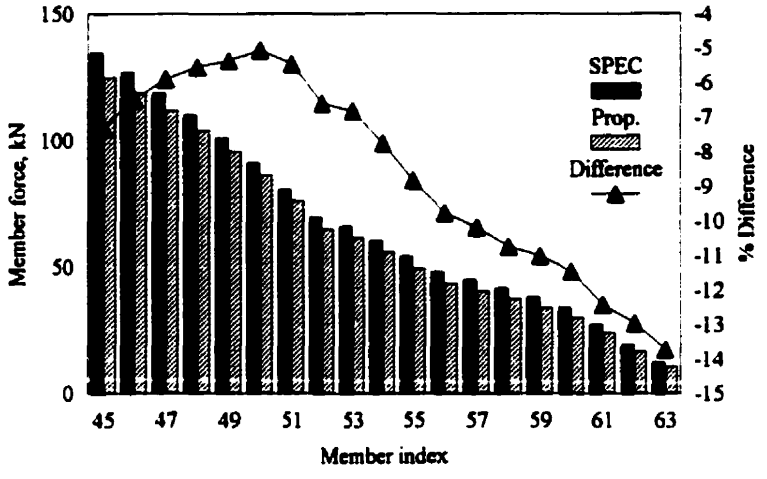

a) Za<Zv

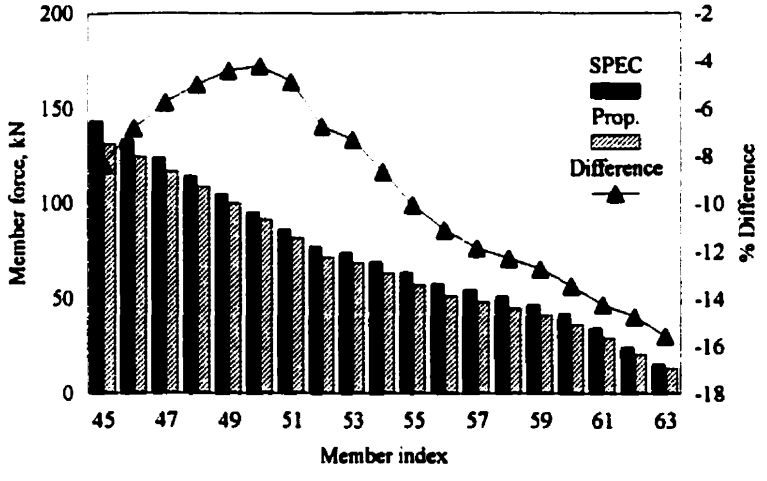

b) Za=Zv

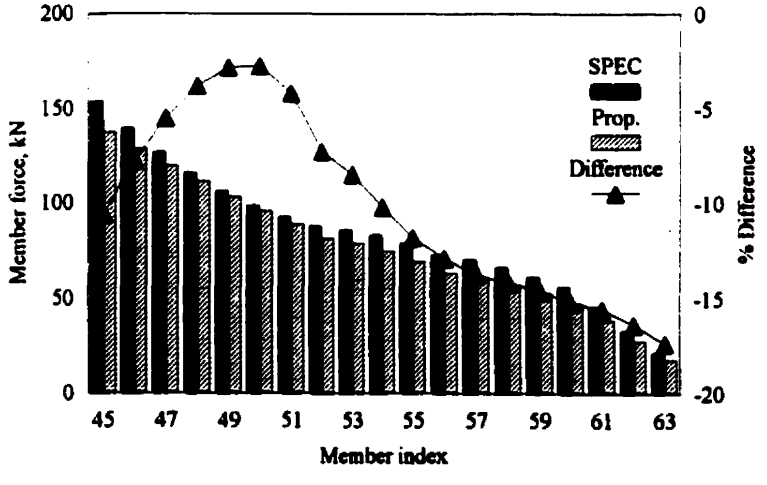

c) Za>Zv

Fig. D.11 Member forces in tower TC5 using NBCC spectrum

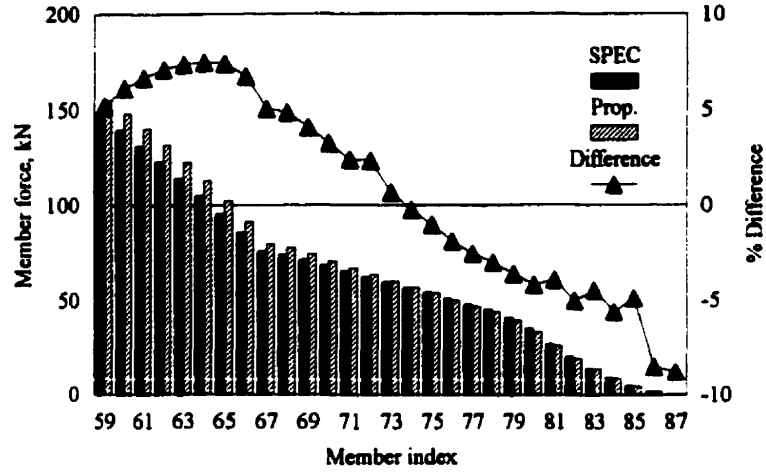

a) Za<Zv

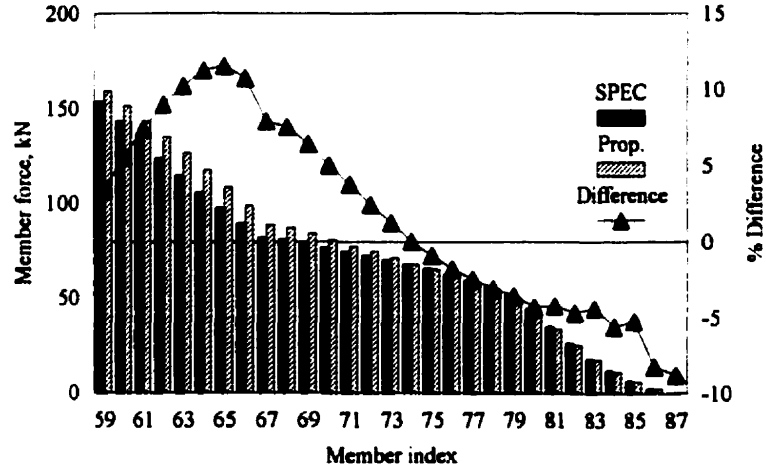

b) Za=Zv

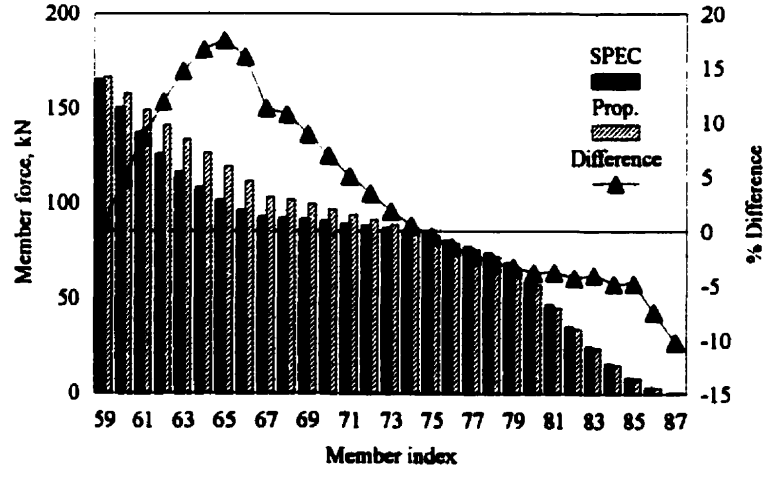

c) Za>Zv

Fig. D.12 Member forces in tower TC6 using NBCC spectrum

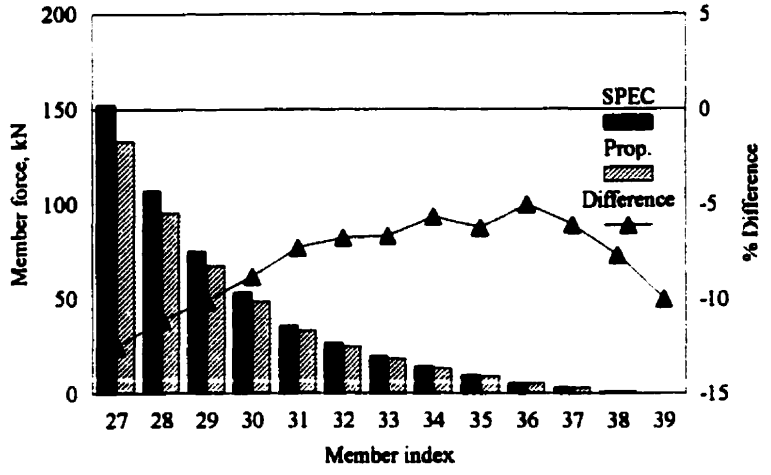

a) Za<Zv

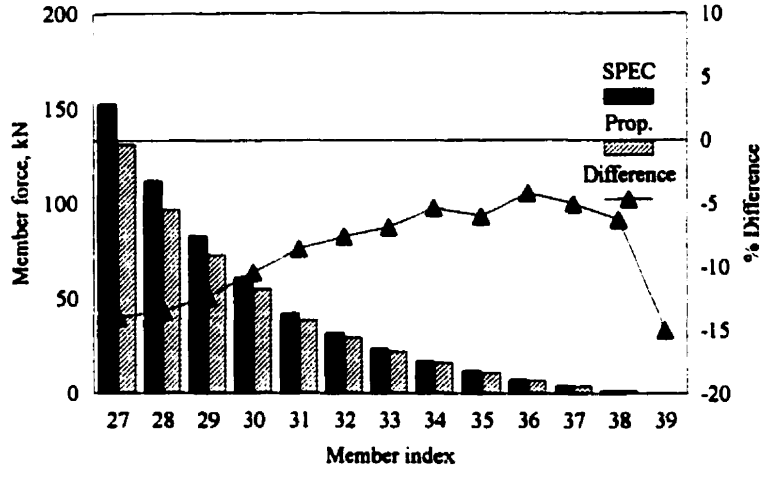

b) Za=Zv

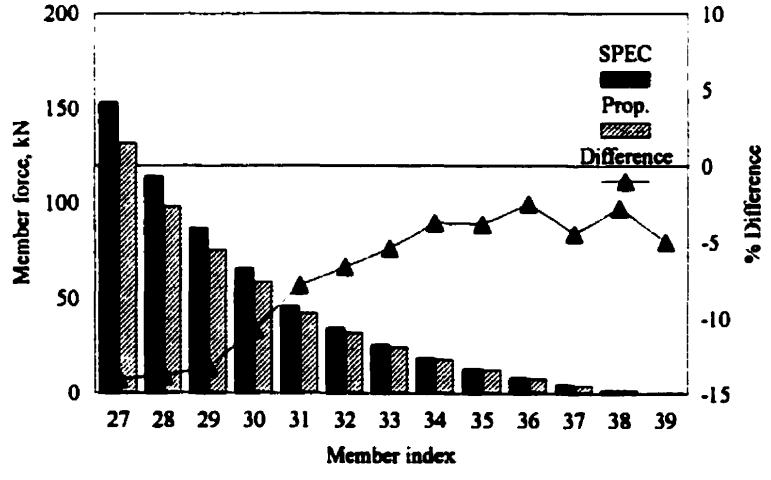

c) Za>Zv

Fig. D.13 Member forces in tower TC7 using NBCC spectrum

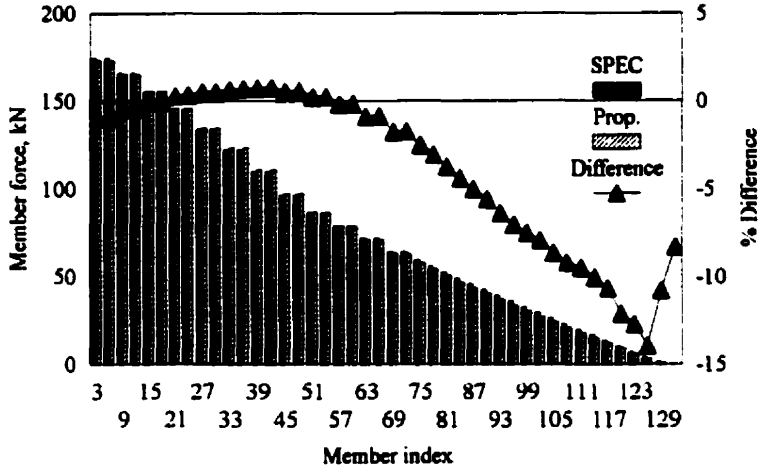

a) Za<Zv

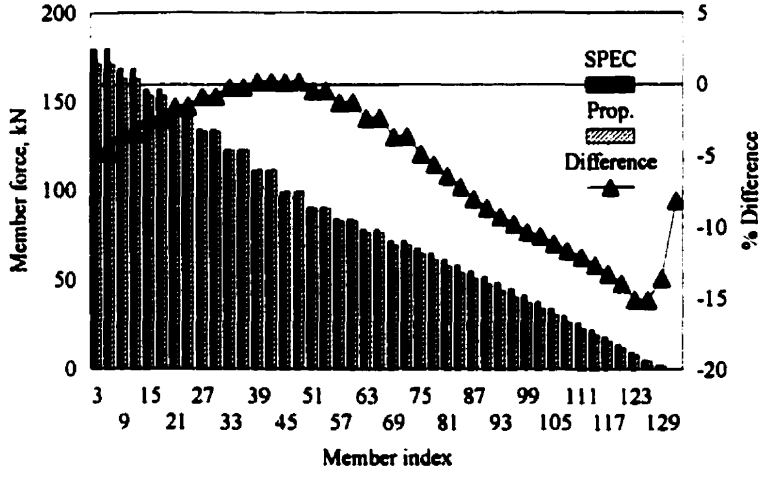

b) Za=Zv

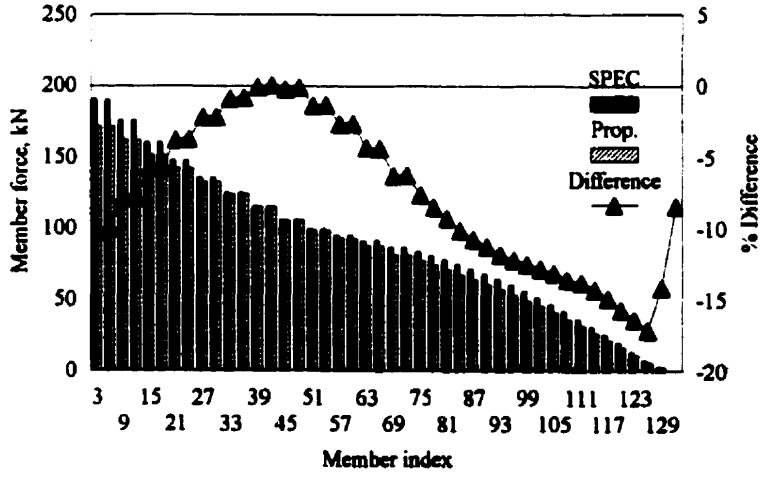

c) Za>Zv

Fig. D.14 Member forces in tower TC8 using NBCC spectrum

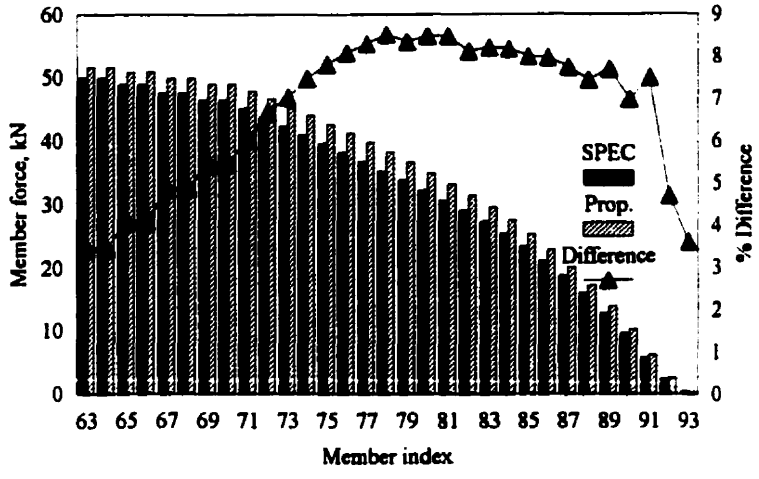

a) Za<Zv

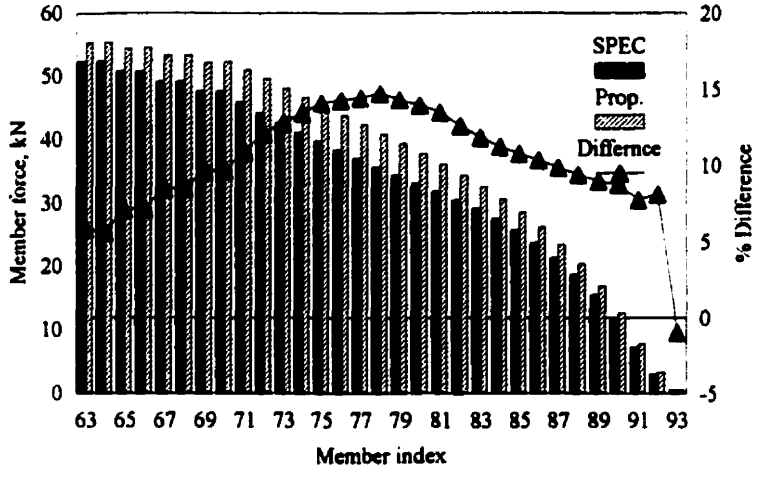

b) Za=Zv

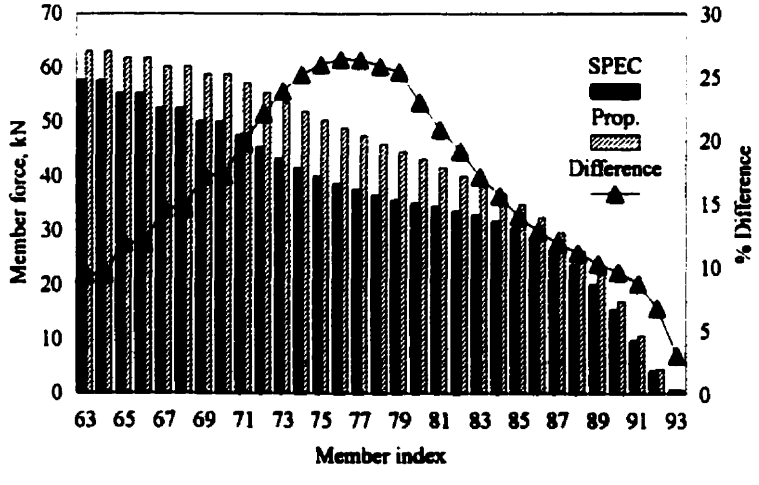

c) Za>Zv

Fig. D.15 Member forces in tower TC9 using NBCC spectrum

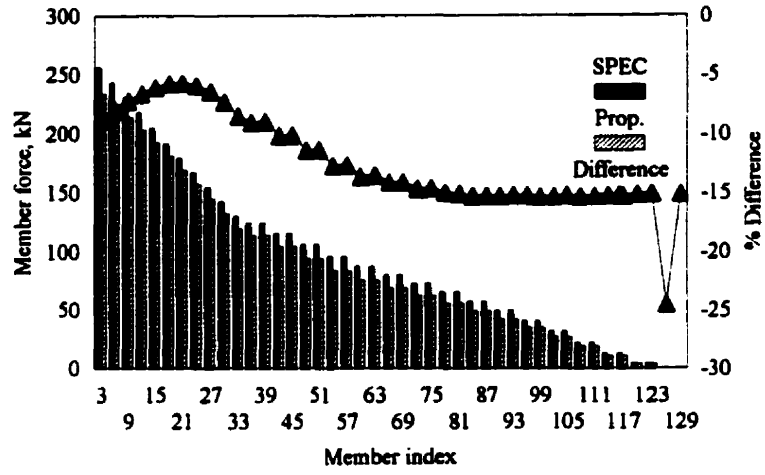

a) Za<Zv

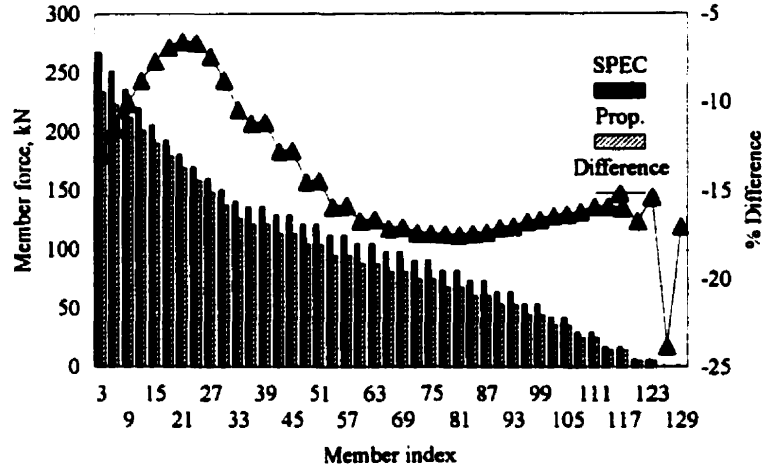

b) Za=Zv

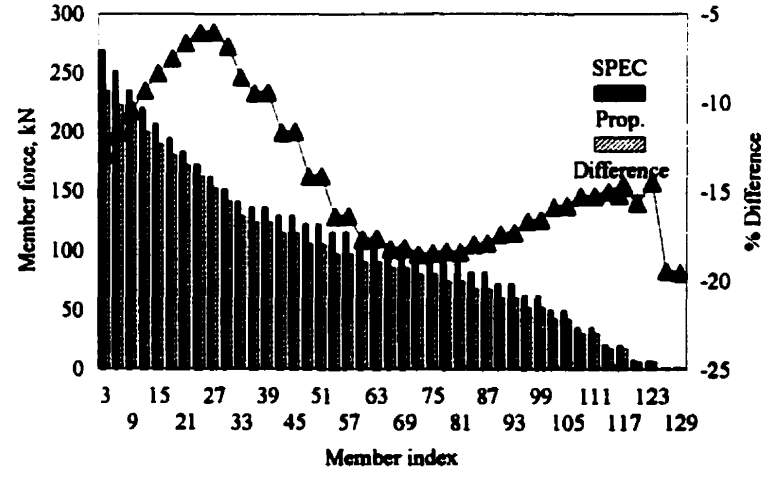

c) Za>Zv

Fig. D.16 Member forces in tower TC10 using NBCC spectrum

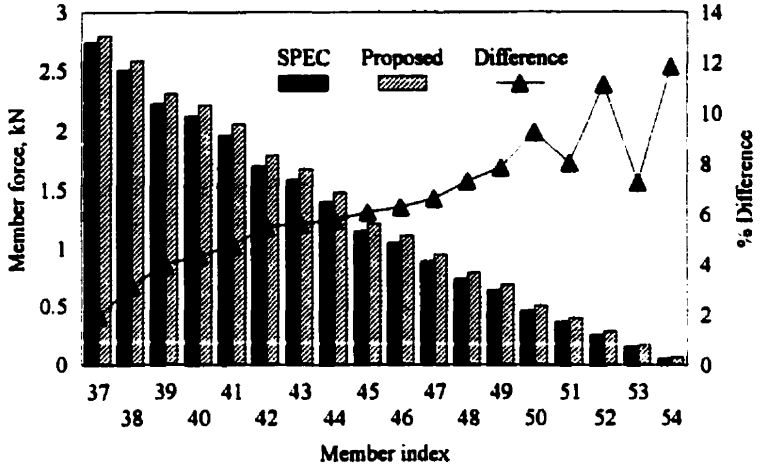

Fig. D.17 Member forces in tower TC2 under vertical excitation

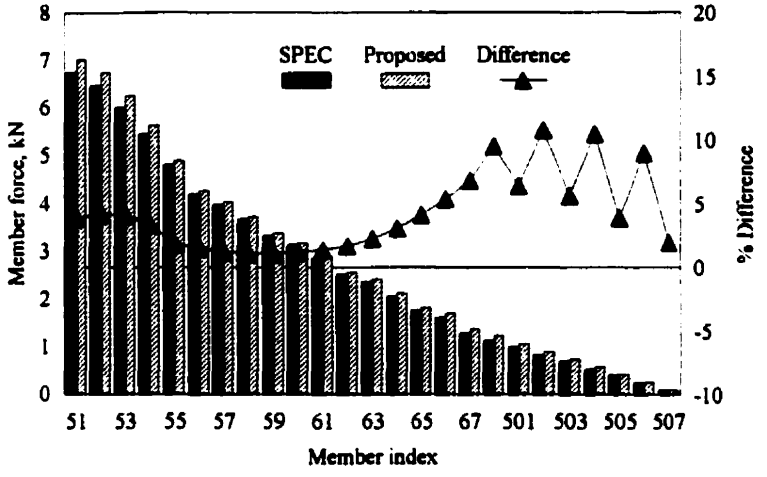

Fig. D.18 Member forces in tower TC3 under vertical excitation

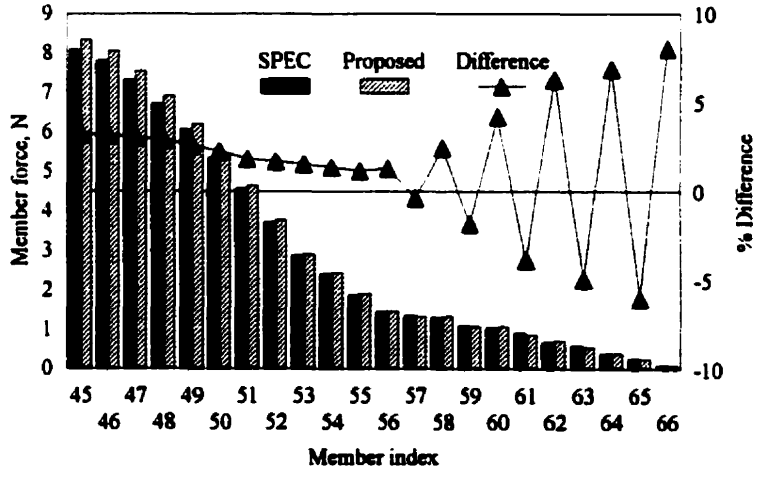

Fig. D.19 Member forces in tower TC5 under vertical excitation

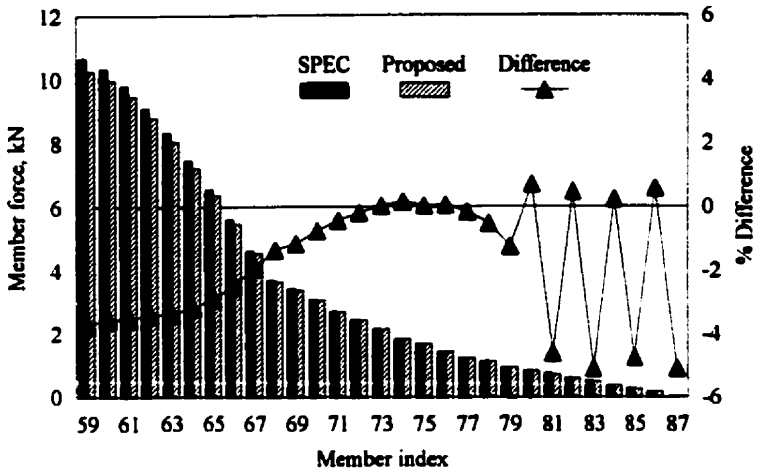

Fig. D.20 Member forces in tower TC6 under vertical excitation

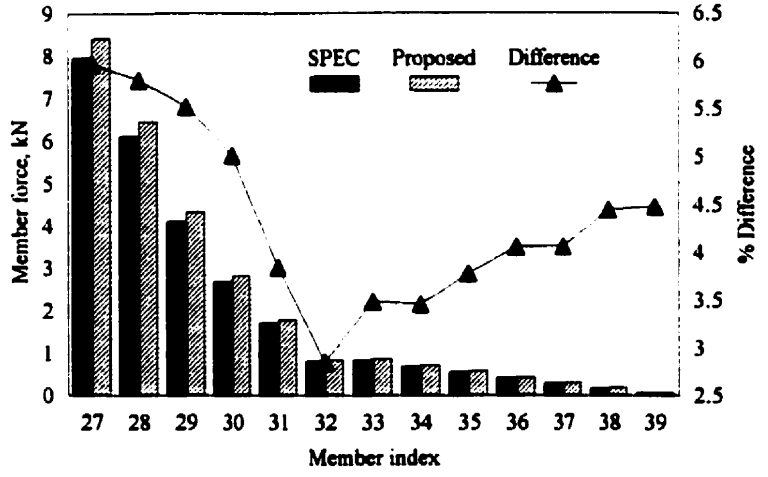

Fig. D.21 Member forces in tower TC7 under vertical excitation

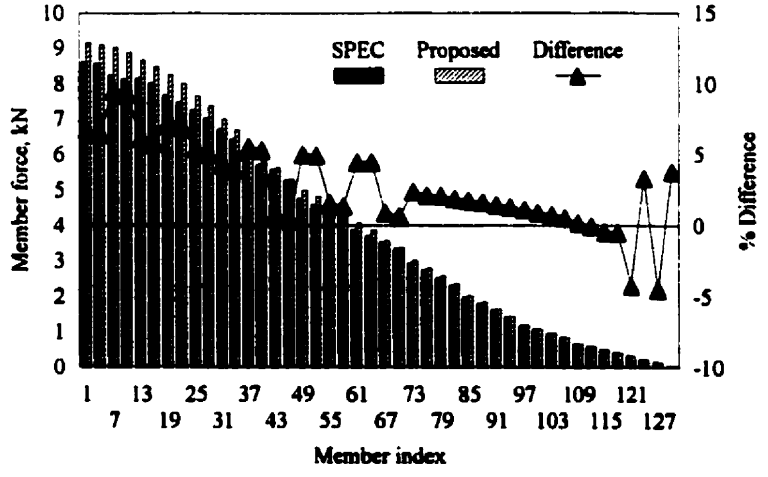

Fig. D.22 Member forces in tower TC8 under vertical excitation

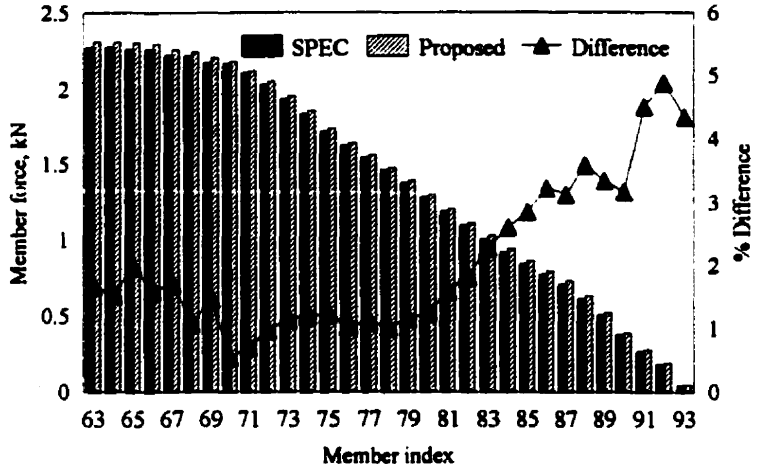

Fig. D.23 Member forces in tower TC9 under vertical excitation

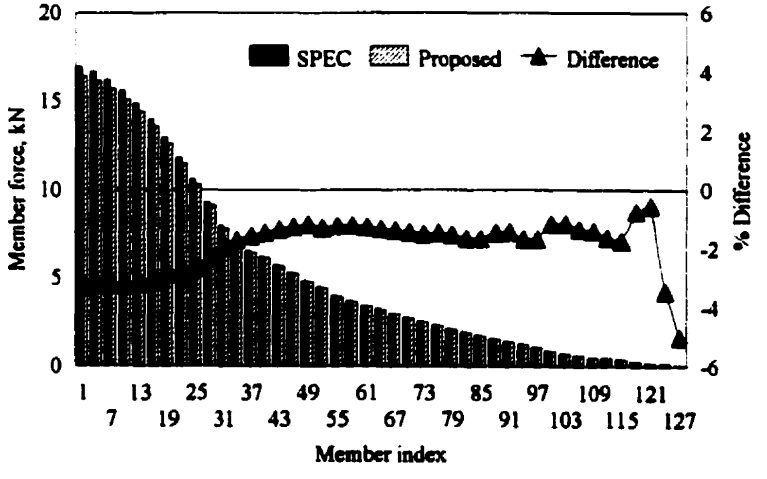

Fig. D.24 Member forces in tower TC10 under vertical excitation